0 0 0 0 5 1 0 5 0 8 6

UC-4
LBL-8011 c.1

Lawrence Berkeley Laboratory
UNIVERSITY OF CALIFORNIA

RECEIVED
LAWRENCE
BERKELEY LABORATORY

FEB 21 1980

LIBRARY AND
DOCUMENTS SECTION

Materials & Molecular Research Division

THERMODYNAMICS OF SOLID AND LIQUID GROUP III-V ALLOYS

Timothy James Anderson
(Ph.D. thesis)

October 1978

For Reference

Not to be taken from this room

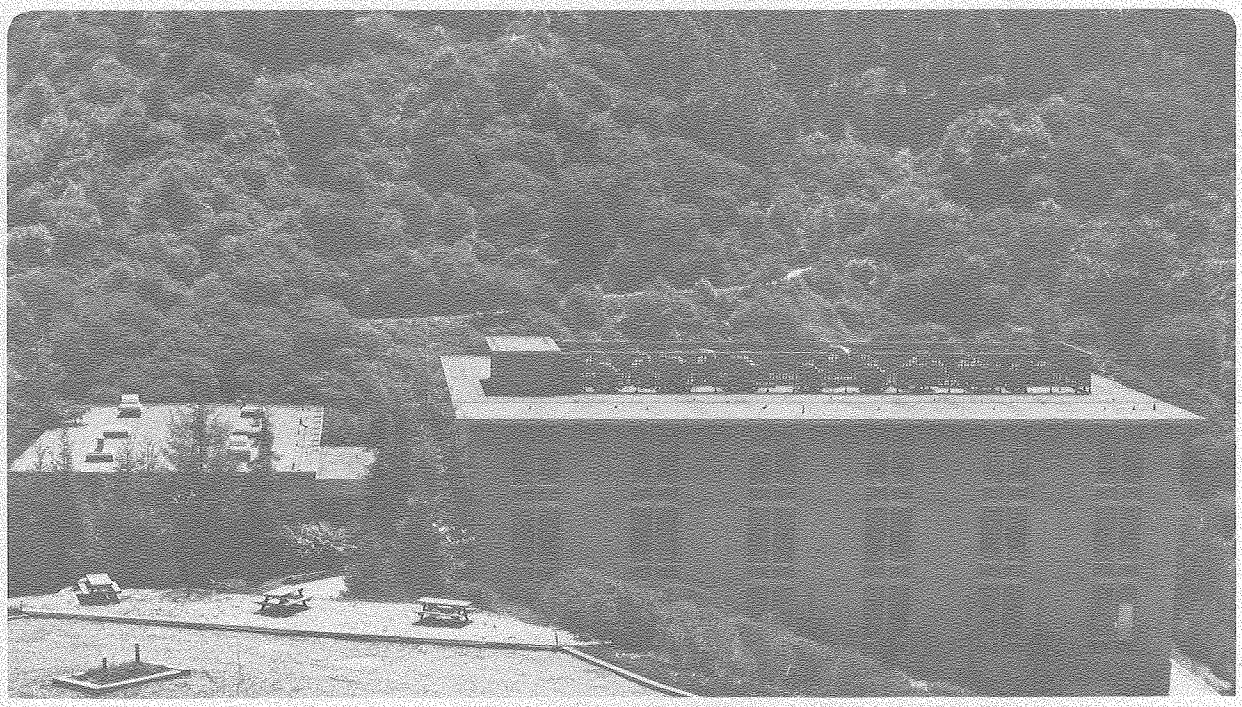

LBL-8011 c.1

Prepared for the U.S. Department of Energy under Contract W-7405-ENG-48

LEGAL NOTICE

This report was prepared as an account of work sponsored by the United States Government. Neither the United States nor the United States Department of Energy, nor any of their employees, nor any of their contractors, subcontractors, or their employees, makes any warranty, express or implied, or assumes any legal liability or responsibility for the accuracy, completeness or usefulness of any information, apparatus, product or process disclosed, or represents that its use would not infringe privately owned rights.

0 0 4 0 3 1 0 0 0 8 7

Contents

		Page
I.	Introduction	1
	A. General	1
	B. Phase Diagrams	3
	References	8
	Figures	9
II.	General Experimental Considerations	12
	A. Introduction	12
	B. Solid Oxide Electrolyte Concentration Cell	13
	C. Calcium Fluoride Electrolyte Concentration Cells	16
	References	23
	Figures	25
III.	Solid State Electrochemical Study of Ga-Sb Liquid Alloys	34
	A. Introduction	34
	B. Experimental	37
	C. Results	38
	D Discussion	42
	E. Conclusion	62
	References	63
IV.	Solid State Electrochemical Study of In-Sb Liquid Alloys	82
	A. Introduction	82
	1. General	82
	2. Phase Diagram	82
	3. Thermodynamics	83

Page

B. Theory and Experimental. 88

C. Results. 90

D. Discussion 96

1. Volume of Mixing 96

2. Calculation of the Phase Diagram 97

3. Gibbs Energy of Formation of InSb(c) 106

E. Conclusion 116

References 117

Figures. 121

V. Thermodynamics of the Gallium-Indium System. 133

A. Introduction 133

B. Thermochemistry. 133

1. Phase Diagram. 134

2. Thermodynamics 135

C. Discussion 139

1. Enthalpy of Mixing 139

2. Phase Diagram. 139

3. Gibbs Energy 139

4. Volume of Mixing 142

5. Short Range Order. 143

D. Conclusion 146

References 147

Figures. 149

0 0 0 0 5 1 0 0 0 8

Page

VI. Solid State Electrochemical Study of $Ga_xIn_{1-x}Sb$ Liquid Alloys. 158

A. Introduction 158

B. Experimental 160

C. Results. 160

D. Discussion 162

1. Introduction 162

2. Composition Dependence of the Liquid Phase Activity Coefficients. 164

3. Enthalpy of Mixing In $Ga_xIn_{1-x}Sb$ Liquid Solutions 169

4. Calculation of Γ_{GaSb} and Γ_{InSb} 175

5. Experimental Ga-In-Sb Phase Diagram Determinations 176

6. Calculation of the $Ga_xIn_{1-x}Sb$ Pseudobinary Phase Diagram. 177

7. Survey of Solution Models Used to Calculate the Pseudobinary Phase Diagram 182

8. Calculation of the Ternary Phase Diagram. 184

E. Conclusion 188

References 189

Figures. 192

VII. Summary. 211

Appendices

I. Solid State Electrochemical Study of the Gibbs Energy of Formation of β-Gallium Sesquioxide . . . 214

A. Introduction 214

B. Theory 215

Pages

C. Experimental 216

1. The Experimental Cell. 216

2. Materials. 218

3. Microcomputer Control System 219

D. Results. 220

E. Discussion 222

F. Conclusion 230

References 232

Figures. . . . . .

II. Solid-State Electrochemical Study of the Gibbs Energy of Formation of Indium Sesquioxide 241

A. Introduction 241

B. Experimental 242

C. Results. 244

D. Discussion 245

E. Conclusion 258

References 259

Figures. 261

III. Calculation of Liquidus Temperatures in a Binary System Forming a Solid Solution of Narrow Homogeneity Range 266

A. Introduction 266

B. Development of the Formation Equation. 266

C. Development of the Fusion Equation 269

D. Development of the Component-Rich Eutectic Liquidus Equations 271

References 273

0 0 0 0 5 1 0 0 0 8 9

Pages

IV. A Lattice Theory for Liquid Metal Solutions . . . 274

A. Introduction 274

B. Approximations 278

1. General Approximations 278

2. Special Cases. 279

a. Constant Interaction Energy. 279

b. Temperature Dependent Interaction Energy 279

c. Composition Dependent Interaction Energy 282

C. Summary. 282

References 283

V. The Important Relationships for Describing Phase Equilibrium in Ternary III-V Systems . . . 284

A. Introduction 284

B. General Results. 285

1. Basic Equilibrium Conditions 285

2. Relationship Between the Standard State Chemical Potentials. 286

3. Development of Working Equations for the Ternary Phase Equilibria 288

C. Pseudobinary Case. 289

D. Ideal Liquid and Solid Solutions 290

Acknowledgments. 292

THERMODYNAMICS OF SOLID AND LIQUID GROUP III-V ALLOYS

Timothy J. Anderson

Materials and Molecular Research Division
Lawrence Berkeley Laboratory
Department of Chemical Engineering
University of California
Berkeley, California 94720

ABSTRACT

Solid-state electrochemical techniques are applied to the Ga-In-Sb-O system to measure some thermodynamic properties important for the analysis of solid-liquid phase equilibria in these important semiconductor materials. The standard Gibbs energies of formation of the most stable oxides of gallium and of induim are determined with a high-temperature solid-state electrochemical cell utilizing calcia-stabilized zirconia as the solid electrolyte and a ($CO + CO_2$) gaseous mixture as the reference electrode. The voltage of the following cell is measured

$$Pt|C|M(\ell),\ M_2O_3(c)||Ca_{0.15}Zr_{0.85}O_{1.85}||\ CO,\ CO_2|Pt \qquad (1)$$

Cell potentials are recorded for M = Ga and In, and cover the temperature ranges from 775 to 1100 K and 950 to 1128 K, respectively. A linear

regression analysis of the results indicate the standard Gibbs energies of formation for the two sesquioxides can be represented by

$$\Delta G_f^o(Ga_2O_3,c,T)/Kcal_{th}mol^{-1} = (-265.83 \pm 0.16) + (0.08345 \pm 0.0016)\ (T/K) \quad (2)$$

$$\Delta G_f^o(In_2O_3,c,T)/Kcal_{th}mol^{-1} = (-223.67 \pm 0.14) + (0.08044 \pm 0.0014)\ (T/K) \quad (3)$$

A third-law analysis of the results show that the standard enthalpies of formation are given by

$$\Delta H_f^o(Ga_2O_3,c,298.15K)/Kcal_{th}mol^{-1} = -261.0 \pm 0.1 \quad (4)$$

and

$$\Delta H_f^o\ (In_2O_3,c,298.15K)/Kcal_{th}mol^{-1} = -229.09 \pm 0.01 \quad (5)$$

These results are in agreement with recent calorimetric determinations. Comparisons with the results of other studies are presented. For Ga_2O_3, the third-law calculation results show a temperature dependence of $0.004\,Kcal_{th}\,mol^{-1}K^{-1}$ which is most probably caused by an error in the estimated high-temperature heat capacity of gallium rather than by electronic conduction in the solid electrolyte. Using the results for In_2O_3 an analysis is presented for assessing the effect of equilibrium partial pressures of In_2O over a mixture of $\{In(\ell) + In_2O_3(c)\}$.

Group III component activities in Ga-Sb and In-Sb liquid alloys are measured in the high-temperature galvanic cell

$$Pt|C|M_xSb_{1-x}(\ell),\ M_2O_3(c)||CSZ||CO,\ CO_2|Pt \quad (6)$$

and

$$Pt|C|M_xSb_{1-x}(\ell),\ M_2O_3(c)||CSZ||M(\ell),\ M_2O_3(c)|Pt \qquad (7)$$

The component activities measured are found to give moderate negative deviations from ideal behavior. Both binary systems exhibit a negative enthalpy of mixing and a positive excess entropy of mixing. This behavior is partially explained by a positive excess volume of mixing. Liquidus temperatures are calculated and the results of this work exhibit excellent consistency with the available calorimetric data and the reported phase diagrams. Furthermore, these calculations suggested the enthalpies of fusion of GaSb and InSb be taken as 7.8 and 5.9 $Kcal_{th}\ g^{\circ}atom^{-1}$, respectively. A new expression for the Gibbs energies of formation of solid GaSb and InSb are derived and given by

$$\Delta G_f^o(GaSb,c,T)/cal_{th}\ g^{\circ}atom^{-1} = -5660 + 3.536\ (T/K) \qquad (8)$$

and

$$\Delta G_f^o(InSb,c,T)/cal_{th}\ g^{\circ}atom^{-1} = -4209 + 3.052\ (T/K) \qquad (9)$$

These results are shown to be consistent with the available calorimetric work, the reported phase diagrams and the activity measurements of this work. The observed tendency of pairing between Group III atoms and Sb is quantified with the aid of a simple statistical model.

The experimental information pertinent to phase equilibria in the Ga-In system is surveyed and an analysis is presented to ascertain the consistency of the reported findings. The reported solidus is considered to be in error as are several determinations of the eutectic

0 0 0 0 5 1 0 5 0 9 1

temperature and composition. Consistent values for the Gibbs energy, enthalpy and entropy of mixing are selected.

Gallium activities in the pseudobinary liquid, $Ga_xIn_{1-x}Sb$ are measured in the solid-oxide galvanic cell

$$Pt|C|Ga_xIn_{1-x}Sb(\ell),\ Ga_2O_3(c)||CSZ|\ Ga(\ell),\ Ga_2O_3(c)|C|Pt \qquad (10)$$

Moderate negative deviations from Raoult's law throughout the entire Group III composition range are found. The literature enthalpy of mixing results in the ternary are analyzed and combined with the results of this study to predict the pseudobinary phase diagram. Excellent agreement with the experimental phase diagram is found. The calculational methods are extended to a complete description of the ternary phase field and results in good consistency with the experimental liquidus and solidus data.

0 0 0 0 5 1 0 0 0 9 2

CHAPTER I. INTRODUCTION

A. GENERAL

The elements aluminum, gallium and indium from the Group IIIA column combine with the Group VA elements phosphorous, arsenic and antimony to form a class of semiconductor materials appropriately termed III-V compounds. These 'second generation' semiconductor materials are isoelectronic analogues to the 'first generation' materials (Group IVA elements silicon and germanium). Though the semiconductor technology is almost completely based on the material silicon, III-V compounds offer several distinct advantages over Si from an electronic device application point of view.

The magnitude of the absolute value of the drift velocity of a charged carrier per unit applied electric field is termed the mobility of that carrier. In general, high purity single crystal semiconductor materials have high electron mobilities that are determined largely by phonon scattering. Though the mobility is a function of the growth technique, the observed III-V compound mobilities are in general much higher than that found in Si. A typical room temperature mobility of InSb is on the order of 7×10^4 cm^2/V sec while the value for Si is near 1×10^3 cm^2/V sec.[1] The higher mobilities in III-V compounds translates into improved electronic device characteristics in terms of decreased response times. For example, faster computer memory switching times and increased upper frequency limitations are possible with III-V compounds.

The second major inherent advantage of III-V compounds over Si arises from an increased range of physical and electrical properties available to the device designer. The use of silicon stipulates a single bandgap (Eg = 1.17 eV, indirect),[2] crystal structure and lattice constant, etc. With the use of III-V compounds the properties of the nine possible compounds are now available. Additionally, III-V compounds exhibit the unusual property of complete cation or anion miscibility in the solid phase. A cation can substitute on the crystal lattice for the host cation throughout the entire composition range and similarly for the anion. For example, InAs can combine with AlSb in any proportion of form the quaternary solid solution $In_xAl_{1-x}As_ySb_{1-y}$, with the Group III to Group V atom ratio remaining nearly unity. Thus the properties of the semiconductor material can now be continuously varied between the binary compound limits. Figure 1 shows the lattice parameter of III-V binary compounds versus the observed room temperature bandgap energy.[2-8] Each point in figure 1 represents the values for the particular compound. The continuous substitition of a cation for another cation or an anion for another anion is represented by a line in the figure. The substitution of both a cation and anion leads to an enclosed area of permissable lattice parameters and corresponding bandgaps. Thus the entire area enclosed in figure 1 is accessible to the designer when employing ternary and quaternary III-V solid solutions. The solid line in figure 1 indicates a direct type of bandgap while the dashed line represents an indirect bandgap. The compounds with an asterick are currently available in bulk single crystal form.

The bandgap is the minimum amount of energy required to promote an electron from the valence band into the conduction band. If the conduction electron retains the same momentum the transition is termed direct, otherwise it is an indirect transition. The magnitude of the bandgap is an important parameter in the construction of optoelectronic devices and the type of bandgap determines the efficiency of electron promotion (direct transition being more favorable.) For example, the bandgap determines the maximum wavelength of radiation produced in a light emitting diode. Thus the use of III-V compounds has greatly expanded the realm of possible solid state electronic devices. Unfortunately, III-V compounds have found limited applications as a result of technological problems.

B. PHASE DIAGRAMS

In general solid state III-V electronic devices require the growth of single crystal epitaxial layers onto a substrate material. The currently best epitaxial material is being produced by growth from liquid phase (liquid phase epitaxy, LPE). Important to this process is knowledge of the liquid phase composition and growth temperature required to produce the specified solid composition. The binary liquid-solid III-V phase diagrams have been experimentally determined.[9] All the binary systems show a similar type of phase field as is illustrated in figure 2. The solid phase is characterized by a single equimolar compound showing a neglible range of stoichiometry. In general the melting temperature of the congruently melting compound is higher than that of the elements. The systems also exhibit degenerate eutectics that are usually located close to the pure components.

The ternary phase diagrams are dominated by the 1:1 solid solutions. The special case of equilibrium between a stoichiometric liquid and solid solution is termed the pseudobinary phase field and these diagrams are isomorphous for all systems. Experimental liquidus-solidus data exists for most of the pseudobinary systems while results outside the pseudobinary phase field exist only for a few technologically important systems. The phase diagrams of quaternary and higher systems have received very little attention.

Because of the potential importance of ternary and quaternary III-V solid solutions knowledge of their phase diagrams is essential. To experimentally determine the possible 18 ternary and 15 quaternary phase diagrams would be a task of immense proportions. The volume of data required alone is limiting, not to mention the experimental difficulties of long equilibration times and the extremely high vapor pressures of As and P encountered. For these reasons recent attention has focused on predicting the phase diagrams on a purely theoretical basis or by forcing a thermodynamic model to perform perfectly in the well known binary limits. Both of these approaches have given qualitatively correct results when compared to the little experimental data available. Unfortunately these approaches have very little physical significance when compared to derived fundamental thermodynamic data.

The purpose of this project is to elucidate some fundamental thermodynamic properties of III-V compounds with the intent of gaining an insight into their solid-liquid phase equilibria. The philosophical approach initiated here involves an accurate and detailed experimental

characterization of a single ternary system. It is hoped that with a fundamentally well defined system in hand various phase equilibria models could be investigated on both a quantitative and physical basis.

A necessary condition for equilibrium to exist in a solid-liquid system at constant temperature and pressure is that the Gibbs energy change of the system be zero for all infinitesimal processes. Since temperature and composition are variables easily specified in crystal growth we seek to map the values of these two variables where this condition occurs. Restricting ourselves to those states that contain both a solid and liquid phase produces a map termed the solid-liquid phase diagram. Thus, of particular interest here would be an experimental elucidation of the Gibbs energy of the system as a function of composition and temperature.

Applying this approach to III-V compounds the ternary system Ga-In-Sb was chosen as the system to investigate mainly in view of its experimental simplicity. An examination of the literature indicated that the three possible binary systems, Ga-Sb, In-Sb and Ga-In, had experimentally well defined binary phase diagrams (See Chapters, 3, 4 and 5). Additionally, calorimetric and emf studies were available for the three binary liquid mixtures and the thermal properties of all solid phases were well characterized. Unfortunately rigorous consistency tests performed with the available data produced erroneous results for the binary systems Ga-Sb and In-Sb. The Gibbs energy measurements of the liquid mixtures for these two systems were suspected to be in error. Thus an experimental program was initiated to better

ascertain the Gibbs energy of mixing in the Ga-Sb and In-Sb binary systems. A solid, oxygen conducting, electrochemical cell was utilized to obtain a direct measurement of the Gibbs energy of mixing. It was hoped that the Gibbs energies generated by these experiments when combined with other literature data would form a consistent fundamental thermodynamic data set. The ramifications of the experimental technique employed are explored in Chapter 2. In order to make the experimental technique used a viable one the Gibbs energy of formation of the two Group III metal oxides was required. Again an analysis of the available literature results generated inconsistencies. Appendices 1 and 2 contain the results of emf measurements performed on the sesquioxides Ga_2O_3 and In_2O_3, respectively. With this preliminary work, the Group III metal activities in the two binary systems of interest were then possible to measure and are discussed in Chapters 3 and 4. Chapter 5 contains a summary and assessment of the available thermodynamic data for the third binary system, Ga-In.

With the binary systems now characterized the ternary system, Ga-In-Sb, was approached. The pseudobinary phase diagram has been investigated by several workers but little work is available for the remainder of the phase field (see Chapter 6). The thermodynamics of the solid solution has received little attention but is more amendable to theoretical calculations than the liquid phase. In Ga-In-Sb liquid mixtures some calorimetric work has been performed but no Gibbs energy measurements were discovered in the literature. Chapter 6 contains the results of emf measurements for Ga-In-Sb pseudobinary liquid

0 0 0 0 3 1 0 0 0 9 5

mixtures and finally assimilates the previous binary work to produce a characterization of the Ga-In-Sb ternary system.

It is hoped that this work will be useful in providing a physical basis for the development of a thermodynamic model that would physical the phase equilibria in other ternary and higher order III-V systems. In this way considerable experimental effort and difficulties could be circumvented.

REFERENCES

1. H. P. R. Frederikse, Am. Inst. Phys. Handbook, 3rd ed.

2. C. Hilsum and A. C. Rose-Innes, "Semiconducting III-V Compounds." MacMillan (Pergamon; New York); 1961.

3. H. Kressel, and H. Nelson, 'Physics of Thin Films', M. H. Francombe, ed., (Academic Press, New York); 1973.

4. G. Giesecke and H. Pfister, Acta Cryst., 11, 369 (1958).

5. Yu. I. Pashintsev and N. N. Sirota, Dokl. Akad. Nauk BSSR, 3, 38 (1959).

6. A. G. Thompson and J. C. Woolley, Can. J. Phys., 45, 255 (1967).

7. R. L. Moon, G. A. Antypas, and L. W. James, J. Electronic Mat., 3, 635 (1974).

8. M. Neuberger, Handbook of Electronic Materials, 2, III-V Semiconducting Compounds (IFI/Plenum, New York); 1971.

9. N. N. Sirota, Semiconductors and Semimetals, 4, R. K. Willardson and A. C. Beer, ed. (1968).

LIST OF FIGURES

Fig. 1 Lattice parameter (Å) of III-V compounds and solid solutions versus bandgap (eV). ●, binary compounds; *, available in bulk single crystal form; ——, direct bandgap, ----, indirect bandgap.

Fig. 2 Generalized Group III-V binary phase diagram.

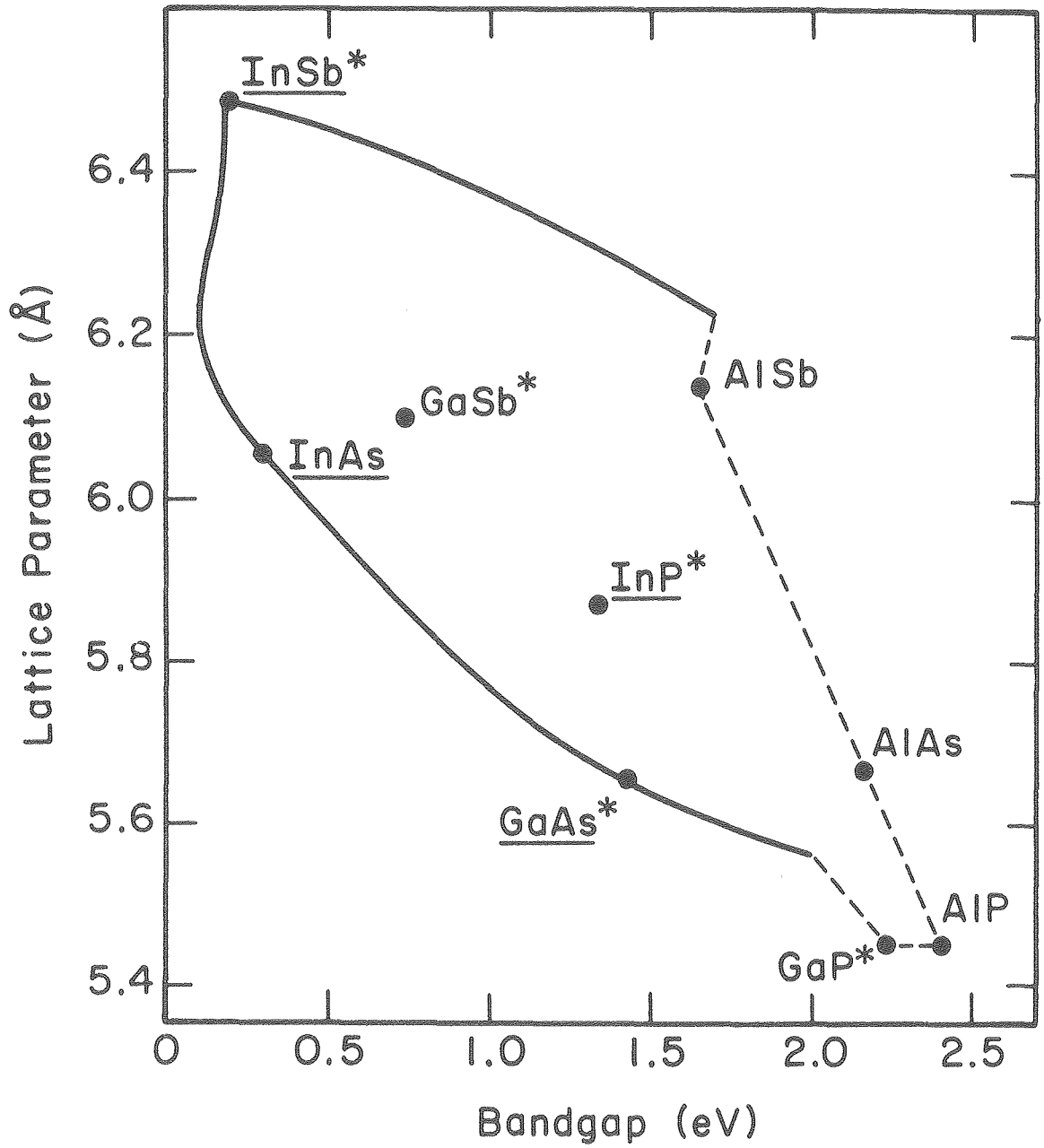

XBL 796-10026

Figure 1.

GENERAL GROUP III-V BINARY PHASE DIAGRAM

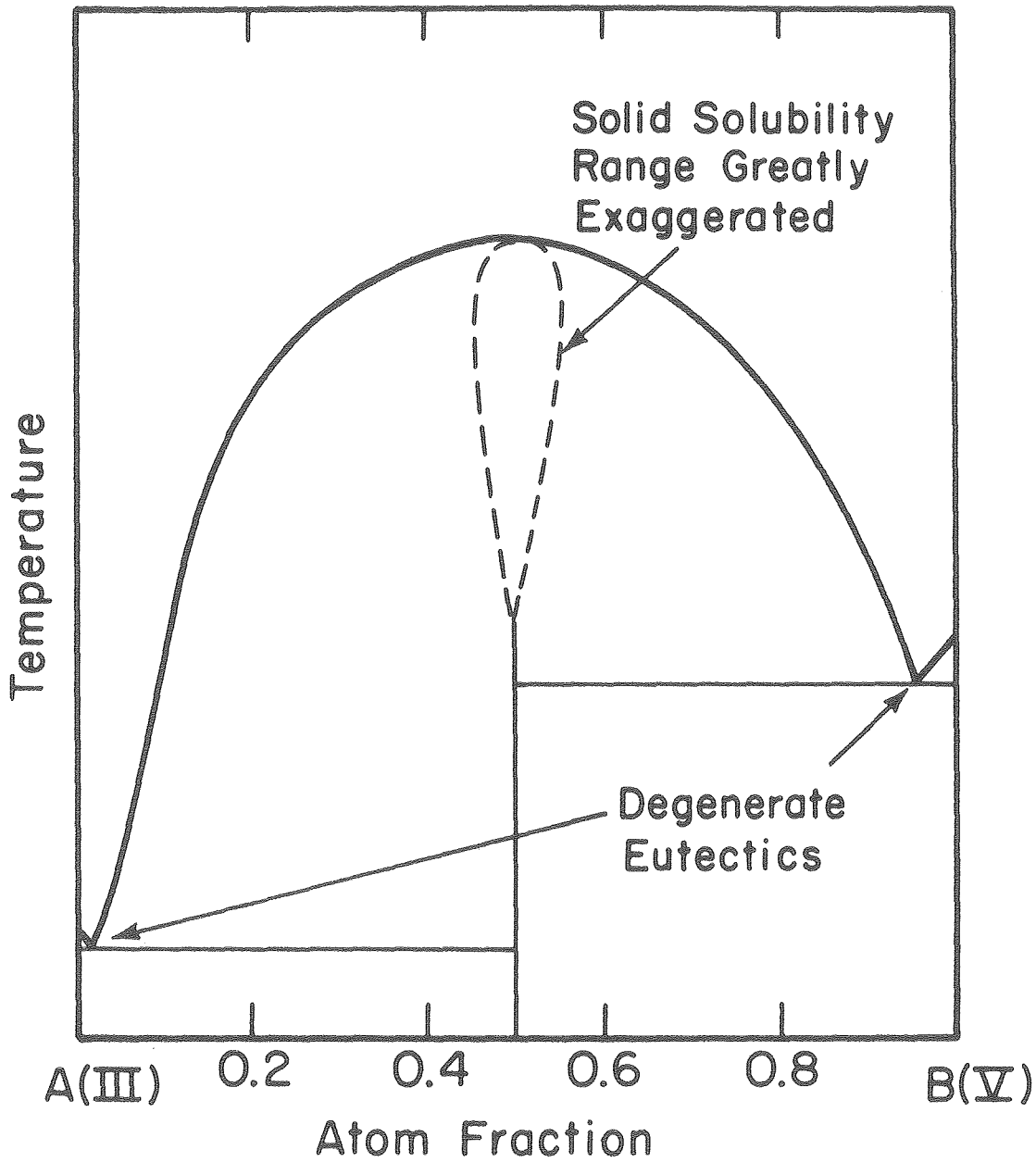

XBL 796-10025

Figure 2.

CHAPTER II. GENERAL EXPERIMENTAL CONSIDERATIONS

A. INTRODUCTION

In general, an open circuit reversible potential, E, is developed in a galvanic electrolytic cell. This cell potential can be related to the Gibbs energy change, ΔG, for the virtual chemical reaction of the cell by the simple relation

$$\Delta G = -nFE \tag{1}$$

where n is the equivalents of charge and F is Faraday's constant. Upon applying this relationship to the measured potential of a solid electrolyte cell, it is implicitly assumed that all charge transfer proceeds exclusively through ion conduction. Thus, electrochemical cells can be designed that yield the Gibbs energy changes for a desired chemical reaction provided a suitable electrolyte can be found. For purposes of characterizing liquid mixtures of Group III metals in antimony the desired chemical reaction is one in which the chemical potential of one of the components can be isolated.

Calcia-stabilized zirconia (CSZ) will conduct oxygen ions solely at elevated temperatures[1] and is suitable for investigating gallium or indium activities. Also of interest would be an investigation of liquid solutions containing the third Group III metal aluminum. Unfortunately, the CSZ solid electrolyte is not suitable due to a favorable reaction of metallic Al with the electrolyte. Thus, in order to investigate Al solution activities a new and stable electrolyte was required. Calcium fluoride was reported[5] to be an exclusive conductor of fluorine ions at high

temperatures and is a possible solid electrolyte in concentration cells containing elemental Al.

Summarized in figure 1 are the two methods for measuring the liquid phase component activities of Group III metal activities with a solid electrolyte concentration cell. Both cells can be thought of as equilibrating the electrochemical potential of the conducting ionic species between a reference electrode and a working electrode. In the schematic shown in figure 1 the conducting species, which exists as a dimer in the gas phase, is fixed at a known reference partial pressure, P''_{x_2}. This known reference state is then compared to the P'_{x_2} established in the working electrode via a cell potential produced by charge transfer of the conducting species which is just balanced by the concentration gradient existing across the electrolyte. The measured cell voltage can be related to the unknown working electrode x_2 partial pressure which in turn is related to the Group III metal activity. In this way, the liquid phase activity of Ga, In or Al in solution with Sb can be measured as a function of composition and temperature.

B. SOLID OXIDE ELECTROLYTE CONCENTRATION CELLS

The predominant defect in zirconia, ZrO_2, is oxygen vacancy-interstitial pairs (Frenkel defects). Doping ZrO_2 with CaO enhances this defect predominance and produces a favorable ionic conductivity ($\sigma = 5.5\ 10^{-2}(\Omega_{\circ}cm)^{-1}$ at 1,000 C and 13 mole-% CaO)[1] while showing negligible electrical conductivity. Several excellent reviews of the conduction mechanism and defect equilibria in CSZ are available in the literature.[2-6] In order to easily interpret the measured cell voltages, electronic conductivity must be negligible. The temperature and pressure range

over which the electronic conductivity is less the 1% (ionic transference, $t_{ion} > 0.99$) is termed the electrolytic domain. Figure 2 shows the electrolytic domain for the solid oxide electrolytes CSZ and yittria doped thoria derived from the results of Schmalzreid[7], Patterson, et al [8,9], Tretyakov and Muan [10], and Hardaway, et al.[11] As the oxygen partial pressure is decreased, electron conductivity increases in importance while very high oxygen pressures introduce hole conduction in these oxides. Shown here are the domain limits as a function of both temperature and oxygen pressure. For CSZ two electrolytic domains are exhibited representing the range found in the literature. The upper conservative limit is indeed too conservative as identical results were found when the Gibbs energy of forming Ga_2O_3 was measured using both the zirconia and thoria based electrolytes (Appendix I). Thus, the domain must lie below the ΔG^o vs T line for the reaction

$$\frac{4}{3}\,Ga(\ell) + O_2 = \frac{2}{3}\,Ga_2O_3(c) \qquad (1)$$

Also shown in figure 2 are the Gibbs energies of forming the various Ga and In oxides. For Ga, the most stable oxide is the sesquioxide and provides an explicit oxygen source. In the case of In it appears that both the monovalent and trivalent indium oxides show nearly equal Gibbs energy changes per mole of oxygen. The viability of this cell is nonetheless shown in Appendix II.

In connection with the measurement of Ga and In activities, two different reference electrodes were employed for establishing a known oxygen partial pressure. The first reference electrode consisted of a mixture of the pure Group III metal in equilibrium with its most stable oxide.

Figure 3 shows the two experimental cell designs used. In cell design (a) a 1.5 inch, (length), 0.25 inch (O.D.) closed one end tube of CSZ (Zirconia Corp. of America, Solon, Ohio) was used as the electrolyte. The metal-metal oxide reference electrode was placed inside this tube in such a way that the oxide powder was put on the top of pure metal, thus providing a vaporization barrier to volatile Sb. Electrical contact was made with a graphite plug that tapered to a thin rod which extended into the liquid metal electrode. A Pt wire (.020 inch) was attached to the graphite plug which was taken out of the cell to the electrometer. The Pt wire was contained in a 1/8 inch single bore alumina sheath. The working electrode was contained in a cylindrical graphite crucible that had a 1/4 inch bore in the top for placement of the CSZ tube. The use of graphite was favorable due to its inertness with respect to reaction with Ga and In. Again, the most stable oxide was placed over the top of the III-V liquid mixture and electrical contact was made with Pt wire. In the second cell design using the metal-metal oxide reference electrode, a 18 inch (length), 1/4 inch (O.D.) CSZ tube was utilized instead. This length allowed the tube to extend beyond the cell head and thus insured isolation of the two electrodes.

A reference oxygen partial pressure can also be established according to the well defined reaction

$$CO_2 = CO + 1/2\ O_2 \qquad (2)$$

With the use of this gaseous electrode a less sluggish reference electrode is insured. A schematic of the cell design is shown in figure 3 (c). A known mixture of CO-CO_2 gas was slowly passed over a porous Pt electrode

on the inside of the CSZ tube. The Pt electrode was formed by repeated application of a Pt paste followed by high temperature firing. Additionally, a wound Pt wire was placed on the inside of the tube. The remainder of the cell design was as described for cell (b).

The assembled experimental cell was contained in an alumina tube as described and shown in Appendix I. Experimental potentials were measured with a Keithley 640 electrometer while temperatures were measured with Pt-Pt10% Rh thermocouple with the aid of an electronic ice bath and amplifier connected to a digital panel meter. Temperature and voltage measurement were coupled with furnace control through an Intel 8008 based microprocessor. Figure 9 shows a picture of the microprocessor while an information flow diagram can be found in Appendix I. The experimental apparatus, procedures and precautions are essentially those described earlier by this author.[12] A list of any materials used and experimental variations is also given.

C. CALCIUM FLUORIDE ELECTROLYTE CONCENTRATION CELLS

As a result of the inaccessibility of Al with the use of a solid oxide electrolyte, and the importance of obtaining thermodynamic data in Al-containing alloys, a new solid electrolyte was investigated. This galvanic cell employed CaF_2 as a flourine ion conducting solid electrolyte. The use of CaF_2 as a functional solid electrolyte has considerable precedence in the literature.[5] Using these successful galvanic cells as a guideline, several cell configurations were tested. The results of these early investigations met with little success even though attempts were made to duplicate previous work. The early results are summarized elsewhere.[12] In these cells a stable cell voltage was not attainable and was attributed

to lack of electrode containment. Escaping metal vapors formed a thin-film electrical conductor around the CaF_2 single crystal. Also, the volatile metal flourides served as a source of vapor phase flourine transport, again short-circuiting the galvanic cell. Thus, a new cell was designed to circumvent this problem.

Shown in figure 4 is the experimental details of the new CaF_2 electrolyte galvanic cell. The electrode material was encased in a crucible of spectrographic grade graphite (5/8 inch O.D.), the perimeter of the opened end being beveled. The electrode was sealed to the electrolyte with a washer made of 0.050 inch carbon foil. The electrolyte was a polished single crystal of CaF_2 having a diameter of 1 inch and thickness of 1/8 inch. Electrical contact was made by contacting platinum foil (0.002 inch) with the bottom of each crucible. Welded to the foil was a Pt wire (0.020 inch). Fitted to the top electrode was an alumina (Al_2O_3) centering block, serving also as an electrical insulator. A spring loaded (1-2 lb. force) alumina pushrod (5/16 inch O.D.) was centered over the top electrode. The tube was ported to allow passage of the inert gas blanket, while a sheathed Pt lead wire passed through the center. The bottom electrode was supported by a tantalum (Ta) plate. An alumina block again served as an insulator and centering device. The Ta plate was suspended from the cell head by means of guy wires and a fluorine gettering material (Th,Y,Zr) was placed on this plate. The two electrode compartments were isolated with two concentric alumina tubes (1 inch O.D. and 1-1/2 inch O.D.). The tubes were sealed to the CaF_2 with carbon foil washers. The annulus of the two tubes was pressurized with either inert gas or oxygen (the oxygen would oxidize and deactivate any possible metal leaks).

The experimental cell was enclosed in a closed one end alumina tube (2-1/4 inch O.D.) and was placed horizontally in a Marshall resistance furnace as shown in figure 5. The horizontal placement allowed the possibility of having both electrodes in the liquid state. The enclosing alumina tube was sealed to a brass cell head by means of a Viton O-ring compression fitting. The isolating concentric tubes were sealed at the cell head with a sliding O-ring seal. The sheathed Pt electrode leads exited through the cell head, with the wires being sealed with teflon ferrules in compression fittings. The sheaths were sealed at the top of the cell head (only one shown) with a Cajon fitting. A Pt-Pt 10%Rh thermocouple placed near the galvanic cell was similarly sealed. Also located on the cell head were three symmetric hooks for attachment of the Ta support plate guy wires. A port was located at the top of the annulus to allow pressurization. Additional ports were located at the spring compartment (inert gas exit for the top electrode (inner compartment) and outside the larger concentric tube /inert gas entrance for the bottom electrode/exterior compartment). The exterior compartment purge gas exited via a alumina tube (1/8 inch O.D., not shown) which extended to the bottom electrode, thus insuring a proper gas blanket. This tube passed through the cell head and was sealed as was the thermocouple. The interior inert gas entrance was fitted into the feedthrough of the top electrode's lead wire. Water cooling coils were provided to insure proper O-ring operation. The furnace was adjusted to have a flat temperature profile (±1 C) in the vicinity of the experimental cell by means of adjustable external resistors.

Special attention was given to obtaining a high purity inert gas stream. The purification scheme utilized is shown in figure 6. Cylinder helium was first passed over Linde 4A molecular sieve to remove any water present. The next stage consisted of passage over hot (600 C) copper turnings followed by hot cupric oxide chips. The copper metal reacted with any oxygen present while the cupric oxide converts hydrogen gas to water. The water vapor subsequently formed was removed in two stages. The bulk drying was achieved with the molecular sieve and then was followed by a liquid nitrogen cold trap. As a final purification step the inert gas was passed over titanium chips at a temperature of 850 C. Before entering the experimental gas manifold, the gas was finally exposed again to a liquid nitrogen cold trap. In this way the impurity levels of oxygen, hydrogen and organics contained in the cylinder helium can be reduced to negligible levels.

Photographs of the new CaF_2 cell design are shown in figures 7 and 8. Figure 7 shows the overall equipment and includes a vacuum system (lower right), microprocessor (upper right), assembled cell and furnace (middle), gas purification and manifold (upper left) and instrument rack (lower left). Figure 8 shows the assembled cell in more detail. Figure 9 depicts the microprocessor used.

Concentration cells of the form

$$Pt\,|M^{I},M^{I}F_{x}|CaF_{2}|M^{II},M^{II}F_{y}|Pt \qquad (2)$$

were tested using this new cell design and with the metals (M^{I} and M^{II}) Al, Ni, Ga, In, Mg, and Y. Various cell mixtures and forms were attempted. These included sintered pellets, powders, liquid melts at the operating

temperature, added CaF_2 to electrode material and pre-drying with SF_4 gas. The cells were tested under atmospheres of purified He and Ar, vacuum (10^{-5} torr) and pure oxygen. In all cells tested the cell voltage would approach an expected value upon reaching a desired operating temperature. Within a few hours of operation, though, the voltage would begin to fall at a moderate rate and reduce to a small value. Titration of the cell could momentarily re-establish the expected cell voltage but again it was unstable. After the cells were disassembled, the electrodes and electrolytes were examined with an X-ray diffractometer and no evidence of any side reaction product could be detected. Visual examination revealed no deposited metal film, and inert gas flow rate changes produced no voltage change during the short period of stable emfs. Though successful operation of many of these concentration cells have been reported in the literature,[5] no successful cells were operated here.

One possible explanation for the lack of a stable emf is to postulate the existence of a CaO pathway between the electrodes, possibly located on the CaF_2 single crystal surface. Hauffe and Tränckler[13] found that CaO was a p-type conductor at oxygen partial pressures above 10^{-5} atm and an n-type conductor at lower oxygen potentials. Alcock and Stavropoulos[14] investigated electrochemical cells of the type

$$M^{I},M^{I}O_{x}|CaO|M^{II},M^{II}O_{y} \qquad (3)$$

with the metals Ni,Co,Cr and Mn. By comparing these results with those obtained using an exclusively ionic conducting electrolyte, they proposed ionic transport numbers for CaO. As a solid electrolyte calcium oxide never has a unity ionic transport number (ionic conduction is probably

due to cation mobility) and drops to less than 0.05 for oxygen potentials less than 10^{-15} atm. Thus, it is possible that the presence of a CaO film could short circuit any cell via electronic conduction.

Calcium fluoride conducts fluorine ions exclusively over a large range of fluorine activities, from atmospheric fluorine pressures down to the stability limit of the electrolyte ($CaF_2 \rightarrow Ca + F_2$). The primary defect responsible for ionic conduction is anti-Frenkel defects according to the defect reaction

$$F_F^X \rightleftarrows F_i^{'} + V_F^{\cdot} \qquad (4)$$

and fluorine ion conduction primarily due to an interstitial mechanism.[15] It is also known that the solubility of oxygen in CaF_2 is near 0.2 mole per cent in the range of the operating temperatures investigated here (600-800 C). Thermogravimetric and total a.c. conductivity studies by Levitskii, et al[17] with CaF_2 as a function of oxygen partial pressures indicate oxygen incorporation in the following manner

$$\frac{1}{2}O_2 + 2F_F^X = V_F^{\cdot} + O_F^{'} + F_2 \qquad (5)$$

This defect reaction provides a mechanism for oxygen ion mobility, and indeed oxygen concentration cells using a CaF_2 electrolyte have established open circuit potentials the same as those using a calcia-stabilized zirconia electrolyte.[18,19] Since the oxygen partial pressure is nearly equal in both electrodes, a reduction in open circuit voltage is possible by the migration of oxygen ions due to the potential drop established by the fluorine concentration gradient. The magnitude of this voltage reduction,

though, is expected to be small since the conductivity of fluorine is much larger than that of oxygen.

In summary, for the solid state galvanic cells investigated here, calcia stabilized zirconia based experiments proved to produce equilibrium voltages while the use of CaF_2 as a solid electrolyte yielded no equilibrium data.

REFERENCES

1. T. H. Estell and S. N. Flengas, Chem Rev., 70, 339 (1970).

2. W. L. Worrell, Topics in Appl. Phys., 21, 143 (1977).

3. C. B. Alcock, Electromotive Force Measurements in High Temperature Systems (American Elsevier Publ. Co., Inc., 1968).

4. R. A. Rapp and D. A. Shores, Physicochemical Measurements in Metals Research, 4 (part 2), 123 (1970).

5. J. Hladick, ed., Physics of Electrolytes, 2, (Academic Press, London, 1972).

6. D. O. Raleigh, Progress in Solid State Chemistry, Vol. 3, ed. by H. Reiss (Pergamon Press, Oxford, 1967).

7. H. Schmalzreid, Z. Elektrochem, 66, 572 (1962).

8. J. W. Patterson, C. C. Bogen, and R. A. Rapp, J. Elec. Soc., 114, 752 (1967).

9. J. W. Patterson, J. Elec. Soc., 118, 1033 (1971).

10. J. D. Tretyakov and A. Muan, J. Elec. Soc., 116, 331 (1969).

11. J. B. Hardaway, J. W. Patterson, D. R. Wilder, and J. D. Schieltz, J. Am. Cer. Soc., 54, 94 (1971).

12. T. J. Anderson, M.S. Thesis, LBL-4148, Lawrence Berkeley Laboratory, Berkeley (Oct. 1975).

13. K. Hauffe and G. Tranckler, Z. Phys., 136, 166 (1953).

14. C. B. Alcock and G. P. Stavropoulos, J. Am. Cer. Soc., 54, 436 (1971).

15. R. W. Ure, J. Chem. Phys, 26, 1363 (1957).

16. W. L. Phillips and J. E. Hanlon, J. Am. Cer. Soc., 46, 477 (1963).

17. V. Levitskii, A. Hammou, M. DuClot, and C. DePortes, J. Chim. Phys., 73, 305 (1976).

18. V. Levitskii and Y. Y. Saolis, J. Chem Thermo., 6, 1181 (1974).

19. V. Levitski, Y. Y. Seolis and Y. Hekimov, J. Solid State Chem., 20, 119 (1977).

List of Figures

Figure 1. Schematic of concentration cells used to measure liquid phase Group III metal activities in solution with antimony. Top arrangement represents use of calcia-stabilized zirconia (CSZ) and bottom depiction indicates use of CaF_2. Here A^{III} is a group IIIA atom and B^{V} is a group VA atom.

Figure 2. Electrolytic domain for calcia stabilized zirconia, ——·——, conservative; - - - -, liberal; ——·—— yittria doped thorea. Also shown as solid lines are the formation Gibbs energies of the In and Ga oxides.

Figure 3. Experimental cells designs using a calcia-stabilized zirconia electrolyte. (a) and (b) - $Ga-Ga_2O_3$ reference electrode, (c) $CO-CO_2$ gaseous mixture reference electrode.

Figure 4. Experimental cell design using a CaF_2 solid electrolyte cell.

Figure 5. Experimental enclosure for the CaF_2 solid electrolyte cell.

Figure 6. Helium purification stream utilized.

Figure 7. Photograph of overall experimental apparatus used with CaF_2 cells.

Figure 8. Experimental apparatus showing assembled cell (middle right).

Figure 9. Photograph of microprocessor.

MEASUREMENT OF LIQUID PHASE COMPONENT ACTIVITIES WITH A SOLID ELECTROLYTE CONCENTRATION CELL

In and Ga Activity — Solid Oxide Electrolyte

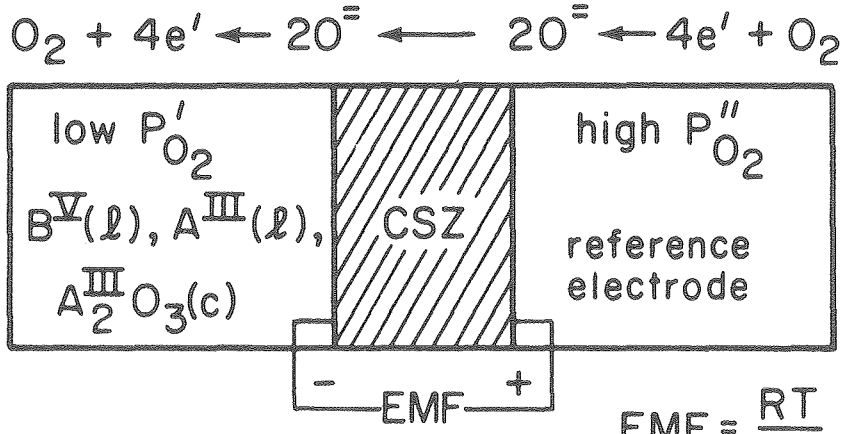

$$EMF = \frac{RT}{4F} \ln \frac{P''_{O_2}}{P'_{O_2}}$$

Al Activity — Solid Fluoride Electrolyte

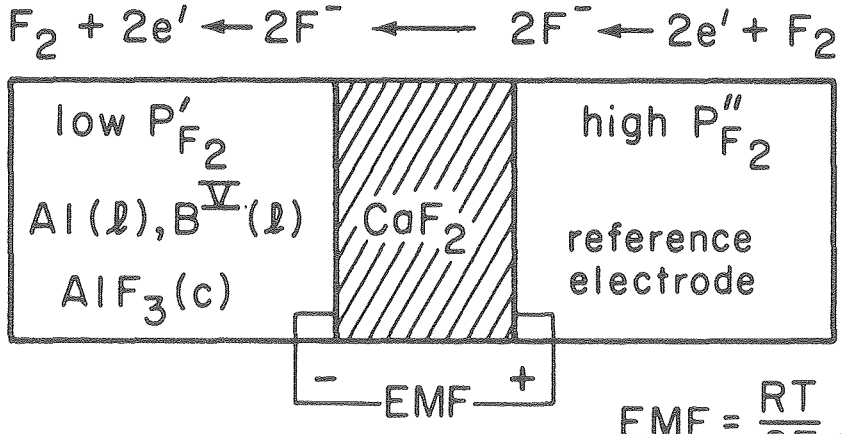

$$EMF = \frac{RT}{2F} \ln \frac{P''_{F_2}}{P'_{F_2}}$$

XBL 796-10027

Figure 1.

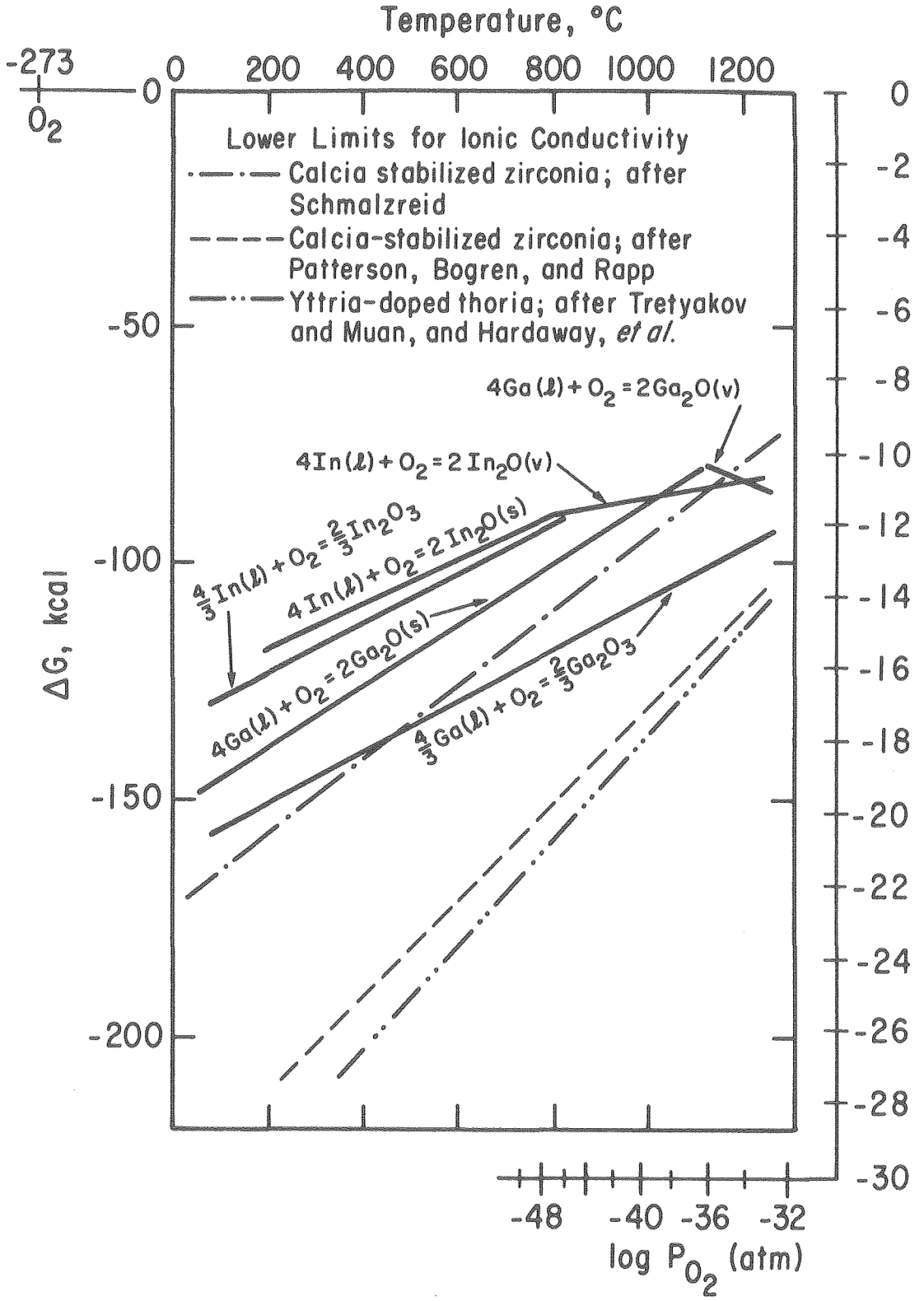

XBL 752-5923A

Figure 2.

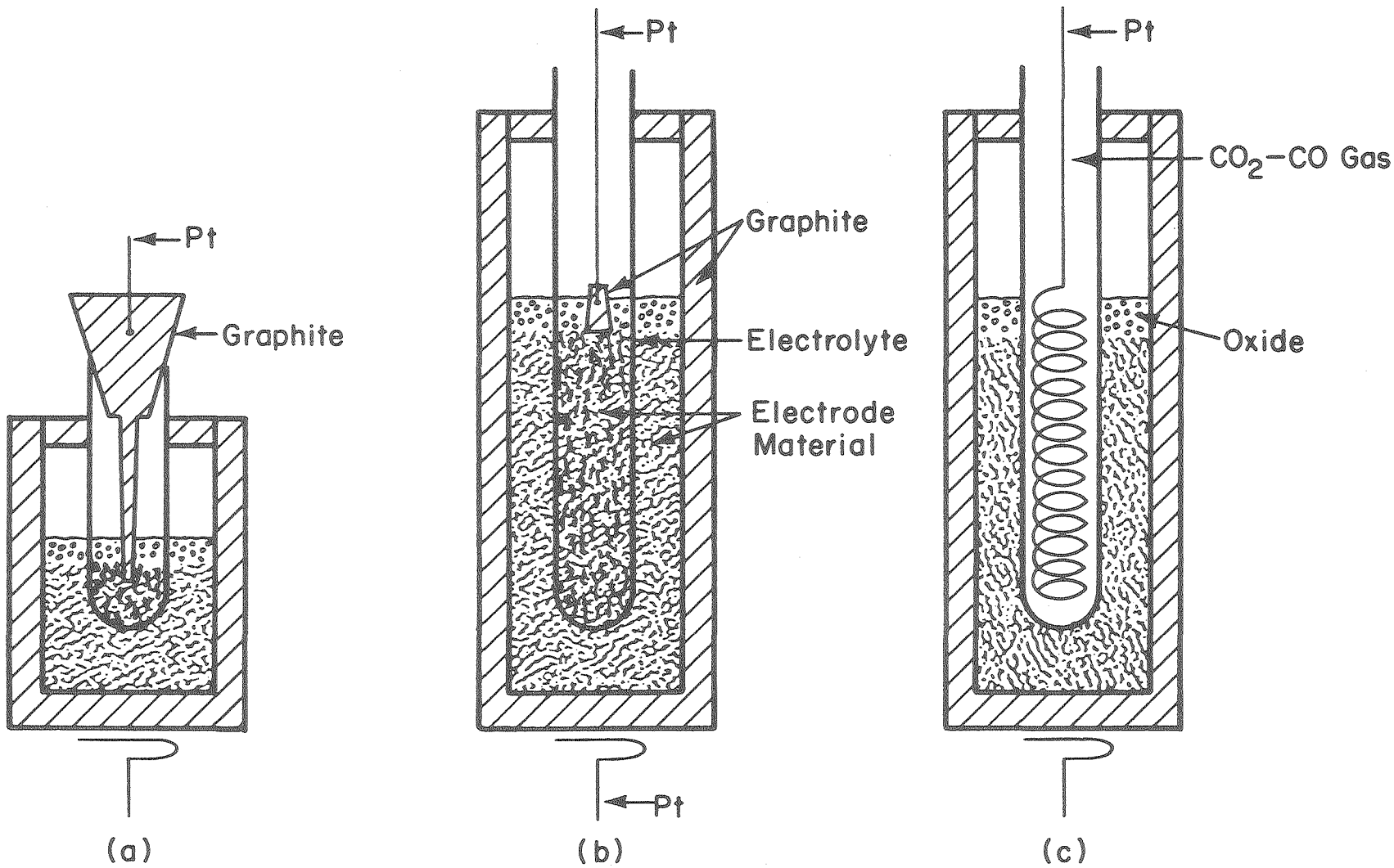

XBL 775-8831

Figure 3.

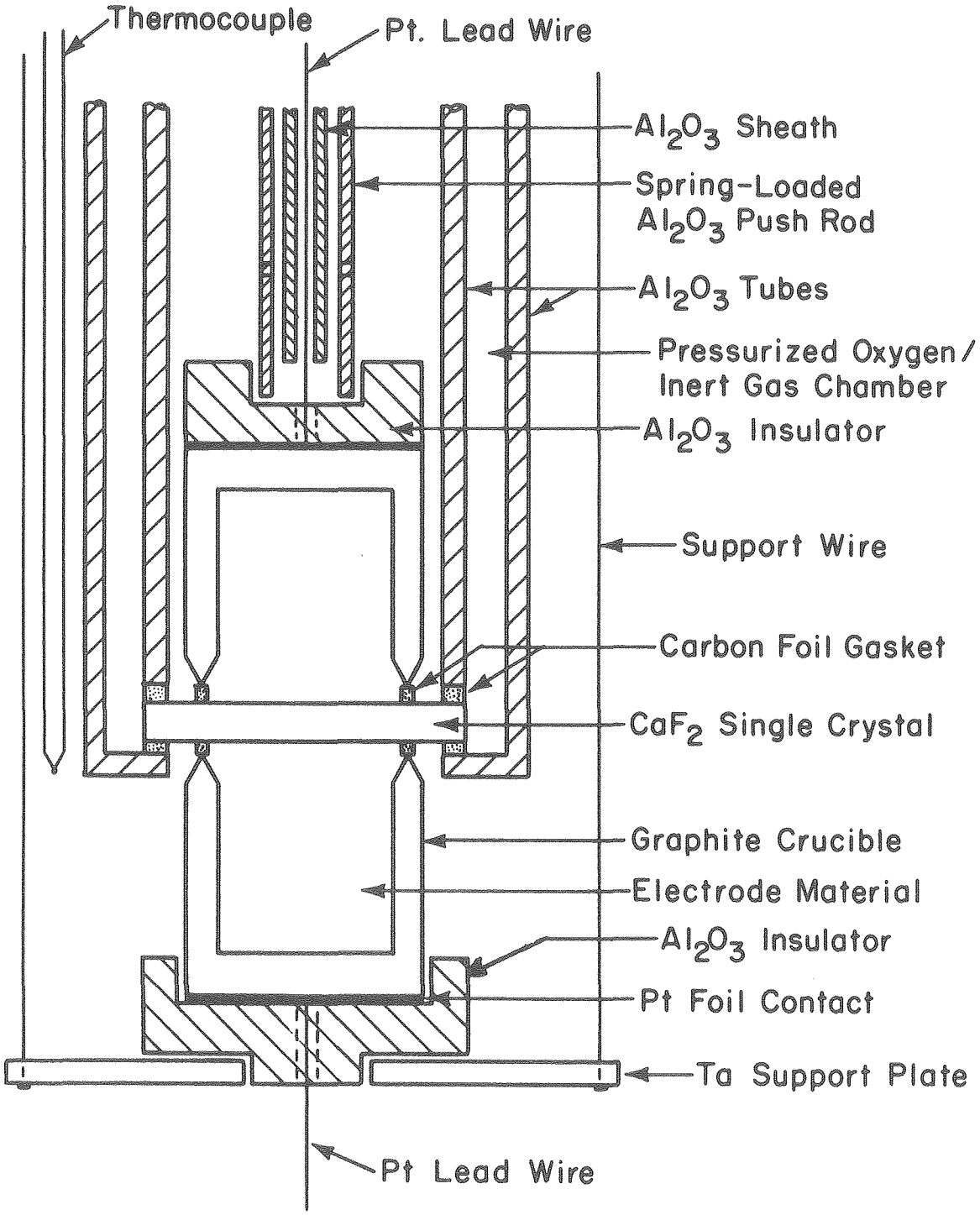

XBL 775-8700

Figure 4.

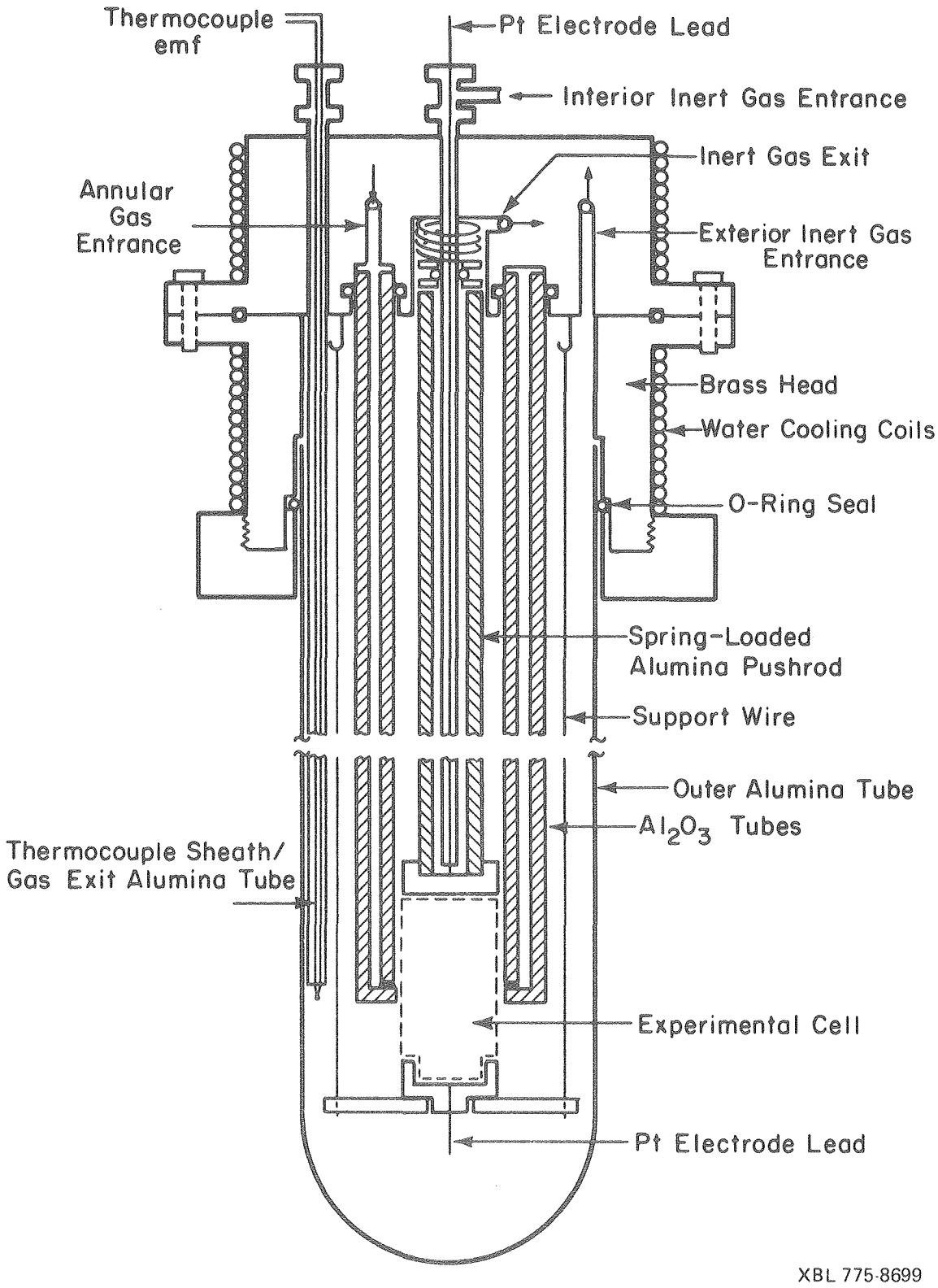
Thermocouple emf
Pt Electrode Lead
Interior Inert Gas Entrance
Inert Gas Exit
Annular Gas Entrance
Exterior Inert Gas Entrance
Brass Head
Water Cooling Coils
O-Ring Seal
Spring-Loaded Alumina Pushrod
Support Wire
Outer Alumina Tube
Al_2O_3 Tubes
Thermocouple Sheath/ Gas Exit Alumina Tube
Experimental Cell
Pt Electrode Lead
XBL 775-8699

Figure 5.

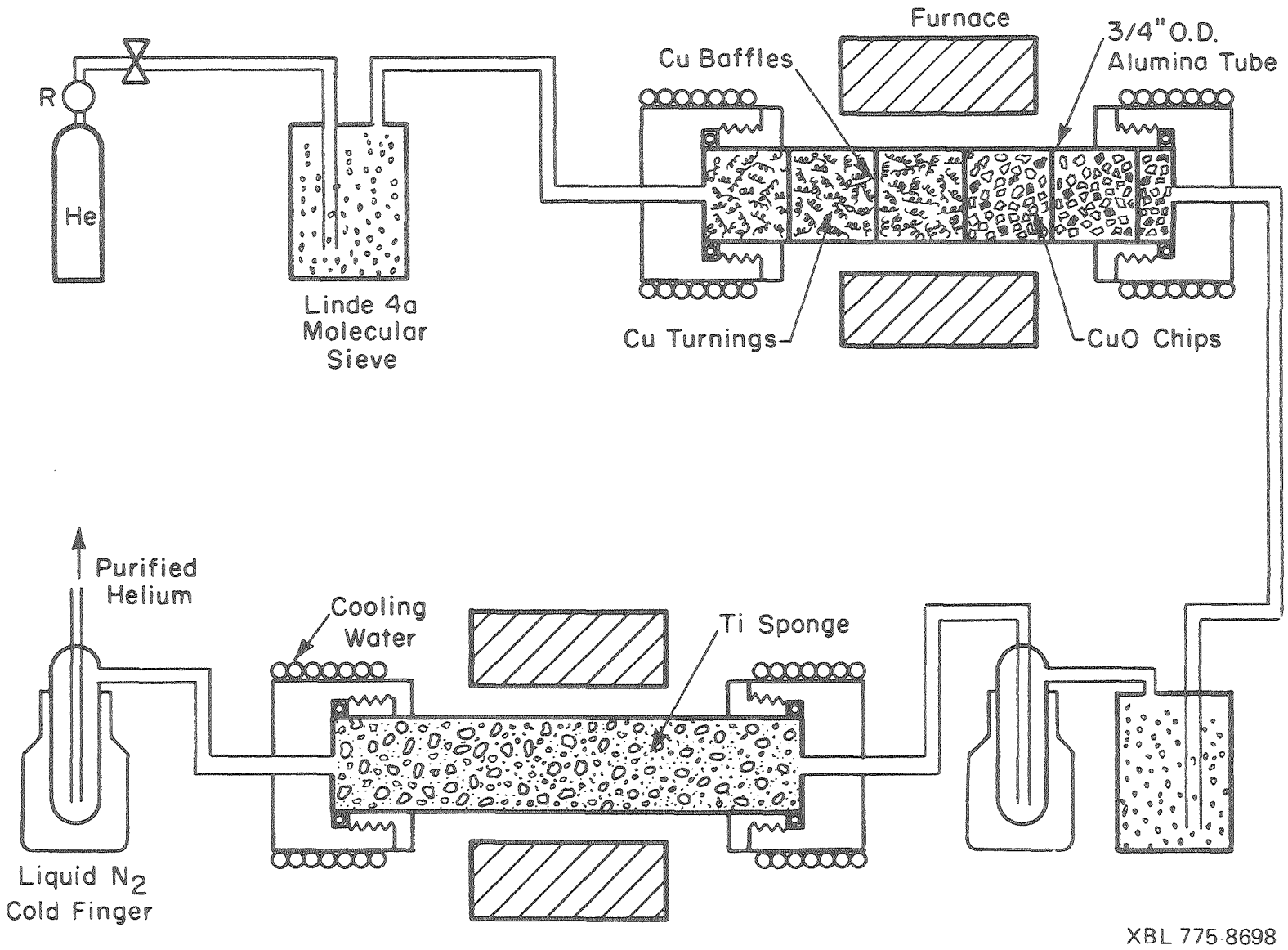
Furnace
3/4" O.D.
Alumina Tube
Cu Baffles
R
He
Linde 4a
Molecular
Sieve
Cu Turnings
CuO Chips
Purified
Helium
Cooling
Water
Ti Sponge
Liquid N_2
Cold Finger
XBL 775-8698

Figure 6.

0 0 0 0 5 1 0 5 1 0 8

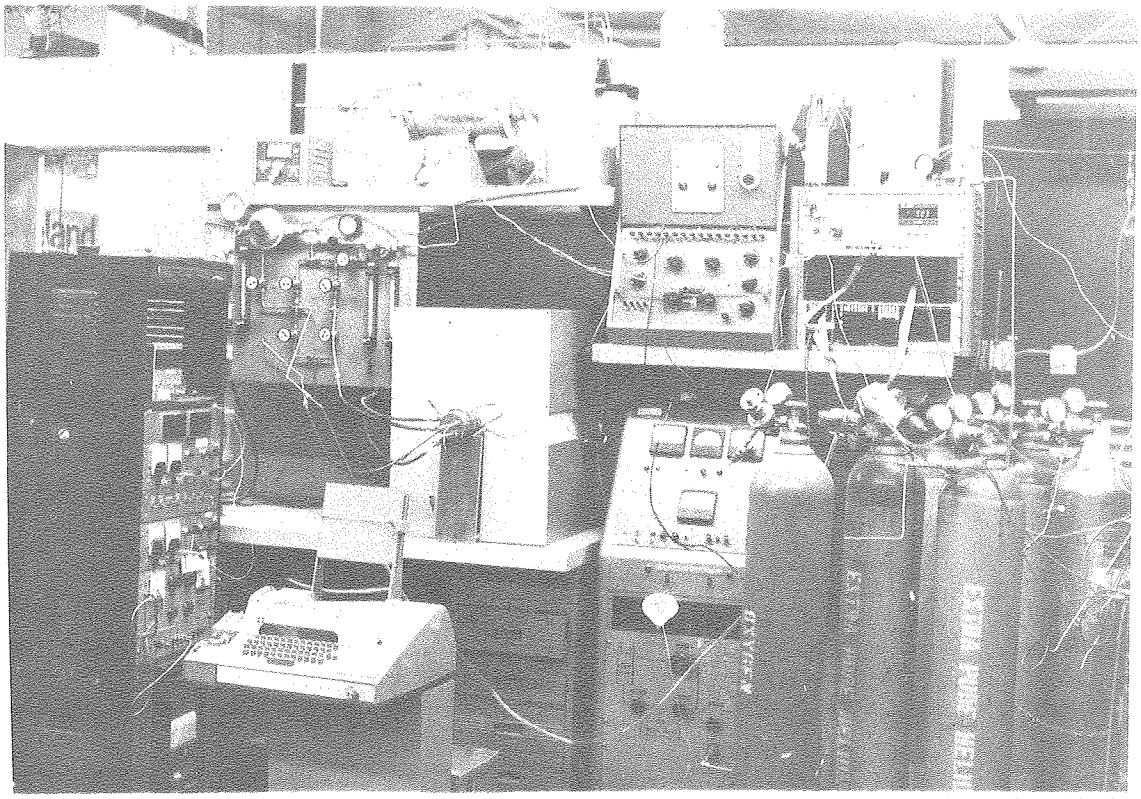

XBB 787-8408

Figure 7.

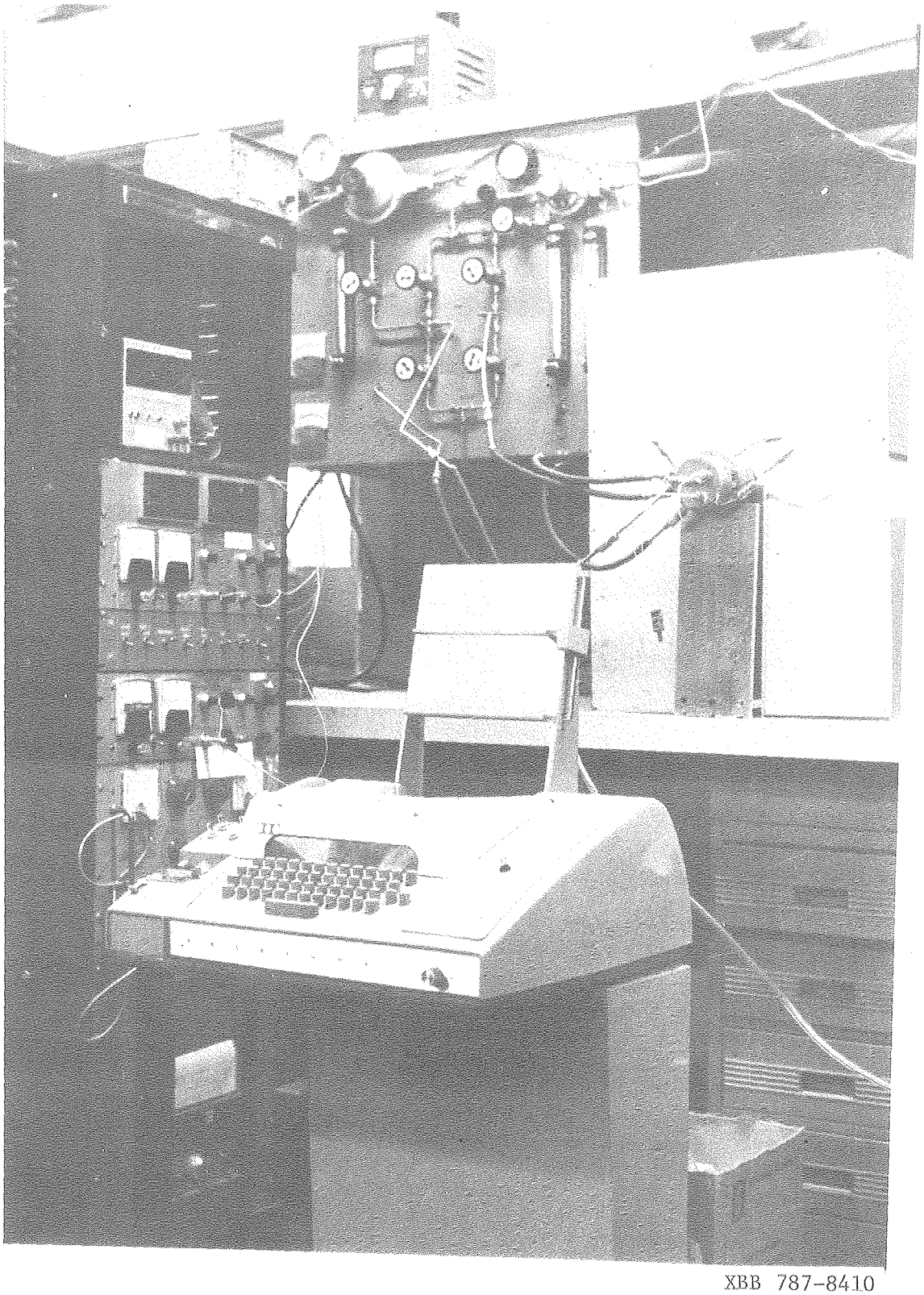

XBB 787-8410

Figure 8.

0 0 1 0 5 1 0 5 1 0 9

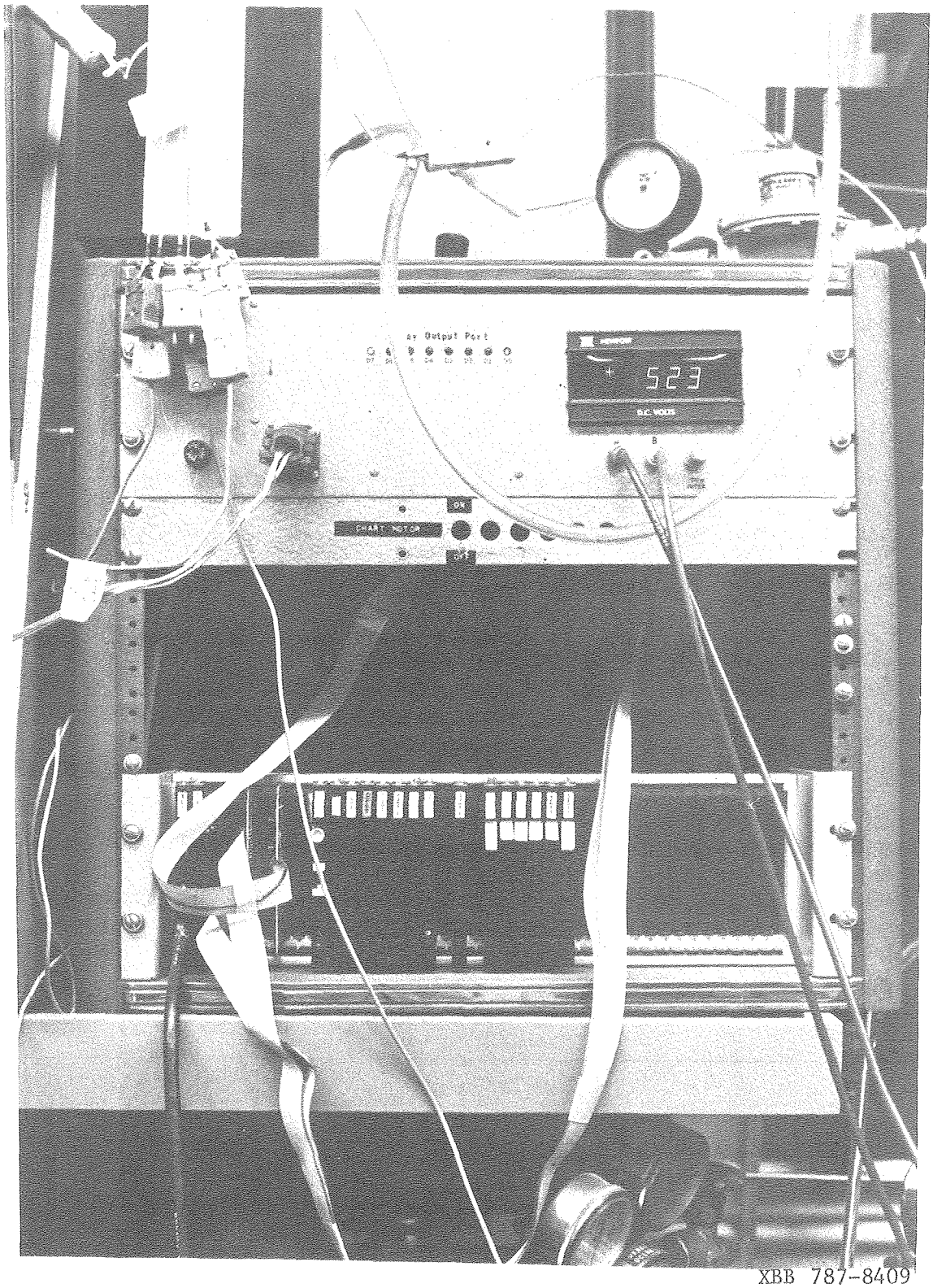

XBB 787-8409

Figure 9.

CHAPTER III. SOLID STATE ELECTROCHEMICAL STUDY OF Ga-Sb LIQUID ALLOYS

A. INTRODUCTION

Gallium and antimony combine to form a single intermetallic compound, gallium antimonide (GaSb) with the sphalerite structure. This compound is of current practical interest for its semiconducting properties, especially in application to Gunn effect diodes.[1]

The thermodynamics of the gallium-antimony system at and above the melting temperature of GaSb, has received considerable attention. Much recent consideration has been given to solution models for the prediction of thermodynamic data from liquidus temperatures. Such indirect methods, however, are sensitive to errors in available liquidus data. For example, the melting point of GaSb determined by different studies varied from 975 to 998 K, as is presented in Table 1. The melting point measured by different investigators shows marked differences though the generally accepted value is 985 K.[18,19] Compiled also in Table 1 is a list of the experimentally determined enthalpy of fusion, $\Delta H_f^c(GaSb)$, and the corresponding entropy of fusion of GaSb, $\Delta S_f^c(GaSb)$, calculated assuming that the melting temperature is 985 K. As can be seen, the large range of 2.0 $Kcal_{th}$ $g^{\circ}atom^{-1}$ occurs for the reported values of $\Delta H_f^c(GaSb)$.

The Ga-Sb phase diagram has been determined by a number of investigators.[4,5,20] All of these determinations are in generally excellent agreement, though all are shifted somewhat below the accepted melting temperature.

Table 1. Comparison of the melting temperature and the enthalpy and entropy of fusion of GaSb, as reported by different investigators, based on a melting temperature for GaSb of 985 K.*

Tm(GaSb) / K	ΔH_f^c(GaSb) / Kcal g°atom^{-1}	ΔS_f^c(GaSb) / cal g°atom^{-1}	Reference
975			2,3
979			4
982			5
985			6,7,8
993			9
998			10
	7.78 (±.1)	7.90 (±.11)	6
	7.9	8.0	11
	6.0 (±.5)	6.1	12
	7.3 (±.3)	7.4	13
	7.5 (±.3)	7.6	14
	8.0 (±.8)	8.1	15
	7.0 (±.3)	7.1	16
	7.2 (±.3)	7.3	17
	7.0 (±.4)	7.1	48

*cal_{th} = 4.184 J

The enthalpy of mixing for liquid alloys has been measured by Predel and Stein,[21] Yazawa, Kawashima and Itagaki,[22] and Gambino and Bros[17] who found maxima in this quantity of -258, -204 and -260 cal_{th} $g \cdot atom^{-1}$, respectively, at an equimolar composition.

Activities in the liquid phase have been measured with electrochemical techniques.[23-25] All of the electrochemical results show extremely large negative deviations from ideality. Small negative deviations were found by Yazawa, Kawashima and Itagaki[22] when they applied a strictly regular solution model to their heat of mixing data, while Predel and Stein[21] calculated moderate positive deviations near the melting temperature of GaSb. On the other hand, vapor pressure studies have shown a moderately negative derivation from ideality.[26,27] Thus the thermodynamic properties of the Ga-Sb system at and above the melting temperature of GaSb are not well defined.

In this study, gallium activities in the liquid phase of the Ga-Sb system were directly determined with a galvanic cell employing a calcia-stabilized zirconia (CSZ) solid electrolyte and both a $CO-CO_2$ gaseous mixture and a gallium-gallium oxide mixture as the reference electrodes. The activity of gallium in Ga-Sb liquid alloys can be measured electrochemically in high temperature galvanic cells. The cells utilized in this study can be represented schematically by

$$Pt\ |C|\ Ga(\ell),\ Sb(\ell),\ \beta\text{-}Ga_2O_3(c)\ ||CSZ||\ CO,\ CO_2\ |C|\ Pt \quad (I)$$

$$Pt\ |C|\ Ga(\ell), Sb(\ell),\ \beta\text{-}Ga_2O_3(c)\ ||CSZ||\ Ga(\ell),\ \beta\text{-}Ga_2O_3(c)\ |C|\ Pt. \quad (II)$$

At thermodynamic equilibrium the electrochemical potential of oxygen is

equilibrated by the passage of oxygen anions through the calcia-stabilized zirconia solid electrolyte, and a Nernst voltage is established with a magnitude given by

$$E = (RT/4F) \ln \{a(O_2;\ ref)/a(O_2;\ Ga\text{-}Sb)\} \ . \qquad (1)$$

Here $a(O_2;\ ref)$ is the oxygen activity in the reference electrode which is a gaseous mixture in cell (I) and a metal-metal oxide coexistence electrode in cell (II). The gallium activity in the working electrode in cell (I) can be calculated from:

$$a(Ga;\ Ga\text{-}Sb) = \left[\frac{p(CO_2)}{p(CO)}\right]^{-3/2} \exp\left\{\frac{3FE}{RT} - \frac{3\Delta G_f^o\ (CO_2;CO\text{-}O_2)}{2RT} + \frac{\Delta G_f^o(\beta\text{-}Ga_2O_3)}{2RT}\right\} . \qquad (2)$$

Here $P(CO_2)/P(CO)$ is the ratio of the partial pressures of CO_2 to CO in the reference gas mixture, E is the open circuit potential, $\Delta G_f^o(CO_2;\ CO\text{-}O_2)$ is the Gibbs energy change of forming CO_2 from CO and O_2 and $\Delta G_f^o(\beta\text{-}Ga_2O_3)$ is the Gibbs energy change of the formation of $\beta\text{-}Ga_2O_3$ and is given in Appendix I. For cell (II) which contains the coexistence electrode, the gallium activity is simply given by

$$a(Ga;\ Ga\text{-}Sb) = \exp\left\{-\frac{3FE}{RT}\right\} \qquad (3)$$

B. EXPERIMENTAL

1. Materials

The alloy coexistence electrodes used in this study were prepared from high purity materials. Semiconductor-grade elemental gallium and

antimony were obtained from Cominco American. Powdered Ga_2O_3 of 99.999% purity was obtained from Alfa Products. The materials were allowed to contact only high-purity alumina during the mixing process. High purity graphite was used in the preparation of the containers for the alloy coexistence electrode. Calcia-stabilized zirconia tubes having a nominal composition of $Ca_{0.15}Zr_{0.85}O_{1.85}$ were obtained from Zircoa Corporation of America, Solon, Ohio. The high temperature part of the experimental cell housing was constructed entirely of high purity recrystallized alumina. The electrode assembly was contained within a split tube of 99.99 tantalum which acted as a support and as an oxygen getter.

A description of the experimental apparatus used and the general procedure can be found in Chapter 2.

C. RESULTS

The activity of Ga in liquid alloys of Ga-Sb was measured electrochemically in two solid-state galvanic cells which can be represented schematically as shown by reactions (I) and (II). At equilibrium, the electrochemical potential of oxygen is equal in both electrodes and is related to the cell emf by Equation (1).

Shown in Figure 1 are the experimental voltages obtained as a function of temperature for the cells with $CO + CO_2$ gaseous reference electrode cells while Figure 2 exhibits the cell voltages measured with the virtual reaction of cell type II.

A linear least squares analysis was applied to the measured equilibrium cell potentials and corresponding temperatures, the results of which are listed in Table 2. Listed in Table 3 are the activity of

Table 2. Emf of the experimental cells as a function of temperature, in the form E/mV = a − b(T/K). The temperature range is 920 to 1100 K.

Reference Electrode	x_{Ga}	a	b x 10^3
CO, CO_2	0.0390	415.71 ± 2.41	−131.16 ± 2.36
CO, CO_2	0.293	434.33 ± 0.86	−75.57 ± 0.83
CO, CO_2	0.500	440.12 ± 1.51	−58.64 ± 1.45
CO, CO_2	0.639	441.48 ± 1.26	−48.60 ± 1.22
CO, CO_2	0.833	449.74 ± 0.44	−48.03 ± 0.41
Ga(ℓ),β-Ga_2O_3	0.242	5.97 ± 2.88	+44.2 ± 2.9
Ga(ℓ),β-Ga_2O_3	0.388	1.86 ± 0.99	+36.5 ± 0.9
Ga(ℓ),β-Ga_2O_3	0.500	4.73 ± 0.94	+24.4 ± 0.9
Ga(ℓ),β-Ga_2O_3	0.687	−7.71 ± 0.68	+22.4 ± 0.6
Ga(ℓ),β-Ga_2O_3	0.896	23.28 ± 1.13	−18.7 ± 1.1
Ga(ℓ),β-Ga_2O_3	0.956	−18.22 ± 1.56	+21.7 ± 1.7

Table 3. Summary of thermodynamic data for Ga-Sb alloys derived from emf measurements at 1003°K.*

x_{Ga}	a_{Ga}	a_{Sb}	$\Delta\bar{H}_{Ga}$	$\Delta\bar{H}_{Sb}$	ΔH^M	$\Delta\bar{S}_{Ga}$	$\Delta\bar{S}_{Sb}$	ΔS^M	ΔG^M
			$cal_{th}g^{\cdot}atom^{-1}$	$cal_{th}g^{\cdot}atom^{-1}$	$cal_{th}g^{\cdot}atom^{-1}$	$cal_{th}g.atom^{-1}$	$cal_{th}g^{\cdot}atom^{-1}$	$cal_{th}g^{\cdot}atom^{-1}$	$cal_{th}g^{\cdot}atom^{-1}$
0.039	0.0124	0.955	-2788	-10	-118	5.944	0.082	0.31	-429
0.293	0.164	0.613	-1499	-240	-609	2.098	.733	1.133	-1745
0.500	0.362	0.370	-1099	-490	-795	0.924	1.487	1.205	-2003
0.639	0.539	0.218	-1005	-790	-927	.226	2.239	0.953	-1883
0.833	0.732	0.075	-433	-2310	-746	.188	2.844	0.632	-1380
0.242	0.174	0.700	-413	-180	-236	3.063	.529	1.143	-1382
0.388	0.263	0.492	-135	-380	-285	2.520	1.031	1.608	-1898
0.500	0.364	0.370	-327	-490	-409	1.682	1.487	1.585	-1998
0.687	0.599	0.178	+529	-960	+63	1.546	2.473	1.836	-1779
0.896	0.856	0.045	-1606	-2990	-1750	-1.292	3.181	0.827	-921
0.956	0.884	0.018	+1280	-4470	+1027	1.521	3.527	1.609	-587

*cal_{th} = 4.184 J

gallium calculated from Equations (2) or (3). The activity of Sb was found by graphical integration of the Gibbs-Duhem equation. Plotted in Figure 3 are the activity coefficients of Ga and Sb as a function of composition.

The relative partial molar enthalpy of Ga was then calculated from the temperature dependence of the cell emf. Then the relative partial molar enthalpy of Sb was obtained by graphical integration. The results for $\Delta\bar{H}_{Ga}$ using the gas reference electrode exhibited a systematic concentration dependence similar to that found in calorimetric studies[17,21,22] while the data obtained using the metal reference electrode showed much scatter. Thus in calculating $\Delta\bar{H}_{Sb}$ only the results with the gas reference electrode were used. The large uncertainty in the temperature derivative of the cell emf is typical of this experimental technique. The fact that the gas reference electrode exhibited more consistent temperature coefficients suggests a possible kinetic problem in establishing an oxygen activity, perhaps as a result of interaction with the surrounding gas blanket or with the electrolyte. The performance of the gas reference electrode might be expected to be superior because it establishes a higher oxygen pressure and because the flowing gas better serves as an oxygen buffer.

The relative partial molar entropies of Ga were then determined as indicated earlier. The resulting values of $\Delta\bar{S}_{Ga}$ and $\Delta\bar{S}_{Sb}$ are also listed in Table 3 along with the integral value of the enthalpy, entropy and Gibbs energy of mixing.

D. DISCUSSION

Figure 4 shows the gallium and antimony activities as a function of the gallium mole fraction, x_{Ga}, obtained from this study. For comparison, the emf results of Danilin and Yatsenko,[24] obtained at 988 K, and those of Gerasimenko, et al.[25] at a temperature of 1023 K are also shown. Neither of these investigators reported an emf temperature derivative. Also shown are the vapor pressure studies of Hsi-Hsiung[26] which showed close agreement with the results of this study. Bergman et al.[27] also directly determined the activity of Ga in Ga-Sb melts by means of a Knudsen cell coupled to a mass spectrometer. Their results are also close to the results of this study though the shape of the measured curve of activity vs composition is somewhat altered.

Also not depicted are the recent results by Pong,[23] determined also with a solid oxygen-conducting electrolyte and with a $Ga(\ell)$-$Ga_2O_3(c)$ reference electrode. Pong found that the activity vs composition curve had the same general shape as that obtained in this study but shifted somewhat to more negative values. Component activities were also reported in conjunction with the three calorimetric studies.[17,21,22] In order to calculate these activities the derivative of the liquidus temperature with respect to composition had to be taken from the experimental phase diagrams. The high temperature calorimeters directly measured integral enthalpies of mixing while calculation of activities required partial molar enthalpies and their derivatives with respect to composition. The reported activities showed

positive deviations from an ideal solution (Predel and Stein[21]), small negative deviations (Yasawa et al.[22]) and moderate negative deviations (Gambino and Bros[17]), while the directly measured integral enthalpies of mixing showed close agreement.

The large negative deviations found in the other two emf studies whose results are shown in Figure 4 might have arisen from problems in the experimental galvanic cell used. Both studies used a chlroide electrolyte and assumed a value of 3 for the number of equivalents in the Nernst equation whereas gallium has known valences of both +3 and +1 and therefore the value of n may be indeterminant. A value for n less than 3 would raise the measured activites, but the general shape of the activity curve would still differ from that found in this study.

Figure 5 shows the Gibbs energy of mixing of the elements in the Ga-Sb liquid alloys, as determined in this study. The values for the enthalpy and entropy changes upon mixing calculated from the temperature dependence of the cell voltages and listed in Table 3 are not shown as they exhibited much scatter. Also shown in Figure 5 is the enthalpy of mixing determined calorimetrically by Predel and Stein[21] and by Yazawa et al.[22] Combining the primary experimental results of this work (component activities) with the primary results of the calorimetric studies (enthalpies of mixing) should produce a reliable entropy of mixing. These results are also shown in Figure 5 along with the entropy change for ideal mixing. This method gives a significant positive excess entropy of mixing.

The experimental data for the liquidus temperature of the Ga-Sb system as well as direct determinations from other sources can be checked for consistency with the following two expressions for the liquidus temperature derived in Appendix III.

$$T_\ell = \frac{2\Delta H_f^c(GaSb)+\Delta\overline{H}_{Ga}(x)+\Delta\overline{H}_{Sb}(x)-\Delta\overline{H}_{Ga}(0.5)-\Delta\overline{H}_{Sb}(0.5)}{2\Delta S_f^c(GaSb) + \Delta\overline{S}_{Ga}(x) +\Delta\overline{S}_{Sb}(x) - \Delta\overline{S}_{Ga}(0.5) - \Delta\overline{S}_{Sb}(0.5)} \qquad (4)$$

and

$$T_\ell = \frac{2\Delta H_f^o(GaSb) - \Delta\overline{H}_{Ga}(x) - \Delta\overline{H}_{Sb}(x)}{2\Delta S_f^o(GaSb) - \Delta\overline{S}_{Ga}(x) - \Delta\overline{S}_{Sb}(x)} \qquad (5)$$

where $\Delta H_f^o(GaSb)$ and $\Delta S_f^o(GaSb)$ are the standard enthalpy and entropy of forming solid GaSb from the pure <u>liquid</u> elements, respectively, and T_ℓ is the liquidus temperature. All other terms are as previously defined. All quantities in Equations (4) and (5) are expressed on a g°atom basis. In the derivation of these equations GaSb(c) is considered an equimolar line compound, and the temperature dependence of the partial molar quantities and formation enthalpy and entropy is neglected.

The liquidus temperature for the Sb-rich region then becomes

$$T_\ell = \frac{\Delta H_f^c(Sb) + \Delta\overline{H}_{Sb}(x)}{\Delta S_f^c(Sb) + \overline{S}_{Sb}(x)} \qquad (6)$$

Tables 4 and 5 show the liquidus temperature calculated from either Equation (4), (5) or (6) for the eleven alloy compositions studied here. In these calculations the partial molar enthalpies of Predel and Stein[21] were used while partial molar entropies were obtained from our experimental results. The fusion data listed in Table 1 was used in Equation (4).

The Gibbs energy of formation of GaSb has been previously measured with emf methods by two other investigators.[27,28] In order to use their results in Equation (5), the enthalpy and entropy change for melting Sb had to be introduced. An enthalpy of fusion value of 4750 $cal_{th}mol^{-1}$ and a melting temperature of 904 K was selected from Hultgren et al.[18] Listed also in Table 4 for comparison is the liquidus temperature as determined by Maglione and Potier.[5] Table 5 shows the liquidus temperature calculated for an antimony-rich Ga-Sb liquid alloy. The accepted temperature is in excellent agreement with the temperature derived from experimental value.

Figure 6 depicts the results listed in Table 4. Also shown is the liquidus curve calculated assuming the liquid solution is ideal. The enthalpy of fusion given by Lichter and Sommelet[6] was used in conjunction with Equation (4) while the standard enthalpy and entropy of formation measured (Sirota, et al.[28]) was employed to give the liquidus temperature plotted in Figure 6.

Based on the results shown in Table 4, several conclusions can be made. The accepted liquidus temperatures in the Ga-Sb system are very well predicted by our activity data and the enthalpy data of Predel

Table 4. Comparison of liquidus temperatures, (T/K) in the Ga-Sb system derived by different methods.

Method	x_{Ga}										Reference Source Data for ΔH_f^c(GaSb) and ΔH_f^o(GaSb)
	.293	.500	.639	.833	.242	.388	.500	.687	.896	.956	
	gas reference electrode				metal electrode						
Equation (4)	948.8	984.6	968.0	889.2	972.2	980.1	985.2	955.9	847.4	772.4	6
Equation (4)	951.9	987.3	970.9	892.8	975.1	982.9	988.0	959.0	851.3	776.7	11
Equation (4)	936.9	983.2	961.6	862.4	967.1	977.4	984.1	946.1	811.4	723.8	12
Equation (4)	948.0	986.2	968.5	884.8	973.1	981.5	987.0	955.6	840.6	762.3	13
Equation (4)	949.4	986.6	969.4	887.6	973.8	982.0	987.3	956.8	844.3	767.3	14
Equation (4)	952.5	987.5	971.3	894.1	975.5	983.1	988.1	959.5	852.9	778.9	15
Equation (4)	945.8	985.7	967.2	880.3	971.9	980.7	986.4	953.8	834.7	754.4	16
Equation (5)	970.2	1006.5	989.7	901.9	994.1	1002.0	1007.1	977.4	866.6	790.0	27
Equation (5)	974.0	1008.7	992.6	908.4	996.9	1004.4	1009.3	980.9	874.4	800.0	28
Ideal	962.3	985.0	975.1	917.4	948.1	978.7	985.0	966.7	876.2	804.6	6
Experimental	952.1	982.4	968.8	894.3	930.3	974.2	982.4	957.4	852.0	-	5

Table 5. Comparison of liquidus temperatures (T/K) of an antimony-rich Ga-Sb alloy.

x_{Ga}	T_ℓ, Equation (6)	T_ℓ, Ideal	T_ℓ, Experimental
0.039	888.6	890.6	890.7

and Stein,[21] along with accepted value for the heat of fusion. The results obtained here show that the value of ΔH_f^c(GaSb) obtained by Schottky and Bever[12] is probably too low. The results of this study are consistent with other literature data, although the measured activity for the alloy x_{Ga} = 0.242 appears to be a few percent high. Figure 7 shows the liquidus temperatures calculated with Equations (4) and (6) and ΔH_f^c(GaSb) given by Lichter and Sommelet.[6] Also shown for comparison are the liquidus temperatures calculated using the electromotive force activity measurement of Danilin and Yatsenko[24] and of Gerasimenko et al.[25] It can be seen that the application of Equations (4) and (6) to these latter two studies produces liquidus temperatures that are lower than the experimental temperatures in Ga-rich solutions.

When calculation of T_ℓ is performed with the aid of activity measurements presented here and with the literature data for the GaSb formation reaction, the liquidus temperatures predicted are much too high, however, Similar calculations employing Equation (5) were performed with the other literature electrochemical studies of Danilin and Yatsenko[24] and Gerasimendko et al.[25] These results are shown in Figure 8. It can be seen that the calculated liquidus temperatures are considerably lower than the experimental temperatures. Owing to the good consistency found with Equations (4) and (6), the probable cause of this error is in the values assigned in previous studies to the standard enthalpy and entropy of the GaSb formation reaction.

A new expression for the Gibbs energy of formation of solid GaSb can be derived utilizing the results of this study. Consider the following reaction scheme:

$$(1/2)Ga(\ell) + (1/2)Sb(\ell) = Ga_{0.5}Sb_{0.5}(\ell) \tag{7}$$

$$Ga_{0.5}Sb_{0.5}(\ell) = (1/2)GaSb(c) \tag{8}$$

$$(1/2)Sb(c) = (1/2)Sb(\ell) \ . \tag{9}$$

The Gibbs energy change for the above reactions can be approximated by

$$\Delta G°(7) = \Delta H^M - \Delta S^M(T/K) \tag{10}$$

$$\Delta G°(8) = -\Delta H_f^c(GaSb)\{1 - (T/K)/Tm(GaSb)\} \tag{11}$$

$$\Delta G°(9) = (1/2)\Delta H_f^c(Sb)\{1 - (T/K)Tm(Sb)\} \ . \tag{12}$$

The overall reaction is the formation reaction given by

$$(1/2)Ga(\ell) + (1/2)Sb(c) = (1/2)GaSb(c) \ . \tag{13}$$

The corresponding Gibbs energy of formation is then

$$\Delta G_f^o(GaSb,c,T) = \Delta H_f^o(GaSb,c,T) - \Delta S_f^o(GaSb,c,T)(T/K) \tag{14}$$

where

$$\Delta H_f^o(GaSb,c,T) = \Delta H^M + (1/2)\Delta H_f^c(Sb) - \Delta H_f^c(GaSb) \tag{15}$$

and

$$\Delta S_f^o(GaSb,c,T) = \Delta S^M + (1/2)\Delta H_f^c(Sb)/Tm(Sb) - \Delta H_f^c(GaSb)/Tm(GaSb). \tag{16}$$

In the above equations all quantities are on a g°atom basis. Using the accepted literature values of $\Delta H_f^c(GaSb) = 7780\ cal_{th}\ g°atom^{-1}$, with Tm(GaSb) = 985 K, $\Delta H_f^c(Sb) = 4750\ cal_{th}\ g°atom$, Tm(Sb) = 904 K and the ΔH^M as given by Predel and Stein[21] along with the Gibbs energy of mixing of this work the following expression is produced

$$\Delta G_f^o(GaSb,c,T) = -5660 + 3.536\ (T/K)\ cal_{th}\ g°atom^{-1}\ . \qquad (17)$$

Figure 9 graphically depicts the liquidus temperatures calculated using Equation (5) in conjunction with Equation (17). Shown are the liquidus temperature calculated using our activity measurements and the molten salt galvanic cell activities of Danilin and Yatsenko[24] and Gerasimenko et al.[25] It can be seen that Equation (17) produces excellent agreement between the experimental and calculated liquidus temperature when used with the results of this study while the results of Danilin and Yatsenko[24] and Gerasimenko et al.[25] show poor agreement. This dichotomy can be partially explained since the derivation of Equation(17) constrains the calculated Tm(GaSb) to the experimental value. This feature suggests that a similar procedure can be applied to the activity measurements of Danilin and Yatsenko[24] and Gerasimenko et al.[25] Performing such calculations yields liquidus temperatures in Ga-rich solutions which are lower than the experimental temperatures, though the temperature was forced to agree with the equimolar melting temperature. Furthermore, calculations of $\Delta G_f^o(GaSb,c,985\ K)$ employing the activity data of Danilin and Yatsenko[24] and Gerasimenko et al.[25] produces the values -3280 and -3680 cal $g°atom^{-1}$, respectively, while

Equation (17) gives a value of -2180 cal g°atom^{-1}. These results can be compared to the primary experimental results of Sirota et al.[28] and Abbasov et al.[27] that yield ΔG_f^o(GaSb,c,985) values of -2375 and -2350 cal$_{th}$ g°atom^{-1}, respectively. Thus ΔG_f^o(GaSb,c,T) as given by Equation (17) exhibits good agreement when compared to the measured electromotive force ΔG_f^o(GaSb,c,T), the reported liquidus temperatures and the other available calorimetric results.

As a further verification of the derived expression for ΔG_f^o(GaSb,c,T) given by Equation (17) a third law calculation was performed. In this calculation the enthalpy of formation of solid GaSb can be found from the following expression

$$\Delta H_f^o\ (\mathrm{GaSb,c,298}) = T \left\{ -\left[\frac{\Delta G_f^o\ (\mathrm{GaSb,c,T}) - \Delta H_f^o(\mathrm{GaSb,c,298})}{T} \right] + \frac{\Delta G_f^o(\mathrm{GaSb,c,T})}{T} \right\}. \tag{18}$$

The first term on the left is the free energy function which can be calculated with the aid of the following equation:

$$-\left[\frac{\Delta G_f^o(\mathrm{GaSb,c,T}) - \Delta H_f^o(\mathrm{GaSb,c,298})}{T} \right] = \Delta S_f^o\ (\mathrm{GaSb,c,298}) + \Delta_f^o[S(T)-S(298)] - \Delta_f^o[H(T)-H(298)]/T \tag{19}$$

Here, ΔS_f^o(GaSb,c,298) is the standard entropy of formation of GaSb at 298 K and can be determined from low temperature heat capacity measurements. The absolute entropy of the elements gallium and antimony is very well determined[17] while that for GaSb is not. Taking the values for the absolute entropy of Ga and Sb from Hultgren et al.[17]

given as $S°(Ga,298) = 9.76\ cal_{th}\ g{\cdot}atom^{-1}K^{-1}$ and $S°(Sb,298) = 10.88\ cal_{th}\ g{\cdot}atom^{-1}K^{-1}$ and the value for GaSb from the work of Piesbergen[29] determined to be $S°\ (GaSb,298) = 18.2\ cal_{th}\ g{\cdot}atom^{-1}K^{-1}$ results in a value of $\Delta S_f^o(GaSb,c,298) = -1.23\ cal_{th}\ g{\cdot}atom^{-1}K^{-1}$. Also $\Delta_f^o[S(T) - S(298)]$ and $\Delta_f^o[H(T) - H(298)]$ are the high temperature entropy and enthalpy contents and can be determined from calorimetric heat capacities and enthalpy contents. A useful feature of this equation is that there is a partial cancellation of possible errors in the high temperature calorimetric work as is easily seen by relating the last two terms to the heat capacities,

$$\Delta_F^o[S(T)-S(298)]-\Delta_f^o[H(T)-H(298)]/T = \int_{298}^{T} \frac{\Delta_f^o C_P}{} dT - \frac{1}{T}\int_{298}^{T} \Delta_f^o C_p dT \qquad (20)$$

Again the high temperature calorimetric data for the pure elements is well investigated and the selected values of Hultgren et al.[17] were utilized. There are three independent examinations of enthalpy contents for solid GaSb available.[6,15,30]

These high and low temperature calorimetric results can then be combined with the experimental values of $\Delta G_f^o(GaSb,c,T)$ of Abbasov et al.[27] and Sirota et al.[28] and the expression for $\Delta G_f^o(GaSb,c,T)$ derived here (Equation (17)), to produce a calculated value for the enthalpy of formation of solid GaSb at 298K. This calculated $\Delta H_f^o(GaSb,c,298)$ can then be compared to the value reported by Schottky and Bever[12] as determined by combustion calorimetry. Thus the consistent values of $\Delta G_f^o(GaSb,c,T)$ should all produce a single value of $\Delta H_f^o(GaSb,c,298)$ and equal to that measured by Schottky and Bever.[12]

The results of such calculations are displayed in Figure 10. The horizontal solid line is the experimental value of $\Delta H_f^o(GaSb,c,298)$ directly measured by Schottky and Bever[12] while the circles indicate the use of Equation (17) for $\Delta G_f^o(GaSb,c,T)$ and the squares and triangles represent the use of the emf work of Abbasov et al.[27] and Sirota et al.[28], respectively. The use of open, closed and half-open symbols differentiate the three available high temperature enthalpy contents. As can be seen, $\Delta G_f^o(GaSb,c,T)$ as given by Equation (17) most clearly reproduces the experimental $\Delta H_f^o(GaSb,c,298)$.

A pair potential analysis was applied to these results. This analysis indicated a preference for Ga-Sb pairing which is consistent with the negative total enthalpy for the alloy. The pairing, though not extensive because of the small values of ΔH^M, would produce a negative contribution to the excess entropy. This contribution is probably offset by a positive excess volume (as has been found for the related In-Sb[31] system and in other metallic solutions) and by possible changes in excitation of internal degrees of freedom resulting from the pairing, which contribute to the positive excess entropy observed.

Scatchard[32] presented a quantitative discussion on the relationship between the volume change on mixing and excess thermodynamic functions. Scatchard assumed a two step process in which the pure components at a pressure P_o were mixed with zero excess volume to a new pressure, P_1, and then taken to P_o. Applying these formulations with the assumption of small fractional volume change ($\Delta V^M/V$) one obtains the following relationships:

$$\Delta S^E_{VOL} = \alpha/\beta_T \ \Delta V^M \tag{21}$$

$$\Delta H^M_{VOL} = T(\alpha/\beta_T) \ \Delta V^M \tag{22}$$

$$G^M_{VOL} = \Delta H^M_{VOL} - T \ \Delta S^E_{VOL} \cong 0 \ . \tag{23}$$

Here, ΔV^M is the volume change upon mixing, α is the thermal coefficient of expansion and β_T is the isothermal compressibility.

No data on the volume of mixing for liquid gallium and antimony is known to exist in the literature. However, an estimate at an equimolar concentration of Ga and Sb can be made from density measurements on the pure components gallium[33-36] and antimony[37-39] and for the equimolar mixture.[40,41] When one performs such calculations a range in the volume of mixing of 0.30 to 0.35 cm^3 $g{\cdot}atom^{-1}$ at a temperature of 1003 K is obtained. The volume of mixing calculated for the equimolar mixture showed a positive temperature coefficient of approximately (0.6 to 2.9) x 10^{-4} cm^3 $g{\cdot}atom^{-1}K^{-1}$.

In order to compute the entropy and enthalpy changes due to the volume change the thermal coefficient of expansion and isothermal compressibility are required. The thermal coefficient of expansion is defined as

$$\alpha_T = -\frac{1}{\rho}(\partial\rho/\partial T)_P \tag{24}$$

where ρ is the density, P the pressure and T the temperature. Thus α_T can be found from density measurements and has the range (0.95 to 1.11) x 10^{-4} K^{-1}.

The isothermal compressibility β_T is proportional to the pressure derivative of the density. This coefficient is also unavailable in the literature for Ga-Sb alloys. However, the literature does provide experimental values for the adiabatic compressibility, β_S, derived from measurements of the ultrasonic velocities of sound in liquid metals. The two compressiblities are related by

$$\beta_T = \beta_S + TM\ \alpha_T^2/(\rho Cp) \tag{25}$$

where M is the molecular weight and Cp is the heat capacity at constant pressure. The coefficients α_T and β_T in Equations (21) and (22) are for the pure isolated components. Thus α_T/β_T is given by

$$\alpha_T/\beta_T = [\beta_S/\alpha_T + TM\ \alpha_T/(\rho Cp)]^{-1} \tag{26}$$

Using the literature values for β_S[42-46] in conjunction with the heat capacities from Hultgren et al.[17], the above densities and thermal expansion coefficients, α_T/β_T was calculated. These results are summarized in Table 6. Also shown are the experimental values of $\Delta S^E/\Delta V^M$ and $\Delta H^M/\Delta V^M$ at 1003 K. As can be seen, the contribution of the volume change to the excess entropy of mixing closely accounts for the observed excess entropy while the enthalpy term shows a contribution opposite in sign. In view of these estimates the liquid solution appears to be strictly regular.

Table 6. Calculated volume contributions to the entropy and enthalpy of mixing.*

$\Delta S^E/\Delta V^M$ $cal_{th}cm^{-3}K^{-1}$	α/β_T $cal_{th}cm^{-3}K^{-1}$	$\Delta H^M/\Delta V^M$ $Kcal_{th}cm^{-3}$	$T\ \alpha/\beta_T$ $Kcal_{th}cm^{-3}$
1.00 to 1.19	0.99 to 1.10	-0.85 to -0.72	1.00 to 1.10

*cal_{th} = 4.184 J

In order to quantify these observations a short-range order parameter, α, was calculated based on a lattice theory discussed in Appendix IV. This parameter is defined as

$$\alpha = 1 - P_{GaSb}/\{ZN_o x_{Ga} x_{Sb}\} \tag{27}$$

where P_{Ga-Sb} is the number of Ga-Sb pairs in the liquid solution, Z is the number of nearest neighbors, N_o is the number of lattice sites and x is the mole fraction of gallium or antimony. Through statistical methods it can be shown that the excess entropy can be approximated by

$$S^E \cong |\alpha|\ kN_o[x_{Ga}\ \ell n\ x_{Ga} + x_{Sb}\ \ell n\ s_{Sb}] - ZN_o\ x_{Ga}x_{Sb}(1 - \alpha)\ \frac{\partial g(T)}{\partial T} \quad . \tag{28}$$

Similarly the enthalpy of mixing is given by

$$\Delta H^M = ZN_o x_{Ga} x_{Sb}(1-\alpha)[\mu + j(x)] \tag{29}$$

where k is the Boltzman constant. The quantities $\mu + j(x)$ and $g(T)$ are defined in terms of the interaction energy, ω, and given by

$$\omega = \mu + j(x) + g(T) \quad . \tag{30}$$

Thus the interaction energy has a temperature dependence contained in $g(T)$ and a composition dependence contained in $j(x)$.

Finally α can be expanded in terms of the mole fraction and the interaction energy, and truncated after the first terms to give

$$\alpha \cong \frac{2N_o x_{Ga} x_{Sb} [\mu + j(x) + g(T)]}{RT} = x_{Ga} x_{Sb} v \ . \qquad (31)$$

If the excess entropy and enthalpy are known, then equations (28), (29) and (31) can be solved simultaneously for α. The temperature dependence of g(T) was assumed to be linear and given by

$$g(T) = \bar{g}T \ . \qquad (32)$$

Listed in Table 7 is the calculated value of α, the terms $N_o[\mu + j(x)]$ and $N_o[\bar{g}]$ and the reduced interaction energy, v, for the eleven compositions studied. In these calculations the heat of mixing of Predel and Stein[21] was used with the excess entropy obtained using the Gibbs energy data. A value of 6 was used for Z which is substantiated by X-ray measurements on In-Sb[47] which showed that the number of nearest neighbors was 5.7. The temperature of calculation was 1003 K.

The values of α listed can be used to predict values of ΔH^M, ΔS^E when used in Equations (28) and (29). It is observed that the effect of a temperature-dependent term g(T) is nearly twice or more than that of the term $[\mu + j(x)]$, therefore the degree of Ga-Sb pairing is much greater than would be predicted by using the heat of mixing data alone.

Figure 11 depicts the short range order parameter as a function of composition and it can be seen that α is symmetrical and nearly parabolic in shape. An examination of Table 8 indicates that the term

Table 7. Short-range order parameter and reduced interaction energies.*

x_{Ga}	α	$\frac{N_o[\mu+j(x)]}{cal_{th}g^{\circ}atom^{-1}}$	$\frac{N_o[\overline{g}]}{cal_{th}g^{\circ}atom^{-1}}$	v
0.039	-0.0165	-149.0	-.297	-0.440
0.293	-0.0985	-145.8	-.327	-0.476
0.500	-0.1169	-152.8	-.313	-0.468
0.639	-0.1095	-151.1	-.321	-0.474
0.833	-0.0908	- 96.7	-.552	-0.652
0.242	-0.0529	-156.2	-.131	-0.288
0.388	-0.1062	-152.3	-.292	-0.446
0.500	-0.1161	-152.9	-.309	-0.464
0.687	-0.1000	-141.6	-.321	-0.466
0.896	-0.0476	- 67.2	-.445	-0.516
0.956	-0.0408	- 79.9	-.833	-0.918

* cal_{th} = 4.184 J

$\mu + j(x)$ is independent of composition except in gallium-rich solutions. The error involved in gallium-rich solutions is magnified as is shown in Figure 12 in which a reduced Gibbs excess energy ($G^E/RT\ x_{Ga}x_{Sb}$) is plotted vs composition. This reduced quantity can be viewed as independent of composition and thus the term $\mu + j(x)$ can be taken as a constant to within the error of measurements.

Table 8 summarizes the important thermodynamic quantities for the compositions studied here and calculated by assuming that j(x) is zero, $N_o\mu = -152.9\ cal_{th}\ g^{\circ}atom^{-1}$ and $N_o\bar{g} = -0.309\ cal_{th}\ g^{\circ}atom^{-1}K^{-1}$. Also shown is the liquidus temperature calculated with the fusion equation and the enthalpy of fusion of GaSb as given by Lichter and Sommelet.[6] As can be seen all these quantities reproduce the experimental values remarkably well for solutions to $x_{Ga} = 0.8$ but deviate slightly for more Ga-rich solutions. This apparent discrepancy arises as a result of this simple model failing to describe the inflection found in the ΔH^M values for Ga-rich solutions.[17,21] This deficiency can be corrected by retaining the j(x) term in this composition range.

Table 8. Summary of thermodynamic quantities calculated with $N_o \mu = -152.9$ cal_{th} g·atom^{-1} and $N_o \bar{g} = -0.309$.

x_{Ga}	$-\Delta\bar{H}_{Ga}$	$-\Delta\bar{H}_{Sb}$	$-\Delta H^M$	$-\Delta\bar{S}_{Ga}$	$-\Delta\bar{S}_{Sb}$	ΔS^M	a_{Ga}	a_{Sb}	T_ℓ
	cal_{th} g·atom^{-1}			cal_{th} g·atom$^{-1}K^{-1}$			T = 1003K		K
0.039	876	1	35	7.951	0.085	0.393	0.012	0.958	889.5
0.293	528	76	208	3.110	0.843	1.507	0.160	0.630	947.7
0.500	256	256	256	1.735	1.735	1.735	0.367	0.367	982.4
0.639	122.5	432	234	1.103	2.754	1.634	0.540	0.220	967.1
0.833	21	711	136	0.428	4.532	1.113	0.798	0.072	885.4
0.242	603	49	183	3.598	0.666	1.375	0.121	0.698	927.3
0.388	395	145	242	2.389	1.214	1.670	0.246	0.505	972.5
0.500	256	256	256	1.735	1.735	1.735	0.367	0.367	982.4
0.687	88	500	217	0.917	2.941	1.550	0.603	0.422	954.3
0.896	7	797	89	0.248	5.694	0.814	0.880	0.038	834.0
0.956	1	870	39	0.097	7.699	0.431	0.952	0.013	753.8

E. CONCLUSION

Previous studies on the Ga-Sb system have concluded that the liquid alloys are either ideal[12,5] or regular[21,22] solutions, while Gibbs energy determinations have indicated that the solutions are highly non-ideal, showing strong negative deviations from ideality. The results of this study have shown the Ga-Sb system to deviate negatively, but moderately so, from Raoults' law with a significantly positive excess entropy of mixing. Liquidus temperatures were calculated and the results of this work exhibited excellent consistency with the available calorimetric data and the reported phase diagram. A new expression for the Gibbs energy of formation of solid GaSb was determined yielding $\Delta H_f^o(GaSb,c,T) = -5660\ cal_{th}\ g^{\circ}atom^{-1}$ and $\Delta S_f^o(GaSb,c,T) = 3.536\ cal_{th}\ g^{\circ}atom^{-1}K^{-1}$. Third law calculations showed these values were consistent with other available calorimetric data. The positive excess entropy of mixing observed was accounted for by a positive excess volume of mixing. Finally the tendency for short range ordering in the liquid phase was quantified with a simple statistical model.

REFERENCES

1. J.C. McGroddy, "Negative Differential Conductivity in Semiconductors," in Proceedings of the Tenth International Conference on the Physics of Semiconductors, U.S. Atomic Energy Commission, 1970.
2. R.F. Blunt, W.R. Hosler, and H.P.R. Frederikse, Phys. Rev., 96, 576 (1954).
3. H. Welker, Z. Naturforsch., 8a, 248 (1953).
4. I.G. Greenfield and R.L. Smith, J. Metals, 7, 351 (1955).
5. M.H. Maglione and A. Potier, J. Chim. Phys., 65, 1595 (1968).
6. B.D. Lichter and P. Sommelet, TMS-AIME, 245, 99 (1969).
7. J. Bednar and K. Smirous, Czech. J. Physics, 5, 546 (1955).
8. V.M. Glazov and D.A. Petrov, Izv. Akad. Nauk SSSR, Otd. Tekhn. Nauk, No. 4, 125 (1958).
9. H. Welker, Physica, 20, 893 (1954).
10. F.A. Cunnell, J.T. Edmond, and J.L. Richards, Proc. Phys. Soc. (London), B67, 848 (1954).
11. R. Hultgren, P.D. Desai, D.T. Hawkins, M. Gleiser, and K.K. Kelley, Selected Values of the Thermodynamic Properties of Binary Alloys, Amer. Soc. Met. (1973).
12. W.F. Schottky and M.B. Bever, Acta Met., 6, 320 (1958).
13. R. Blachnik and A. Schneider, Z. Anorg. Allgem. Chem., 372, 314 (1970).
14. L.A. Mechkovskii, A.A. Savitskii, V.F. Skums, and A.A. Vecher, Russ. J. Phys. Chem., 45, 1143 (1971).
15. R.H. Cox and M.J. Pool, J. Chem. Eng. Data, 12, 247 (1967).

16. R. Blachnik, Ph.D. Dissertation, Technischen Hochschule, Clausthal (1967).

17. M. Gambino and J.P. Bros, J. Chem. Thermodynamics, 7, 443 (1975).

18. R. Hultgren, P.D. Desai, D.T. Hawkins, M. Gleiser, K.K. Kelly, and D.D. Wagman, Selected Values of the Thermodynamic Properties of the Elements, Amer. Soc. Met. (1973).

19. R.N. Hall, J. Electrochem. Soc., 110, 385 (1963).

20. W. Koster and B. Thoma, Z. Metallk., 46, 291 (1955).

21. B. Predel and D.W. Stein, J. Less-Common Metals, 24, 391 (1971).

22. A. Yazawa, T. Kawashima, and K. Itagaki, J. Japan Inst. Metals, 32, 1288 (1968).

23. R. Pong, M.S. Thesis, "Thermodynamic Studies of Ga-In, Ga-Sb and Ga-In-Sb Liquid Alloys by Solid State Electrochemistry with Oxide Electrolytes," April (1975).

24. V.N. Danilin and S.P. Yatsenko, Tr. Inst. Khim., Akad. Nauk SSSR, Ural. Finial No. 20, 142 (1970).

25. L.N. Gerasimenko, I.V. Kirichenko, L.N. Lozhkin, and A.G. Morachevskii, Zashchitn. Metal. i Oksidyne Pokrytiya, Korroziya Metal. i Issled. v Obl. Electrokhim., Akad. Nauk SSSR, Otd. Obshch. i Tekhn. Khim., Sb. Statei (1965) p. 236.

26. C. Hsi-Hsiung, C. Peng-Nien, and Mo Chin-Chi, Acta. Met. Sinica, 9, 113 (1966).

27. A.S. Abbasov, A.V. Nikolskaya, Ya.I. Gerasimov, and V.P. Vasilev, Dokl. Akad. Nauk SSSR, 156, 1399 (1964).

28. N.N. Sirota and N.N. Yushkevich, Khim. Svyas v Poluprov. i Tverd. Telakh, Inst. Fiz. Tverd. Tela i Poluprov., Akad. Nauk Belorussk. SSR, p. 122 (1965).

29. U. Piesbergen, Z. Naturforsch. 18a, 141 (1963).

30. M.J. Pool, R.W. Sullivan, and C.E. Lundin, Denver Research Institute, Tech. Report. DRI 2115 (1963).

31. H. Hoshino, Y. Nakamura, M. Shimoji, and K. Niwa, Ber. Bensenges, 69, 114 (1965).

32. G. Scatchard, Trans. Far. Soc., 33, 160 (1937).

33. W.H. Hoather, Proc. Phys. Soc., 48, 699 (1936).

34. V.I. Nizhenko, L.I. Sklyarenko and V.N. Eremenko, Ukrain. Khim. Zhur., 31, 559 (1965).

35. H. Koster, F. Hensel, and E.U. Franck, Ber. Buns. Ges. Phys. Chem., 74, 43 (1970).

36. A.F. Crawley, Int. Met. Rev., 19, 32 (1974).

37. A.F. Crawley and D.R. Kiff, Met. Trans., 3, 157 (1972).

38. P.E. Berthou and R. Tougas, Met. Trans., 1, 2978 (1970).

39. W. Klemm, H. Spitzer, and H. Niermann, Angew. Chem., 72, 985 (1960).

40. N.P. Mokrovskii and A.R. Regel, Zh. Tekhn. Fiz., 22, 1281 (1952).

41. V.M. Glasov, S.N. Chizhevskaya and N.N. Glagoleva; Liquid Semiconductors, Plenum Press, New York (1969).

42. B.N. Oshcherin, Rev. Roum. Chim., 21, 351 (1976).

43. M.B. Gitis and I.G. Mikhailov, Sov. Phys. Acoustics, 11, 372 (1966).

44. V.M. Glasov, A.A. Aivazov and V.I. Timoshenko, Sov. Phys. Solid State, 18, 1236 (1976).

45. O.J. Kleppa, J. Chem. Phys., 18, 1331 (1950).

46. A.A. Magomedov, M.A. Ismailov, and B.P. Pashaev, Teplofiz. Vys. Temp., 13, 1106 (1975).

47. R. Buschert, I.G. Gelb, and K. Lark-Horovitz, Bull. Am. Phys. Soc. Ser., 11, 1, 111 (1956).

48. L. Garbato and F. Ledda, Thermochimica Acta, 19, 267 (1977).

LIST OF FIGURES

Figure 1. Corrected experimental cell voltages as a function of temperature for cell type I. Least squares lines are shown.

Figure 2. Corrected experimental cell voltages as a function of temperature for cell type II. Least squares lines are shown.

Figure 3. Logarithm of the activity coefficients of gallium and antimony in the liquid phase: 1003 K; 0, $\ln \gamma$ (Ga); ■, $\ln \gamma$ (Sb); closed symbols, gas reference electrode; open symbols, metal reference electrode.

Figure 4. Activities of gallium and antimony in the liquid mixture at 1003 K ———, this work; ■, this work - gas reference electrode; 0, this work - metal reference electrode; ....., 1003 K, Yazawa, Kawashima and Itagaki; ——— - ———, 988 K, Danilin and Yatsenko; ------, 1023 K, Gerasimenko et al.

Figure 5. Gibbs energy, enthalpy and entropy of mixing for Ga-Sb liquid alloys at 1003 K. ■, this work - gas reference electrode, 0, this work - metal reference electrode; ——— - ——— Predel and Stein, ... Yazawa et al.

Figure 6. Liquidus temperatures for the gallium-antimony system from Table 4. ———, phase diagram of Magilone and Porter[5]; ----, calculated assuming ideal liquid phase; 0, this work by Equations (4) and (6); Δ, this work by Equation (5).

Figure 7. Liquidus temperatures for the gallium-antimony system calculated from Equations (4) and (6). 0, this work; ■, Danilin and Yatsenko; Δ, Gerasimenko et al.; ———,

Maglione and Potier. ΔH_f^c(GaSb) was taken as 7780 cal g°atom^{-1}.

Figure 8. Liquidus temperatures for the gallium-antimony system calculated from Equation (5), with ΔG_f^o(GaSb,c) of Sirota and Yushkevich. ●, this work; ■, Danilin and Yatsenko; ▲, Gerasimenko et al.; with ΔG_f^o(GaSb,c) of Abbasov et al.; 0, this work; □, Danilin and Yatsenko; Δ, Gerasimenko et al.; ———, phase diagram of Maglione and Potier.

Figure 9. Liquidus temperatures for the gallium-antimony system using the formation Equation (5) with the derived ΔG_f^o(GaSb,c,T). ———, phase diagram of Magilone and Porter[5]; 0, this work; □, Danilin and Yatsenko[24]; Δ, Gerasimenko et al.[25]

Figure 10. Standard enthalpy of formation of GaSb(c) obtained by a third-law analysis. ———, Schottky and Bever[12]; 0, this work; □, Abbasov et al;[27] Δ, Sirota and Yushkevich[28]; GaSb enthalpy content data used: open symbols, Lichter and Sommelet[6]; closed symbols, Pool, et al.[30] half open, Cox, et al.[15]

Figure 11. Short range order parameter, α as a function of the gallium mole fraction calculated at 1003 K. □, this work - gas reference electrode; 0, this work - metal reference electrode.

0 0 1 3 3 1 0 3 1 2 7

Figure 12. Reduced excess Gibbs energy as a function of the gallium mole fraction calculated at 1003K. ●, this work - gas reference electrode; O, this work - metal reference electrode.

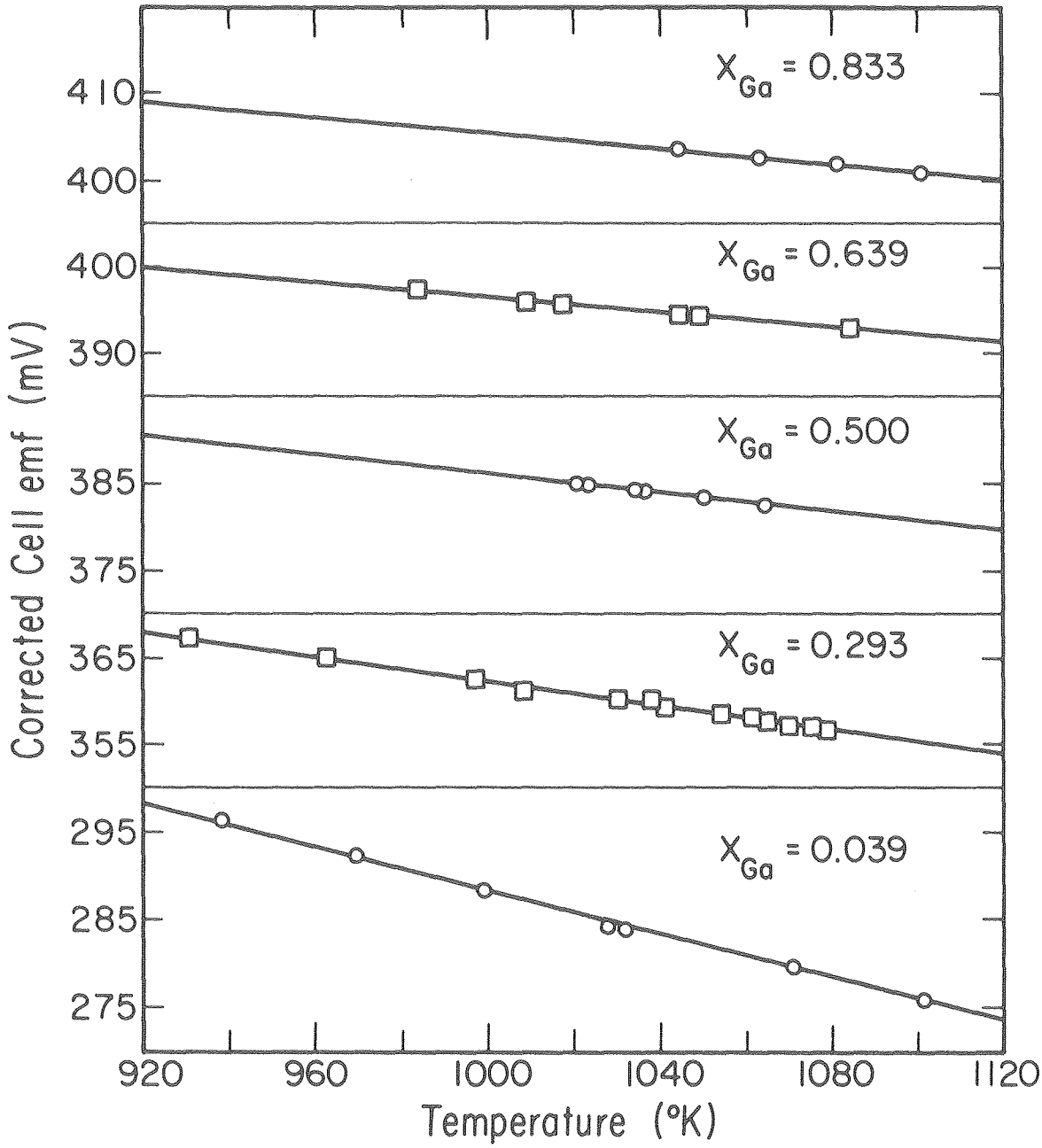

XBL 757-6794

Figure 1.

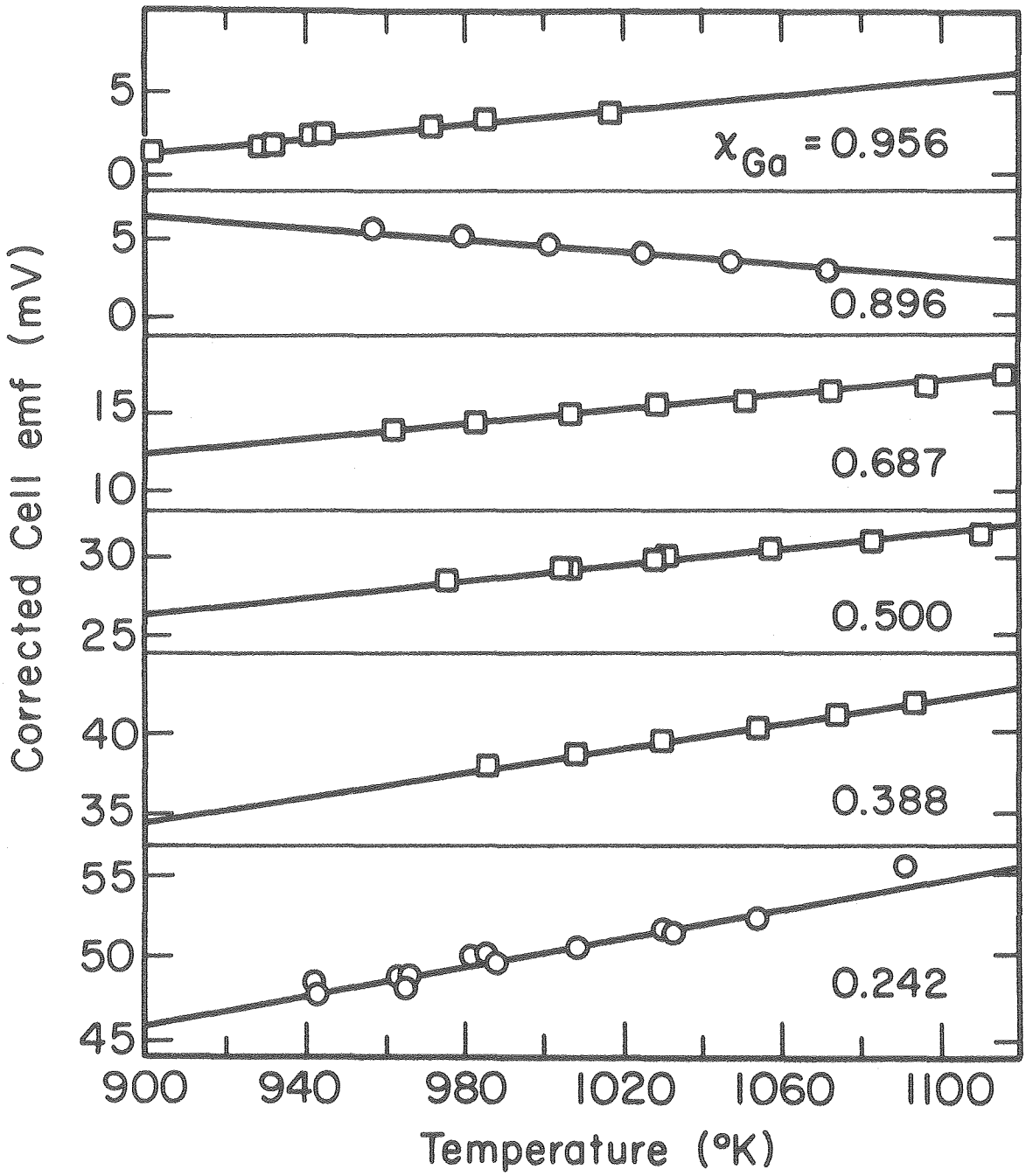

XBL 7711-10676

Figure 2.

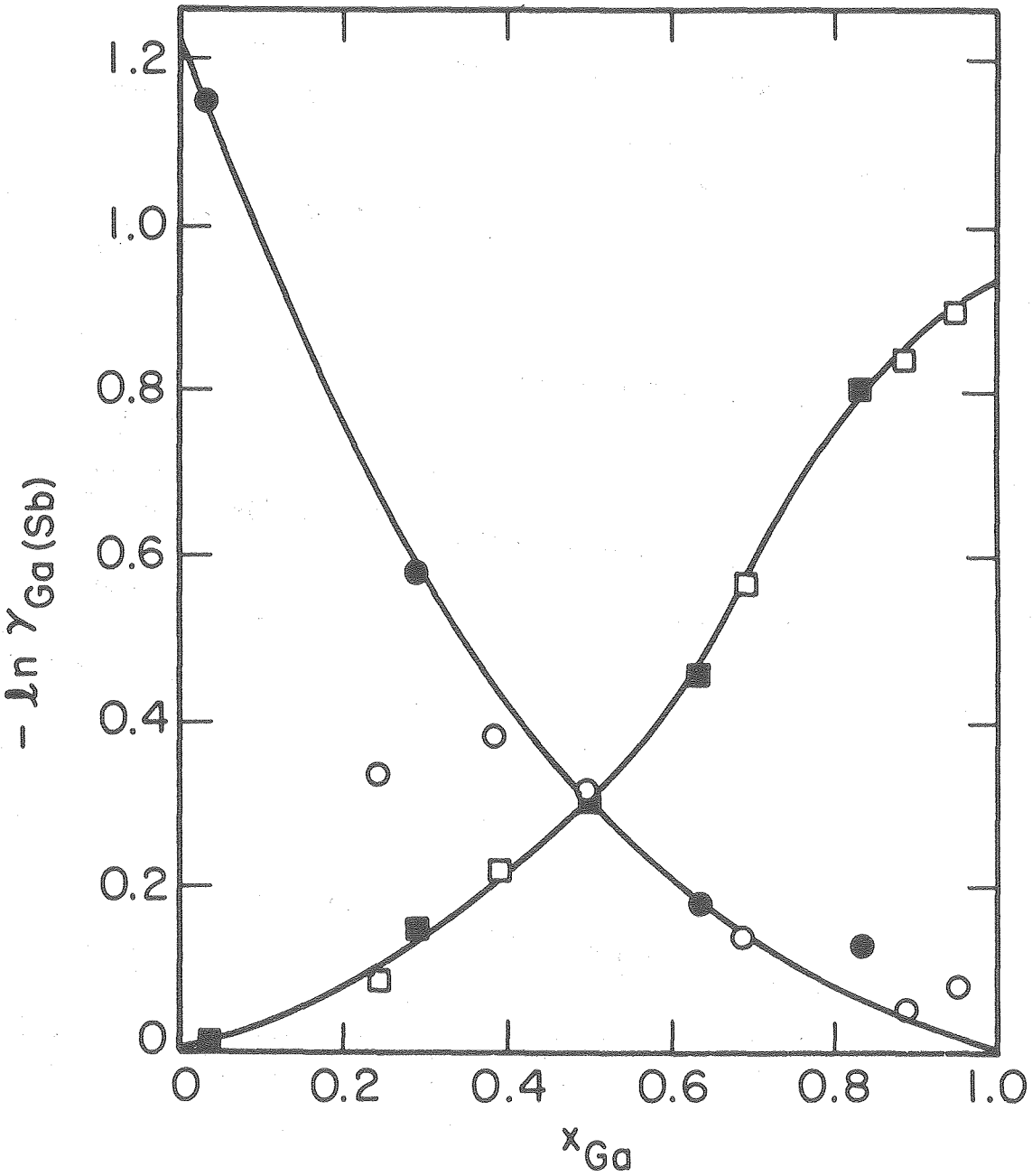

XBL 786-9412

Figure 3.

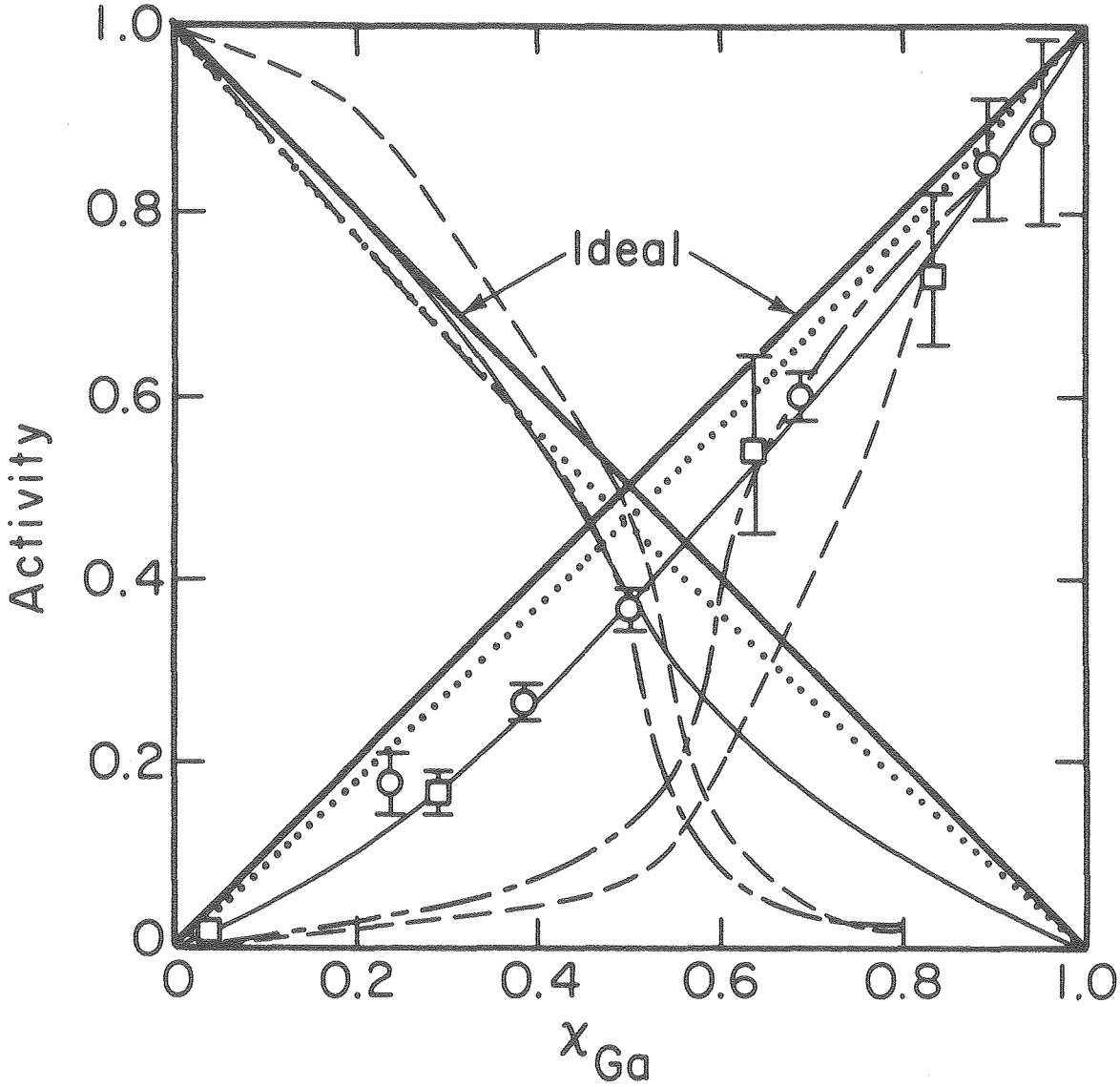

XBL 775-8834

Figure 4.

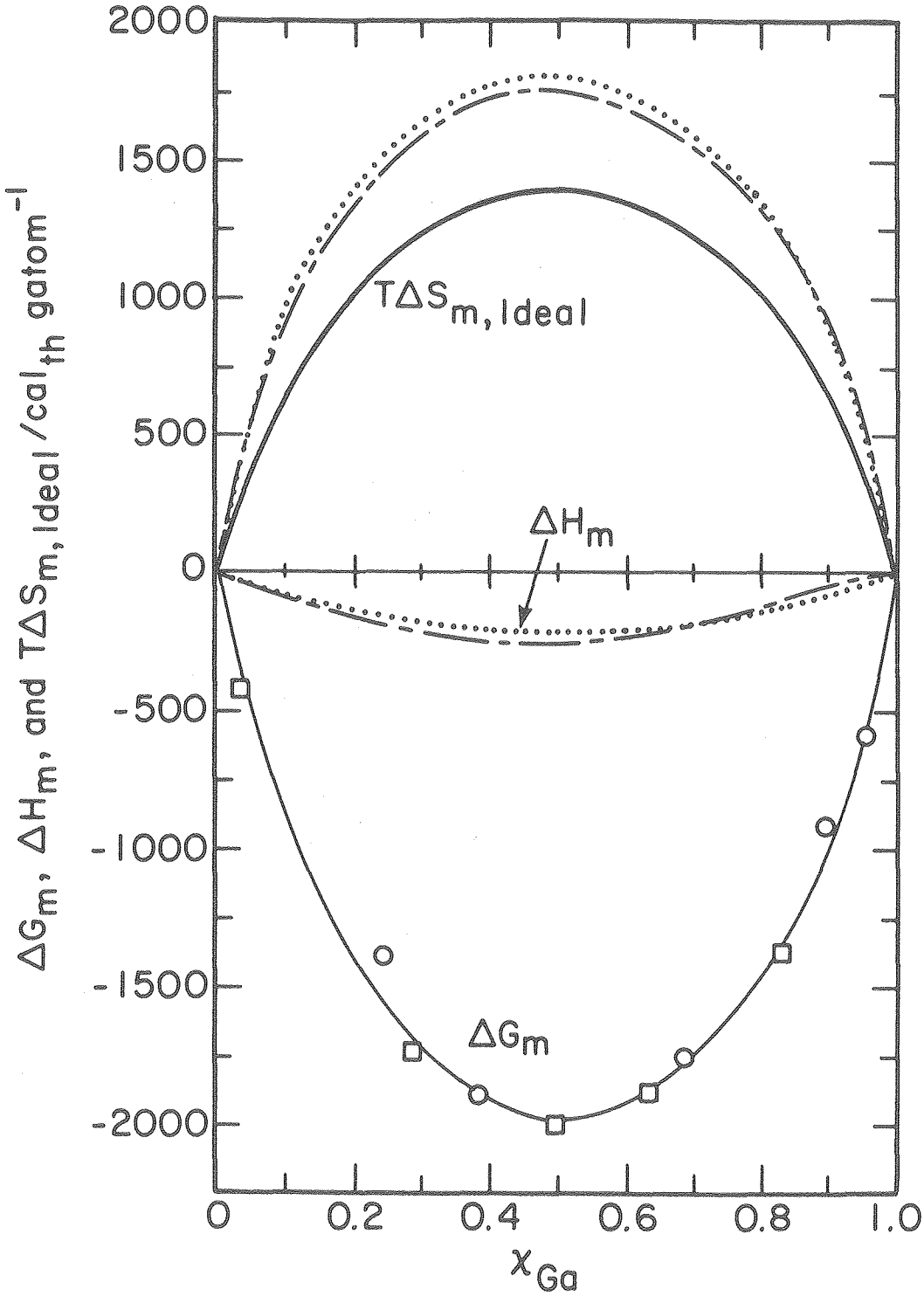

XBL 775-8833

Figure 5.

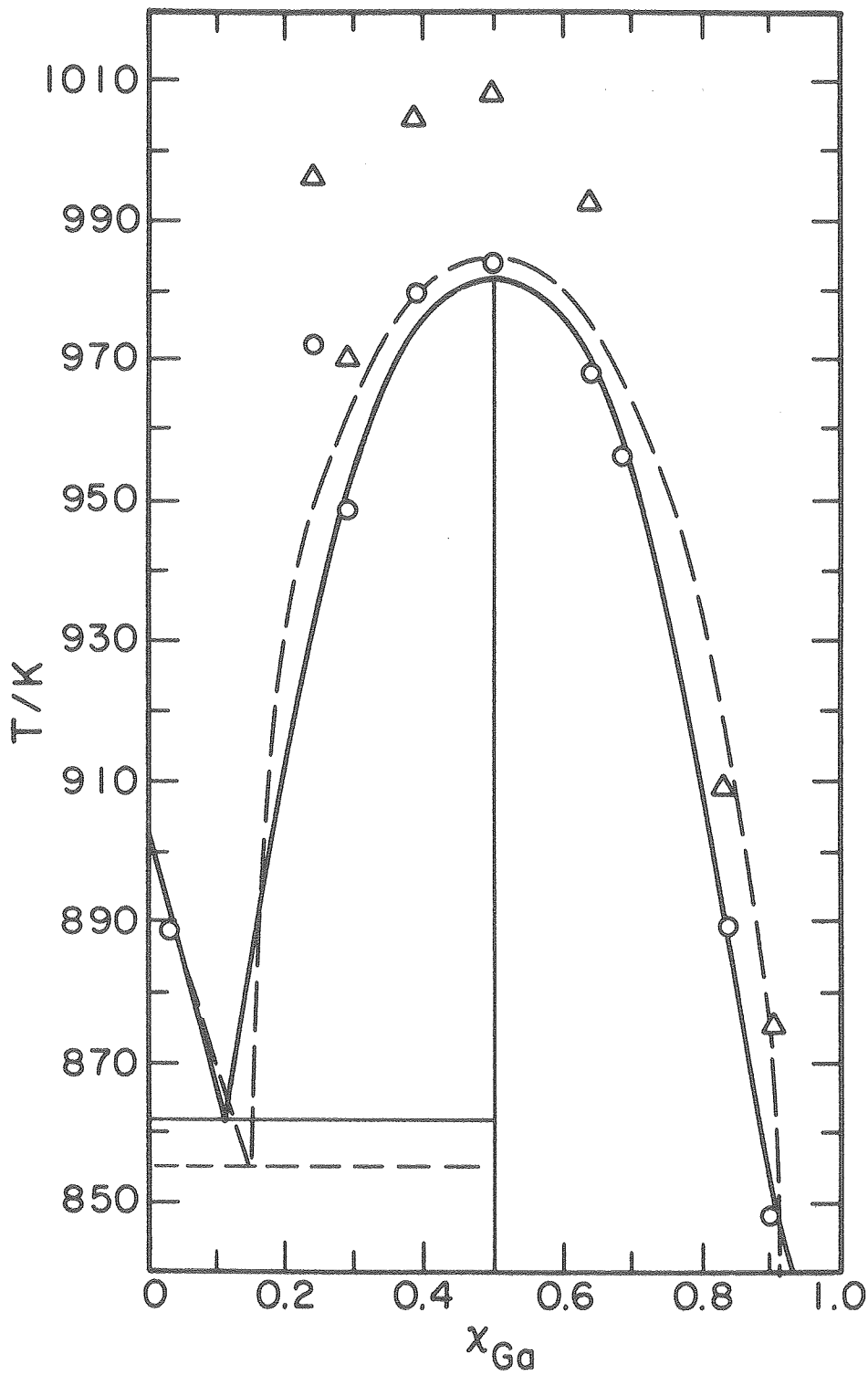

XBL 775-8832

Figure 6.

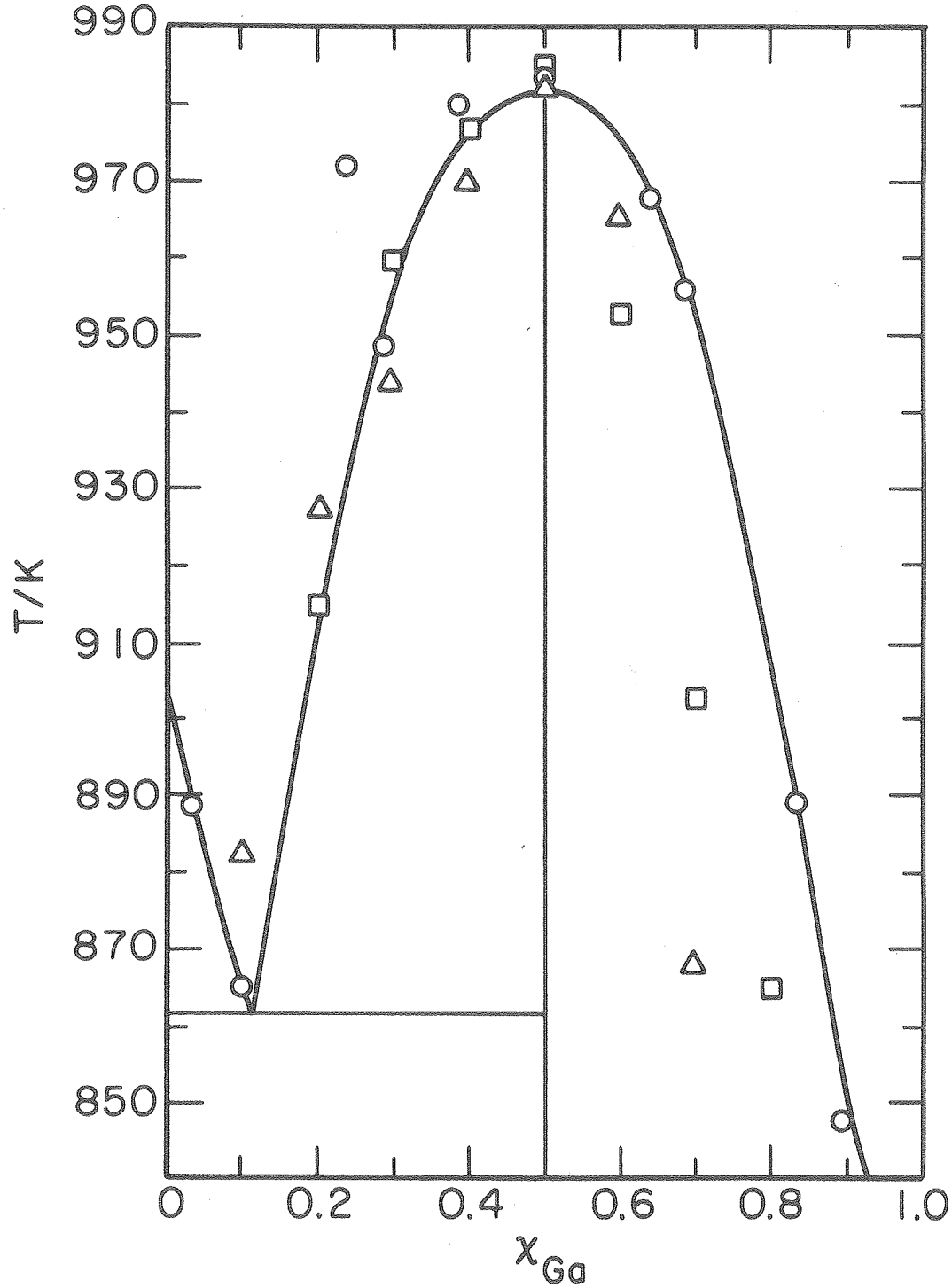

XBL 7711-10646

Figure 7.

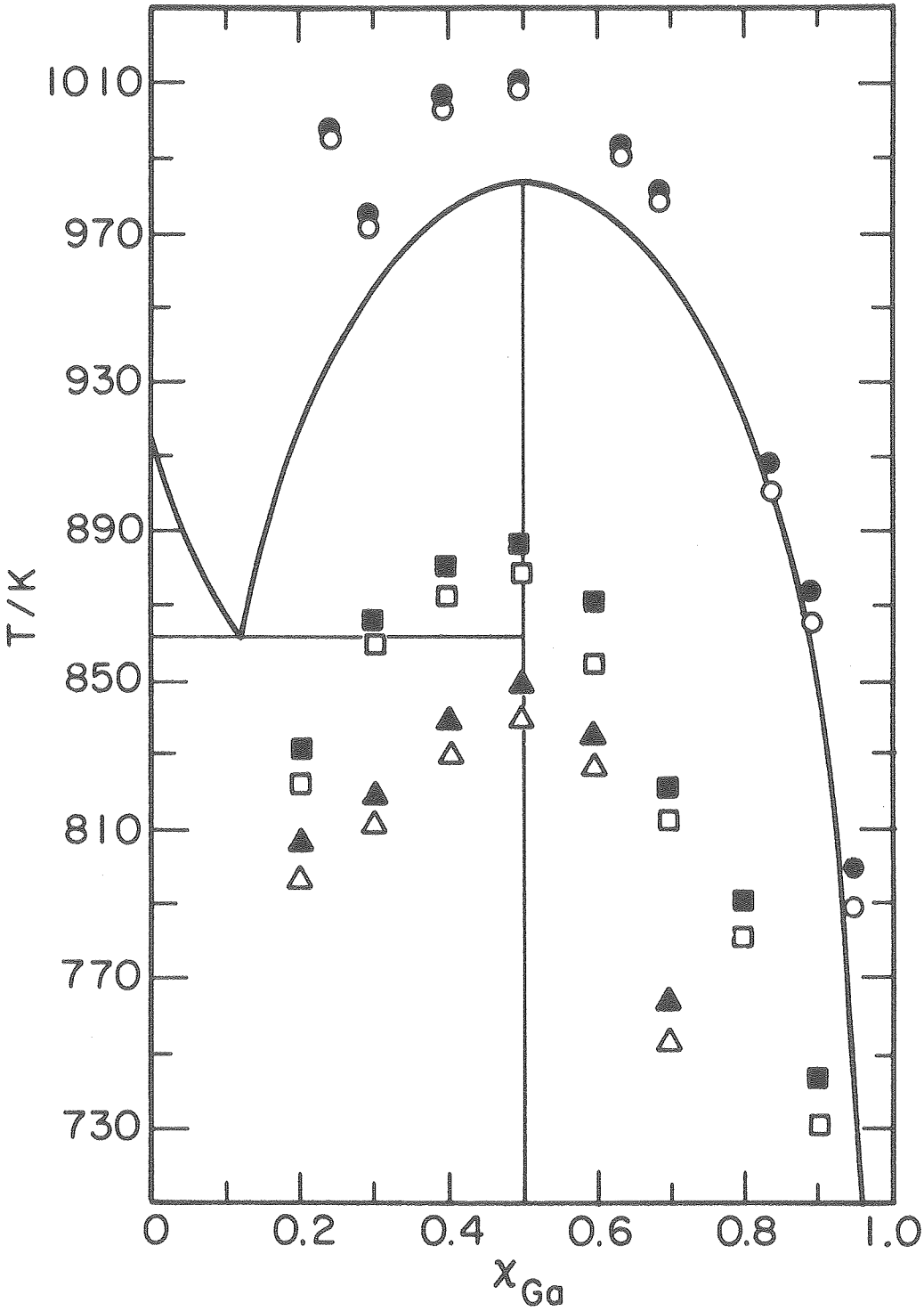

XBL 7711-10647

Figure 8.

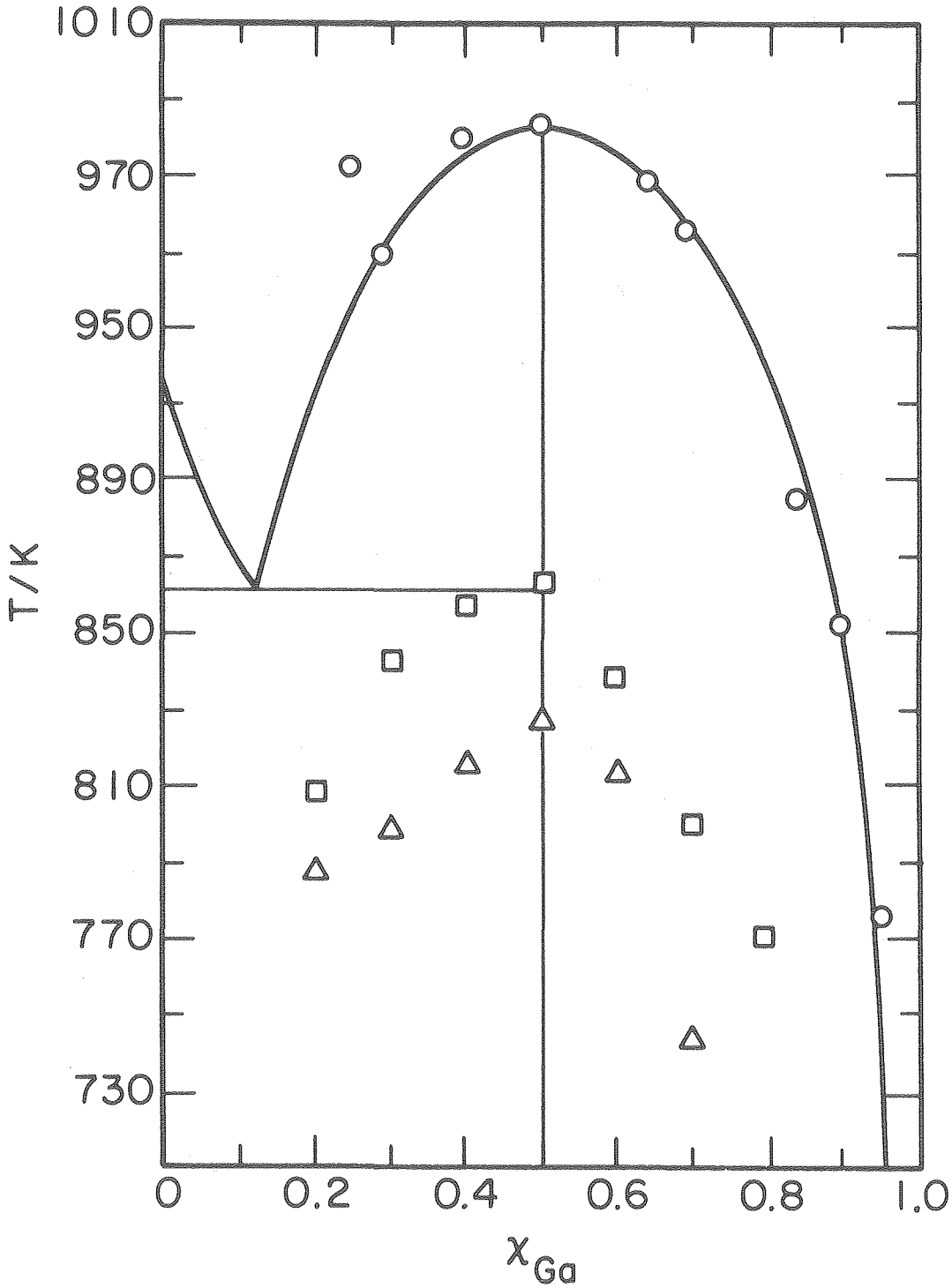

XBL 7711-10645

Figure 9.

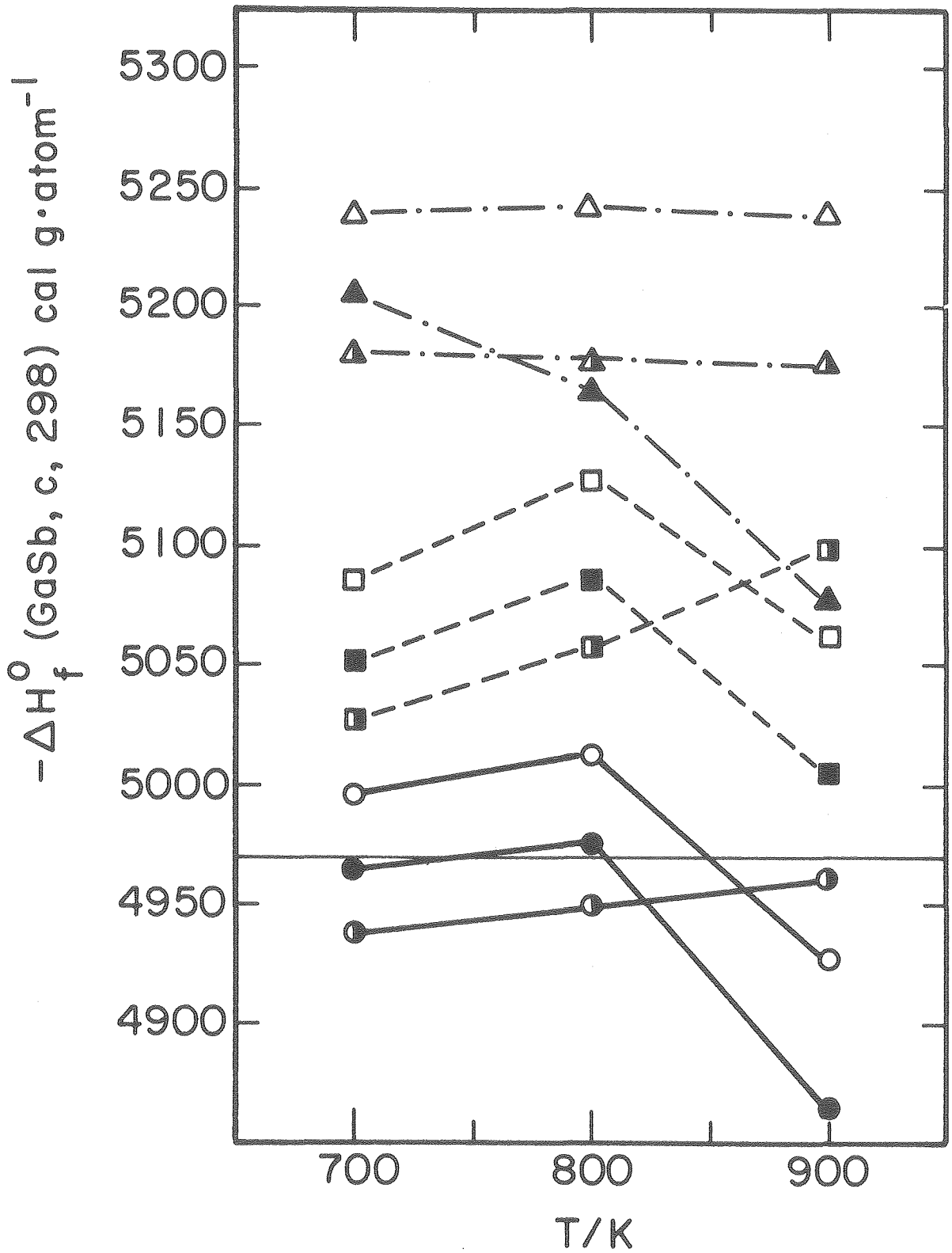

XBL 787-9539

Figure 10.

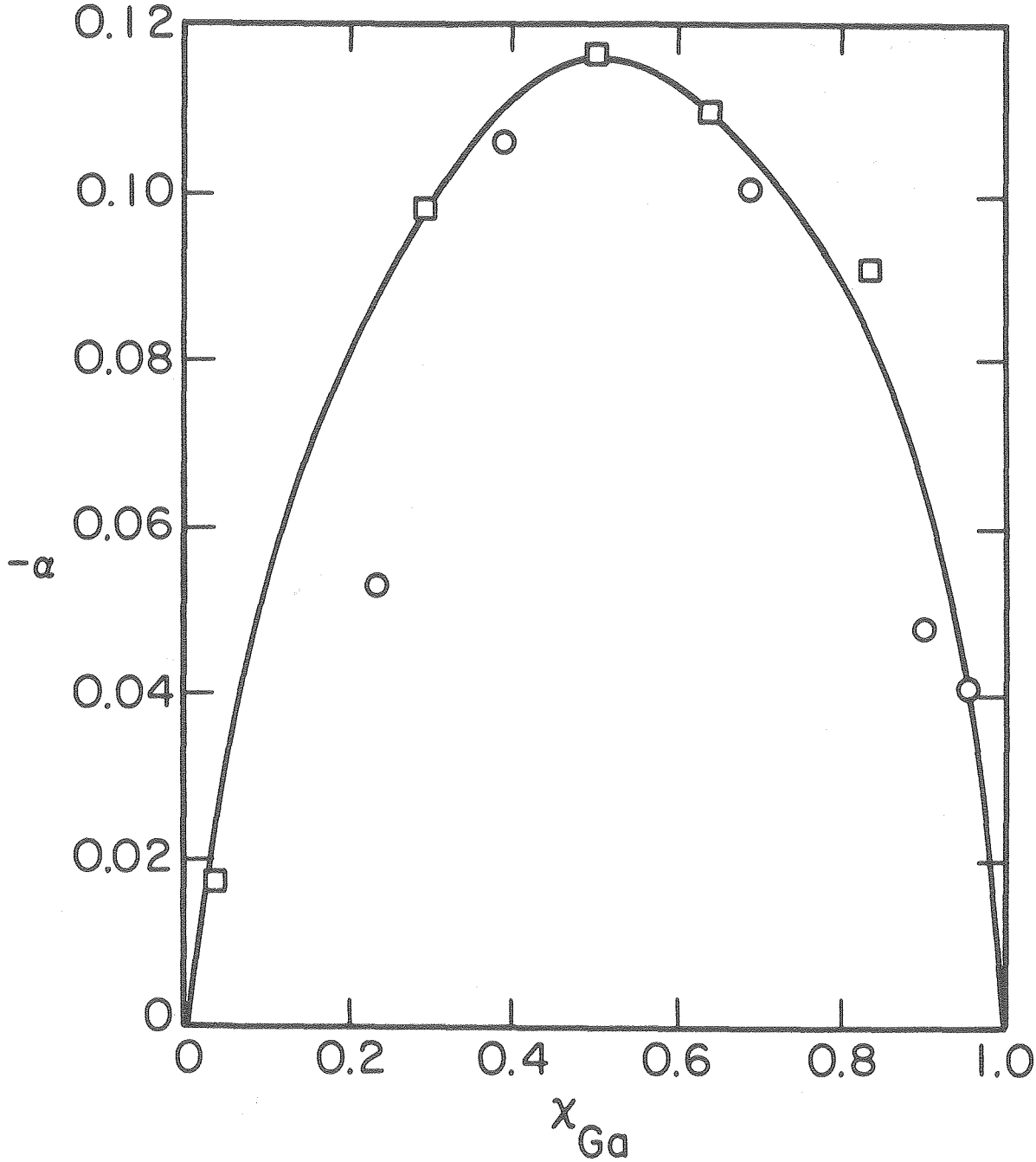

XBL 775-8835

Figure 11.

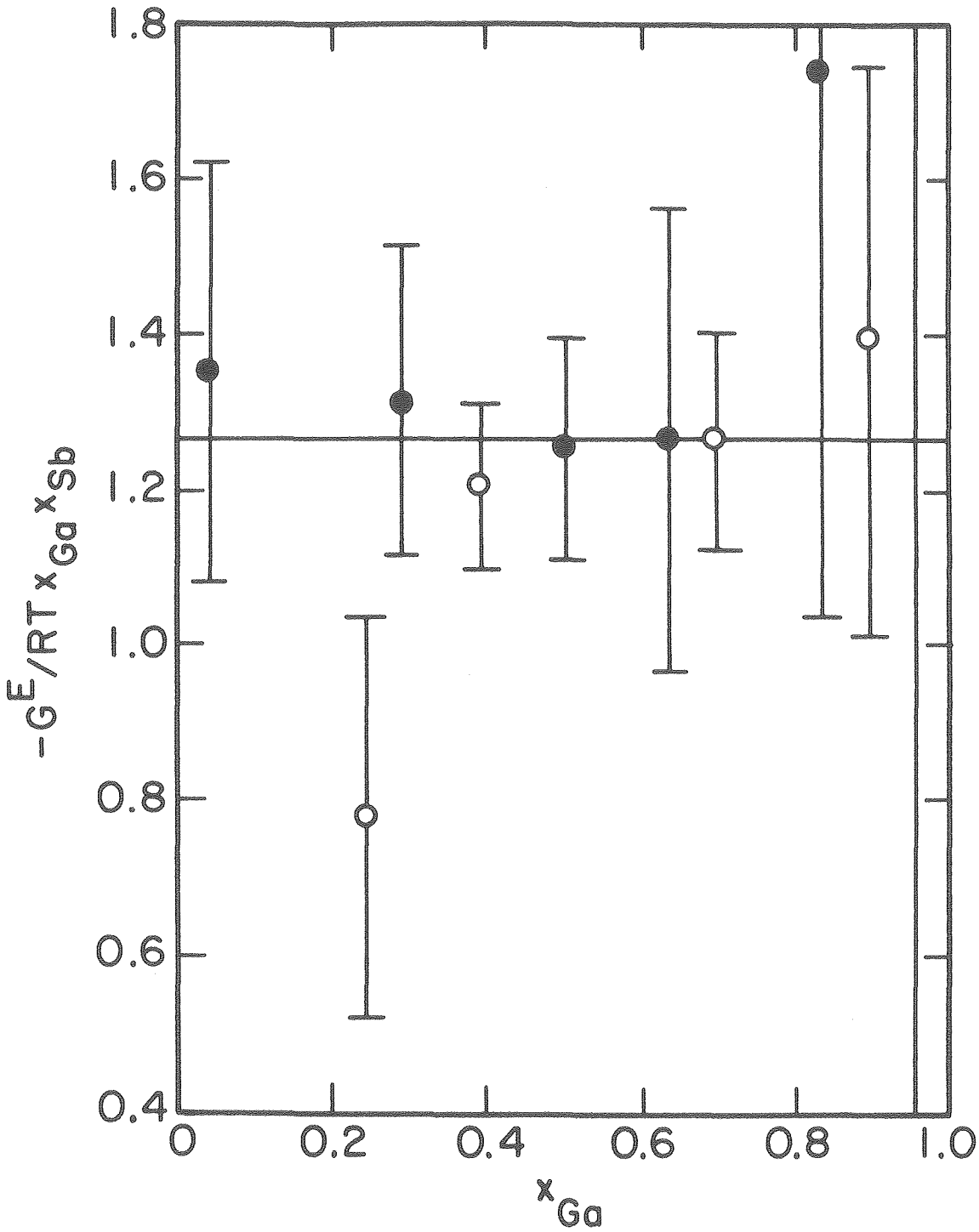

XBL 786-9373

Figure 12.

CHAPTER IV. SOLID STATE ELECTROCHEMICAL STUDY OF In-Sb LIQUID ALLOYS

A. INTRODUCTION

1. General Introduction

Indium antimonide (InSb) is the only existing intermetallic compound in the indium-antimony system and crystallizes in the sphalerite structure. This compound is a very well known semiconductor exhibiting interesting electrical properties, namely, an extremely high electron mobility (6500 $cm^2V^{-1}s^{-1}$ at room temperature) and the lowest bandgap of the III-V semiconducting compounds (0.18 eV).[1-3] Thus devises which have been fabricated from InSb include MOS capacitors,[4-6] MOS field effect transistors[7,8] and solid state lasers.[9] The small bandgap has been utilized in infrared charge coupled devices and the high electron mobility increases the sensitivity and response time in photo detectors operating in the millimeter to submillimeter wavelength range.[10-12] The growth of very thin epitaxial layers of InSb required for device fabrication is generally carried out by solidification from the liquid phase. Since the electrical characteristics are primarily defined by the degree of crystal perfection, the thermodynamic properties of the In-Sb system are important for defining the solid-liquid phase equilibria, and for the design and understanding of solidification phenomena.

2. Phase Diagram

Growth of epitaxial InSb is usually performed from a liquid solution rich in In due to the considerably higher vapor pressure of

Sb. Knowledge of the liquidus temperatures in the composition range is thus essential for predicting growth conditions. The phase diagram of the In-Sb system has been reported by several investigators[13-16] and forms a simple eutectic on the antimony rich side at a composition $x_{Sb} = 0.682$ and a temperature of 767 K. The In-InSb eutectic is practically degenerated having a melting point approximately one degree below that of pure indium and $x_{Sb} = 0.007$ and 428 K. The liquidus temperatures are accurate to within a few degrees and are more than sufficient for predicting growth temperatures.

Currently there is considerable interest in multicomponent solid solutions containing InSb and the experimental liquidus temperatures of these intermetallic solid solutions is lacking. The important phase equilibria of these solid solutions can be predicted by knowledge of the liquid and solid phase solution thermodynamics. As a prerequisite to predicting the multicomponent phase equilibria, an accurate description of the binary system is essential and thus the availability of an accurate binary phase diagram provides a consistency test for any developed thermodynamic model.

3. Thermodynamics

A considerable amount of experimental thermodynamic information has been compiled on the In-Sb system. Shown in Table 1 is the melting temperature (Tm) of InSb as determined by several investigators, generally taken to be 798 K, and is the only III-V compound having a Tm below that of a corresponding the element (Sb). Also shown in Table 1 is a summary of the enthalpy of fusion of InSb, ΔH_f^c(InSb).

Table 1. Comparison of melting temperature and enthalpy of fusion of InSb, as reported by different investigators.*

Tm K	$\Delta H_f^o(InSb)$ $Kcal_{th}\ g^{\circ}atom^{-1}$	Reference
798		13
809		14
813		16
798	6.1	17
	5.61 ± 0.2	18
	5.6	19
	6.1 ± 0.25	20
803	5.8	21
	5.9 ± 0.2	22
800 ± 3	5.75 ± 0.20	23
798 ± 3	4.5 ± 1.5	24
797 ± 1	5.71 ± 0.10	25
798.4 ± 0.3		26
	5.8 ± 0.35	62

*cal_{th} = 4.184 J

As can be seen there exists a maximum difference of 1.6 $Kcal_{th}$ $g^{\circ}atom^{-1}$ in the reported values of $\Delta H_f^c(InSb)$.

The mixing of pure In and pure Sb produces a negative enthalpy change as determined calorimetrically by four investigators.[27-30] Wittig and Gering[27] found a maximum exothermic enthalpy of mixing of 795 cal_{th} $g^{\circ}atom^{-1}$ at x_{Sb} = 0.41 and a temperature of 973 K, while Vecher et al.[28] found a maximum of 730 cal_{th} $g^{\circ}atom^{-1}$ at x_{Sb} = 0.43 and 910 K. The results of Itagaki and Yazawa[29] indicate the maximum ΔH^M to be 890 cal_{th} $g^{\circ}atom^{-1}$ measured at x_{Sb} = 0.42 and 923 K and Yazawa and coworkers[30] reported a ΔH^M maximum of 691 cal_{th} $g^{\circ}atom^{-1}$ at x_{Sb} = 0.39 and 945 K.

Of primary importance in understanding the solid-liquid phase equilibria in III-V compounds is an accurate description of the liquid phase solution behavior. The multicomponent solid solutions are nearly ideal but the liquid phase for most III-V systems show negative deviations from ideal behavior. The calculation of liquidus temperatures proves to be very sensitive to the assumed model for the liquid phase thermodynamics. To date there have been only three experimental determinations of component activities in liquid In-Sb solutions. Terpilowski[31] measured In activities in an electrochemical cell using a double bromide salt and found negative deviations throughout the entire composition range. Similarly Hoshino et al.[32] using a double iodide salt concentration cell measured In activities and found very close agreement with the results of Terpilowski. However, the excess enthalpies and entropies reported in these two studies were quite different and further discrepancies are found when compared to calorimetric data.

Furthermore, Terpilowski and Hoshino and coworkers assumed that the In ions transported in the fused salt electrolytes were monovalent and this assumption is directly related to the activitiy calculated from the measured cell emf by the relationship,

$$\ell n\ a(In) = -nFE/RT \qquad (1)$$

The analogous sytem Ga-Sb was extensively studied by this investigator (Chapter III) using a solid state electrochemical cell with calcia-stabilized zirconia (CSZ) as the electrolyte, and schematically represented as

$$Pt|C|Ga_xSb_{1-x}(\ell),\beta\text{-}Ga_2O_3(c)||CSZ||CO,CO_2|Pt \qquad (I)$$

or

$$Pt|C|Ga_xSb_{1-x}(\ell),\beta\text{-}Ga_2O_3||CSZ||Ga(\ell),\beta\text{-}Ga_2O_3(c)|C|Pt \qquad (II)$$

In these electrochemical cells the mobile ion, $O^{=}$, is clearly doubly charged and the +3 oxidation state of Ga is stable by more than 20 $Kcal_{th}$ g•mole oxygen.$^{-1}$

The results of the Ga activities measured in cells (I) and (II) were found to be in considerable disagreement with the activities determined in the fused salt electrochemical cells. Further thermodynamic analysis indicated the results obtained on the Ga-Sb system with the solid electrolyte were most consistent with the available calorimetric data and the reported phase diagram.

A third indium activity study was performed by Chatterji and Smith[33] using a solid electrolyte and found close agreement with the earlier work. This study investigated only four compositions, all

in the In-rich portion of the phase field. Returning to the Ga-Sb system, the analysis indicated fairly close agreement in the Group III, Ga, rich side (between the fused salt and solid electrolyte work) but found considerable discrepancy in Group V rich solutions. In addition Chatterji and Smith [33] used air as the reference electrode thus requiring knowledge of the Gibbs energy of forming In_2O_3 from the elements. Therefore those investigators evaluated a second electrochemical cell using a mixture of pure In metal and indium sesquioxide as the working electrode and air as the reference electrode. The resulting logarithm of the indium activity is then proportional to the difference in the measured emf of the above two types of cells. This difference is small in value (6.5 to 37 mV for the compositions studied) compared to the measured emfs of the two individual cells (920 to 1160 mV) and includes the uncertainties of two experiments. A thermodynamic analysis on the expression of Chatterji and Smith[33] reported for $\Delta G_f^o(In_2,O_3,c,T)$ was found to be inconsistent with other available thermodynamic data (Appendix II). For example, the expression for $\Delta G_f^o(In_2O_3,c,T)$ given earlier by the same authors[34] produces an error of 5 mV in the calculated emf difference while the expression for $\Delta G_f^o(In_2O_3,c,T)$ determined here and found in Appendix II gives the following equation for the emf difference

$$\text{Emf error/mV} = 102.9 - 0.032T/K \qquad (2)$$

and yields an error of 74.3 mV in the difference at 900K (which is twice the value of the emf used to calculate a(In) at the equimolar

composition). Thus the measurements of Chatterji and Smith[33] are questionable though the errors introduced are systematic and possibly cancelling.

B. THEORY AND EXPERIMENTAL

For these reasons the following solid state electrochemical cells were investigated:

$$Pt|C|In_xSb_{1-x}(\ell),In_2O_3||CSZ||CO,CO_2|Pt \qquad (III)$$

$$Pt|C|In_xSb_{1-x}(\ell),In_2O_3||CSZ||In(\ell),In_2O_3|C|Pt \qquad (IV)$$

In both cells the working electrode consisted of a mixture of the liquid alloy In-Sb at the composition of interest and the most stable oxide, indium sesquioxide. In the first cell type the reference oxygen partial pressure was established with a mixture of $CO + CO_2$ of known composition, while the second cell type utilized pure liquid indium and its stable oxide as the reference electrode. The open circuit potential of these concentration cells can be related to the indium activity by the following expressions:

$$a(In;In\text{-}Sb) = [P(CO_2)/P(CO)]^{-3/2} \exp\{3FE/RT - 3\Delta G^\circ(CO\text{-}CO_2)/2RT + \Delta G_f^o(In_2O_3)/2RT\} \qquad (3)$$

where $P(CO_2)/P(CO)$ is the ratio of the partial pressures of CO_2 to CO in the reference gas mixture, a(In;In-Sb) is the indium activity, E is the measured cell potential, $\Delta G^\circ(CO\text{-}CO_2)$ is the Gibbs energy change for the reaction

$$CO + \frac{1}{2}O_2 = CO_2 \qquad (4)$$

and $\Delta G_f^o(In_2O_3)$ is the Gibbs energy change for the formation of indium sesquioxide

$$2In(\ell) + \frac{3}{2}O_2(v) = In_2O_3(c) \qquad (5)$$

The simplest arrangement possible is cell type II where the logarithm of the indium activity can be directly related to the measured voltage by

$$\ell n\ a(In;In\text{-}Sb) = -3FE/RT \qquad (6)$$

The first cell is advantageous in that the gaseous reference electrode provides a more reversible electrode and generally serves as a better buffer for oxygen. Thus temperature coefficients of these cells were found to be in closer agreement with calorimetric values though the calculated activities are subject to larger uncertainties. In addition the use of $CO\text{-}CO_2$ is superlative to air since the O_2 partial pressure can be adjusted to match nearly with that established in the working electrode. The use of pure $In\text{-}In_2O_3$ as a reference electrode is superior for measuring In activities in that the only errors involved are those associated with the measurement of one emf and temperature. Thus in this study indium activities were measured in liquid solutions with antimony by means of the oxygen ion conducting solid electrolyte calcia stabilized zirconia. Both the investigation of solutions throughout the entire composition range and the use of a solid oxide electrolyte should illuminate possible ambiguities in the oxidation

state of the In ion assumed by earlier workers employing a halide-based concentration cell. An elucidation of the experimental apparatus used and procedure followed can be found in Chapter II.

The alloys were formed by mixing powdered InSb (Orion Chemical Co., 325 mesh, 99.999 percent purity) with either pure antimony (Cominco American, high purity, LOT EM 2139) or pure indium (Orion Chemical Co., 325 mesh, 99.999 percent purity, LOT #2449) to obtain the desired composition. Indium sesquioxide (Alfa Inorganics, 99.999 percent purity) was placed on the top of the alloy or the pure indium in cell type IV. The $CO-CO_2$ reference gas mixture (22.169 ($\pm$ 0.02) percent CO_2, 2.349 ($\pm$ 0.02) percent CO, and balance Ar) was a primary standard procured from Matheson Gas Products.

When a new alloy composition was formed by adding pure elemental material to a previously studied composition it was found to give inconsistent results. This inconsistency was apparent in a changing emf temperature coefficient as the temperature was cycled and probably due to incomplete mixing. Thus a new alloy had to be formed for each composition studied.

C. RESULTS

Concentration cells of the type schematically shown in Equations (III) and (IV) were employed to determine component indium activities in liquid solution with antimony. The open circuit equilibrium potentials for these cells were measured throughout a predetermined temperature range and these results are plotted in Figures 1 and 2. Figure 1 shows the measured cell emf for cells using the $CO-CO_2$ gaseous mixture

as a reference electrode while Figure 2 depicts the direct measurements employing the simple metal reference electrode. Only shown are the measurements made in one complete temperature cycle. However, it was found that several cycles were required before reproducible emf temperature variations existed. As can be seen, over the temperature range investigated the measured potentials are linear in temperature. Thus a simple linear regression analysis was performed to produce equations of the form

$$E/mV = a - b(T/K) \qquad (7)$$

The results of this statistical treatment are shown as the solid lines in Figures 1 and 2 and the regression coefficients are tabulated in Table 2 for the twelve compositions studied.

The activity of indium was calculated by means of Equations (3) or (6) at a temperature of 973 K, and using Equation (7) and the coefficients given in Table 2. These results are given in Table 3 for both types of electrodes. The activity of antimony is listed in Table 3 and was calculated by integration of the Gibbs-Duhem equation. Also shown in Table 3 are the corresponding activity coefficients. The temperature dependence of the equilibrium cell potential can be directly related to the partial molar enthalpy and entropy of indium. The indium partial molar enthalpy is thus shown in Table 3 and is seen to show considerable scatter. When these results are compared to the calorimeter values of $\Delta\overline{H}_{In}$ a large discrepancy is found. This inconsistency is common in these types of measurements and does not reflect on the

Table 2. Emf as a function of temperature, in the form E/mV = a-b(T/K) of the experimental cells. Temperature range is 820 to 1190 K.

Reference Electrode	x_{Ga}	a	b x 10^3
$CO-CO_2$	0.145	94.5	54.5
$CO-CO_2$	0.202	76.6	26.0
$CO-CO_2$	0.260	91.7	30.5
$CO-CO_2$	0.656	-93.0	-203.7
$CO-CO_2$	0.703	-68.5	-184.3
$CO-CO_2$	0.787	122.1	1.45
$CO-CO_2$	0.890	126.9	0.93
$In(\ell)-In_2O_3$	0.398	349.2	23.0
$In(\ell)-In_2O_3$	0.500	56.9	20.4
$In(\ell)-In_2O_3$	0.500	19.0	-0.66
$In(\ell)-In_2O_3$	0.600	337.5	317.6
$In(\ell)-In_2O_3$	0.647	128.7	107.2

Table 3. Summary of thermodynamic data for In-Sb liquid alloys derived from emf measurements at 973K.*

x_{In}	a_{In}	γ_{In}	a_{Sb}	γ_{Sb}	$\Delta\bar{H}_{In}$ $cal_{th}g^{\circ}atom^{-1}$	ΔG^{M} $cal_{th}g^{\circ}atom^{-1}$
0.145	0.051	0.352	0.828	0.968	-3,890	-1,150
0.202	0.072	0.356	0.741	0.929	-5,190	-1,490
0.260	0.106	0.408	0.659	0.890	-4,150	-1,730
0.656	0.435	0.663	0.158	0.459	-16,930	-2,280
0.703	0.544	0.774	0.107	0.360	-15,170	-2,110
0.787	0.760	0.966	0.043	0.197	-1,800	-1,710
0.890	0.915	1.028	0.012	0.110	-1,720	-1,090
0.398	0.142	0.357	0.475	0.789	-23,990	-2,370
0.500	0.265	0.530	0.343	0.685	-3,940	-2,320
0.500	0.261	0.522	0.343	0.685	-1,320	-2,330
0.600	0.364	0.607	0.218	0.544	-23,750	-2,350
0.647	0.418	0.646	0.166	0.471	-8,920	-2,320

*cal_{th} = 4.184 J

primary results of emf measurements - Gibbs energy changes. Finally the measured indium activity and calculated antimony activity were combined to yield the Gibbs energy change upon mixing pure indium and pure antimony and this quantity is given in Table 3. The results of the activity measurements are graphically shown in Figure 3 and the results indicate a negative deviation from ideal solution behavior. Shown for comparison are the molten salt electrolyte results of Terpilowski[31] at 923 K and of Hoshino and coworkers[32] at 900 K and also the solid oxide electrolyte results of Chatterji and Smith[33] at 973 K. As can be seen, the results of all four investigations show relatively good agreement. The results of the molten salt electrolyte work shows a slightly more negative deviation in component rich solutions than this work though the difference is within the experimental error involved.

For purposes of calculation smooth values for both the indium and antimony activity were extracted from Figure 3 and these results are tabulated in Table 4. Also listed here is the Gibbs energy of mixing calculated with these activities and the enthalpy of mixing In and Sb taken from the work of Yazawa et al.[30] The primary results of this work, Gibbs energy changes, can be combined with the primary results of calorimetric investigations, enthalpy changes, to produce the product of temperature and entropy of mixing which is given in Table 4. In addition Table 4 lists the values of the partial molar Gibbs energy and partial molar entropy for both components. Figure 4 summarizes this table in plotting the Gibbs energy change of mixing against the

Table 4. Summary of thermodynamic data for the In-Sb system derived from smooth activity data at 973K.*

x_{In}	a_{In}	a_{Sb}	$-\Delta G^M$ $cal_{th}g^{\circ}atom^{-1}$	$-\Delta H^M$ $cal_{th}g^{\circ}atom^{-1}$	$T\Delta S^M$ $cal_{th}g^{\circ}atom^{-1}$	$-\Delta G_{In}$ $cal_{th}g^{\circ}atom^{-1}$	
0.1	0.021	0.884	942	256	686	7471	238
0.2	0.062	0.754	1512	480	892	5377	546
0.3	0.112	0.605	1950	638	1150	4234	972
0.4	0.180	0.470	2203	693	1313	3316	1460
0.5	0.262	0.335	2353	684	1669	2590	2115
0.6	0.378	0.218	2307	621	1537	1881	2946
0.7	0.538	0.114	2100	512	1469	1199	4200
0.8	0.785	0.048	1549	366	1099	468	5872
0.9	0.915	0.010	1045	192	795	172	8906

*cal_{th} = 4.184 J

indium mole fraction. Figure 4 also contains a depiction of the available experimental enthalpy of mixing data of which there were four studies.[27-30] The combination of these two thermodynamic quantities yields information on the entropy of mixing which is also shown. For comparison the ideal entropy of mixing is plotted and the excess entropy of mixing can be seen to be nearly zero in the composition range $0.0 < X_{In} < 0.4$ and positive in more indium-rich solutions.

D. DISCUSSION

1. Volume of Mixing

When pure indium and pure antimony are mixed a mixture volume is produced that is larger than the volume of the pure components. This positive excess volume of mixing leads to a positive contribution to the excess entropy of mixing. Scathchard[35] first treated the quantitative relation between the volume change in mixing and other thermodynamic excess functions. In his analysis the mixing process was considered to be a two-step process where in the first step the mixing of the two pure components was performed at constant volume, allowing the pressure to vary as required, and followed by a compression or expansion step to recover the original pressure. If the fractional volume change ($\Delta V^M/V$) is small, higher order terms may be neglected in Scatchard's derivations and the volume contribution to the excess functions may be simply written as

$$\Delta S^{ex}_{Vol} \cong \alpha/\beta_T \, \Delta V^M$$

$$\Delta H_{Vol} \cong T \, \alpha/\beta_T \, \Delta V^M$$

Here α denotes the thermal coefficient of expansion and β_T is the isothermal compressibility, where both of these properties are for the pure components. Unfortunately no volume of mixing data is available for In-Sb but the volume change in mixing for an equimolar mixture can be calculated from available density determinations . Using the literature density volume for molten InSb,[36,37] pure In[38-40] and pure Sb[38,41,42] a range of ΔV^M of 0.399 to 0.561 cc g·atom^{-1} is obtained. The thermal coefficient of expansion can be found from the temperature dependence of the density measurements[38,42] while the isothermal compressibility can be calculated from velocity of sound measurements in the molten metals.[43-46] Summarized in Table 5 are the volume contributions to the enthalpy and entropy of mixing. Also shown is the experimentally observed values of these quantities. Thus it is seen that the entropy contribution is in the correct direction but more than twice that observed while the enthalpy term is opposite in sign. This discrepancy is partially explained by the tendency of In and Sb to form pairs in the liquid state as will be discussed later.

2. Calculation of the Phase Diagram

The In-Sb binary phase diagram is very well determined and thus a convenient check of the consistency of the available solution thermodynamic data is a calculation of the liquidus temperatures. Two

Table 5. Volume contributions to the excess entropy and enthalpy of mixing liquid equilmolar In-Sb at 973K.*

$\Delta S^E/\Delta V^M$ $cal_{th}cm^{-3}K^{-1}$	α/β_T $cal_{th}cm^{-3}K^{-1}$	$-\Delta H^M/\Delta V^M$ $Kcal_{th}cm^{-3}$	$T\alpha/\beta_T$ $Kcal_{th}cm^{-3}$
0.279 to 0.393	0.489 to 0.558	1.22 to 1.71	0.87 to 1.40

*cal_{th} = 4.184 J

equations for calculating the liquidus temperature can be employed and are derived in Appendix III. The first equation is termed the "fusion" equation and is given by

$$T_\ell = \frac{2\Delta H_f^c(InSb)+\Delta\overline{H}_{In}(x)+\Delta\overline{H}_{Sb}(x)-\Delta\overline{H}_{In}(0.5)-\Delta\overline{H}_{Sb}(0.5)}{2\Delta S_f^c(InSb)+\Delta\overline{S}_{In}(x)+\Delta\overline{S}_{Sb}(x)-\Delta\overline{S}_{In}(0.5)-\Delta\overline{S}_{Sb}(0.5)} \tag{10}$$

where ΔH_f^c and ΔS_f^c are the enthalpy and entropy of fusion of InSb respectively and $\Delta\overline{H}_i(x)$ and $\Delta\overline{S}_i(x)$ are the relative partial molar enthalpy and entropy of component i at mole fraction x, respectively. All quantities here are expressed on a g°atom basis. A second expression for calculating liquidus temperatures, the "formation" equation, can be derived in terms of the standard enthalpy and entropy of formation of solid InSb from the pure <u>liquid</u> elements, $\Delta H_f^o(InSb,c,T)$ and $\Delta S_f^o(InSb,c,T)$, and is given by

$$T_\ell = \frac{2\Delta H_f^o(InSb,c,T) - \Delta H_{In}(x) - \Delta\overline{H}_{Sb}(x)}{2\Delta S_f^o(InSb,c,T) - \Delta\overline{S}_{In}(x) - \Delta\overline{S}_{Sb}(x)} \tag{11}$$

The InSb phase diagram also shows a simple eutectic in the antimony rich region. In this portion of the phase diagram the liquidus temperature can be calculated from the following equation also developed in Appendix III:

$$T_\ell = \frac{\Delta H_f^c(Sb) + \Delta H_{Sb}(x)}{\Delta S_f^c(Sb) + \Delta S_{Sb}(x)} \tag{12}$$

where $\Delta H_f^c(Sb)$ and $\Delta S_f^c(Sb)$ are the enthalpy and entropy of fusion of pure antimony.

Given in Table 6 are the results of calculating the liquidus temperatures with either the "fusion" or "formation" equations. Required for these calculations is the partial molar enthalpy of both components which is readily obtained from the calorimetric enthalpy of mixing investigations, while the partial molar entropy can be calculated from the measured component activities of this work. A melting temperature of 800 K was used in conjunction with the experimental enthalpies of fusion listed in Table 1 to calculate the liquidus temperatures with the "fusion" equation. There are four emf studies of the Gibbs energy of formation of solid InSb available in the literature.[47-50] The standard enthalpy and entropy of formation of InSb required in the "formation" equation can be found from the temperature dependence of these measurements. Finally in order to express these quantities with respect to the formation of solid InSb from the pure <u>liquid</u> elements, the enthalpy of fusion and melting temperature of pure antimony was required. The value for $\Delta H_f^c(Sb)$ was taken from Hultgren, et al.[51] as 4750 cal g°atom^{-1} and Tm was assumed to be 904K.

Table 7 gives the liquidus temperatures determined from Equation (12) using the activity measurements of this work and also of

Table 6. Comparison of liquidus temperatures, (T/K) in the In-Sb system.

Method	x_{Sb}							Reference	
	0.1	0.2	0.3	0.4	0.5	0.6	0.7	$\Delta H_f^c(InSb)/\Delta H_f^o(InSb)$	ΔH^M
fusion	596.9	707.5	760.5	792.7	800.0	795.6	771.7	17	30
"	582.6	699.8	757.3	792.1	800.0	795.2	769.2	18	30
"	582.3	699.7	757.2	792.1	800.0	795.2	769.2	19	30
"	588.4	702.9	758.7	792.4	800.0	795.4	770.2	21	30
"	585.7	701.5	758.0	792.3	800.0	795.3	769.8	25	30
"	591.3	704.5	759.4	792.5	800.0	795.5	770.7	22	30
"	586.9	702.1	758.3	792.3	800.0	795.3	770.0	23	30
"	541.4	676.9	747.2	790.2	800.0	794.0	761.9	24	30
"	594.5	705.3	760.1	792.6	800.0	796.5	771.4	17	27
"	537.9	673.6	746.4	790.0	800.0	794.0	761.6	24	27
formation	576.6	687.3	741.6	774.3	781.7	777.2	752.8	47	30
"	582.3	697.8	754.4	788.5	796.3	791.6	766.1	48	30
"	585.1	698.4	653.6	786.9	794.5	789.9	765.0	49	30
"	597.2	705.9	758.1	789.5	796.6	792.3	768.9	50	30
"	570.2	681.6	738.3	771.8	779.4	774.7	750.0	47	27
"	591.4	700.8	755.1	787.3	794.6	790.2	766.4	50	27
ideal	701.8	753.0	779.9	793.8	798.2	793.8	-	-	-
experimental	607.2	699.3	756.9	787.6	798.2	788.6	774.3	13	-

Table 6. Comparison of liquidus temperatures, (T/K) in the In-Sb system.

Method	x_{Sb}							Reference	
	0.1	0.2	0.3	0.4	0.5	0.6	0.7	ΔH_f^c/or ΔH_f^o	ΔH^M
fusion	596.9	707.5	760.5	792.7	800.0	795.6	771.7	17	30
"	582.6	699.8	757.3	792.1	800.0	795.2	769.2	18	30
"	582.3	699.7	757.2	792.1	800.0	795.2	769.2	19	30
"	588.4	702.9	758.7	792.4	800.0	795.4	770.2	21	30
"	585.7	701.5	758.0	792.3	800.0	795.3	769.8	25	30
"	591.3	704.5	759.4	792.5	800.0	795.5	770.7	22	30
"	586.9	702.1	758.3	792.3	800.0	795.3	770.0	23	30
"	541.4	676.9	747.2	790.2	800.0	794.0	761.9	24	30
"	594.5	705.3	760.1	792.6	800.0	796.5	771.4	17	27
"	537.9	673.6	746.4	790.0	800.0	794.0	761.6	24	27
formation	576.6	687.3	741.6	774.3	781.7	777.2	752.8	47	30
"	582.3	697.8	754.4	788.5	796.3	791.6	766.1	48	30
"	585.1	698.4	653.6	786.9	794.5	789.9	765.0	49	30
"	597.2	705.9	758.1	789.5	796.6	792.3	768.9	50	30
"	570.2	681.6	738.3	771.8	779.4	774.7	750.0	47	27
"	591.4	700.8	755.1	787.3	794.6	790.2	766.4	50	27
ideal	701.8	753.0	779.9	793.8	798.2	793.8	-	-	-
experimental	607.2	699.3	756.9	787.6	798.2	788.6	774.3	13	-

Terpilowski[31] and Hoshino et al.[32] Also found in Tables 6 and 7 are the liquidus temperatures found assuming that the solutions behave ideally. Finally, these results can be compared to the experimental liquidus temperatures as determined by Liu and Peretti.[13] Figure 5 graphically depicts the high temperature portion of the InSb phase diagram. The solid line represents the experimental phase diagram while the dashed line indicates the assumption of ideal solution behavior. The points plotted here are those calculated with the "fusion" equation and using the smoothed values of activity from this work, $\Delta H_f^c(InSb) = 5.9\ Kcal_{th} g^{\circ} atom^{-1}$[22] and the enthalpy of mixing of Yazawa et al.[30] As can be seen, the "fusion" equation exhibits good consistency with the experimental phase diagram. For purposes of comparison, similar calculations were performed with the other available emf activity measurements. Figure 6 shows the results of such calculations using the "fusion" equation, the enthalpy data given above, and the smoothed activity measurements of Hoshino et al.[32] or the actual measurements of Terpilowski.[31] The results of Chatterji and Smith[33] were over an insufficient composition range to be investigated.

Several conclusions can be drawn from these calculations. First, the negative deviations found in all emf activity measurements is supported by these calculations as is seen by comparing with the ideal case. The enthalpy of fusion reported as $4.5\ Kcal_{th}\ g^{\circ} atom^{-1}$[24]

Table 7. Comparison of liquidus temperatures, (T/K) in the In-Sb system rich in Sb.

Method	x_{Sb}			Reference	
	0.7	0.8	0.9	ΔH^M	Activity
equation 12	755.2	815.6	863.6	30	this work
" "	755.1	815.6	863.6	27	this work
" "	765.7	819.5	866.5	30	32
" "	730.5	797.0	860.1	30	31
ideal	796.6	833.6	869.4		
experimental	774.3	825.1	867.7		13

appears to be too low while the use of the experimental ΔH_f^c(InSb) (range of 5.6 to 6.1 $Kcal_{th}$ $g^{\circ}atom^{-1}$) give liquidus temperatures within the experimental range of the data used for at least one of the three activity measurements used. Our results tend to support a higher ΔH_f^c(InSb) while the results of Terpilowski support the lower ΔH_f^c(InSb) values. Also the use of the different enthalpy of mixing data is seen to have a negligible effect on the results. Finally the results in the antimony rich region indicate the activities of this work or Hoshino et al.[32] give close agreement while the work of Terpilowski[31] produces considerably lower liquidus temperatures.

A more stringent test of the thermodynamic consistency of our results is found in using the "formation" equation in that the partial molar quantities are not dominated as greatly by the integral enthalpy and entropy. Figure 7 displays the results found using the "formation" equation. Of the four experimental values for ΔH_f^o(InSb,c,T) and ΔS_f^o(InSb,c,T) available the values given by Nikol'skaya et al.[48] and Sirota and Yushkevich[49] produced similar results. Figure 7 shows the liquidus temperatures calculated using the results of Sirota and Yushkevich,[49] Abbasov and Mamedov[47] and of Terpilowski and Trzebiatowski[50] for the standard enthalpy and entropy and the smooth activities of this work. As can be seen, fairly close agreement is found though the use of the work of Abbasov and Mamedov[47] produced significantly lower values. Again for comparison the "formation" liquidus temperatures were calculated with the other emf activity data. Figure 8 depicts the results of using either the work of Hoshino

et al.[32] or Terpilowski[31] in conjunction with the extremum for $\Delta H_f^o(InSb,c,T)$ and $\Delta S_f^o(InSb,c,T)$.[47,50]

Again several conclusions can be drawn from these calculations. The results of Terpilowski[31] show considerable discrepancy with the reported phase diagram while good consistancy is found only with this work or that of Hoshino et al.[32] and use of the lowest values of $\Delta H_f^o(In,Sb,c,T)$ and $\Delta S_f^o(InSb,c,T)$.[50] Also as expected the use of the various enthalpy of mixing results produces a somewhat larger range in the calculated temperatures.

3. Gibbs Energy of Formation of InSb(c).

An alternate expression for $\Delta G_f^o(InSb,c,T)$ can be derived using the results of this study as follows. Consider the following reaction scheme:

$$(\tfrac{1}{2})In(\ell) + (\tfrac{1}{2})Sb(\ell) = In_{0.5}Sb_{0.5}(\ell) \qquad (13)$$

$$In_{0.5}Sb_{0.5}(\ell) = (\tfrac{1}{2})InSb(c) \qquad (14)$$

$$(\tfrac{1}{2})Sb(c) = (\tfrac{1}{2})Sb(\ell)\ . \qquad (15)$$

The Gibbs energy change for the first reaction is simply the Gibbs energy change in mixing equal moles of In and Sb while the Gibbs energy change for reactions (14) and (15) can be approximated by

$$\Delta G^\circ(14) = -\Delta H_f^c(InSb)\{1 - (T/K)/Tm(InSb)\} \qquad (16)$$

$$\Delta G^\circ(15) = (\tfrac{1}{2})\Delta H_f^c(Sb)\{1 - (T/K)/Tm(Sb)\} \qquad (17)$$

where the small temperature dependence on the enthalpy and entropy of fusion of InSb and Sb has been neglected. Upon summation of the above reactions the overall reaction is found to be the desired formation reaction and the Gibbs energy change is given by

$$\Delta G_f^o(InSb,c,T) = \Delta H_f^o(InSb,c,T) - T\ \Delta S_f^o(InSb,c,T) \qquad (18)$$

where

$$\Delta H_f^o(InSb,c,T) = \Delta H^M + (\tfrac{1}{2})\Delta H_f^c(Sb) - \Delta H_f^c(InSb) \qquad (19)$$

and

$$\Delta S_f^o(InSb,c,T) = \Delta S^M + (\tfrac{1}{2})\Delta H_f^c(Sb)/Tm(Sb) - \Delta H_f^c(InSb)/Tm(InSb)\ . \qquad (20)$$

In the above equations all quantities are on a g°atom basis. Using the results of Yazawa et al.[30] for ΔH^M, the enthalpy of fusion as given by Blachnik and Schneider,[22] $\Delta H_f^c(InSb) = 5.9$ $Kcal_{th}$ $g°atom^{-1}$, the results of this work to determine ΔS^M, and taking $\Delta H_f^c(Sb) = 4750$ $Kcal_{th}$ $g°atom^{-1}$, Tm(Sb) = 904 K and Tm(InSb) = 798 K the following equation is derived for $\Delta G_f^o(InSb,c,T)$.

$$\Delta G_f^o(InSb,c,T) = -4209 + 3.052(T/K)\ cal_{th}\ g°atom^{-1} \qquad (21)$$

Table 8 summarizes the various results reported for the standard enthalpy and entropy of formation of solid InSb. The values determined by molten salt emf studies are given for the average temperature of those measurements. Also listed are two investigations of the standard formation enthalpy performed with a high temperature calorimetry and can be seen to give excellent agreement with the value derived here.

Table 8. Summary of results for the standard enthalpy and entropy of formation of InSb.*

Method	$-\Delta H_f^o(InSb,c,T)$ $cal_{th}\ g^{-1}\cdot atom^{-1}$	(T/K)	Reference
emf	4083	703	47
emf	3980 ± 200	703	48
emf	4500 ± 210	703	50
emf	4110	703	49
calorimetry	4320 ± 20	723	52
mass spectroscopic	4100	798	53,22
calorimetry	4233 ± 100	750	21
derived	4209	-	30,22,51

Method	$-\Delta S_f^o(InSb,c,T)$ $cal_{th}\ g^{-1}\cdot atom^{-1}$	(T/K)	Reference
emf	3.045	703	47
emf	2.78 ± 0.25	703	48
emf	3.43 ± 0.20	703	50
emf	2.96	703	49
derived	3.052	-	this work, 22, 30,51
derived	2.667	-	31, " " "
derived	3.120	-	32, " " "

cal_{th} = 4.184 J

Also listed in Table 8 is the standard entropy derived from the equimolar activity results of the two other studies.

There are several different ways to test the consistency of these various results. The primary result of the emf formation work is the Gibbs energy of formation of InSb. Thus the consistent derived equations should produce $\Delta G_f^o(InSb,c,T)$ values in close agreement with the emf ones. Table 9 lists the value of $\Delta G_f^o(InSb,c,T)$ calculated from the derived equations and are compared to the measured results. As can be seen the equations derived with the activity measurements of this work and of Hoshino et al.[32] are within the range of experimental error for the emf results and the range produced by varying the enthalpy of fusion of InSb (approximately $\Delta G_f^o(InSb,c,T) \pm 150\ cal_{th}\ g^{\circ}atom^{-1}$). The results found in using the activity work of Terpilowski[31] give Gibbs energies which are too low.

A second consistency test involves a third law calculation of $\Delta H_f^o(InSb,c,T)$ from the following equation

$$\Delta H_f^o(InSb,c,298) = T/K \left\{ -\left[\frac{\Delta G_f^o(InSb,c,T) - \Delta H_f^o(InSb,c,298)}{T/K}\right] + \frac{\Delta G_f^o(InSb,c,T)}{T/K} \right\} \quad (22)$$

The first term on left is the free energy function and can be calculated from

Table 9. Summary of Gibbs energy of formation of InSb.*

Method	$-\Delta G_f^o(InSb,c,T)$ $cal_{th}\ g^{\circ}atom^{-1}$		Reference
	643 K	763 K	
derived	2247	1880	this work
derived	2494	2174	31
derived	2203	1828	32
emf	2125	1760	47
emf	2192	1859	48
emf	2207	1852	49
emf	2295	1883	50

*cal_{th} = 4.184 J

$$-\left[\frac{\Delta G_f^o(InSb,c,T)-\Delta H_f^o(InSb,c,298)}{T/K}\right] = \Delta S_f^o(InSb,c,298)$$

$$+ \Delta_f^o[S(T) - S(298)] - \Delta_f^o[H_T(T) - H(298)]/T/K \qquad (23)$$

Thus the free energy function, calculated from both low and high temperature heat capacities, can be combined with the Gibbs energy of formation of InSb from the various sources to give a calculated value of $\Delta H_f^o(InSb,c,298)$. The calculated result can then be compared to that measured independently with calorimetry. Taking the high temperature heat capacity of In from Hultgren et al.,[51] for Sb from Glassner[54] and for InSb from Lundin et al.[21] and the absolute entropy for the elements from Hultgren et al.[51] and for InSb from Renner[55] and combining this with the values of $\Delta G_f^o(InSb,c,T)$ produces the results displayed in Figure 9. The results of the four emf formation studies are shown by the solid lines while the experimental value shown is that selected by Hultgren et al.[23] ($\Delta H_f^o(InSb,c,T)$ = $-$ 3700 ± 100 cal_{th} $g^{\cdot}atom^{-1}$) though the direct measurements available in the literature show considerable scatter and are summarized in Table 10.

Thus the results of these calculations are not too definitive, though the derived $\Delta G_f^o(InSb,c,T)$ using the data of Terpilowski[31] produces values which are low. It should also be noted that the results of this work produce constant values of the calculated $\Delta H_f^o(InSb,c,298)$ as required.

Table 10. Summary of the standard enthalpy of formation of InSb at 298 K or 273 K.*

Method	$-\Delta H_f^o(InSb,c,T)$ $Kcal_{th}\ g^{\circ}atom^{-1}$		Reference
tin solution calorimetry	3.47 ± 0.07	273K	17
" " "	3.661 ± 0.1	273K	21
calculated	3.65	273K	56,57
calorimetry	3.4 ± 0.3	298K	58
bomb calorimetry	3.89 ± 0.04	298K	59
calculated	3.7 ± 0.1	298K	25,23

*cal_{th} = 4.184 J

As a final comparison, the phase diagram for InSb is again calculated using the standard enthalpy and entropy given in Equation (21). These results are presented in Figure 10 and it is found that the activity measurements of this work and Hoshino et al.[32] give excellent agreement while the temperatures calculated with the data of Terpilowski[31] are low. It should be noted that this method requires the melting temperature of the compound to be predicted exactly thus essentially fixing the zero temperature on the ordinate. Similar liquidus temperature calculations with the other derived equations again gave excellent agreement thus supporting the common compositional activity dependence reported. In summary, it may be concluded that the expression for ΔG_f^o(InSb,c,T) derived here (Equation (21)) is consistent with other available Gibbs energy determinations, calorimetric results and the reported phase diagram.

An equimolar liquid solution of In and Sb exhibits unusual properties near the melting temperature. These properties include anomalous heat capacities,[25] viscosity[37] and velocity of sound[23] for temperatures to 20 degrees above the melting temperature. Direct X-ray scattering curves for liquid InSb have been measured at 813 K[60,61] and result in a radial distribution function having a first maximum at 3.2Å with a corresponding coordination number of 5.7. Crystalline InSb, on the other hand, exhibits a peak at 2.80Å and has a coordination number of 4, thus indicating the zinc-blende structure is not retained upon melting. In addition, an examination of the radius of the first coordination sphere for both the pure liquid elements

and the liquid solution establishes that the nearest neighbors in InSb are atoms of different kinds. Thus the atoms in liquid InSb tend to form unlike pairs and may even form covalent clusters in a small temperature range above Tm.

These observations can be quantified with the aid of a statistical model developed in Appendix IV. In this model a short range order parameter, α, is defined and is related to a reduced interaction energy v by

$$\alpha = x_{In}x_{Sb}v = 2N_o x_{In}x_{Sb}(\mu + j(x) + \bar{g}T)/RT \qquad (24)$$

where No is the equivalent number of lattice sites, $\mu + j(x)$ accounts for the composition dependence of the interaction energy and $\bar{g}$ relates to the temperature dependence. The interaction energy can then be calculated from experimental enthalpy and Gibbs energy data for the liquid phase. The results of these calculations are shown in Table 11. The smooth values of the component activities of this work at 973 K were used along with the enthalpy of mixing of Yazawa et al.[30] As can be seen liquid In-Sb solutions exhibit a considerable degree of pairing.

The fact that the enthalpy of mixing is not symmetrical about the compound composition requires that the term j(x) be present and is apparent in Table 11. Unfortunately, the assumed linear temperature dependence of the interaction energy did not bear out in these calculations as indicated by the variable calculated value of $\bar{g}$.

Table 11. Short range order parameter and reduced interaction energy for the In-Sb system.*

x_{In}	$-\alpha$	$-N_o(\mu + j(x))$ $cal_{th}\ g^{\circ}atom^{-1}$	$-N_o g$ $cal_{th}\ g^{\circ}atom^{-1}K^{-1}$	$-v$
0.1	0.057	449	0.168	0.633
0.2	0.077	464	-0.001	0.479
0.3	0.115	454	0.076	0.547
0.4	0.134	424	0.117	0.557
0.5	0.183	385	0.337	0.733
0.6	0.158	372	0.272	0.659
0.7	0.146	354	0.328	0.696
0.8	0.093	349	0.216	0.579
0.9	0.065	334	0.370	0.718

*cal_{th} = 4.184 J

E. CONCLUSION

Component activities in liquid solutions containing In and Sb were measured and found to give moderate negative deviations from ideal behavior. The activities measured showed close agreement with the other reported emf activity measurements and supports the assumption that the indium ion is monovalent in the fused salt electrolytes used in previous emf work.[31,32] The system exhibited a negative enthalpy of mixing[27-30] having a maximum value near $x_{In} = 0.42$. The combination of these results produced a significant positive excess entropy of mixing that was partially explained by an observed positive excess volume of mixing. Comparison of the reported phase diagram[13] to various thermodynamic results indicated the results of Hoshino et al.[32] and this work were consistent while the work of Terpilowski[31] showed marked discrepancies. Furthermore, these calculations suggested the enthalpy of fusion of InSb be taken as 5.9 $Kcal_{th}$ $g^{\circ}atom^{-1}$. A new expression for the Gibbs energy of formation of solid InSb was derived with the standard enthalpy and entropy give by -4209 cal_{th} $g^{\circ}atom^{-1}$ and 3.052 cal_{th} $g^{\circ}atom^{-1}K^{-1}$, respectively. This result was shown to be consistent with the available calorimetric work, the reported phase diagram and the activity measurements of this work. Liquid phase X-ray scattering investigations[60,61] suggested the tendency of pairing between In and Sb atoms. This observation was quantified with the aid of a simple statistical model. Thus it may be concluded that the high temperature thermodynamic properties of the liquid In-Sb system are experimentally well-defined.

REFERENCES

1. H. Welker, Z. Naturforsch, 7a, 744 (1952).
2. H. Welker, Z. Naturforsch, 8a, 248 (1953).
3. R.G. Breckenridge, R.F. Blunt, W.R. Hosler, H.P.R. Fredricks, J.H. Becker, and W. Oshinsky, Phys. Rev., 96, 571 (1954).
4. A. Etchells and C.W. Fischer, J. Appl. Phys., 47, 4605 (1976).
5. W.E. Krag, R.J. Phelan, and J.O. Dimmock, J. Appl. Phys., 40, 3661 (1969).
6. A. Heime and H. Pagnia, Appl. Phys., 15, 79 (1978).
7. D.L. Lile, and J.C. Anderson, Solid-State Electron., 12, 735 (1969).
8. H. Sewell and J.C. Anderson, Solid-State Electron., 18, 641 (1975).
9. T. Yoshida, K. Miyazaki, and K. Fujisawa, Jap. J. Appl. Phys., 14, 1987 (1975).
10. E. Spenke, Phys. in uns. Zeit, 6, 134 (1975).
11. F. Nakajima and M. Kobayashi, Jap. J. Appl. Phys., 17, 149 (1978).
12. K. Sakai and J. Sakai, Jap. J. Appl. Phys., 15, 1335 (1976).
13. T.S. Liu and E.A. Peretti, Trans. J. Metals, 3, 791 (1951).
14. S.A. Pogodin and S.A. Dubinskii, Izv. Sektora Fiz. Khim. Analiza, Inst. Obshch. i Neorgan. Khim. Akad. Nauk SSSR, 17, 204 (1949).
15. R.N. Hall, J. Elect. Soc., 110, 385 (1963).
16. V.M. Glasov and D.A. Petrov, Izv. Akad. Nauk SSSR, Otd. Tekhn. Nauk, No. 4, 125 (1958).
17. W.F. Schottky and M.B. Bever, Acta Metallurg., 6, 320 (1958).
18. N.H. Nachtrieb and N. Clement, J. Phys. Chem., 62, 876 (1958).
19. R.H. Cox and M.J. Pool, J. Chem. Eng. Data, 12, 247 (1967).

20. L.A. Mechkovskii, A.A. Savitskii, V.F. Skums, and A.A. Vecher, Russ. J. Phys. Chem., 45, 1143 (1971).

21. C.E. Lundin, R.W. Sullivan, and M.J. Pool, Denver Research Report AFCRL-63-156 (1963).

22. R. Blachnik and A. Schneider, Z. Anorg. Alleg. Chem., 372, 314 (1970).

23. R. Hultgren, P.D. Desai, D.T. Hawkins, M. Gleiser, and K.K. Kelley, Selected Values of the Thermodynamic Properties of Binary Alloys, Am. Soc. Met. (1973).

24. D. Richmond and E.F. Hockings, J. Elec. Soc., 112, 461 (1965).

25. L.D. Lichter and P. Sommelet, Trans. Met. Soc. AIME, 245, 99 (1969).

26. J. Bednar and K. Smirous, Czech. J. Phys., 5, 546 (1955).

27. F.E. Wittig and E. Gehring, Z. Electrochem., 71, 29 (1967).

28. A.A. Vecher, E.I. Voronova, L.A. Mechkovskii, and A.S. Skoropanov, Russ. J. Phys. Chem., 48, 584 (1974).

29. K. Itagaki and A. Yazawa, Nippon Kinzoko Gakkai-Shi, 38, 880 (1975).

30. A. Yazawa, T. Kawashima, and K. Itagaki, J. Japan Inst. Metals, 32, 1288 (1968).

31. J. Terpilowski, Arch. Hutn., 4, 355 (1959).

32. H. Hoshino, Y. Nakamura, M. Shimoji, and K. Niwa, Ber. Bensenges, 69, 114 (1965).

33. D. Chatterji and J.V. Smith, J. Elect. Soc., 120, 770 (1973).

34. D. Chatterji and J.V. Smith, J. Am. Ceram. Soc., 55, 575 (1972).

35. G. Scatchard, Trans. Faraday Soc., 33, 160 (1937).

36. N.P. Mokrovskii and A.R. Regel, Zh. Tekhn. Fiz., 22, 1281 (1952).

37. V.M. Glasov, S.N. Chizhevskaya, and N.N. Glagoleva, Liquid Semiconductors, Plenum Press, New York (1969).

38. P.E. Berthou and R. Tougas, Met. Trans., 1, 2978 (1970).

39. L. Ganovici and I. Ganovici, Rev. Romaine Chim., 14, 1011 (1969).

40. P.J. McGonigal, J.A. Cahill, and A.D. Kirshenbaum, J. Inorg. Nucl. Chem., 24, 1012 (1962).

41. W. Klemm, H. Spitzer, and H. Niermann, Angew. Chem. 72, 985 (1960).

42. A.F. Crawley, Int. Met. Rev., 19, 32 (1974).

43. V.M. Glazov, A.A. Aivazov, and U.I. Timoshenko, Sov. Phys. Solid State, 18, 1236 (1976).

44. M.B. Gitis and I.G. Mikhailov, Sov. Phys. - Acoustics, 11, 372 (1966).

45. O.J. Kleppa, J. Chem. Phys., 18, 1331 (1950).

46. B.N. Osherin, Rev. Romaine Chim., 21, 351 (1976).

47. A.S. Abbasov and K.N. Mamedov, Isv. Akad. Nauk, Azerb. SSR, Ser. Fiz Mat. i Tekhr. Nauk, 3, 86 (1970).

48. A.N. Nikol'skaya, V.A. Geiderikh, Ya.I. Gerasimov, Doklady Akad. Nauk SSSR, 130, 1074 (1959).

49. N.N. Sirota and N.N. Yushkevich, Chemical Bonds in Semiconductors, N.N. Sirota, ed., Consultants Bureau, New York, 95 (1967).

50. J. Terpilowski and W. Trzebiatowski, Bull. Acad. Poln. Sci., Ser. Sci. Chim., 8, 95 (1960).

51. R. Hultgren, P.D. Desai, D.T. Hawkins, M. Gleiser, K.K. Kelley, and D.D. Wagman, Selected Values of the Thermodynamic Properties of the Elements, Am. Soc. Met. (1973).

52. O.J. Kleppa, J. Am. Chem. Soc., 77, 897 (1955).

53. G. De Maria, J. Drowart, and M.G. Inghram, J. Chem. Phys., 31, 1076 (1959).

54. A. Glassner, Argonne National Laboratory Report ANL-5760 (1957).

55. T. Renner, Solid State Elec., 1, 39 (1960).

56. A.K. Jena, M.B. Bever, and M.D. Banus, Trans. Met. Soc. AIME, 239, 1232 (1967).

57. A.K. Jena, M.B. Bever, and M.D. Banus, Trans. Met. Soc. AIME, 239, 725 (1967).

58. A. Schneider, H. Klotz, J. Stendel, and G. Strauss, Pure and Appl. Chem., 2, 13 (1961).

59. S.N. Gadzhiev and K.A. Sharifov, Doklady Akad. Nauk SSSR, 136, 1339 (1961).

60. H. Krebs, H. Weyand and M. Haucke, Angew. Chem. 70, 468 (1958).

61. R. Buschert, I.G Geib, and K. Lark-Horovitz, Bull. Am. Phys. Soc., 1, 111 (1956).

62. L. Garbato and F. Ledda, Thermochimica Acta, 19, 267 (1977).

LIST OF FIGURES

Figure 1. Experimental cell voltages as a function of temperature for cell type III. Least squares line shown.

Figure 2. Experimental cell voltages as a function of temperature for cell type IV. Least squares line shown.

Figure 3. Activities of indium and antimony in the liquid mixture _____, 973 K, this work; ●, this work - gas reference electrode; ■, this work - metal reference electrode; ○, Chatterji and Smith[33]; X, Hoshino et al.[32]; Δ, Terpilowski.[31]

Figure 4. Gibbs energy, enthalpy and entropy of mixing for In-Sb liquid alloys at 973 K. o, this work; ----, Wittig and Gehring[27]; _____, Vecher, et al.[28]; ....., Yazawa et al.[30]

Figure 5. Liquidus temperatures for the In-Sb system calculated from Equations (10) and (12). o, this work; ----, ideal solution _____, experimental results of Liu and Peretti[13] . ΔH_f^o(InSb) was taken as 5900 cal_{th} g°atom^{-1} and ΔH^M from Yazawa et al.[30]

Figure 6. Liquidus temperatures for the In-Sb system calculated from Equations (10) and (12). o, this work; Δ, Terpilowski[31]; □, Hoshino et al.[32]; _____, experimental results of Liu and Peretti.[13]

Figure 7. Liquidus temperatures for the In-Sb system calculated from Equation (11) and the results of this work _____, experimental results of Liu

and Peretti.[13] The standard enthalpy and entropy of formation of InSb(c) taken from; o, Terpilowski and Trzebiatowski[50]; □, Sirota and Yushkevich[49]; Δ, Abbasov and Mamedov[47]; _____, experimental results of Liu and Peretti.[31] ΔH^M from Yazawa et al.[30]

Figure 8. Liquidus temperatures for the In-Sb system calculated from Equation (11) and the emf activity results of; o, Terpilowski[31]; □, Hoshino et al[32]; and the standard enthalpy and entropy of formation of InSb; open, Terpilowski and Trzebiatowski[49]; closed, Abbasov and Mamedov[46]; _____, experimental results of Liu and Peretti.[13]

Figure 9. Standard enthalpy of formation of InSb(c) at 298 K obtained by a third law analysis. a, Abbasov and Mamedov[46]; b, Nikol'skaya et al.[47]; c, Sirota and Yushkevich[48]; d, Terpilowski and Trzebiatowski[49]; e, Hultgren et al.[23]; ---, derived - this work; ....., derived - Terpilowski[31]; ——— -———, derived - Hoshino et al.[32]

Figure 10. Liquidus temperatures for the InSb system calculated from Equations (11) and (21). o, this work; Δ, Terpilowski[31]; □, Hoshino et al.[32]; _____, experimental results of Liu and Peretti.[13]

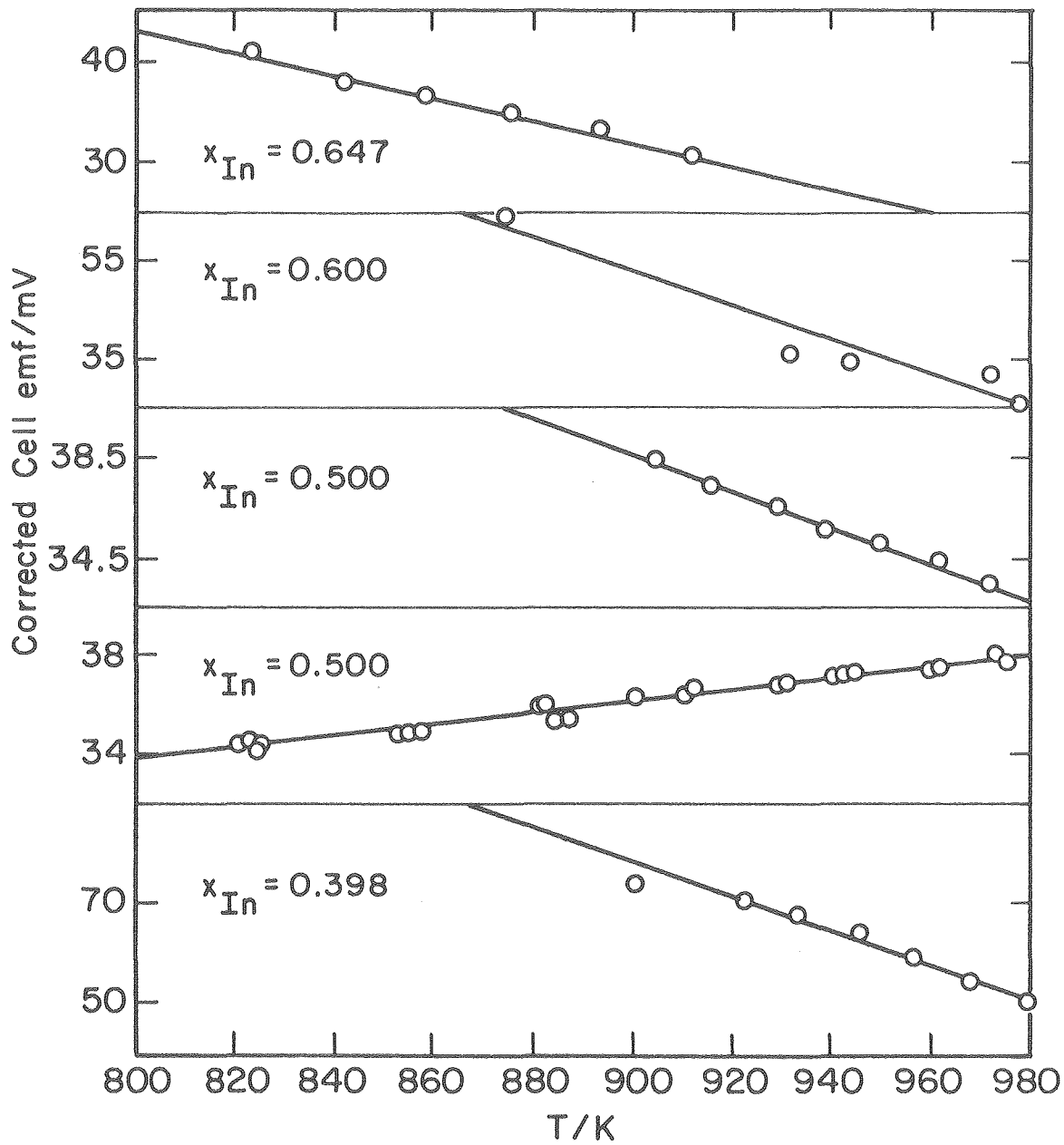

XBL 786-9372

Figure 1.

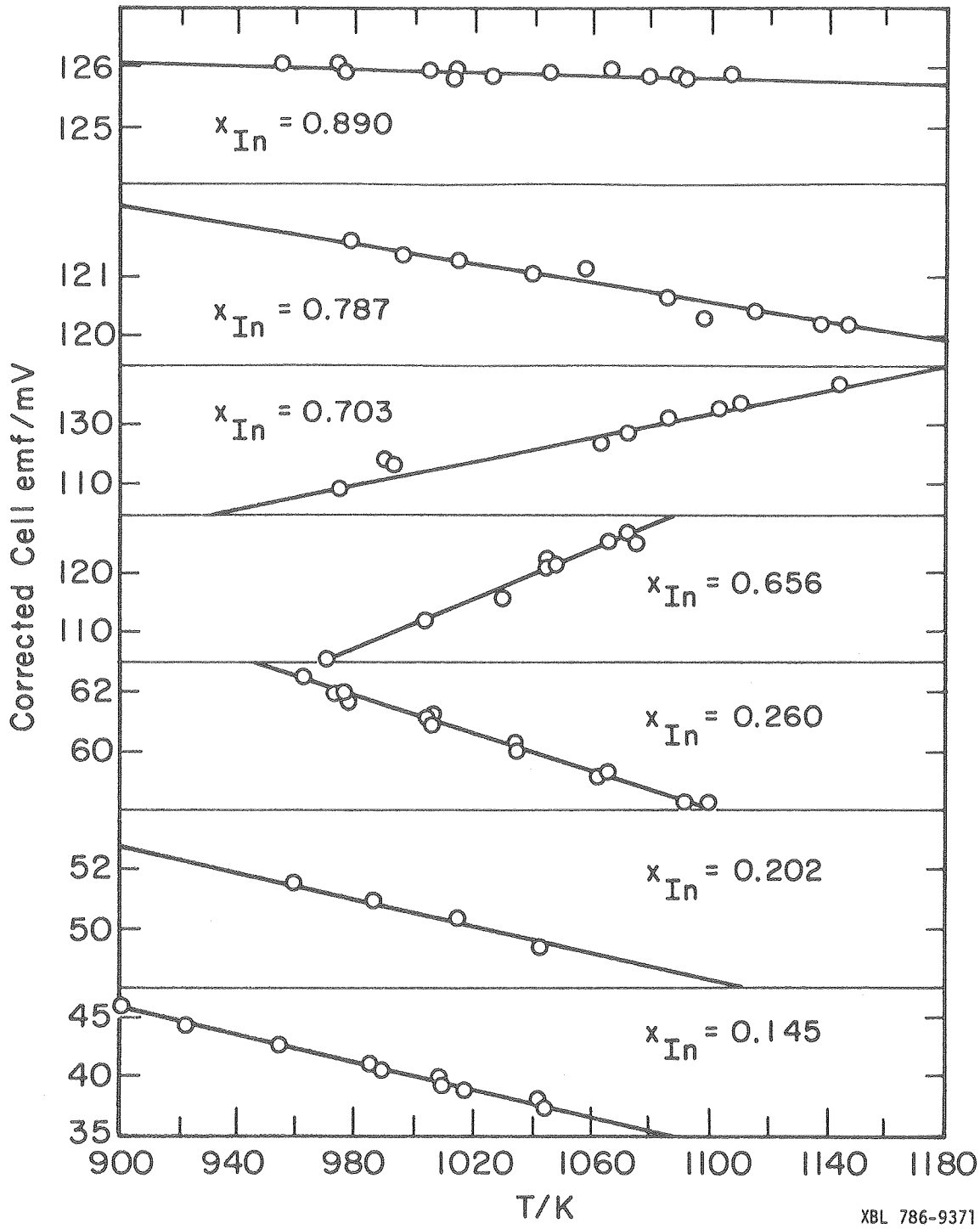
126
125
x_{In} = 0.890
121
120
x_{In} = 0.787
130
110
x_{In} = 0.703
120
110
x_{In} = 0.656
62
60
x_{In} = 0.260
52
50
x_{In} = 0.202
45
40
35
x_{In} = 0.145
Corrected Cell emf/mV
900
940
980
1020
1060
1100
1140
1180
T/K
XBL 786-9371

Figure 2.

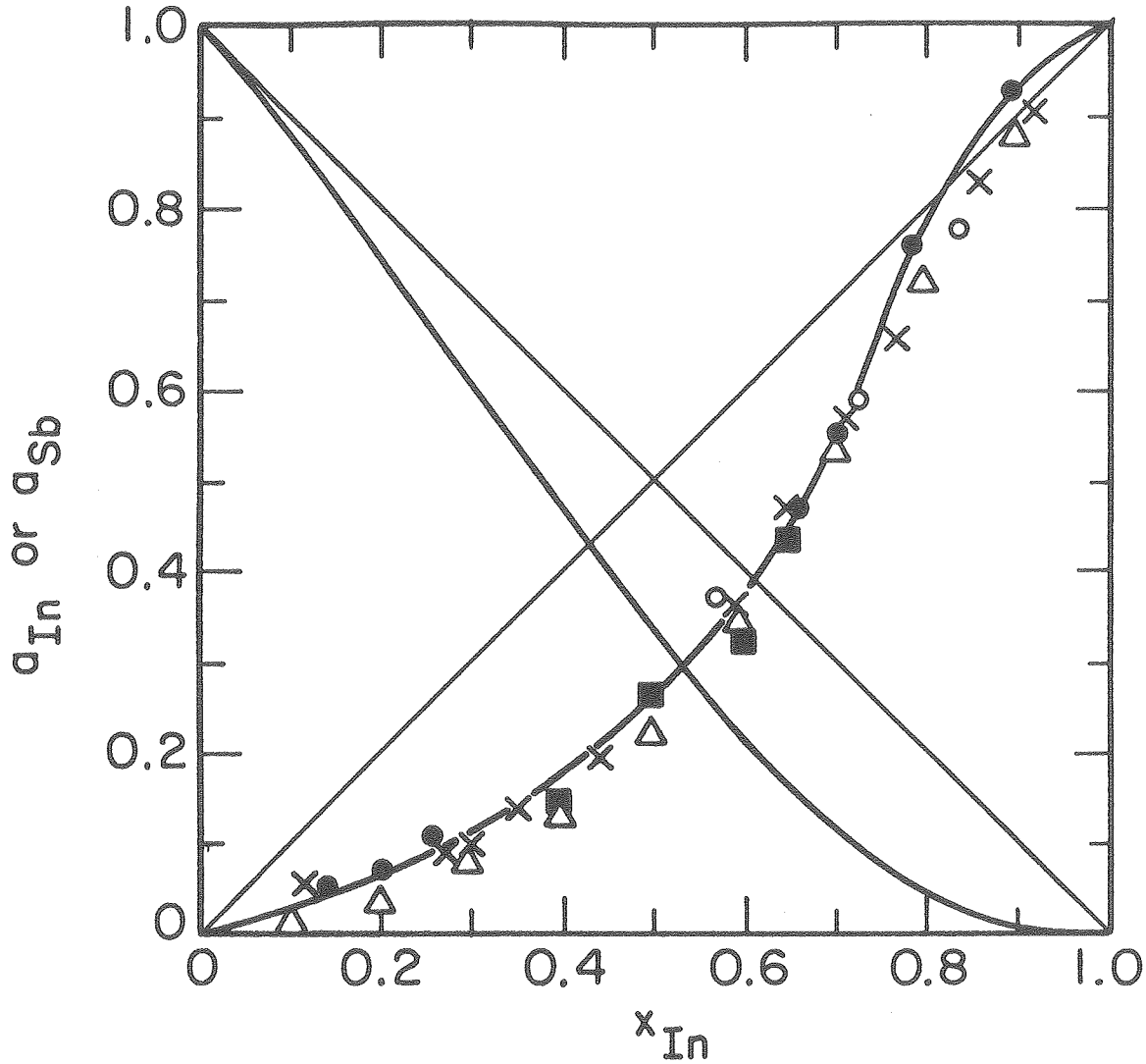

XBL 786-9370

Figure 3.

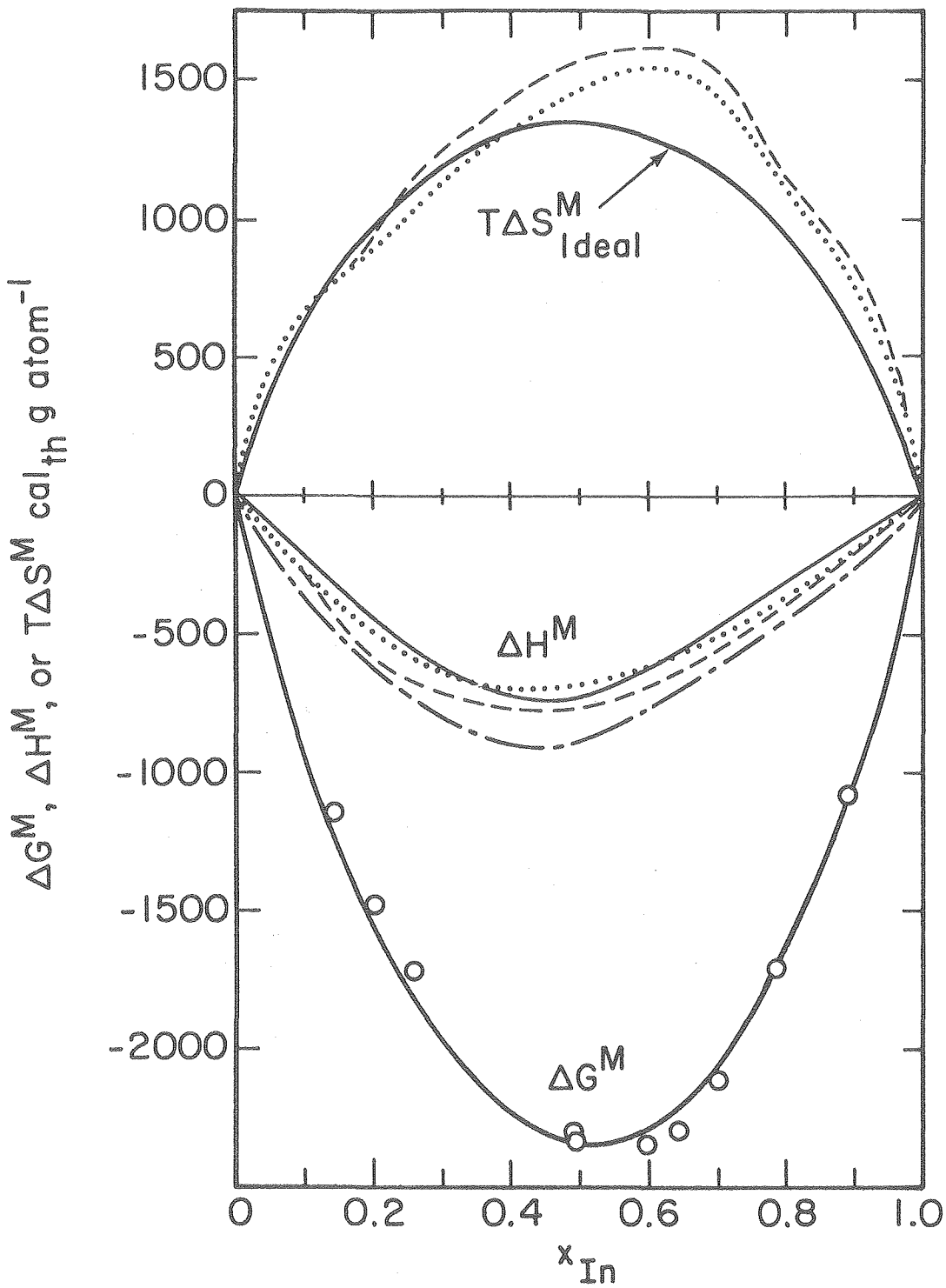

XBL 786-9369

Figure 4.

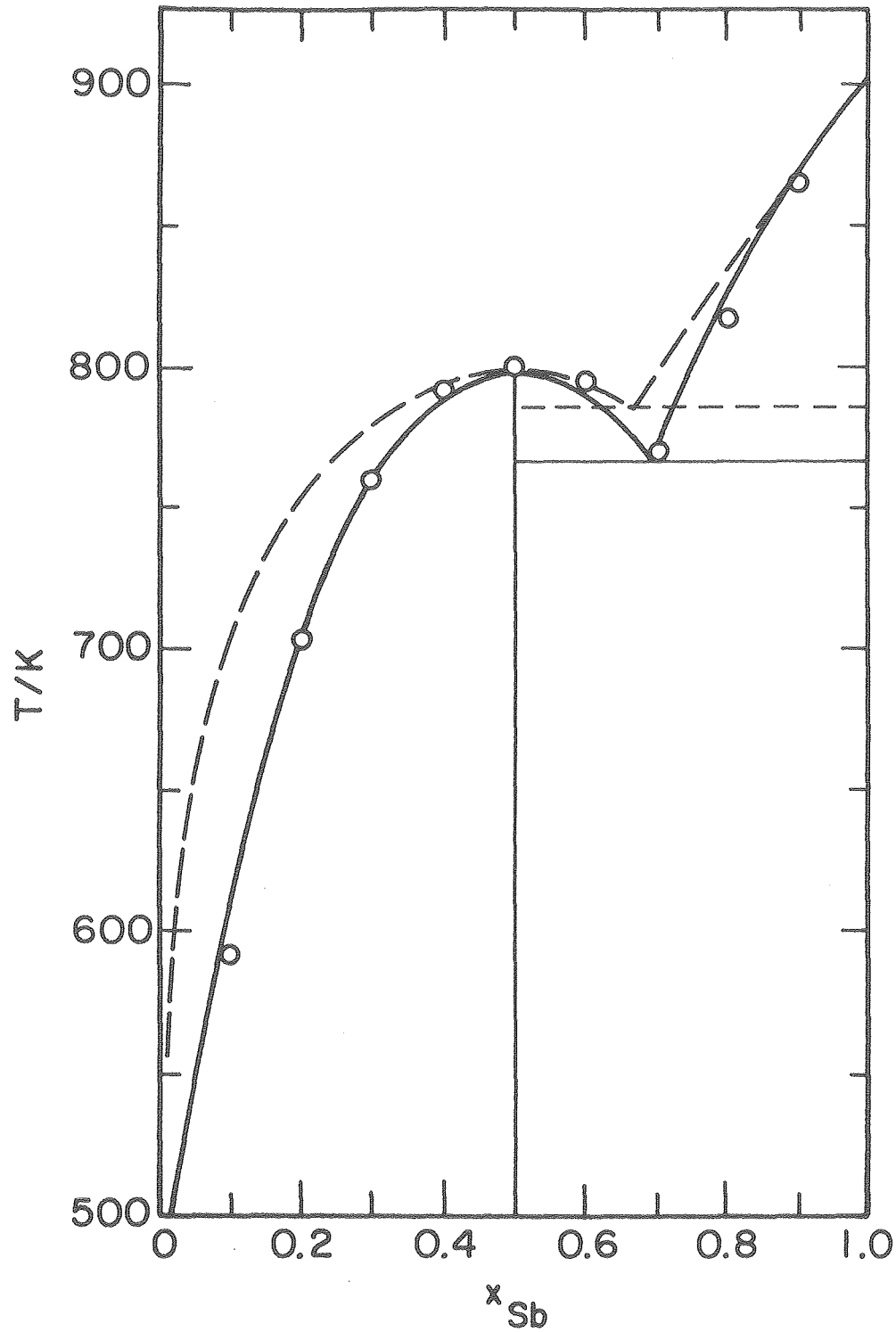

XBL 786-9368

Figure 5.

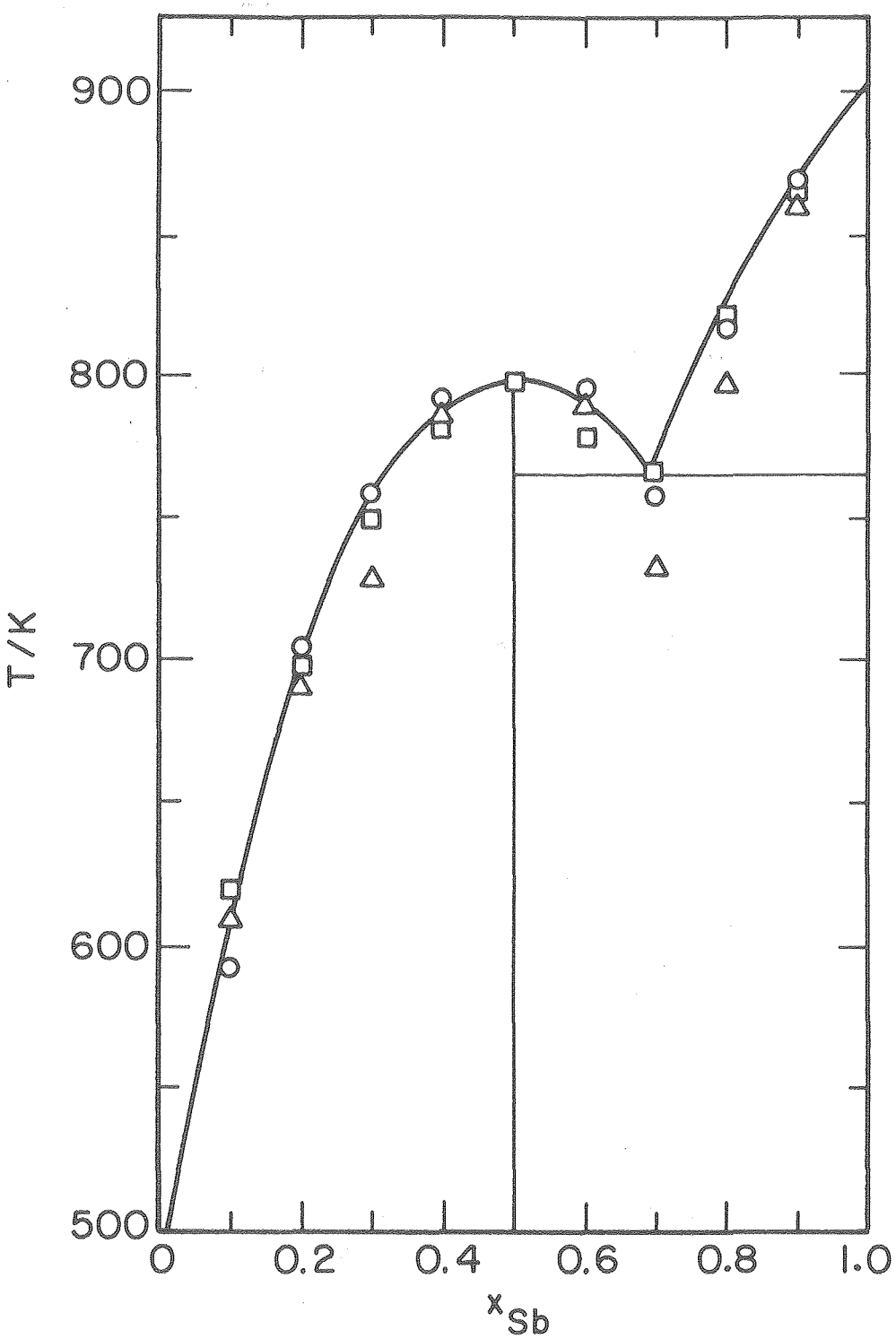

XBL 786-9367

Figure 6.

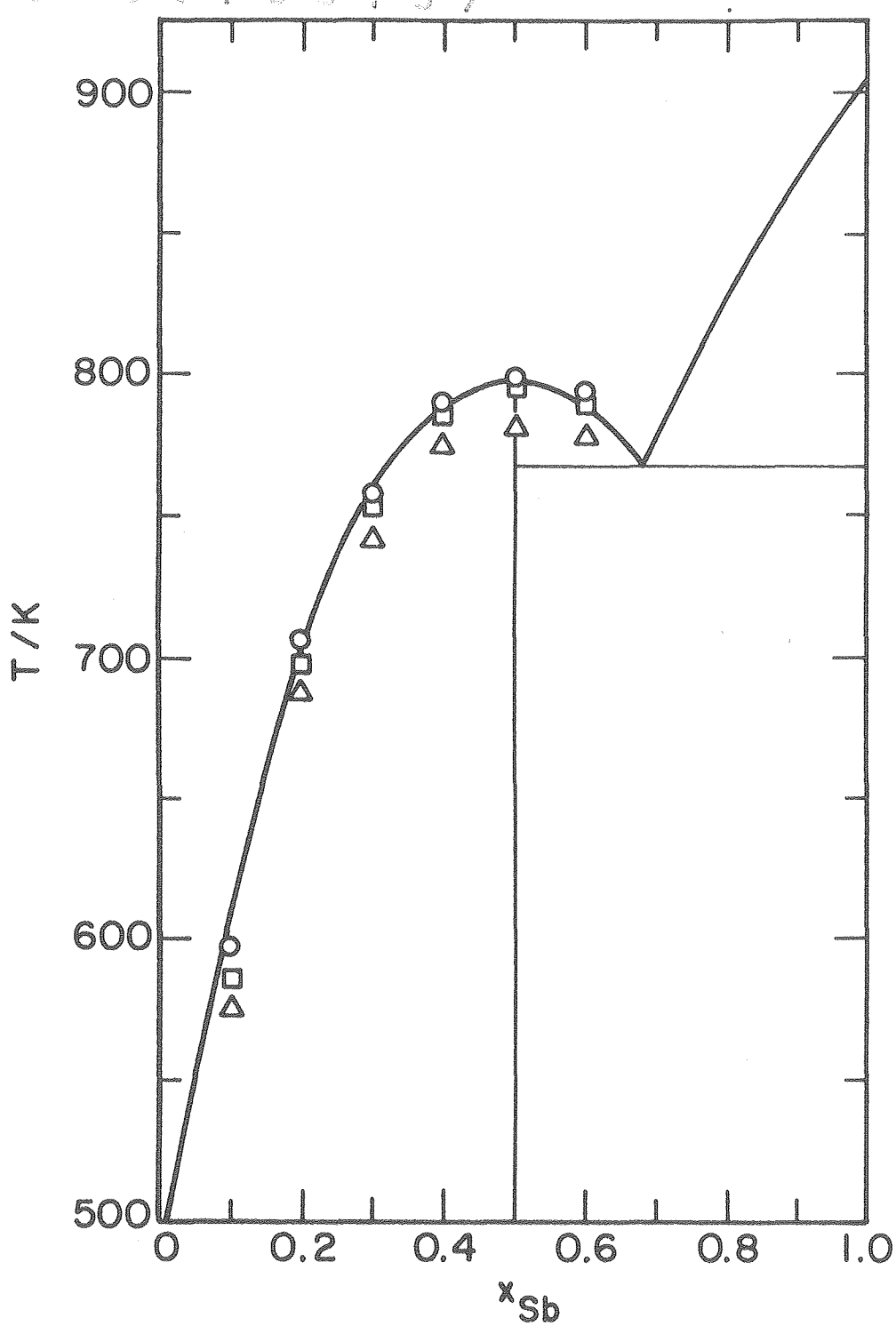

XBL 786-9366

Figure 7.

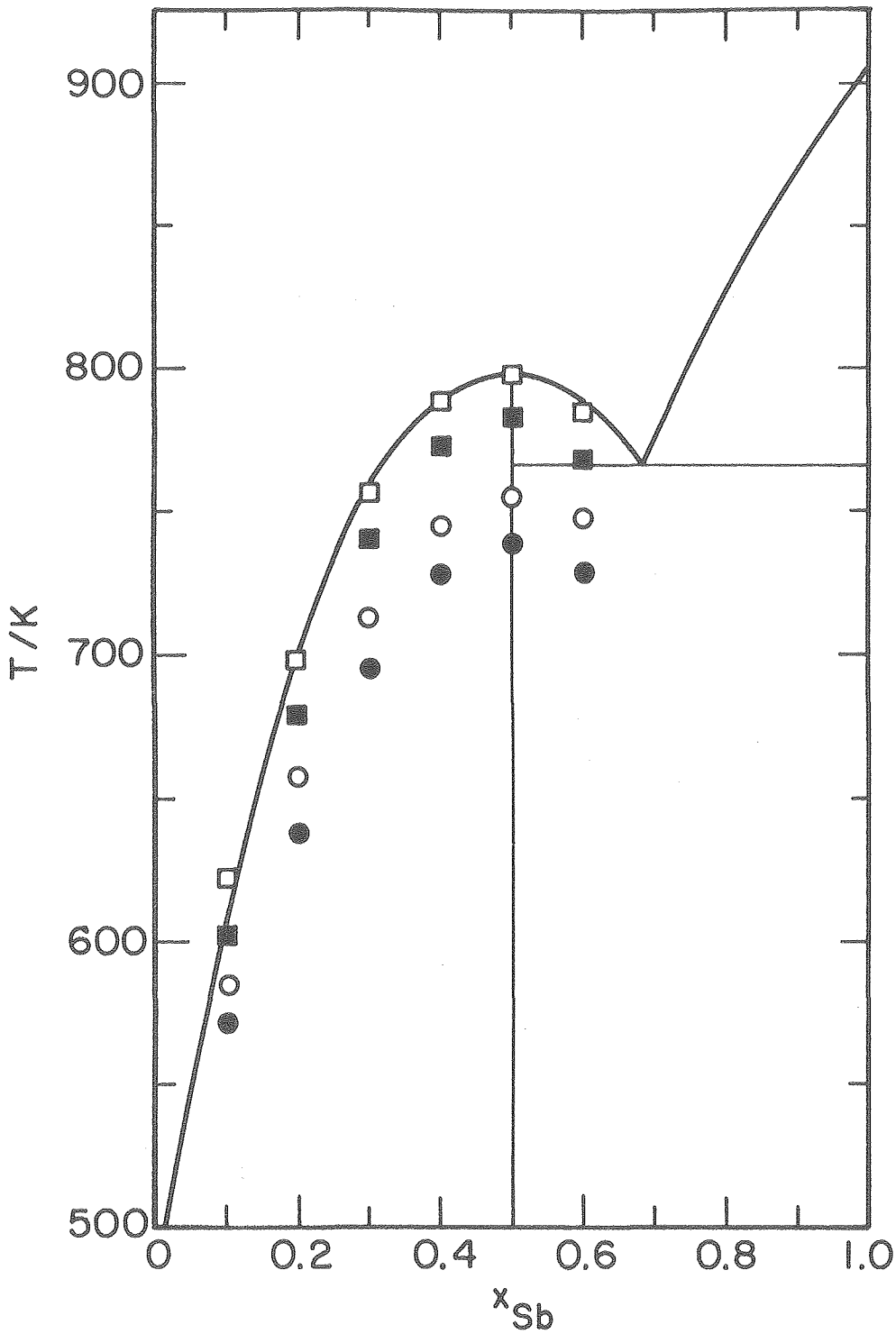

XBL 786-9365

Figure 8.

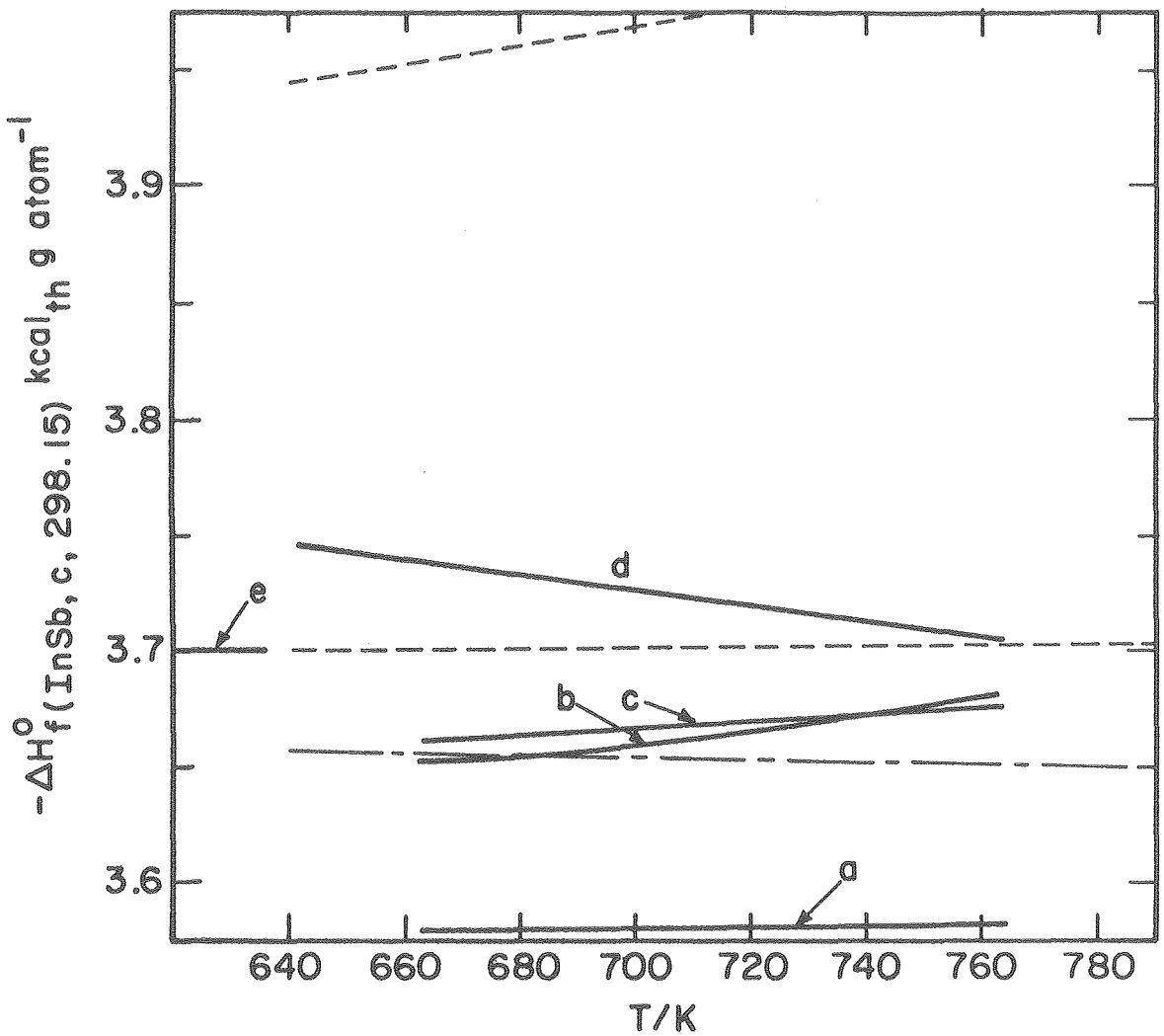

XBL 786-9364

Figure 9.

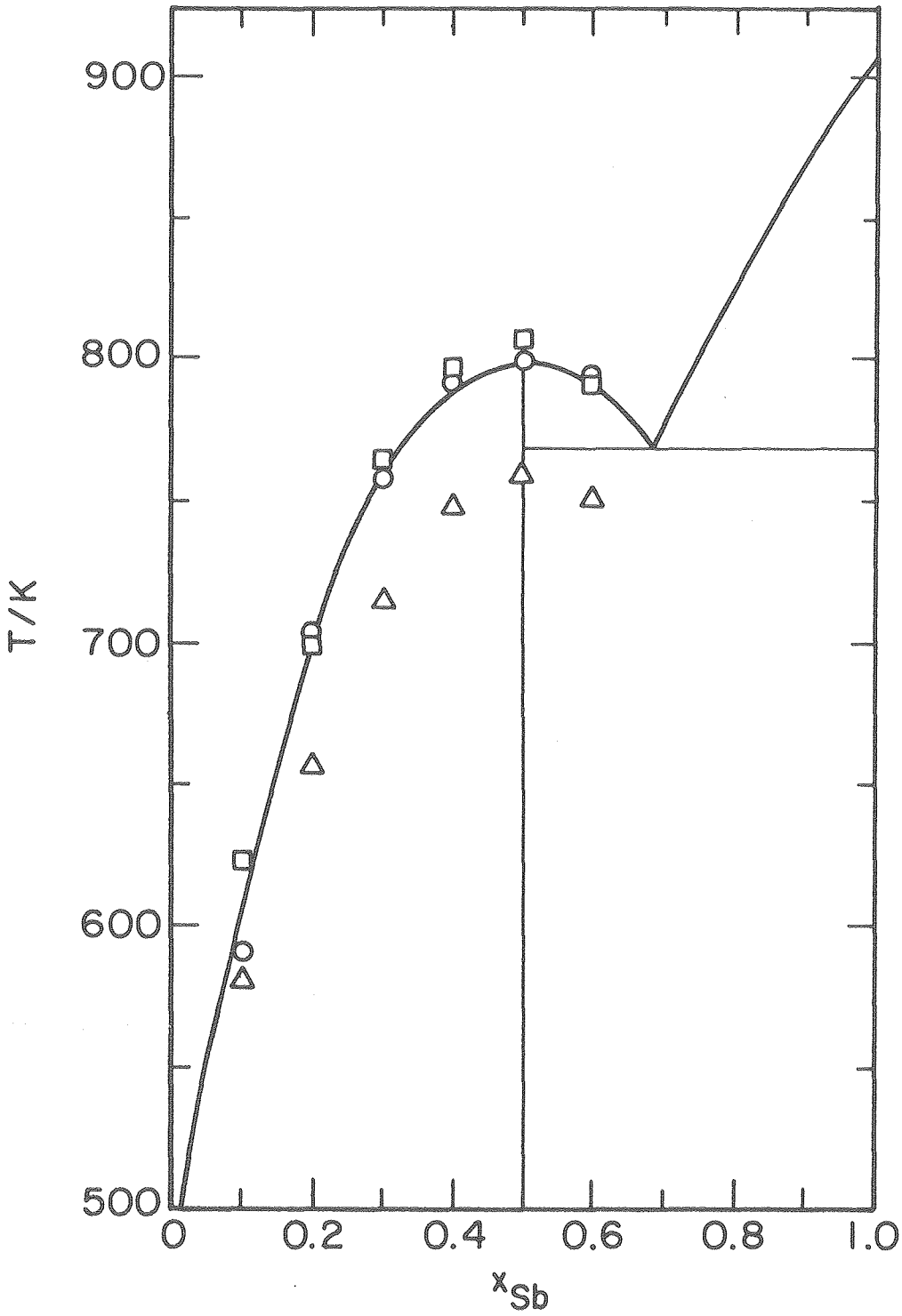

XBL 786-9363

Figure 10.

CHAPTER V. THERMODYNAMICS OF THE GALLIUM - INDIUM SYSTEM

A. INTRODUCTION

The gallium-indium system is currently under considerable investigation primarily as a result of applications of gallium and indium as solvents for liquid phase epitaxial growth of III-V semiconductor films for electronic device application. The binary system Ga-In is metallic and extremely low melting. This system is of importance principally because it constitutes the solvent alloy for the growth of III-V compound solid solutions such as $In_xGa_{1-x}As$, $In_xGa_{1-x}Sb$ and $In_xGa_{1-x}As_yP_{1-y}$ which are stable phases in the In-Ga-As, In-Ga-Sb, and In-Ga-P ternary systems. The arsenide and phosphide ternary compound solid solutions exhibit direct bandgaps in the visible region over a large composition range and provide the designer with both a variable bandgap and lattice parameter. As a result these solid solutions have found applications as solid state luminescence devices.[1-6] The $Ga_xIn_{1-x}Sb$ alloy is of interest due to the observation of Gunn microwave oscillations in this material.[7,8] Ternary III-V semiconductor alloys are generally fabricated by liquid phase epitaxy for which accurate knowledge of the phase diagram is essential.

B. THERMOCHEMISTRY

The high temperature thermochemistry of the Ga-In system has been investigated extensively and presented here is a review of the available literature thermodynamic data and accompanied with a critical assessment of their consistency.

1. Phase Diagram

Lecoq de Boisbaudran,[9] the discoverer of gallium, conducted the first investigation on the Ga-In system in 1885. Hansen[10] constructed a eutectic-type phase diagram for Ga-In alloys, employing the results of Boisbaudran. In 1938 French and coworkers[11], using a thermal method, first measured both liquidus and solidius temperatures throughout the entire composition range. Their results indicate the solid solution range of indium in gallium is zero, while the solid solution range of gallium in indium extends up to 9.5 weight per cent gallium. The system also was found to form a eutectic at a composition of 76 per cent gallium by weight and a temperature of 289 K. The liquidus curve determined by these investigators was uniquely concave - upwards. The constitution of the Ga-In system has also been determined by thermal analysis by Denny and coworkers[12] who found a eutectic composition of 76 weight per cent gallium at 288.9 K. The liquidus curve measured was found to contain an inflection point. Using an electrical resistance-temperature method, Svirbley and Selis[13] measured the Ga-In phase diagram and essentially reproduced the results of Denny and coworkers.[12] This work and that of French et al.[11] are the only investigations of the solidus line on the indium-rich side of the phase diagram. More recently Heubner and Wincierz[14] and Predel and Stein[15] have reported experimental liquidus temperatures showing excellent consistency for $x_{In} > 0.6$ but showing slight discrepancies from the inflection point to the eutectic composition. Finally, Shuray et al.[16] have measured liquidus temperatures up to 40 weight per cent indium. The results of several of the phase diagram determinations

are condensed in Figure 1. Table 1 contains a summary of the reported eutectic temperatures and compositions.

2. Solution Thermodynamics

Several investigations of the solution thermodynamic properties of liquid phase Ga-In solutions have been performed. Bros[18] measured low temperature (423 K) integral enthalpies of mixing and found positive and nearly symmetric values of ΔH^M exhibiting a maximum value of 256 cal_{th} g°atom^{-1} at an equimolar composition. Bros and coworkers[19] repeated these measurements with a microcalorimeter at a higher temperature (742 K) and the results indicated a maximum ΔH^M of 265 cal_{th} g°atom^{-1} occurring again at an equimolar composition. It is significant that these results showed no temperature dependence in the measured integral enthalpy of mixing. Mechkovskii and Veecher[20] reported the following expression for ΔH^M based on a quantitative differential thermal analysis of the system:

$$\Delta H^M = 1039\ (\pm 43)\ x_{Ga} x_{Sb}\ . \qquad (1)$$

Predel and Stein[15] using a high temperature calorimeter found somewhat higher heats of mixing but the scattering exhibited in the data is large enough for their results to be consistent with the other investigations. Finally Ansara et al.[34] reported measurements at the highest temperature (995 K) and their results showed nearly symmetrical behavior with a maximum enthalpy of mixing of 265 cal g°atom^{-1} at the equimolar composition. The results for the various enthalpy of mixing data are shown graphically in Figure 2.

Table 1. Summary of eutectic compositions and temperatures for the Ga-In system reported by several investigators.

x_{Ga}	T/K	reference
0.835	288.9	10
0.839	289.2	11
0.839	288.9	12
0.837	288.9	13
0.875	289.1	15
0.860	289.0	16
0.858	288.9	17

Svirbeley and Read[21] first reported component activities for the binary liquid solution. These results were calculated from emf measurements on the Zn-In-Ga ternary system. The gallium activity exhibited strong positive deviations from Raoult's law while the indium activity showed negative deviations for $x_{In} > 0.5$. Macur et al.[22] employing a Knudsen-cell effusion technique measured In activities at three temperatures and several compositions. Positive deviations throughout the entire composition range were found and the indium activity coefficient, γ_{In} was suggested to be calculated by

$$\log_{10}\gamma_{In} = 0.42\ (1 - x_{In})^2 \qquad (2)$$

at 1269 K. Component activities were also measured with a more accurate solid state electrochemical technique by Klinedinst et al.[23] and Pong and Donaghey.[24] Klinedinst et al[23] determined positive deviations in the temperature range 1073 to 1223 K and proposed that the gallium activity coefficient can be calculated from

$$\ln \gamma_{Ga} = (-8.9093 \times 10^{-4} + 1.0945 \times 10^{-3} x_{In} + 800.42/T - 135.41 x_{In}/T)(1-x_{Ga})^2 \qquad (3)$$

Four indium-rich compositions were measured by Pong and Donaghey[24] in the same temperature range and found slightly more positive deviations that are described by the following expression for the gallium activity coefficient

$$\ln \gamma_{Ga} = (0.2862 + 0.0352\ x_{Ga} + 398.3/T + 220.0\ x_{Ga}/T)(1 - x_{Ga})^2 \quad (4)$$

Using numerical techniques with the reported enthalpy of mixing and the phase diagram Rao and Tiller[25] determined the following expression for the In activity coefficient

$$\ln \gamma_{In} = (-0.258 + 0.497\ x_{Ga} + 513.5/T)(1 - x_{In})^2 \quad (5)$$

The activity coefficient here was made to match the enthalpy of mixing reported by Bros[18] and the liquidus measured by Svirbley and Selis.[13] Figure 3 shows the component activities as a function of the gallium mole fraction and summarizes these results. Shown in Figure 4 is the integral Gibbs energy of mixing at 1223 K while Figure 5 shows the excess entropy of mixing calculated at 1223 K using the enthalpy of mixing of Bros.[18] As can be seen, the system shows a small positive excess entropy of mixing.

Unfortunately no thermodynamic data exists for the solid solution in the indium-rich side of the phase diagram. The only thermodynamic investigation reported is a measurement of the enthalpy of fusion at the eutectic composition.[26]

C. DISCUSSION

1. Enthalpy of Mixing

The enthalpy of mixing data reported in the literature[15,18,19] was fit to the following expression with good accuracy

$$\Delta H^M = x_{Ga}x_{In}(a_0 + a_1x_{In} + a_2x_{In}^2) \ . \qquad (6)$$

The values of the constants are listed in Table 2. These results all show excellent consistency between different studies, and the results of Bros[18] were taken as correct and used for all following calculations. Also shown in Table 2 are the values of the constants suggested by the other two available studies.[20,34]

2. Phase Diagram

Though there have been numerous determinations of the In-Ga phase diagram the results near the eutectic composition show considerable scatter. Also, as pointed out by Rao and Tiller,[25] the solidus temperatures are inconsistent with the observed liquidus. This is probably due to the low temperatures involved and the subsequent slow rates of equilibration as exemplified in the similar Ga-Zn system.[27] Combining these conclusions with lack of thermodynamic information for the solid solution indicates that the numerical results of Rao and Tiller[25] provide the best description of the Ga-In solid solution.

3. Gibbs Energy

There has been three determinations of liquid phase component activities[22-24] of which only one contained measurement throughout the entire composition range. Since there is no information available

Table 2. Summary of constants for calculating the enthalpy of mixing in Ga-In alloys
$\Delta H^M = x_{Ga}x_{In}(a_0 + a_1x_{In} + a_2x_{In}^2)cal_{th}\ g^{\cdot}atom^{-1}$.

a_o	a_1	a_2	reference
1458	-1059	800	15
1103	- 195	252	18
951	337	-311	19
1039	0	0	20
1060	0	0	24

on the Ga-In solid solution in the In-rich region, a consistency test involving a calculation of the liquidus temperatures cannot be performed in the range of $x_{Ga} < 0.84$. However, it has been reported that In shows negligible solubility in Ga.[13] Therefore, the Ga-rich portion of the phase diagram can be calculated by the expression developed in Appendix III and given by

$$T_\ell = \frac{\Delta H_f^c(Ga) + \Delta \overline{H}_{Ga}(x_{Ga})}{\Delta S_f^c(Ga) + \Delta \overline{S}_{Ga}(x_{Ga})} \qquad (7)$$

where $\Delta H_f^c(Ga)$ and $\Delta S_f^c(Ga)$ are the enthalpy and entropy of fusion of pure Ga and taken as 1336 cal_{th} g°atom^{-1} and 4.411 cal_{th} g°atom$^{-1}K^{-1}$,[28] respectively and $\Delta \overline{H}_{Ga}(x_{Ga})$ and $\Delta \overline{S}_{Ga}(x_{Ga})$ are the partial molar enthalpy and entropy of gallium. In this calculation the partial molar enthalpy was taken from Equation (6) and the constants computed from the work of Bros[18] while the partial molar entropy was calculated with the expressions reported by the various activity determinations and at a temperature of 1223 K. The results of these calculations are presented in Figure 6 along with the experimental phase diagram. The activity measurements of Klinedinst et al.[23] are found to nearly reproduce the experimental liquidus temperatures of Svirbley and Selis[13] while the expression for the gallium activity suggested by Macur et al.[22] yields a eutectic composition of $x_{Ga} = 0.894$ and is clearly in error. Employing the extrapolated results of Pong and Donaghey[24] and the numerical solution of Rao and Tiller[25] one obtains nearly identical results for the phase diagram liquidus temperature fit, and a eutectic

composition x_{Ga} = 0.86 which is near the upper limit of the reported range of the eutectic composition as shown in Table 2. It should also be pointed out the concave-upward curvature of the liquidus curve is indeed an unusual case and that the reported liqudus does show both cases.

4. Volume of Mixing

The Ga-In system is one of the few systems for which experimental data on the volume of mixing exists. Using an aerometric method Khokonov and coworkers[29] measured the density of Ga-In solutions at 473 K over the entire composition range. The excess volume of mixing was calculated using their results and is shown in Figure 7. As can be seen, the system shows a small positive excess volume of mixing and having a maximum value of 0.06 cc g°atom^{-1}. The reported error in the density measurement is 0.10 per cent and this translates into a maximum tolerance of 0.016 cc g°atom^{-1}, thus the scatter shown is expected. Following the reasoning outlined in Chapters III and IV, this volume of mixing can be related to the corresponding excess entropy and enthalpy of mixing. Table 3 shows these results using an excess volume of 0.06 cc g°atom^{-1} and the enthalpy of mixing reported by Bros[18] and ΔS^M calculated with the results of Klinedinst et al.[23] Values for the volume coefficient of expansion and isothermal compressibility were taken from the literature.[30-32] The excess volume, enthalpy and entropy of mixing are dependent upon the changes of the bonding relationships and the atomic radii difference of the alloy partners. Atom

radii differences, which imply a considerable strain, produce a positive enthalpy of mixing.

With strong interactions between unequal atom types, strong negative mixing enthalpies occur. X-ray scattering experiments[33] have indicated no unlike atom pairing and have even suggested the existence of micro-regions of pure components at low temperatures. Thus these concepts are consistent with the observed positive excess entropy, enthalpy and volume of mixing.

5. Short Range Order

Following the analysis presented in Appendix IV and applied in Chapters III and IV short range order parameters were calculated. The results of these calculations are shown in Table 4 using both the activity measurements of Klinedinst et al.[23] and Pong and Donaghey.[24] The enthalpy of mixing of Bros[18] was used and the temperature of calculation was 1223 K.

As expected these results indicate a small preference for pairing of like atoms and shows a maximum at the equimolar concentration. It is also seen that the term j(x) is nearly zero and the assumption of a linear g(T) is consistent with the experimental thermodynamic quantities. These conclusions are in agreement with the symmetrical nature of the enthalpy and entropy of mixing.

Table 3. Volume contribution to the excess entropy and enthalpy of mixing a liquid equimolar mixture of In-Ga at 1223 K.

$\Delta S^E/\Delta V^E$ * $cal_{th}\ cm^{-3}K^{-1}$	α/β_T ** $cal_{th}\ cm^{-3}K^{-1}$	$\Delta H^M/\Delta V^E$ *** $Kcal_{th}\ cm^{-3}$	$T\ \alpha/\beta_T$** $Kcal_{th}\ cm^{-3}$
0.91	0.49	4.54	0.6

* calculated from data of reference 23 and 29
** calculated from data of reference 30 to 32
*** calculated from data of reference 18 and 29

0 0 0 0 5 1 0 0 1 6 5

Table 4. Short range order parameter for the Ga-In system at 1223 K.*

	x_{Ga}	α		$N_o(\mu+j(x))$ $cal_{th}\ g^{\circ}atom^{-1}$		$N_o\bar{g}$ $cal_{th}\ g^{\circ}atom^{-1}K^{-1}$	
reference		24	23	24	23	24	23
	0.1	0.017	0.016	185	184	0.039	0.021
	0.2	0.030	0.026	185	184	0.034	0.009
	0.3	0.039	0.034	185	184	0.032	0.009
	0.4	0.044	0.038	186	185	0.031	0.005
	0.5	0.047	0.040	187	185	0.034	0.008
	0.6	0.046	0.039	188	186	0.037	0.009
	0.7	0.042	0.036	190	188	0.042	0.014
	0.8	0.033	0.028	191	190	0.047	0.020
	0.9	0.019	0.015	193	192	0.057	0.009

*cal_{th} = 4.184 J

D. CONCLUSION

The experimental information pertinent to the phase equilibria in the Ga-In system has been surveyed in order to ascertain their consistency and to develop a thermodynamic model useful in predicting multicomponent phase equilibria. Though several determinations of the phase diagram have been made, there is still some discrepancy near the eutectic composition. The reported solidus is considered to be in error probably due to unusually long times required for equilibration.

The experimental liquid phase enthalpy of mixing shows excellent agreement among the various studies and is positive and nearly symmetric in nature. The enthalpy of mixing can also be considered to be temperature independent. The Gibbs energies reported by Svirbely and Read[21] and Macur et al.[22] were found to be inconsistent with the liquidus temperatures reported while the high temperature measurements of Klinedinst et al.[23] and Pong and Donaghey[24] were found to be consistent. In addition, the tendency for like atom pairing was quantified with a simple statistical model. The degree of pairing was found to be small as expected.

REFERENCES

1. C. Hilsum, Proc. Seventh Intenat. Conf. Phys. Semiconductors, Paris, 1027 (1864).

2. M.R. Lorentz, W. Reuter, W.P. Dumke, R.J. Chieotka, G.D. Pettit, and J.M. Woodall, Appl. Phys. Letters, 13, 421 (1968).

3. G.M. Blom, J. Electrochem. Soc., 118, 1834 (1971).

4. I.V. Bodnar, E.E. Matyas, and L.A. Makovetskaya, Phys. Stat. Sol. 36(a), K141 (1976).

5. Yu.B. Bolkhovityanov and H.B. Zembatov, J. Crystal Growth, 37, 101 (1977).

6. G.A. Antypas, J. Electrochem. Soc., 117, 1393 (1970).

7. J.C. MacGroddy, M.R. Lorentz, and T.S. Plaskett, Solid State Commun., 7, 901 (1969).

8. C. Hilsum and A.D. Rees, Elect. Letters, 6, 277 (1970).

9. L. de Boisbaudran, Compt. rend., 100, 701 (1885).

10. M. Hansen, Aufbau der Zweistofflegierungen, (1936).

11. S.J. French, D.J. Saunders and G.W. Ingle, J. Phys. Chem., 42, 265 (1938).

12. J.P. Denny, J.H. Hamilton, and J.R. Lewis, Trans. AIME, 194, 39 (1952).

13. W.J. Svirbely and S.M. Selis, J. Phys. Chem., 42, 33 (1954).

14. U. Heubner and P. Wincierz, Metall., 20, 703 (1966).

15. B. Predel and D.W. Stein, J. Less-Common Metals, 18, 49 (1969).

16. P.E. Shuray, V.N. Danilin, and I.T. Sryvalin, Zh. Fiz. Khim., 48, 1325 (1974).

17. F.H. Hayes and O. Kubaschewski, J. Inst. Metals, 97, 381 (1969).

18. J.P. Bros, Compt. rend. C, 263, 977 (1966).

19. J.P. Bros, R. Castanet, and M. Laffite, Compt. rend. C, 264, 184 (1967).

20. L.A. Mechkovski and A.A. Vecher, Russ. J. Phys. Chem., 43, 751 (1969).

21. W.J. Svirbely nd S.M. Read, J. Phys. Chem., 66, 658 (1962).

22. G.J. Macur, R.K. Edwards and P.G. Wahlbech, J. Phys. Chem., 72, 1047 (1968).

23. K.A. Klinedinst, M.W. Rao, and D.A. Stevenson, J. Electrochem. Soc., 119, 1261 (1972).

24. R. Pong and L.F. Donaghey, J. Chem. Eng. Data, 21, 370 (1976).

25. M.V. Rao and W.A. Tiller, J. Mat. Sci., 7, 14 (1972).

26. L.S. Topchyyan, D.M. Zakharov, R.B. Lyudvigov, and M.I. Orvelashvili, Russ. J. Phys. Chem., 47, 158 (1973).

27. O. Kubaschewski and T.G. Chart, J. Inst. Metals, 93, 329 (1964-5).

28. R. Hultgren, P.D. Desai, D.T. Hawkins, M. Gleiser, K.K. Kelley, and D.D. Wagman, Selected Values of the Thermodynamic Properties of the Elements, Am. Soc. Metals (1973).

29. Kh.B. Khokonov, B.B. Akhigirov, and S.N. Zadumkin, Ind. Lab., 40, 56 (1974).

30. P.E. Berthou and R. Tougas, Met. Trans., 1, 2978 (1978).

31. L. Ganovici and I. Ganovici, Re. Romaine Chim., 14, 1011 (1969).

32. M.B. Gitis and I. G. Mikhailov, Sov. Phys. - Acoustics, 11, 372 (1966).

33. A.V. Romanova and B.A. Melnik, Russ. Metall., 6, 99 (1970).

34. I. Ansara, M. Gambino, and J.P. Bros, J. Crystal Growth, 32, 101 (1976).

0 0 1 0 5 1 0 5 1 6 7

LIST OF FIGURES

Figure 1. The Ga-In phase diagram. ____, French et al.[11]; ----, Denny et al[12]; o, liqudus of Svirbley and Selis[13], ●, solidus of Svirbley and Selis[13]; □, liquidus of Heubner and Wincierz[14]; ■, solidus of Huebner and Wincierz[14]; ——— - ———, Predel and Stein[15]; △, Hayes and Kubaschewski.[17]

Figure 2. Enthalpy of mixing liquid Ga-In. ——— - ———, Predel and Stein[15]; _____, Bros[18]; ----, Mechkovski and Vecher.[20]

Figure 3. Gallium and indium activities in the liquid phase. --- Svirbely and Read[21] (743 K); ■, Macur et al.[22] (1269 K); o, Klinedinst et al.[23] (1223 K); , Pong and Donaghey[24] (1223K); ....., Rao and Tiller[25] (1223K).

Figure 4. Gibbs energy of mixing Ga and In at 1223 K. ---, Macur et al.[22]; ——— - ———, Klinedinst et al.[23]; _____, Pong and Donaghey[24]; ....., Rao and Tiller[25].

Figure 5. Excess entropy of mixing in the Ga-In system as a function of the gallium mole fraction at 1223 K. ----, Macur et al.[22]; ——— - ———, Klinedinst et al.[23]; _____, Pong and Donaghey[24].

Figure 6. The gallium rich portion of the Ga-In phase diagram. Experimental results o, Svirbely and Selis[13]; Δ, Shuray et al.[16] Liquidus temperatures calculated from equation (7), ΔH^M of Bros[18] and the Gibbs energy taken from: ----,

Macur et al.[22]; ——— - ———, Klinedinst et al.[23];

———, Pong and Donaghey[24]; ....., Rao and Tiller.[25]

Figure 7. The excess volume of mixing in the Ga-In system versus the indium mole fraction.[33]

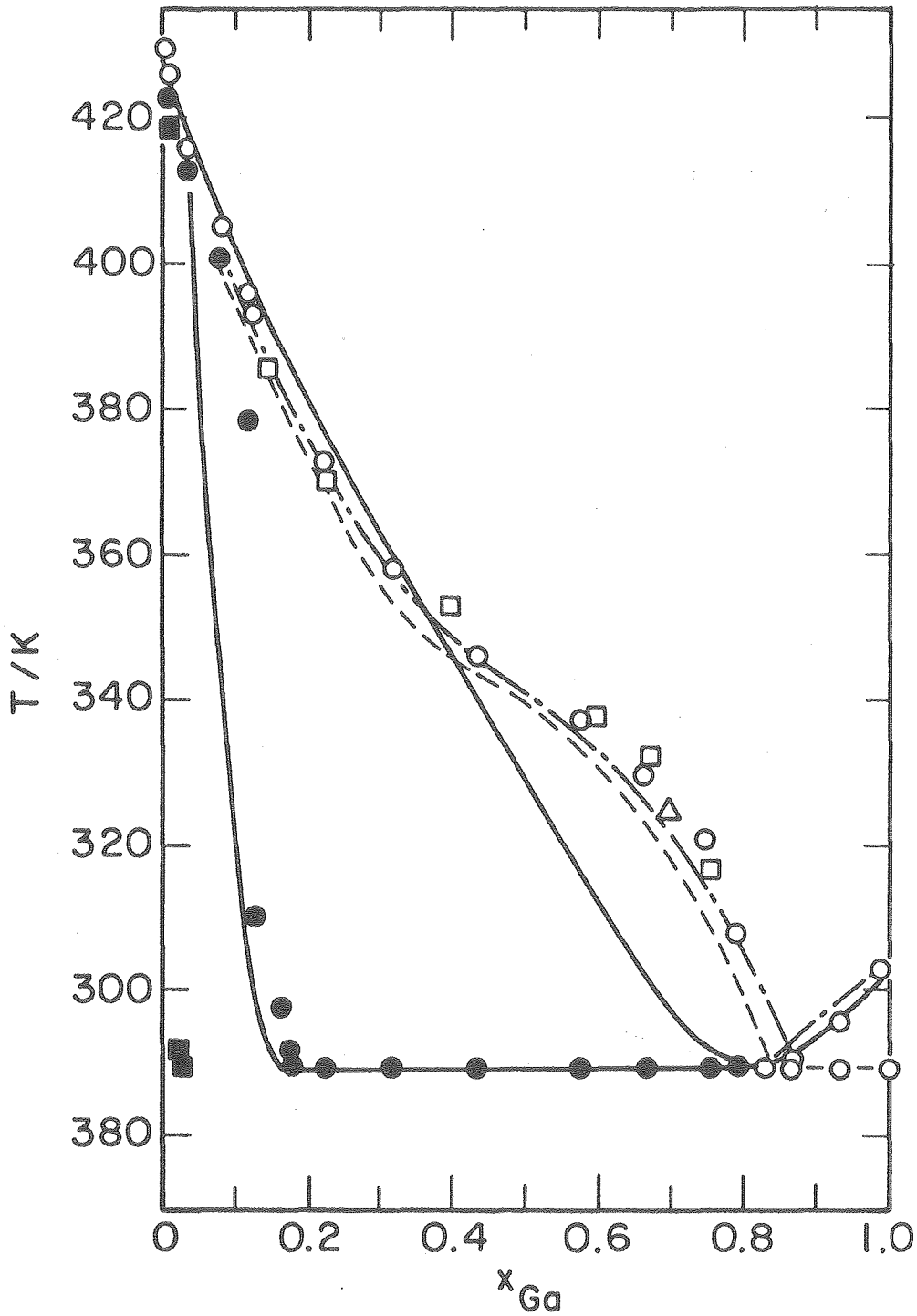

XBL 787-9544

Figure 1.

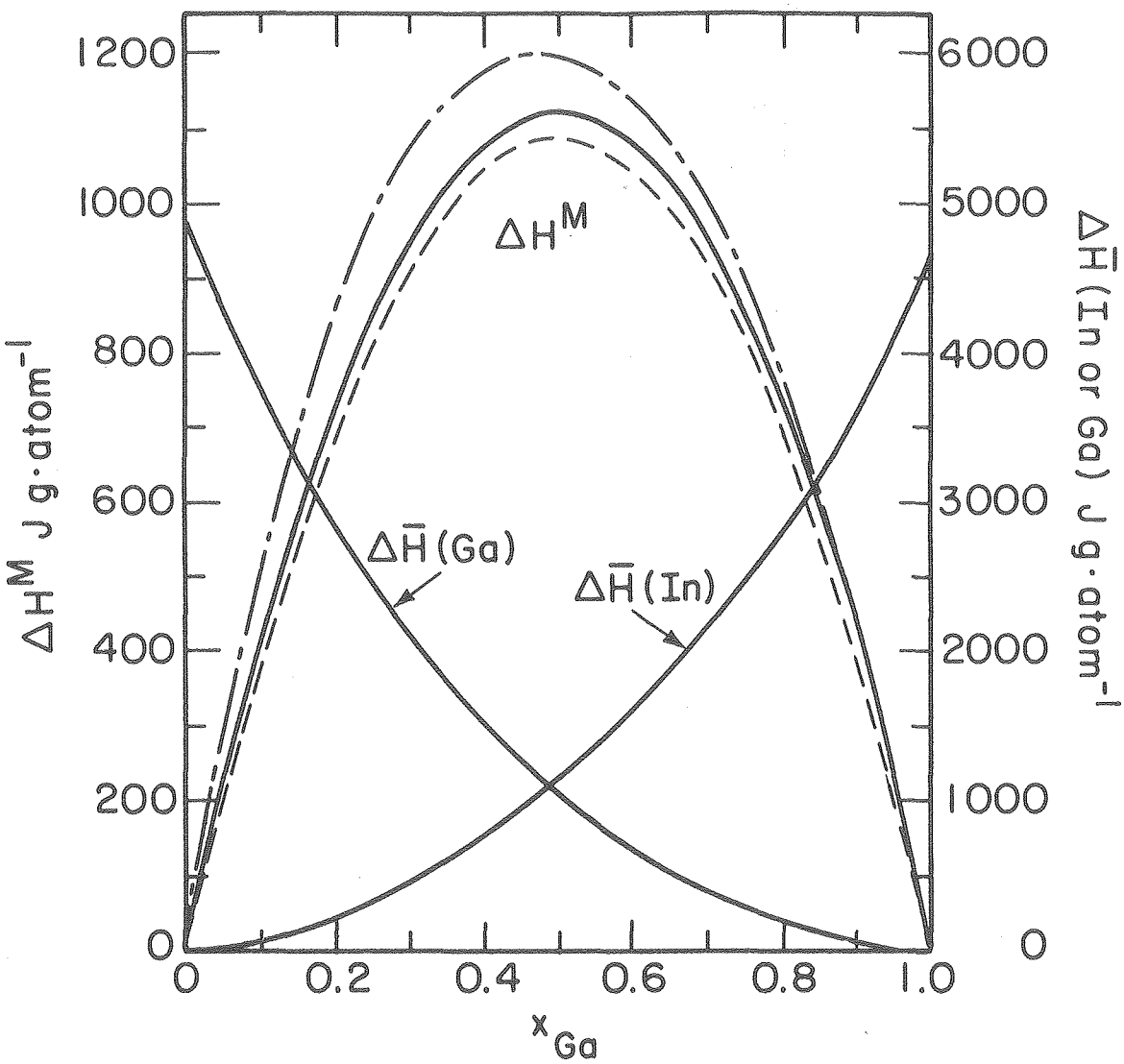

XBL 787-9546

Figure 2.

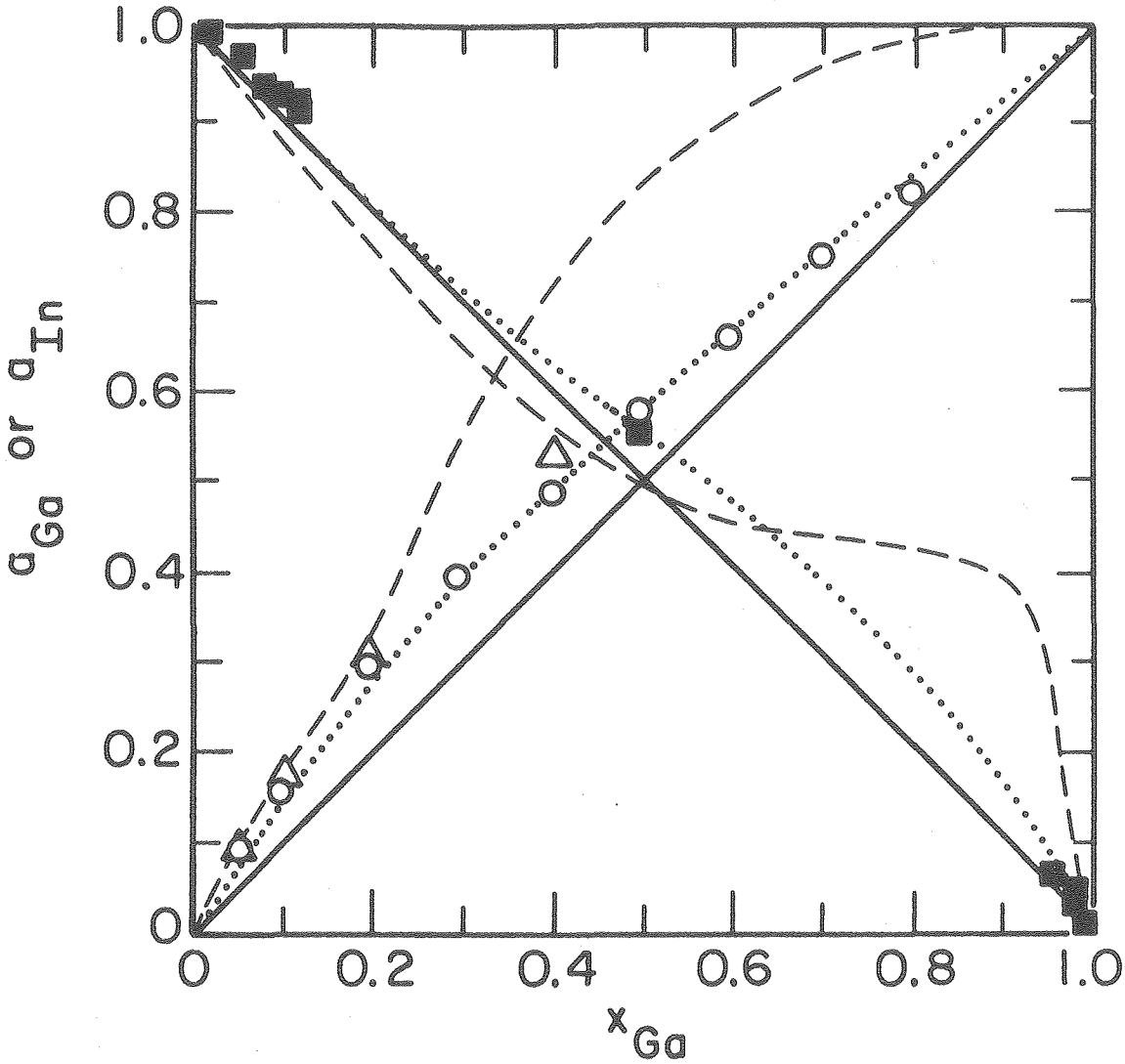

XBL 787-9542

Figure 3.

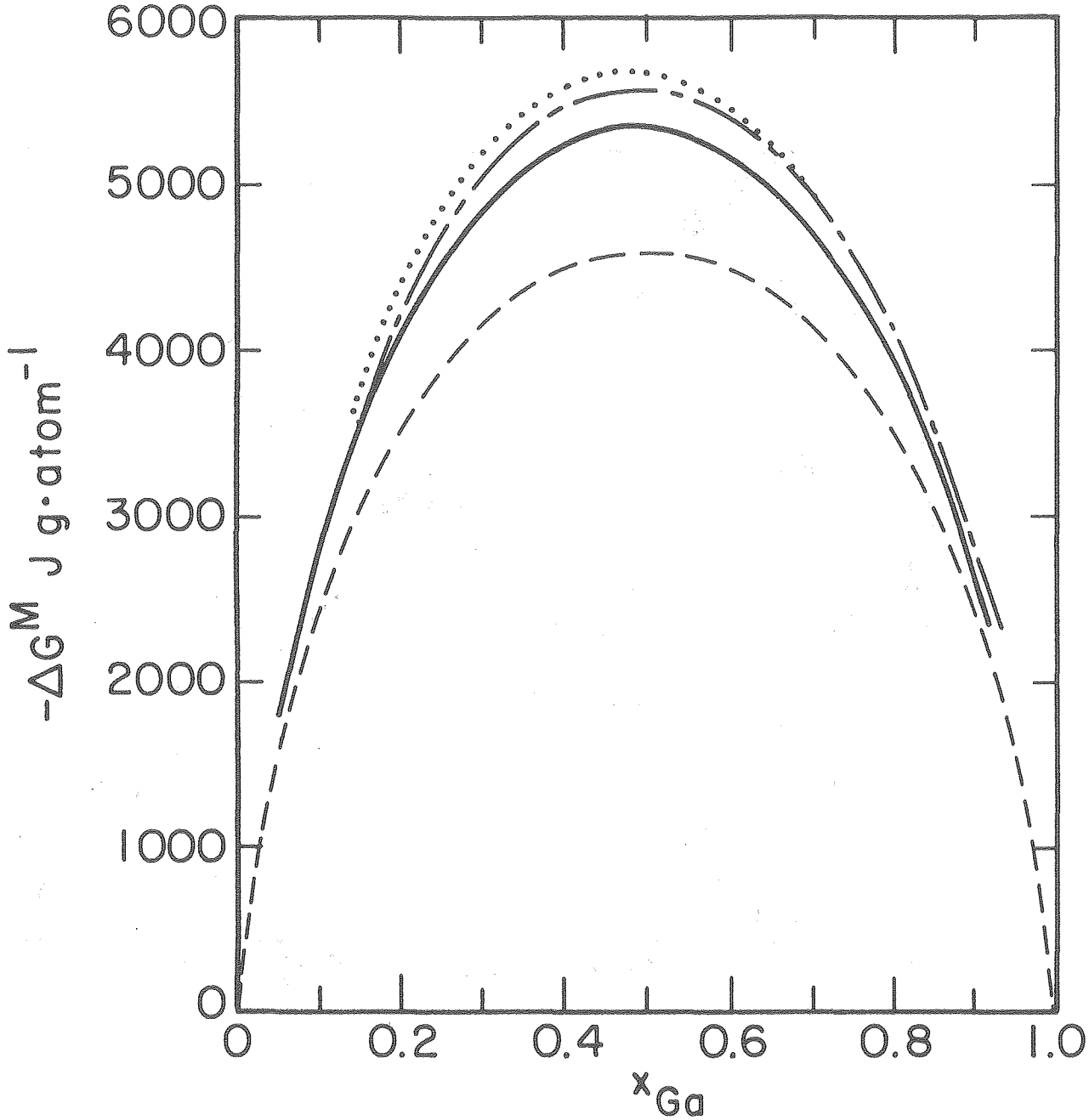

XBL 787-9545

Figure 4.

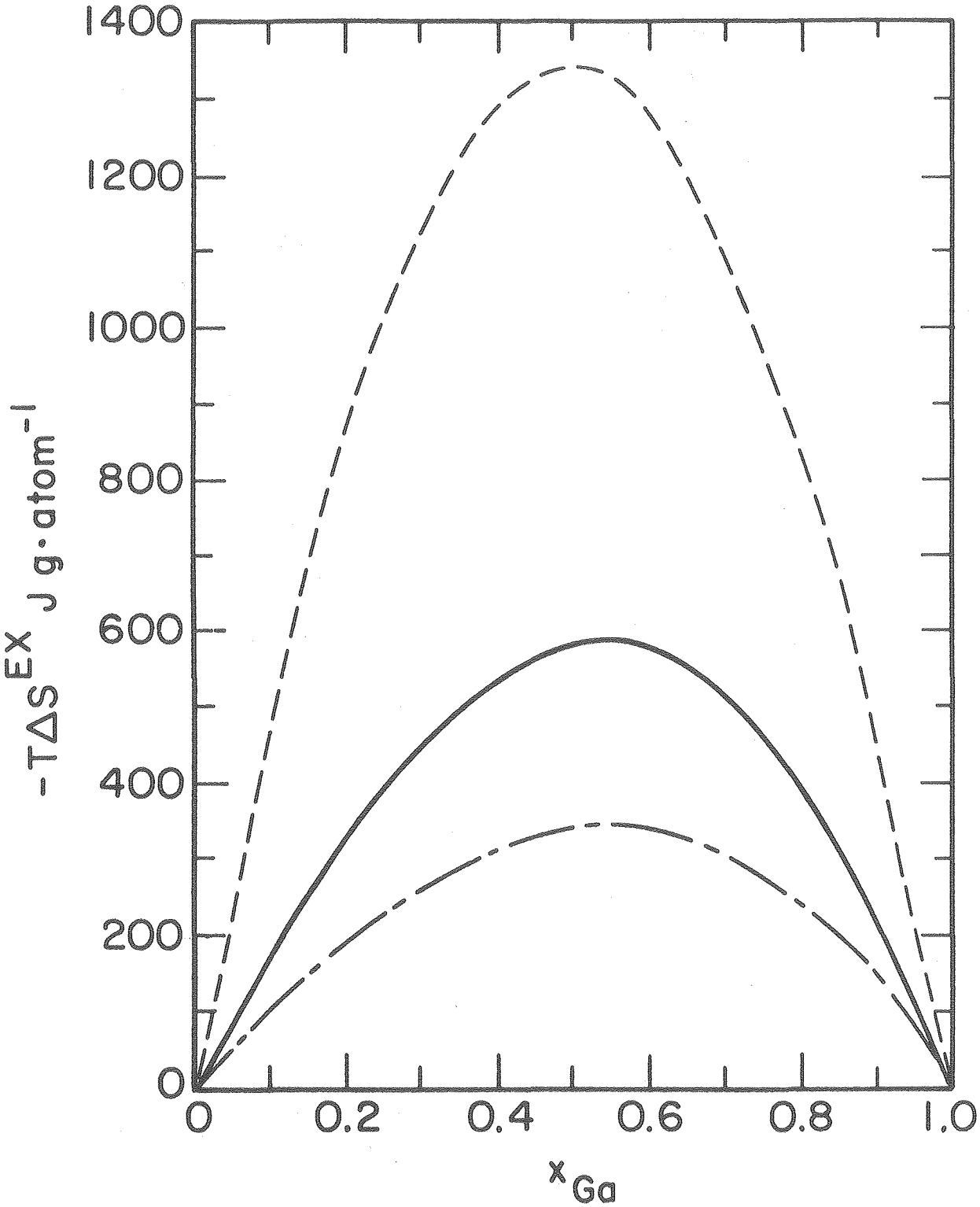

XBL 787-9543

Figure 5.

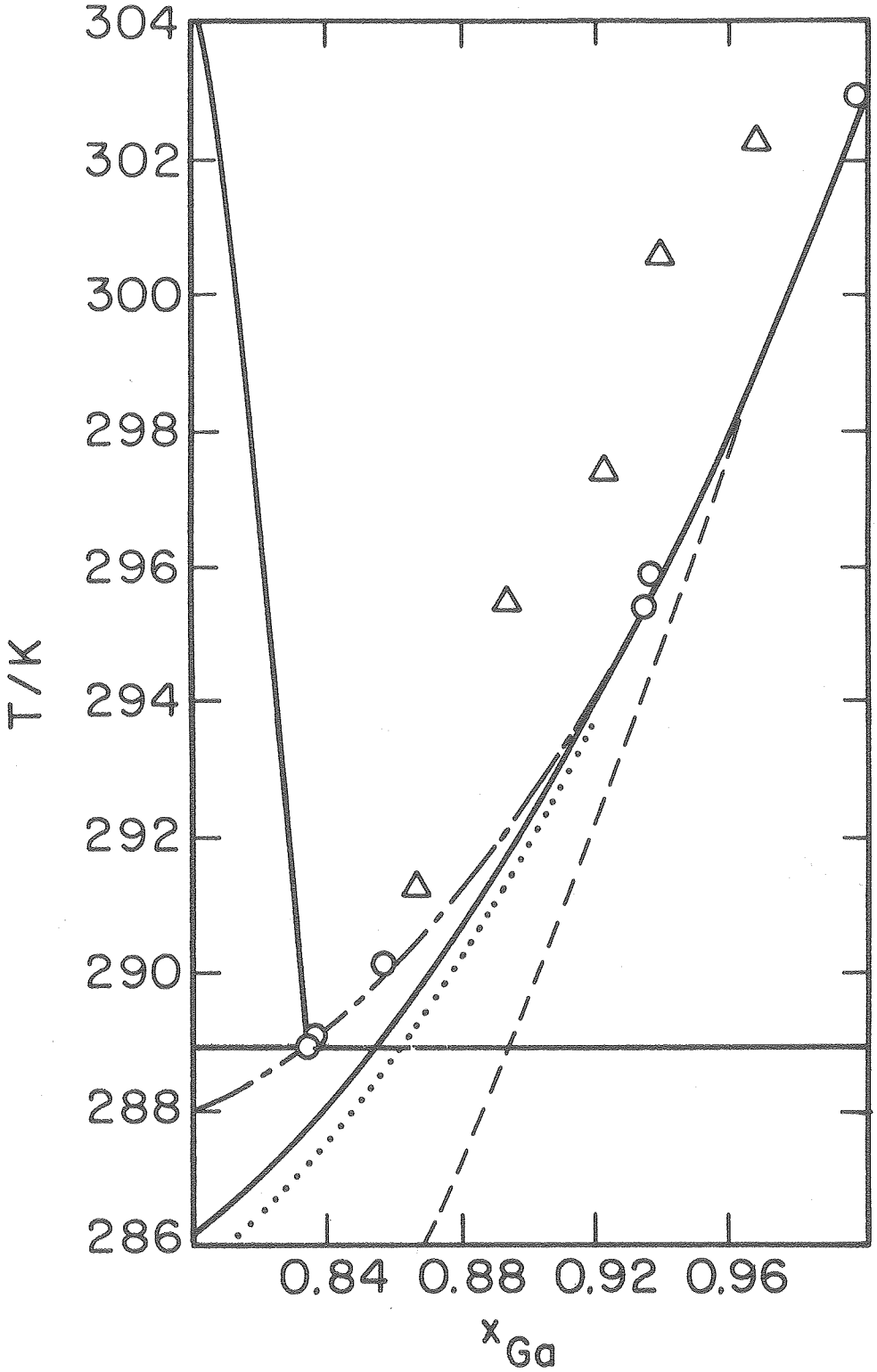

XBL 787-9541

Figure 6.

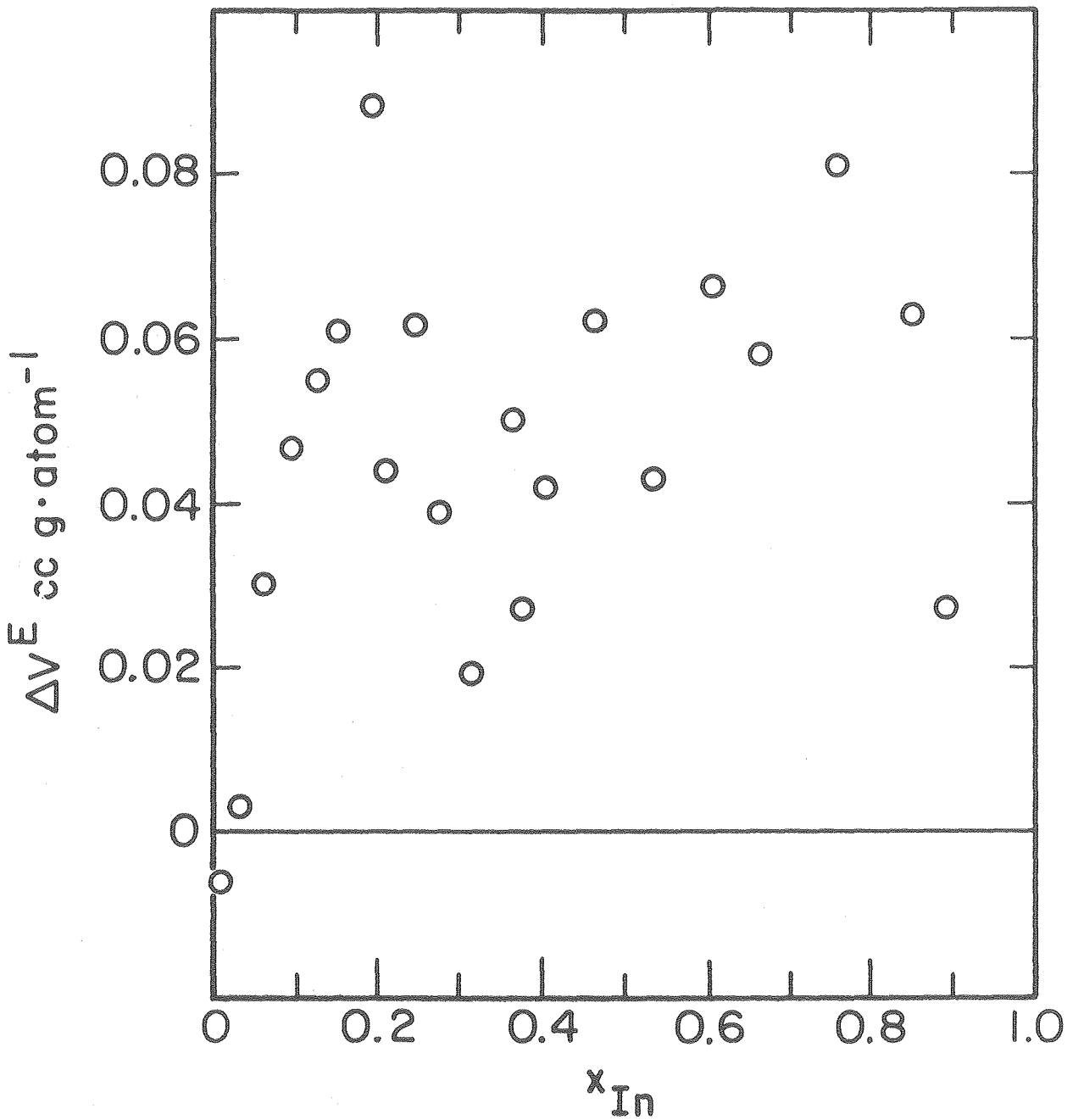

XBL 787-9540

Figure 7.

CHAPTER VI. SOLID STATE ELECTROCHEMICAL STUDY OF $Ga_xIn_{1-x}Sb$ LIQUID ALLOYS

A. INTRODUCTION

The Group III elements gallium and indium are completely miscibile in the liquid phase with the Group V element antimony. The only solid compound formed from these elements is a solid solution containing equal atomic numbers of the Group III element and of antimony. This solid phase can be thought of as either a substitutional solid solution, where Ga is substituted on the crystal lattice for In in the binary compound InSb, or as a binary mixed crystal GaSb-InSb.

The ternary system Ga-In-Sb has received considerable attention recently due to its potential applications in microwave devices.[1,2] The availability of the GaSb-InSb mixed crystal puts at the disposal of the designer a continuous range of electronic and physical properties between the limits of the two binary compounds and thus allows for optimal device performance. Because of this important technological application, considerable interest has been shown for the prediction and investigation of the ternary phase diagram. The theoretical predictions to date have been applied using a very simple solution model for the well known binary counterparts. More recently this model has been extended to the ternary system with adjustable parameters introducted to provide a best fit to phase diagram liquidus tempertures. These models generally contain little physical information. The experimental investigations have been limited to determinations of liquidus and solidus temperatures and enthalpies of mixing and fusion. The

solidus results are somewhat suspect in that long equilibration times (1-2 months) are generally required to achieve equilibrium conditions and to counteract the presence of a large supercooling effect. As was found in the binary limit (see Chapters 3, 4 and 5), the entropy contribution to the liquid phase thermodynamics is expected to be considerable.

To date no experimental investigation of the liquid phase Gibbs energies has been reported. In this study liquid phase gallium activities have been measured with a solid state galvanic cell throughout the entire composition range of the pseudobinary liquid $Ga_xIn_{1-x}Sb$. These results have been combined with other available thermodynamic data to predict the ternary phase diagram.

The gallium activity in the ternary liquid mixture Ga-In-Sb was measured in the high temperature electrochemical cell

$$Pt|C|Ga(\ell),In(\ell),Sb(\ell),\beta\text{-}Ga_2O_3(c)||CSZ||Ga(\ell),\beta\text{-}Ga_2O_3(c)|C \qquad (I)$$

In this cell, calcia-stabilized zirconia (CSZ) was employed as a solid state oxygen ion-conducting electrolyte. At thermodynamic equilibrium the electrochemical potentials of the oxygen ion in the two electrodes are equal. The most stable oxide is β-Ga_2O_3, which is by more than 20 $Kcal_{th}$ g°mole O_2^{-1} than In_2O_3, and is in the solid phase at the temperatures investigated and considered to be at unit activity. Under equilibrium conditions the gallium activity is simply given by

$$a(Ga;Ga\text{-}In\text{-}Sb) = \exp\left\{\frac{-3FE}{RT}\right\} \qquad (1)$$

B. EXPERIMENTAL

The metal electrodes were prepared from electronic grade materials. When preparing the electrodes from the elements semiconductor-grade elemental gallium was obtained from Cominco American, pure indium from Orion Chemical Co. (325 mesh, 99.999 per cent purity, LOT #2449) and antimony from Cominco American (high purity, LOT Em 2139). Cells were also investigated using a working electrode prepared from the binary compounds InSb and GaSb. InSb was purchased from Orion Chemical Co. (325 mesh, 99.999 per cent purity) and GaSb also from Orion Chemical Co. (99.999 per cent purity). Powdered β-Ga_2O_3 was obtained from Alfa Products with a reported purity of 99.999 per cent. Spectroscopic grade grahpite was used for the electrode containers and pure 0.020 inch Pt wire as the contact leads. Calcia stabilized zirconia tubes having a nominal composition of $Ca_{0.15}Zr_{0.85}O_{1.85}$ were obtained from Zircoa Corporation of America, Solon, Ohio. A complete description of the experimental equipment and the procedure followed is given in Chapter 2.

C. RESULTS

A total of fourteen solid state electrochemical cells were investigated of cell type I. Experimentally, the working electrode composition was formulated by four different techniques. In the first design the pseudobinary liquid solution was constructed by adding the desired proportion of pure GaSb and InSb powders. The most stable oxide, gallium sesquioxide, was then placed on the top of this mixture in powdered form. In the second type the composition was

Table 1. Summary of gallium activity measurements in $Ga_xIn_{1-x}Sb$ pseudobinary liquid solutions.

Run	X(Ga)	a(Ga)	T/K	T/K range	a(Ga) range	Cell Formation
1	0.399	0.245	990	915-1056	0.05↔0.53	1
2	0.227	0.018	1008	981-1036	0.012↔0.22	2
3	0.081	0.033	946	877-1015	0.017↔0.062	1
4	0.169	0.123	887	820-953	0.055↔0.203	2
5	0.233	0.120	884	840-927	0.063↔0.141	3
6	0.289	0.116	906	871-940	0.047↔0.205	4
7	0.133	0.114	903	867-939	0.060↔0.214	4
8	0.100	0.064	1028	979-1077	0.059↔0.068	3
9	0.050	0.060	1006	965-1046	0.055↔0.062	4
10	0.200	0.157	1004	965-1043	0.134↔0.182	3
11	0.150	0.149	1015	989-1040	0.138↔0.160	4
12	0.399	0.304	1024	991-1057	0.254↔0.359	3
13	0.351	0.288	1003	972-1033	0.249↔0.304	4
14	0.299	0.253	1072	1041-1103	0.240↔0.267	3

The cell variation in which the elemental powders were intimately mixed (cell formation 3) exhibited much better behavior. The measured emf was found to be linear with temperature and reproducible after both titration and temperature cycling. The temperature coefficients were also in better agreement with those expected. Good performance in this case indicates excellent liquid phase mixing. This might be expected since the elements Ga and In are very low melting and would serve as good solvent for the higher melting Sb, Tm(Sb) = 904 K. Additionally, antimony oxide would be reduced in the presence of Ga or In metal, thus removing any oxide coating present.

Finally the cell variations designed to extend the electrolyte lifetime by the addition of material to a previously investigated cell (cell types 2 and 4) showed inconsistent results. The recorded emfs were found to be similar to that found in the parent cell. This is probably due again to incomplete mixing as a result of the β-Ga_2O_3 powder barrier. Thus only the results found will cell variation 3 are considered to be valid. Figure 1 graphically depicts the results found with the use of cell formation 3 for one of the reproducible temperature cycles. As can be seen, the emf is a linear function of temperature.

D. DISCUSSION

1. Introduction

The results of this study indicate that the pseudobinary liquid solution shows negative deviations from ideal behavior, this result is in agreement with the results found for the binary limits (see Chapters

3 and 4). The purpose of this investigation was to elucidate the liquid phase Gibbs energies which would facilitate the development of models for predicting the ternary Ga-In-Sb phase diagram. The technologically important portion of the phase diagram is for temperatures and compositions in the range that includes the two-phase equilibrium between the mixed crystal GaSb-InSb and tie lines to the ternary liquid. A condition for the existence of this equilibrium at a given temperature and pressure is that the total Gibbs energy should be minimized. An alternate and equally valid statement is that the chemical potentials of each component in both phases must be equal. Developed in Appendix V are the following working expressions to be used in calculating the ternary phase diagram.

$$\ln(X_{GaSb}\gamma_{GaSb}) = \ln\left(\frac{4\gamma^{\ell}_{Ga}\gamma^{\ell}_{Sb}x^{\ell}_{Ga}x^{\ell}_{Sb}}{\gamma^{s\ell}_{Ga}\ \gamma^{s\ell}_{Sb}}\right) + \Gamma_{GaSb} \qquad (2)$$

and

$$\ln(X_{InSb}\gamma_{InSb}) = \ln\left(\frac{4\gamma^{\ell}_{In}\gamma^{\ell}_{Sb}x^{\ell}_{In}x^{\ell}_{Sb}}{\gamma^{s\ell}_{In}\ \gamma^{s\ell}_{Sb}}\right) + \Gamma_{InSb} \qquad (3)$$

Here X_i is the mole fraction of compound i (GaSb or InSb) in the mixed crystal $Ga_XIn_{1-X}Sb$, x_i is the mole fraction of component i (Ga, In or Sb) in the liquid phase, γ_i is the activity coefficient of component i (GaSb, InSb, Ga, In or Sb) in the solid or liquid solution and the $s\ell$ superscript indicates that the activity coefficient is evaluated for the stoichiometric binary liquid GaSb or InSb.

Finally, the terms Γ_{GaSb} and Γ_{InSb} account for the difference in the standard state chemical potentials of the solid and liquid phases and are given by

$$\Gamma_{GaSb} = [\Delta S_f^c(GaSb)(Tm(GaSb)-T) - \int_T^{Tm}\int_T^{Tm} \frac{\Delta C_p^{GaSb}}{T} dT^2]/RT \qquad (4)$$

$$\Gamma_{InSb} = [\Delta S_f^c(InSb)(Tm(InSb)-T) - \int_T^{Tm}\int_T^{Tm} \frac{\Delta C_p^{InSb}}{} dT^2]/RT \qquad (5)$$

Here ΔS_f^c is the entropy of fusion of the binary compound GaSb or InSb and ΔC_p is the difference between the heat capacity of the supercooled stoichiometric binary liquid and the binary compound GaSb or InSb. If this heat capacity difference is considered independent of temperature the integral in Equations (4) and (5) reduces to

$$\Delta C_p \int_T^{Tm} \int_T^{Tm} \frac{dT^2}{T} = \Delta C_p \{Tm-T-T\ell n[\frac{Tm}{T}]\} \qquad (6)$$

Thus, in order to calculate the ternary phase diagram expressions for the activity coefficients as a function of temperature and composition must be developed and the terms Γ_{GaSb} and Γ_{InSb} must be assigned values.

2. Composition Dependence Of The Liquid Phase Activity Coefficients.

The binary activity coefficients at a given tempreature can be expressed in terms of a Margules series as

$$\ell n\gamma_1 = a_2x_2^2 + a_3x_2^3 + a_4x_2^4 + \ldots \qquad (7)$$

and

$$\ell n\gamma_2 = (a_2+3/2\ a_3+2a_4+\ldots)x_1^2-(a_3+8/3\ a_4+\ldots)x_1^3+(a_4+\ldots)x_1^4+\ldots \qquad (8)$$

These expansions are to be truncated where the limits of error in the data indicates. A plot of $\ln\gamma_1/x_2^2$ versus x_2 would thus aide in clarifying how many terms should be retained: A horizontal linear line would stipulate keeping only the first term, a non-linear plot having a non-zero slope would indicate retaining two constants, and so forth.

For the binary systems Ga-Sb and In-Sb the values of $\ln\gamma_{Ga,\ In}/x_{Sb}^2$ are shown plotted against x_{Sb} in Figure 2. For the Ga-Sb binary system the activity measurements presented in Chapter 3 at a temperature of 1003 K are shown. This system is seen to produce a horizontal plot thus dictating the retention of a single constant. The analysis of the available activity measurements presented in Chapter 4 on the In-Sb system indicated that the results of this work (see Chapter 4) and that of Hoshino et al[3] were most consistent with the reported diagram and other available thermodynamic data. Figure 2 also shows the values $\ln\gamma_{In}/x_{Sb}^2$ versus x_{Sb} using these measurements. The results for the In-Sb system exhibited some scatter but is very close to linear. Finally, the Group III binary Ga-In system was analyzed in Chapter V and the activity measurements of Klinedinst and Stevenson[4] deemed most accurate. Using their proposed expression for $\ln\gamma_{Ga}$ at a temperature of 1003 K produces a linear expression again. Summarized in Table 2 are the values of the constants for the Margules equation determined from data for the three binary systems of interest. These constants are found to reproduce the activity results excellently.

The three suffix Margules equations can be extended to the ternary system by Wohl's method.[5,6] The results take the form

Table 2. Summary of Margules constants for the binary systems Ga-Sb, In-Sb and Ga-In at a temperature of 1003 K.
$\ln\gamma_i = a_2x_j^2 + a_3x_j^3$

SYSTEM	i	j	a_2	a_3
Ga-Sb	Ga	Sb	-1.27	0
" "	Sb	Ga	-1.27	0
In-Sb	In	Sb	-3.591	2.065
" "	Sb	In	-0.494	-2.065
Ga-In	Ga	In	0.797	-0.134
" "	In	Ga	0.596	0.134

$$\ln\gamma_1 = A_{12}x_2^2(1-2x_1) + 2A_{21}x_1x_2(1-x_1) + A_{13}x_3^2(1-2x_1) + 2A_{31}x_2x_3(1-x_1) - 2A_{23}x_2x_3^2 - 2A_{32}x_2^2x_3 + [1/2\ (A_{12}+A_{21}+A_{13}+A_{23}+A_{32}) - Q][x_2x_3 - 2x_1x_2x_3] \quad (9)$$

where the terms A_{12}, A_{21}, A_{13}, A_{31}, A_{32} and A_{23} are constants related to the binary Margules constants by

$$A_{ij} = a_2 + 1/2\ a_3 \quad (10)$$

Margules constants a_2 and a_3 are taken from the binary expression

$$\ln\gamma_j = a_2x_i^2 + a_3x_i^3 \quad (11)$$

The only constant that is not able to be determined from the binary parameters is Q, which accounts for the three body interactions. Expressions similar to equation (9) for the remaining 2 components are easily determined. The expression for $\ln\gamma_2$ abd $\ln\gamma_3$ are found by interchanging the subscripts of equation (9) as follows: 1 to 2, 2 to 3 and 3 to 1, and 1 to 3, 2 to 1 and 3 to 2, respectively.

In order to determine the constant Q, Equation (9) was applied to the measured gallium activities of this study. Table 3 summarizes these findings using the activities measured at 1003 K. As can be seen Q is not constant over the composition range studied but for purposes of calculation a value of Q = 4.5 was selected. Also shown in Table 3 are the activities calculated for the compositions studied with Q = 4.5 and the binary constants listed in Table 2. Figure 3 graphically depicts the measured gallium activities as a function of the gallium antimonide liquid mole fraction. Also shown in Figure 3 are the gallium and indium activities calculated from Equation (9).

Table 3. Summary of measured and calculated* gallium activities in the pseudobinary liquid system (GaSb-InSb at 1003 K).

x_{Ga}	a (Ga) measured	Q	a (Ga) calculated	a (In) calculated
0.100	0.068	3.6	0.058	0.208
0.200	0.124	5.3	0.132	0.142
0.299	0.219	4.2	0.216	0.081
0.399	0.278	11.0	0.297	0.032

Mean Value = 6.0

* a (Ga) calculated from Equation (9) with Q = 4.5, $A_{Ga-Sb} = A_{Sb-Ga} = -1.27$, $A_{In-Sb} = -1.526$, $A_{Sb-In} = -2.5585$, $A_{Ga-In} = 0.663$ and $A_{In-Ga} = 0.730$.

These values reproduce the measured values to within the experimental error involved.

Liquid phase concentrations of constant activity of all three components were calculated by successive approximation using Equation (9) and the constants listed at the bottom of Table 3. The iso-activity lines for a temperature 1003 K are shown in Figure 4 in triangular coordinates. The antimony activity shows negative deviations throughout the entire composition range while both the gallium and indium activities shift from negative to positive deviations from ideality as the antimony content decreases.

3. Enthalpy of Mixing $Ga_xIn_{1-x}Sb$ Liquid Solutions

The liquid phase activity coefficients needed in Equations (2) and (3) were evaluated at the composition and temperature of the equilibrium liquidus solution. The three suffix Margules equation developed earlier accounts for the composition dependence at a constant temperature of 1003 K, while knowledge of the partial molar enthalpy of each component is required to ascertain the temperature dependence. This factor can be very pronounced as liquidus temperatures in this system can be several hundred degrees removed from 1003 K.

Two independent investigations of the enthalpy of mixing the ternary liquid solution Ga-In-Sb have been reported in the literature. Vecher and coworkers[7] measured enthalpies of mixing at 910 K by quantitative differential thermal analysis in the ternary system. The liquid ternary solution showed both positive and negative deviations from ideality and exhibited a maximum exothermic heat of mixing of -820 ± 25 cal_{th} $g \cdot atom^{-1}$

for an alloy containing In, Sb, and Ga in the proportion of 39, 50 and 11 atom percent, respectively. Ansara et al.,[8,9] measured the molar enthalpies of mixing for Ga-In-Sb liquid mixture with a high temperature microcalorimeter at 995 K. Their results are less exothermic than those of Veecher et al.[7] and showed no maximum exothermic mixing enthalpy.

The enthalpy of mixing for binary systems are often correlated with expressions of the form

$$\Delta H^M = x_1 x_2 \xi_{12}(x_2) \tag{12}$$

where x_1 and x_2 are the binary mole fractions and the $\xi_{12}(x_2)$ parameter is generally taken in the form

$$\xi_{12}(x_2) = a_0 + a_1 x_2 + a_2 x_2^2 + \ldots \tag{13}$$

Equations of this form can be extended to ternary systems by considering that the ternary system is a modified binary solution, with component 1 considered to be in solution with component 2 which is a mixture of the other two ternary components in constant proportions. The ternary model takes the form

$$\Delta H^M = \left(\frac{x_1}{1-x_2}\,\Delta H^M_{1-2} + \frac{x_3}{1-x_2}\,\Delta H^M_{2-3}\right)\Big|_{x_2} + (1-x_2)^2 (\Delta H^M_{1-3})\Big|_{x_1/x_3} + x_1 x_2 x_3 \xi_{123}(x_1, x_2) \tag{14}$$

where the mole fractions listed are of the ternary liquid solution. The binary enthalpies of mixing ΔH^M_{1-2} and ΔH^M_{2-3} are evaluated for a

binary liquid at composition x_2 and the binary enthalpy of mixing ΔH^M_{1-2} is evaluated at the constant proportion composition x_2/x_3. Combining Equations (13) and (14) and evaluating the binary enthalpies of mixing at the prescribed composition one obtains the following equation in terms of the ternary mole fractions,

$$\Delta H^M = x_1x_2\xi_{12}(x_2) + x_2x_3\xi_{23}(x_2) + x_1x_3\xi_{13}(\frac{x_3}{1-x_2}) + x_1x_2x_3\xi_{123}(x_1,x_2) \qquad (15)$$

The activity coefficient at any temperature can now be evaluated from the activity coefficient calculated at 1003 K with Equation (9) by

$$\ln\gamma_i^T = \ln\gamma_i^{1003K} + \Delta\overline{H}_i\{\frac{1}{T} - \frac{1}{1003}\}/R \qquad (16)$$

where $\Delta\overline{H}_i$ is the partial molar enthalpy of component i. Using Equation (15) as the expression for ΔH^M the partial molar quantities are easily found, which for component 1 is given by

$$\Delta\overline{H}_1 = x_2x_3(\xi_{12}-\xi_{23}+\xi_{13}) + x_2^2[\xi_{12}-x_1\xi'_{12} + x_3(\xi_{123}-\xi'_{23})] + x_3^2(\xi_{13}-x_1\xi'_{13}(1 + \frac{x_2}{1-x_2})\ x_2\ \xi_{123}) - x_1x_2x_3(\xi_{123} + x_3(\frac{123}{\partial x_3})_{x_2} + x_2(\frac{\partial\xi_{123}}{\partial x_2})_{x_3}) \qquad (17)$$

for component 2, by

$$\Delta\overline{H}_2 = x_1x_3(\xi_{12}+\xi_{23}-\xi_{13}) + x_1^2[\xi_{12}+x_2\xi'_{12}+x_3(\xi_{123} + \frac{x_3}{1-x_2}\xi'_{13})]$$

$$+ x_3^2[\xi_{23}-x_2\xi'_{23}+x_1(\xi_{123}-\xi'_{13}(1 - \frac{x_3}{1-x_2}))] - x_1x_2x_3(\xi_{123} + x_3 \frac{\partial\xi_{123}}{\partial x_3})_{x_1}$$

$$+ x_1(\frac{\partial\xi_{123}}{\partial x_1})_{x_3} - \xi'_{12} - \xi_{23}) \qquad (18)$$

and for component 3 by

$$\Delta\overline{H}_3 = x_1x_2(\xi_{23}+\xi_{13}-\xi_{12}) + x_1^2(\xi_{13}+x_3\xi'_{13}+x_2\xi_{123}) + x_2^2(\xi_{23}$$

$$-x_3\xi'_{23}-x_1\xi'_{12}+x_1\xi_{123}) - x_1x_2x_3[\xi_{123}+x_2(\frac{\partial\xi_{123}}{\partial x_2})_{x_1}$$

$$+ x_1(\frac{\partial\xi_{123}}{\partial x_1})_{x_2} + \xi'_{13}(\frac{x_3}{1-x_2} - 1] \qquad (19)$$

where ξ'_{12} and ξ'_{23} are the x_2 partial derivatives of the ξ parameters and ξ'_{13} is the x_3 partial derivative. Provided the ξ parameters are known the activity coefficient of each liquid phase component is now readily calculated at any composition and temperature.

Considerable experimental information is available on the enthalpy of mixing of the binary systems and has been summarized in Chapters 3, 4 and 5. The results of the various investigations showed remarkable consistency and were generally found to be independent of temperature. For the Ga-Sb system the results of Predel and Stein[10] were used while the work of Wittig and Gehring[11] was utilized for the In-Sb binary system and the 742 K results of Bros and coworkers[12] for the Ga-In system. The constants describing the ξ parameters are summarized in Table 4. The constants for the ternary parameter ξ_{123} were found by

a linear regression analysis with the results of Ansara et al.[8,9] to obtain the functional form

$$\xi_{123} = \alpha x_2 + \beta x_1 + \gamma x_3 \qquad (20)$$

Figure 5 illustrates the enthalpy of mixing for the pseudobinary liquid. Shown are the experimental results of both Vecher et al.[7] and Ansara et al.[8,9] Also shown as the solid line is the enthalpy of mixing calculated with Equation (15) and the constants listed in Table 4. The experimental results of the two studies can be seen to show marked discrepancies. The enthalpy of mixing for the Ga-Sb binary limit is reported by Vecher et al.[7] as -350 cal_{th} $g \cdot atom^{-1}$ and by Ansara et al.[8,9] as -258 cal_{th} $g \cdot atom^{-1}$. These results can be compared to the other available literature ΔH^M values of -258,[10] -204,[13] and -260[14] cal_{th} $g \cdot atom^{-1}$. This the comparison indicates that the work of Ansara et al.[8,9] to be more consistent with the present results than are the other values for H^M.

Using Equation (15) with the constants listed in Table 4, contours of constant enthalpy of mixing at 1003 K were calculated. The results of these calculations are graphically depicted in Figure 6.

The entropy of mixing in the Ga-In-Sb system can now be ascertained from the experimental Gibbs energy measurements of this study and the enthalpy of mixing values measured by Ansara et al.[8,9] Figure 7 shows the temperature-entropy of mixing product calculated at 1003 K from the above equation representing the activity coefficients and ΔH^M.

Table 4. Summary of function representations for describing the experimental enthalpies of mixing in the Ga-In-Sb system.*

SYSTEM	ξ $cal_{th}\ g^{\cdot}atom^{-1}$	ΔH^M reference
Ga-Sb	$\xi_{13} = -438 - 2040x_{Sb} + 1699x_{Sb}^2$	10
In-Sb	$\xi_{23} = -4002.4 + 1845.1x_{Sb}$	11
Ga-In	$\xi_{12} = 951 + 337x_{In} - 311x_{In}^2$	12
Ga-In-Sb	$\xi_{123} = 5137x_{In} - 4603x_{Ga} + 165x_{Sb}$	8,9

*$cal_{th} = 4.184J$

Also shown in Figure 7 is the ideal entropy of mixing for the pseudobinary liquid. As was found in the binary cases the pseudobinary exhibits a positive excess entropy of mixing. Figure 7 also contains the calculated Gibbs energy of mixing for the pseudobinary liquid.

4. Calculation of Γ_{GaSb} and Γ_{InSb}

In order to calculate the ternary Ga-In-Sb phase diagram values must be assigned to the terms Γ_{GaSb} and Γ_{InSb} and defined by Equations (4) and (5). The entropy of fusion and melting temperatures for the binary compounds have been reviewed in Chapters 3 and 4. For GaSb the entropy of fusion has the reported range of 6.1 to 8.1 cal_{th} $g^{\circ}atom^{-1}K^{-1}$ (see Chapter 3). The analysis presented in Chapter 3 indicated the higher entropy of fusion values agreed more closely with the measurements of this work and with the reported phase diagram. Thus the value 7.90 cal_{th} $g^{\circ}atom^{-1}K^{-1}$ reported by Lichter and Sommelet[15] was adopted for $\Delta S_f^c(GaSb)$, while a melting temperature of 985 K as selected by Hultgren et al[16] was employed. Similarly, for the InSb system the range of reported values for $\Delta S_f^c(InSb)$ is 5.6 to 7.6 cal_{th} $g^{\circ}atom^{-1}K^{-1}$ (see Chapter 4). The analysis given in Chapter 4 indicated the higher values are more consistent with the other available thermodynamic measurements and therefore the value of $\Delta S_f^c(InSb) = 7.393$ cal_{th} $g^{\circ}atom^{-1}K^{-1}$ suggested by Hultgren et al[16] was used along with $T_m(InSb) = 798$ K.[16]

The temperature dependence of the entroy of fusion is accounted for by the term containing the heat capacity difference, ΔC_p^{AC}, between the stoichiometric binary liquid and the binary compound. Evaluation

of this heat capacity difference requires knowledge of the heat capacity in a temperature range where one of the phases is metastable or unstable. Experimentally this is a difficult proposition. An estimate of ΔC_p can be made by examining this difference at the melting temeprature of the compound for which experimental data is readily available. Using the values for C_p of the solid and liquid phases selected by Hultgren et al[16] the following values are found for ΔC_p: $\Delta C_p^{GaSb} = 0.681$ cal_{th} $g \cdot atom^{-1}$ K^{-1} and $\Delta C_p^{InSb} = 1.32$ cal_{th} $g \cdot atom^{-1}$ K^{-1}. If ΔC_p is assumed to be independent of temperature the ΔC_p term in Equations (4) or (5) for calculating Γ_{GaSb} and Γ_{InSb} is then given by Equation (6). For the larger estimated values of ΔC_p(InSb) this term represents 0.6 and 2.9 per cent of the value of Γ_{InSb} at 100 and 300 K below the melting temperature, respectively. This contribution is well within the experimental error of the reported entropy of fusion. Thus, for calculation purposes, ΔC_p is assumed independent of temperature and having the values assigned above.

5. Experimental Ga-In-Sb Phase Diagram Determinations

The determination of the Ga-In-Sb phase diagram has received some attention. Koster and Thomas[17] first investigated the GaSb-InSb system and reported a degenerate eutectic diagram without appreciable terminal solid solution. Goryunova and Fedorova[18] investigated two alloys and found a single phase after conducting high temperature anneal of samples initially consisting of several components. The formation of a complete solid solution in the GaSb-InSb system was fully substantiated by Woolley et al.[19-21] Using X-ray, thermal and metallographic techniques, these investigators discovered single phase

equilibrium could be attained within a reasonable length of time by annealing approximately two months near the solidus temperature only in the case of compressed powder specimens. Gorshkov and Goryunova[22] used thermal methods to find close agreement with the work of Woolley et al. More recent measurements of the pseudobinary phase diagram have been reported by Nikitina and Romanenko,[23] Ufimtsev et al[24] and Blom and Plaskett[25] and these measurements agree well with the earlier work. Solidus and liquidus temperatures have also been reported for liquid compositions other than the pseudobinary ones.[25,26] Also less accurate phase diagram results obtained from investigations of rate processes in liquid phase epitaxy, crystal pulling and zone melting have also been reported for the Ga-In-Sb system.[27-31] Summarized in Figure 8 are the various experimental results for the isomorphous pseudobinary phase field.

6. Calculation of the $Ga_xIn_{1-x}Sb$ Pseudobinary Phase Diagram

In order to calculate the pseudobinary phase diagram all that remains is a description of the solid solution thermodynamics. As a first approximation the solid solution may be considered to be ideal. In this case the activity coefficients of both components are considered to be unity. For the condition that the liquid phase is also ideal the liquidus and solidus compositions are given by Equations (A-30) and (A-31) found in Appendix V. Figure 9 shows the pseudobinary phase diagram calculated assuming both the liquid and solid phases are ideal. Also shown are the experimental results of Woolley et al.[19-21]

The assumption of ideal behavior produces liquidus and solidus temperatures that are higher than the expeimental values.

An improvement in the calculated phase diagram can be made by accounting for the negative deviations from ideality present in the liquid phase as was found in this work. Figure 9 also contains is the pseudobinary phase diagram calculated using the expression for the liquid phase activity coefficients (Equation (9)) in conjunction with the partial molar enthalpies given by Equations (17) to (19) and the constants tabulated in Table 4. The solid solution was again assumed to be ideal. This improvement in the model produced liquidus temperatures that were in good agreement with the experimental data but produced little improvement in the solidus temperatures, thus indicating the mixed crystal is indeed non-ideal.

Unfortunately little experimental information is available on the thermodynamic properties of the solid solution. Reported in the literature is the total antimony vapor pressure of antimony over the solid solution as a function of composition.[32] Unfortunately antimony exists primarily as two species in the vapor phase (Sb_2 and Sb_4) in almost equal proportions and therefore the activity of antimony in the solid phase can not be estimated. The only other experimental work available in the literature is a determination of the enthalpy of fusion of the solid solution at various compositions.[33] The enthalpy of mixing solid GaSb and InSb to form the solid mixed crystal can be derived as follows: Consider the reaction sequence where the pseudobinary solid solution is first formed from a stoichiometric liquid

$$Ga_{\frac{1}{2}(1-X)}In_{\frac{1}{2}X}Sb_{\frac{1}{2}}(\ell) = \tfrac{1}{2}Ga_{(1-X)}In_{(X)}Sb(c) \tag{21}$$

followed by the formation of the stoichiometric liquid solution from the pure elements and represented as

$$\tfrac{1}{2}(1-X)Ga(\ell) + \tfrac{1}{2}XIn(\ell) + \tfrac{1}{2}Sb(\ell) = Ga_{\frac{1}{2}(1-X)}In_{\frac{1}{2}X}Sb_{\frac{1}{2}}(\ell) \tag{22}$$

Finally the line compounds are melted and separated into the pure elements

$$\tfrac{1}{2}(1-X)GaSb(c) = \tfrac{1}{2}(1-X)GaSb(\ell) \tag{23}$$

$$\tfrac{1}{2}X\ InSb(c) = \tfrac{1}{2}XInSb(\ell) \tag{24}$$

$$\tfrac{1}{2}(1-X)GaSb(\ell) = \tfrac{1}{2}(1-X)Ga(\ell) + \tfrac{1}{2}(1-X)Sb(\ell) \tag{25}$$

$$\tfrac{1}{2}X\ InSb(\ell) = \tfrac{1}{2}XIn(\ell) + \tfrac{1}{2}XSb(\ell) \tag{26}$$

The overall reaction is the formation of the solid solution from the pair binary compounds.

$$\tfrac{1}{2}(1-X)GaSb(c) + \tfrac{1}{2}XInSb(c) = \tfrac{1}{2}Ga_{(1-X)}In_{(X)}Sb(c) \tag{27}$$

The corresponding enthalpy changes are listed below

$$\Delta H(21) = -\Delta H_f^c(s.s.) \tag{28}$$

where $\Delta H_f^c(s.s.)$ is the enthalpy of fusion of the solid solution $Ga_{1-x}In_xSb$. The enthalpy changes for reactions (22), (25), and (26) are simply the enthalpy of mixing of the liquid ternary solution and the negative enthalpy of mixing of the two III-V binary solutions,

respectively. The enthalpy change of the reactions (23) or (24) is the enthalpy of fusion of the corresponding binary compound. The overall enthalpy change is then given by

$$\Delta H^M(s.s.) = -\Delta H_f^c(s.s.) + \Delta H^M(l.s.) + (1-X)\{\Delta H_f^c(GaSb) - \Delta H^M(Ga\text{-}Sb)\} + X\{\Delta H_f^c(InSb) - \Delta H^M(In\text{-}Sb)\} \quad (29)$$

Here all thermodynamic quantities are on a g°atom basis.

Using the enthalpies of fusion of the solid solution reported by Mechkovskii et al.[33] with the enthalpies of mixing the liquid solutions and enthalpies of fusion of the binary compounds suggested previously, the solid solution enthalpies of mixing were determined. The enthalpy of mixing calculated was small and exothermic and exhibited much scatter. The results were quantified in equation form of type Equation (12). The scatter warranted the retention of only the first constant in the $\xi_{s.s.}$ expansion. The enthalpy of mixing can be calculated from the expression

$$\Delta H^M(s.s.) = -1.7(\pm 1.0)X_{GaSb}(1-X_{GaSb})\ \mathrm{Kcal}_{th}\ g^{\circ}atom^{-1}\ . \quad (30)$$

The large uncertainty in the ξ parameter arises from the combined errors in the various enthalpies used in Equation (29). Upon employing Equation (30) and assuming the entropy of mixing is ideal yields calculated solidus temperatures that are even higher.

An estimate for the excess entropy can be made by evaluating the the entropy changes for reactions (21) to (27). In order to make such a determination knowledge of the solidus temperature is necessary.

Performing these calculations with experimental solidus temperatures again produces much scatter.

In order to bring the solidus line calculated into agreement with the experimental values an excess entropy given by the following expression was used.

$$\Delta S^{E}(s.s.) = -2.9\ X_{GaSb}(1-X_{GaSb}) \tag{31}$$

Under this assumption and using the enthalpy of mixing given by Equation (30) yields the activity coefficient expressions

$$\ln\gamma_{GaSb} = (1.46 - 855/T(K))(1-X_{GaSb})^{2} \tag{32}$$

and

$$\ln\gamma_{InSb} = (1.45 - 855/T(K))(X^{2}_{GaSb}) \tag{33}$$

The pseudobinary phase diagram calculated with the above model for the solid and liquid phases produced the solidus and liquidus line represented by the solid line in Figure 9. This model is seen to produce much closer agreement with the experimental solidus line than the assumption of ideality for the solid solution.

As in the case of the binary compounds, the electrical conductivity greatly increases upon melting the solid solution $Ga_{X}In_{1-X}Sb$. The composition dependence of the viscosity, electrical conductivity and density[34] in addition to X-ray data[34] for the pseudobinary liquid solution indicates a tendency for interaction between the Group III and V atoms. The results have even suggested the formation of the ternary

complexes In_2GaSb_3 and $InGa_2Sb_3$ in the liquid phase. The ordering found in the liquid phase is carried into the solid phase producing an exothermic enthalpy of mixing. This tendency of the different components of the solid solution toward interaction is supported by the concentration dependence of the density isotherms for the solid solution[34] in which positive deviations were found from the additive line. Similarly, the total antimony vapor pressure[32] over the solid solutions exhibited negative deviations from the additive line. The GaSb-InSb solid solution has been analysed by Foster and Woods.[35] Calculations they performed suggested that a significant size effect contribution to ΔG^E can be excluded whereas they calculated a distortion energy of 1900 cal_{th}/mole for the equimolar mixture. This positive distortion energy more than balances the chemical effects to yield a small positive excess Gibbs energy. In the liquid phase the distortion energy contribution is absent and the large negative excess Gibbs energy of mixing observed in this study reflects the chemical interactions present in both phases.

7. Survey of Solution Models Used to Calculate the Pseudobinary Phase Diagram

A survey of the available literature reveals several approaches to calculating the Ga-In-Sb pseudobinary phase diagram.[36,37] Stringfellow calculated the phase diagram using a model with no adjustable parameters. The liquid phase was treated as a regular solution and

the interaction parameters were calculated from solubility parameters, electronegativities and molar volumes of the individual elements. The thermodynamic properties of the solid solution were calculated using a spectroscopic theory of chemical bonding. In this model the solid solution entropy of mixing was assumed zero and the enthalpy of mixing given by

$$\Delta H^M \text{ (s.s.)} = 1846\ X_{GaSb}\ (1-X_{GaSb})\ \text{cal}_{th}/\text{mole} \qquad (34)$$

The calculations of Stringfellow gave good agreement with the experimental solidus but produced liquidus temperatures that were high.

Foster and Woods[35] also calculated the pseudobinary phase diagram by assuming the liquid phase to be ideal and the activity coefficient of the two solid phase binary components to be given by

$$\ln \gamma_i^s = (B^s/RT)X_j^2 \qquad (35)$$

Using a fitted value for B^s that showed a small composition dependence the phase diagram was easily reproduced. Several other investigators[25,28,38,31] have also assumed that both the solid and liquid solutions are simple solutions with component activity coefficients given by equations of type Equation (35). Here the parameter B was sometimes allowed to also have a temperature dependence. The procedure was to obtain the liquid B parameters from the binary phase diagrams and extend this model to the ternary system. The solid phase B parameter was then obtained form the pseudobinary phase diagram. In general, these methods could reproduce the pseudobinary phase diagram very well but the thermodynamic properties calculated from these models were in sharp

disagreement with the available experimentally determined properties.

8. Calculation of the Ternary Phase Diagram

The method used to calculate the pseudobinary phase diagram was extended to calculate the complete ternary phase diagram. The general equations used to describe the important phase equilibria are Equations (20) and (21) found in Appendix V. For this calculation the values of the entropy of fusion of the compounds and the ΔCp terms were taken to be the same as in the pseudobinary case.

For purposes of comparison the phase diagram was first calculated under the assumption that the liquid and solid phases both behave as ideal solutions. The governing equations describing the ideal liquidus surface have been developed in Appendix V and yields the following for the gallium liquid phase mole fraction

$$x_{Ga}^{IDEAL} = \frac{\frac{1}{4}\, xSb-(1-xSb)\exp(\Gamma InSb)}{\exp(\Gamma GaSb)-\exp(\Gamma InSb)} \qquad (36)$$

where the terms in the above equation are the same as those described following the presentation of Equations (2) and (3). The solidus composition expressed as the GaSb mole fraction in the solid solution can be determined by

$$X_{GaSb}^{IDEAL} = \frac{4xSb(1-XSb)-\exp(-\Gamma InSb)}{\exp(-\Gamma GaSb)-\exp(-\Gamma InSb)} \qquad (37)$$

The ideal solution ternary phase diagram was generated by first choosing a temperature and antimony liquid phase mole fraction and then calculating the remaining liquid and solid phase compositions with Equations (36) and

(37). The results of these calculations for five different temperatures are shown in figure 10 where liquidus lines are drawn in the three component phase field. The dashed line in figure 10 represents the liquidus line under ideal conditions while the solid line was drawn through the available literature data. The solid line in the antimony rich corner represents a eutectic valley formed at the ends by the eutectic points of the two Group III antimonides. As can be seen, the assumption of ideality is indeed poor as liquidus temperatures show disagreements of as much as 100 K.

As was found in the pseudobinary case, an improvement can be made in the predicted liquidus temperatures by accounting for the negative deviations present in the liquid phase. Employing the expressions describing the liquid phase behaviour developed earlier, the liquidus lines were recalculated. The results of this calculation are shown in figure 11 along with the available experimental liquidus data. As can be seen, good correlation is found with the use of this description.

Finally, the enthalpy and entropy of mixing proposed for the solid solution formation was incorporated into the model to yield the isothermal liquidus compositions depicted as solid lines in figure 11. This consideration produced very little influence on the calculated liquidus compositions, with the greater influence occurring at the higher temperatures as expected since the multiplying exp (Γ) terms are also increasing with temperature.

For comparison, the binary limits of the ternary phase diagram were calculated with the model presented here. Figure 12 shows, as

open circles, the calculated liquidus line for the GaSb binary system. The solid line represents the experimental phase diagram of Maglione and Potier.[39] Shown in figure 13 is a similar plot for the In-Sb binary system. Here the experimental liquidus line of Liu and Peretti[40] is shown (solid line). The model developed here performs exceptionally well in the binary limits.

With the aid of this model it was also possible to calculate solid-liquid tie lines and solidus compositions. Figure 14 depicts the isothermal solidus compositions at various temperatures calculated under the assumption that both the liquid and solid phases are ideal. Plotted here is the mole fraction of GaSb in the solid phase versus the liquid phase Ga mole fraction. Such a plot completely specifies the ternary equilibrium compositions as the remaining compositions can be easily ascertained from the liquidus lines (figures 10 or 11) and simple material balances. For equilibrium temperatures below the melting temperature of the lowest melting binary compound (InSb) it is possible to precipitate solid solutions throughout the entire composition range while for temperatures higher than Tm(InSb) the GaSb solid composition in this case is constrained to $X_{Gasb} > X_{GaSb\ (pseudobinary)}$.

For comparison, figure 15 shows the isothermal solidus compositions calculated with the model that accounts for both the liquid and solid phase deviations from ideal behaviour. As was found before, marked differences exist between the real and ideal cases. Such plots as shown in figures 11 and 14 are extremely useful to educe growth conditions in that device characteristics generally define the solid composition

required. Unfortunately very little experimental information is available where both the equilibrium liquidus and solidus composition have been measured. In these measurements generally one composition is measured and the other is calculated from an appropriate model.

A more direct comparison between the ideal and real cases can be made as follows: First a GaSb distribution coefficient defined as

$$K_{GaSb} = X_{GaSb}/x_{Ga} \tag{38}$$

is formulated. In the case of ideal solution behaviour substitution of Equations (36) and (37) into (38) produces the simple result

$$K^{Ideal}_{GaSb} = 4x_{Sb}\ \exp(\Gamma_{GaSb}) \tag{39}$$

Thus, in the ideal case a plot of K_{GaSb} versus X_{Sb} should be linear and have a zero intercept at constant temperature. The slope of the line is proportional to the temperature only. Further a log-log plot would yield the GaSb term as the intercept.

For solid and liquid solutions that deviate from ideal behavior, an equation similar to Equation (39) can be derived and has the form

$$K_{GaSb} = 4A\ x_{Sb}\ \exp(\Gamma_{GaSb}) \tag{40}$$

where the term A is given by

$$A = \frac{\gamma^{\ell}_{Ga}\ \gamma^{\ell}_{Sb}}{\gamma_{GaSb}\ \gamma^{s.l.}_{Ga}\ \gamma^{s.l.}_{Sb}} \tag{41}$$

and is a function of both temperature and composition and therefore this term is responsible for deviations from the ideal line given by Equation (39).

Plotted in figure 16 as the solid line is K_{GaSb} versus x_{Sb} calculated with the model presented here. For comparison the dashed line represents

the values calculated with Equation (39). As can be seen in the real case, the curves are shifted to the right of the ideal solution line and are non-linear though in the range of $6 > K_{GaSb} > 2$ the real curve is nearly linear and has a slope very close to the ideal case. Also plotted are the available experimental results although the liquidus composition data of Gratton and Woolley[26] were calculated rather than measured. The results of these calculations show good agreement with the experimental data.

E. CONCLUSION

For the first time Gibbs energies were measured in the liquid phase pseudobinary system Ga-In-Sb. Moderate negative deviations throughout the entire Group III composition range were found in the high temperature solid state electrochemical cell used. Component activity coefficients were developed in the form of a Margules function with the aid of binary solution data and the results presented here. The literature enthalpy of mixing results in the ternary system were analyzed. This analysis, combined with the measurements of this study, allowed the prediction of the pseudobinary phase diagram and showed excellent agreement with the experimental results. The calculational methods were extended to a description of the complete ternary system phase diagram and again good consistency with experimental liquidus and solidus data was found.

REFERENCES

1. C. Hilsum and H.D. Rees, Elect. Letters, 6, 277 (1970).
2. J.C. MacGroddy, M.R. Lorentz, and T.S. Plaskett, Solid State Commun., 7, 901 (1969).
3. H. Hoshino, Y. Nakamura, M. Shimoji, and K. Niwa, Ber. Bensenger, 69, 114 (1965).
4. K.A. Klinedinst and D.A. Stevenson, J. Chem. Thermo, 4, 565 (1972).
5. K. Wohl, Trans. Am. Inst. Chem. Engrs., 42, 215 (1946).
6. J.M. Prausnitz, Molecular Thermodynamics of Fluid-Phase Equilibria, Prentice-Hall, Inc., 1969.
7. A.A. Vecher, E.I. Voronova, L.A. Mechkovskii, and A.S. Skoropanov, Russ. J. Phy. Chem., 48, 584 (1974).
8. I. Ansara, M. Gambino, and J.P. Bros, J. Cryst. Growth, 32, 101 (1976).
9. I. Ansara, J.P. Bros, and M. Gambino, Conf. Int. Thermo. Chim, 4th, Montpellier, France, Vol. 3, 29 (1975).
10. B. Predel and D.W. Stein, J. Less-Common Metals, 24, 391 (1971).
11. F.E. Wittig and E. Gehring, Z. Elekt., 71, 29 (1967).
12. J.P. Bros, R. Gastanet, and M. Laffite, Compt. rend. C, 264, 184 (1967).
13. A. Yazawa, T. Kawashima, and K. Itagaki, J. Japan Inst. Metals, 32, 1288 (1968).
14. M. Gambino and J.P. Bros, J. Chem. Thermodynamics, 7, 443 (1975).
15. B.D. Lichter and P. Sommelet, TMS-AIME, 245, 99 (1969).
16. R. Hultgren, P.S. Desai, D.T. Hawkins, M. Gleiser, and K.K. Kelley, Selected Values of the Thermodynamic Properties of Binary Alloys, Amer. Soc. Met. (1973).

17. W. Koster and B. Thoma, Z. Metallk., 46, 293 (1955).

18. N.A. Goryunova and N.N. Fedorova, J. Tech. Phys. (USSR), 25, 1339 (1955).

19. J.C. Woolley and D.G. Lees, J. Less-Common Metals, 1, 192 (1959).

20. J.C. Woolley, B.A. Smith, and D.G. Lees, Proc. Phys. Soc. London, 69B, 1339 (1956).

21. J.C. Woolley and B.A. Smith, Proc. Phys. Soc. London, 72, 214 (1958).

22. I. Ye. Gorshkov and N.A. Goryunova, Zh. Neorg. Khim, 3, 668 (1958).

23. L.V. Nikitina and V.I. Romanenko, Izv. Akad. Nauk SSSR, Metallurgia i Gornoe Delo, 6, 156 (1964).

24. V.B. Ufimtsev, A.S. Timoshin and G.V. Kostin, Neog. Mat., 7, 2090 (1971).

25. G.M. Blom and T.S. Plaskett, J. Electrochem. Soc., 118, 1831 (1971).

26. M.F. Gratton and J.C. Woolley, J. Electrochem. Soc., 125, 657 (1978).

27. V.I. Ivanov-Omskii and B.T. Kolomiets, Sov. Phys. Solid State, 2, 363 (1960).

28. A. Joullie, R. Dedies, J. Chevrier, and G. Bougnot, Rev. Phys. Appl., 9, 455 (1974).

29. G.A. Antypas, J. Cryst. Growth, 16, 181 (1972).

30. F.A. Trumbore, P.E. Freeland, and D.A. Mills, J. Elect. Soc., 109, 645 (1962).

31. A. Joullie, R. Aulombard, and G. Bougnot, J. Cryst. Growth, 24/25, 276 (1974).

32. V.B. Ufimtsev, A.S. Timoshin, and G.V. Kostin and A.N. Krestovnikov, Neorg. Mat. 7, 2088 (1971).

33. L.A. Mechkovskii, A.A. Savitskii, V.F. Skums, and A.A. Veecher, Russ. J. Phys. Chem., 45, 1143 (1971).

34. V.M. Glazov, A.S. Timoshin, and V.B. Ufimstev, Dolk. Akad. Nauk SSSR, 218, 1097 (1974).

35. L.M. Foster and J.F. Woods, J. Electrochem. Soc., 118, 1175 (1973).

36. G.B. Stringfellow, J. Phys. Chem. Solids, 33, 665 (1972).

37. G.B. Stringfellow, J. Phys. Chem. Solids, 34, 1749 (1973).

38. M.B. Panish and M. Ilegems, Progress in Solid State Chemistry, eds. H. Reiss and J.O. McCaldin (Pergamon Press, New York, 1972), 7, p. 39-83.

39. M.H. Maglione and A. Potier, J. Chim. Phys., 65, 1595 (1968).

40. T.S. Liu and E.A. Peretii, A.S.M. Trans., 44, 539 (1952).

List of Figures

Fig. 1 Typical measured open circuit voltages as a function of temperature in the liquid $Ga_XIn_{1-X}Sb$ pseudobinary system.

Fig. 2 Margules representation of the liquid Ga-Sb and In-Sb binary systems. ○ - gallium activity coefficients this work; □ - indium activity coefficients this work, △ - indium activity coefficients reference 3. Solid line represents linear regression results.

Fig. 3 Gallium and indium liquid phase activities in the $Ga_XIn_{1-X}Sb$ pseudobinary system as a function of GaSb liquid phase mole fraction. ○ - gallium activities this work; □ - indium activity this work. Solid line represents activities calculated with Equation (9) and constants listed in Table 2. Temperature is 1003 K.

Fig. 4 Iso-activity curves for the ternary Ga-In-Sb liquid phase system at 1003 K. Calculated with equation (9) and constants listed in Table 2. ———, constant gallium activity; ——— - ———, constant antimony activity; - - - - - - -, constant indium activity.

Fig. 5 Enthalpy of mixing in the $Ga_XIn_{1-X}Sb$ pseudobinary liquid system. □, results of Vecher et al; ○, results of Ansara et al.; - - - - - -, regression results with data of Vecher et al; , regression results with data of Ansara et al. Measurements on entire ternary system used in regression analysis.

Fig. 6 Lines of constant enthalpy of mixing (cal_{th} $g^{\circ}atom^{-1}$) in the ternary Ga-In-Sb liquid system calculated with Equation (15) and the parameters listed in Table 4 at 1003 K.

Fig. 7 Gibbs energy and entropy of mixing in the $Ga_XIn_{1-X}Sb$ pseudobinary liquid system at 1003 K. ————, ΔG^M this work; ----------, $T\Delta S^M$ this work with ΔH^M results of Ansara et al; ——— - ——— $T\Delta S^M$ ideal solution.

Fig. 8 The experimental $Ga_XIn_{1-X}Sb$ pseudobinary phase diagram. ○, DTA results of Woolley et al; □, ordinary thermal analysis results of Woolley et al; Δ, X-ray results of Woolley et al; X, Blom and Plaskett; Gorshkov and Goryunova; ■ Ufimtsev et al; ▲ Hultgren et al.

Fig. 9 The calculated $Ga_XIn_{1-X}Sb$ pseudobinary phase diagram; ---------, ideal solid and liquid solution; ——— - ———, real liquid and ideal solid solution; ———, real liquid and solid solution, Experimental results of Woolley et al; ○, DTA; □, OTA; Δ, X-ray.

Fig. 10 Liquidus isotherms in the Ga-In-Sb system: ----------, calculated assuming ideal liquid and solid solution behaviour; smooth values of experimental results; ○, Blom and Plaskett; □, Maglione and Potier, △, Liu and Peretii; X, Joullie et al; ○, Woolley et al; ▲, Antypas.

Fig. 11 Liquidus isotherms in the Ga-In-Sb system: ——— - ———, calculated assuming ideal solid and real liquid solution behavior; ———, calculated assuming real liquid and solid solution behavior; experimental data same as listed in figure 10.

Fig. 12 The Ga-Sb phase diagram: ○, calculated with model developed here; ————, experimental results of Maglione and Potier.

Fig. 13 The In-Sb phase diagram: ○, calculated with model developed here; ———, experimental results of Liu and Peretii.

Fig. 14 Solidus composition in $Ga_XIn_{1-X}Sb$ as a function of liquidus composition along the isotherms of figure 10 (ideal liquid and solid solutions assumed): a, 948 K; b, 873 K; c, 773 K; d, 673 K; e, 573 K.

Fig. 15 Solidus composition in $Ga_XIn_{1-X}Sb$ as a function of liquidus composition along the isotherms of figure 11 for real liquid and solid solutions: a, 948 K; b, 873 K; c, 773 K, d, 673 K.

Fig. 16 The GaSb distribution coefficient as a function of the liquidus composition along the isotherms of figures 10 and 11. --------, ideal liquid and solid solution; ————, real liquid and solid solution; ○, Gratton and Woolley; ●, Joullie et al; a, 948 K, b, 873 K; c, 773 K; d, 673 K.

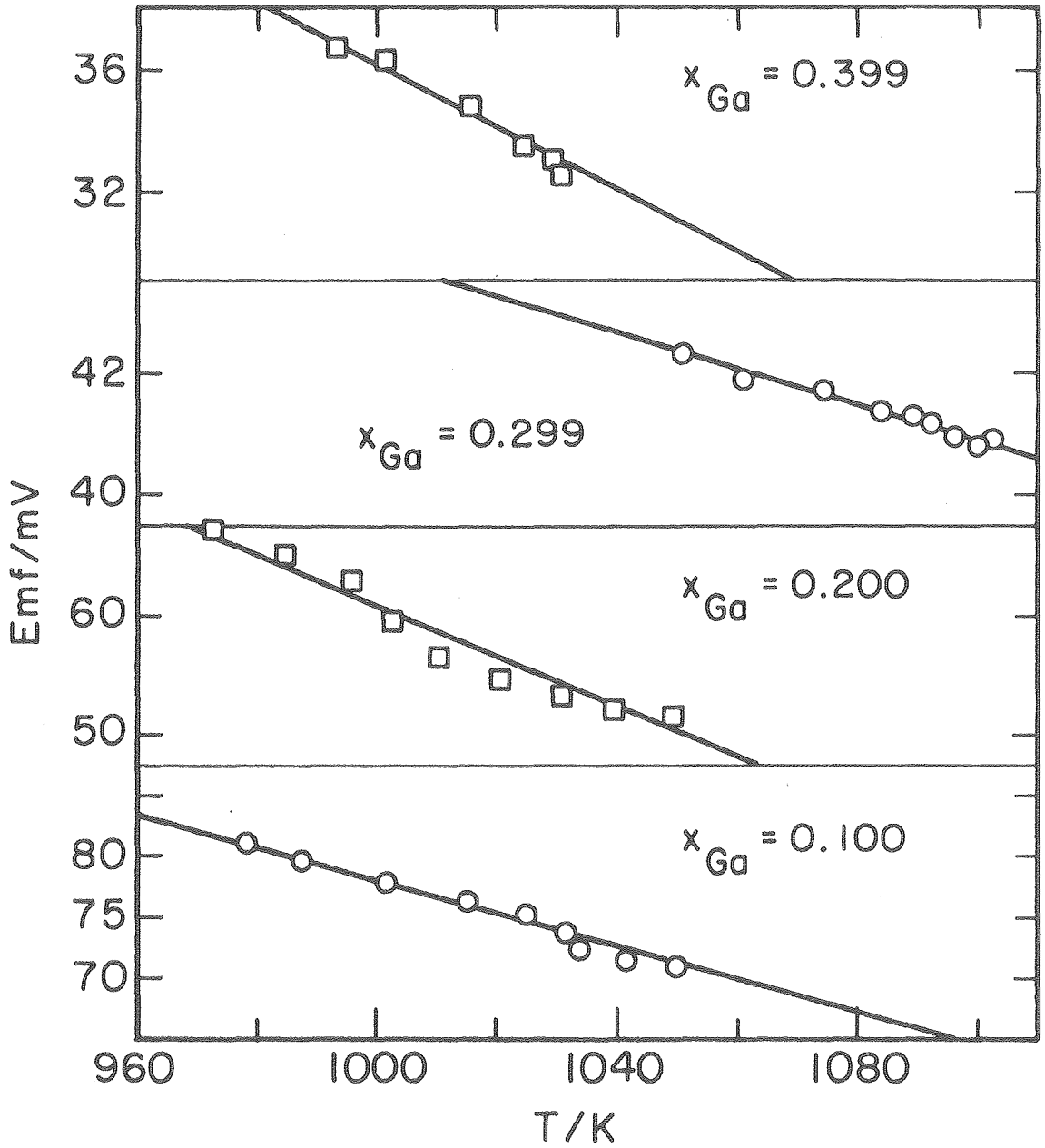

XBL 788-10384

Figure 1.

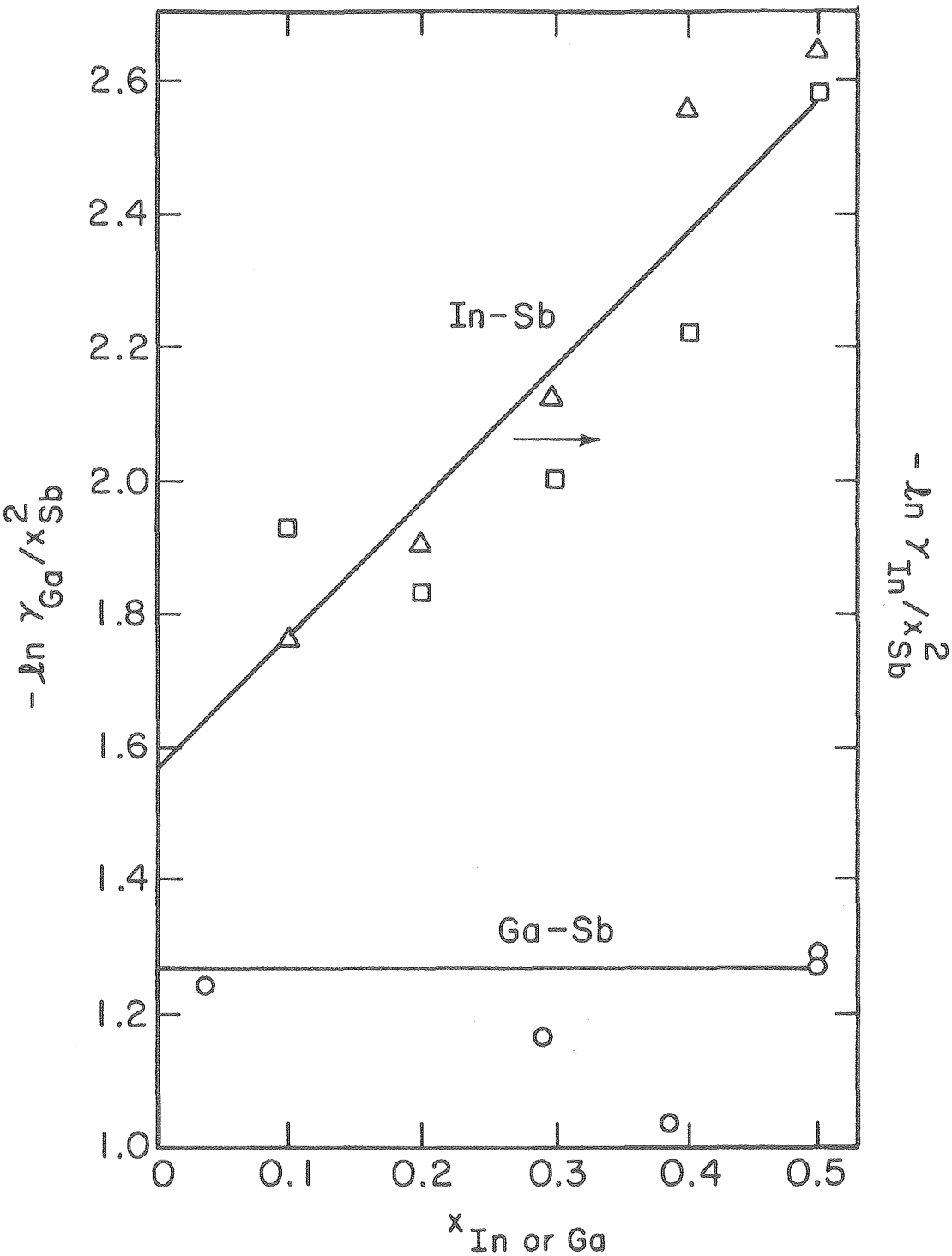

XBL 788-10383

Figure 2.

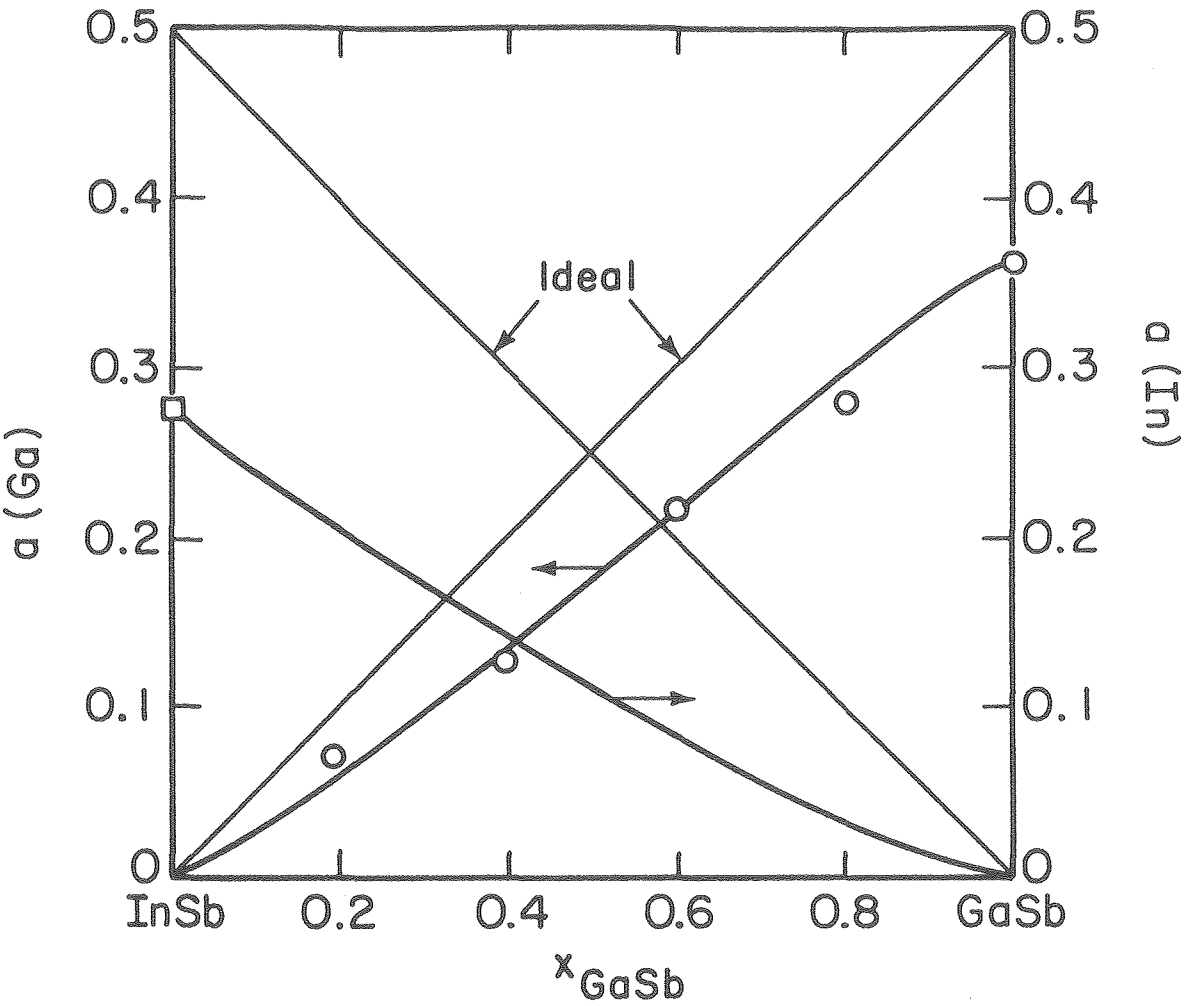

XBL 788-10385

Figure 3.

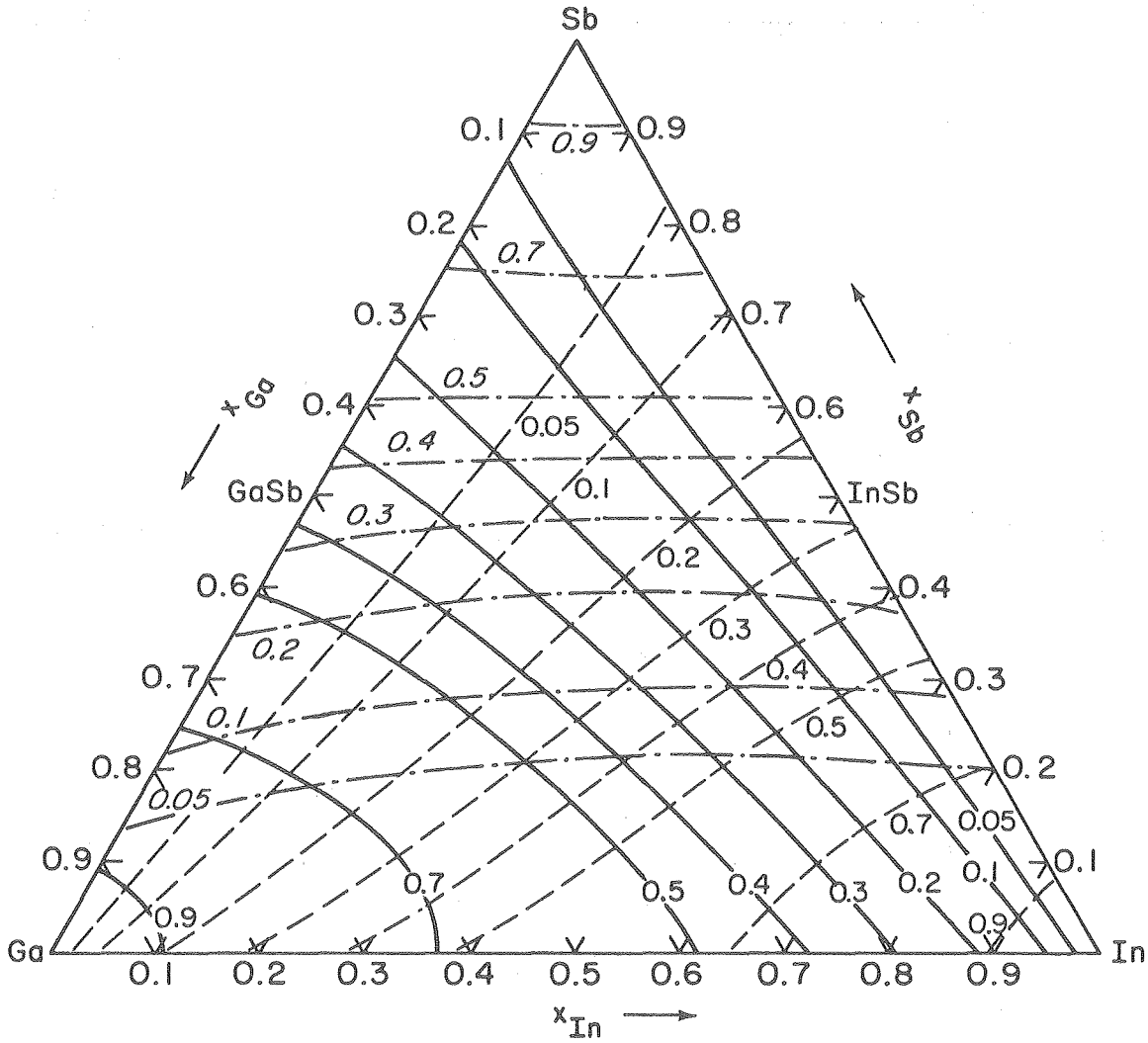

XBL 788-10386

Figure 4.

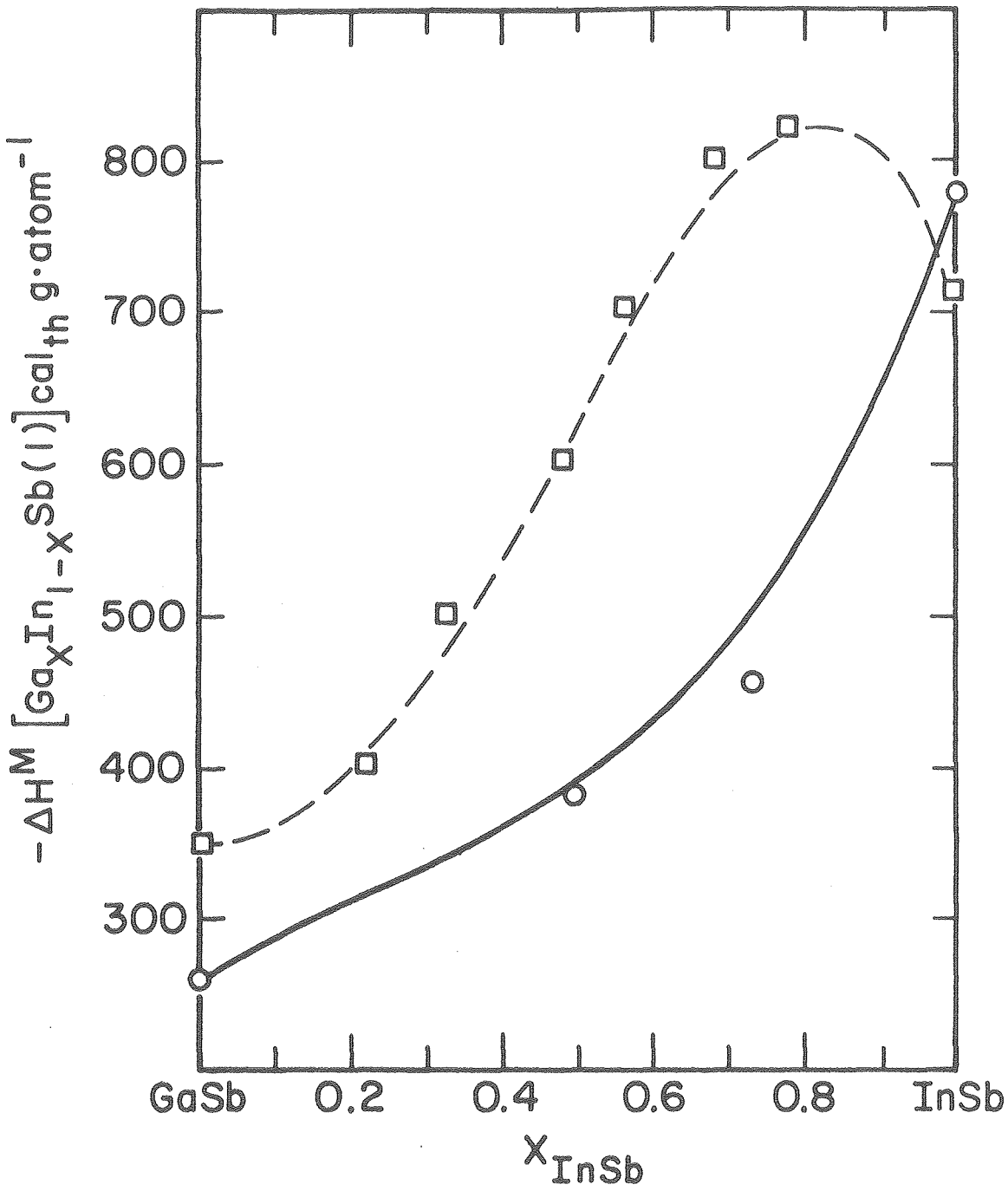

XBL 788-10379

Figure 5.

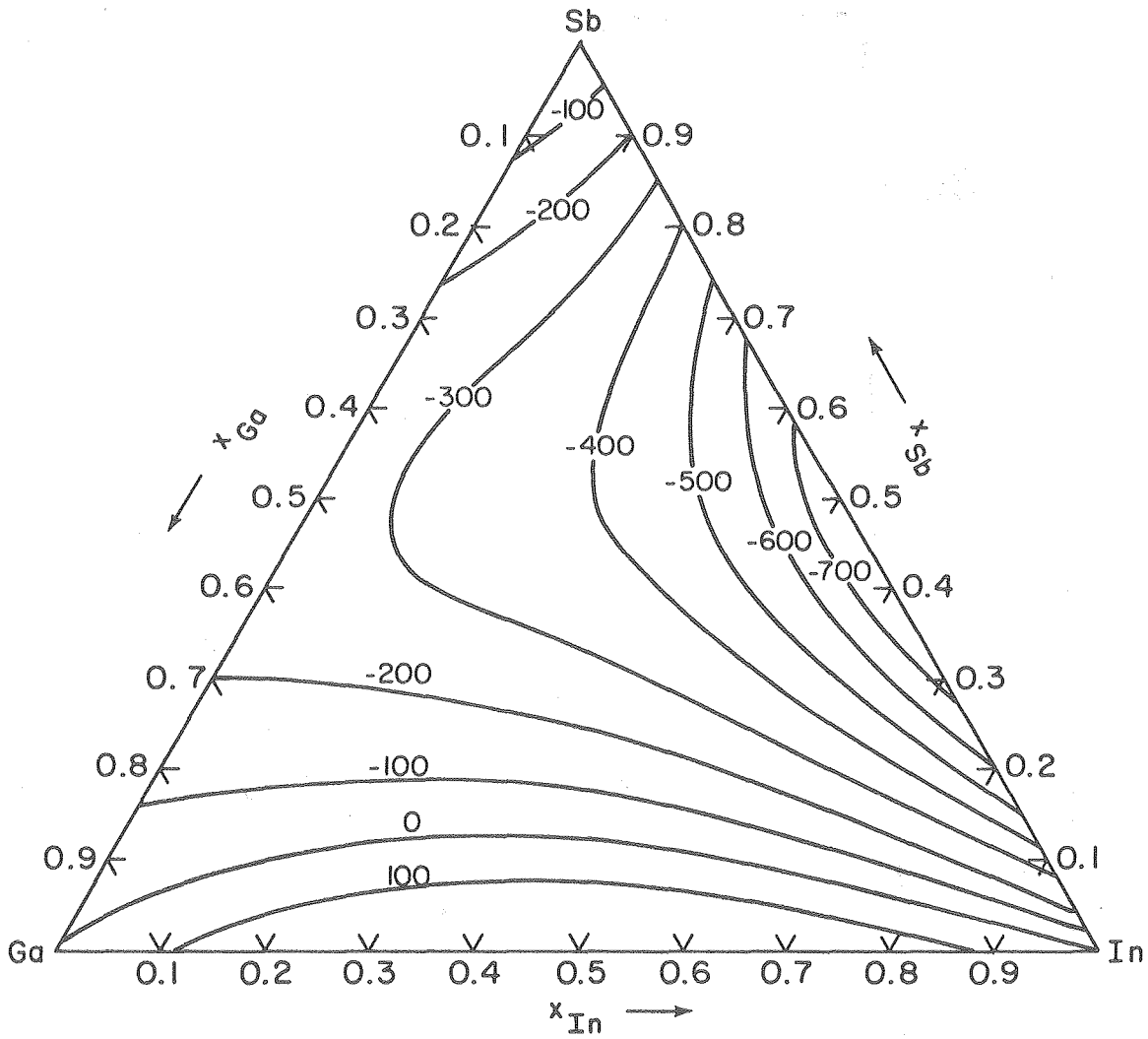

XBL 788-10387

Figure 6.

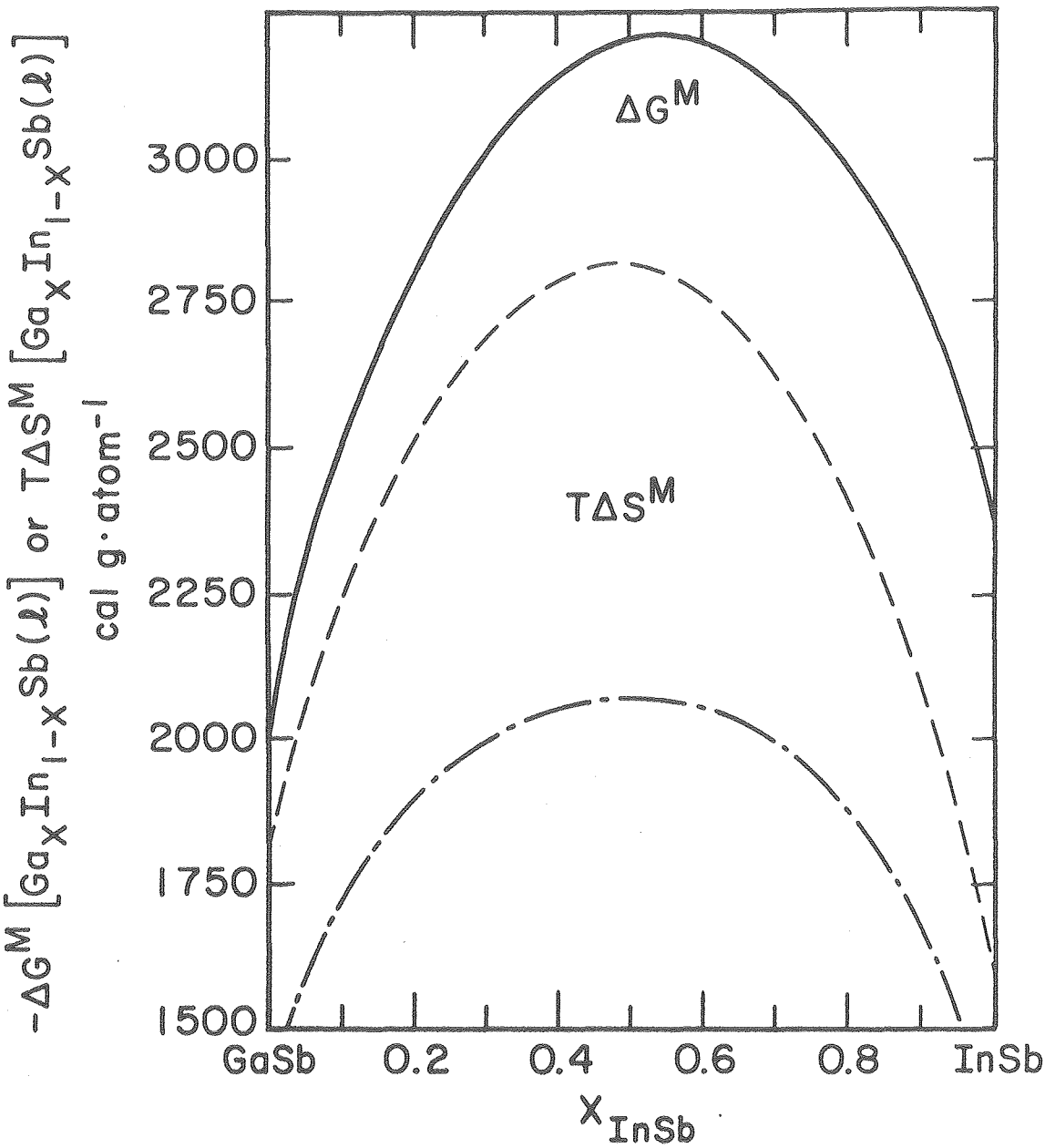

XBL 788-10378

Figure 7.

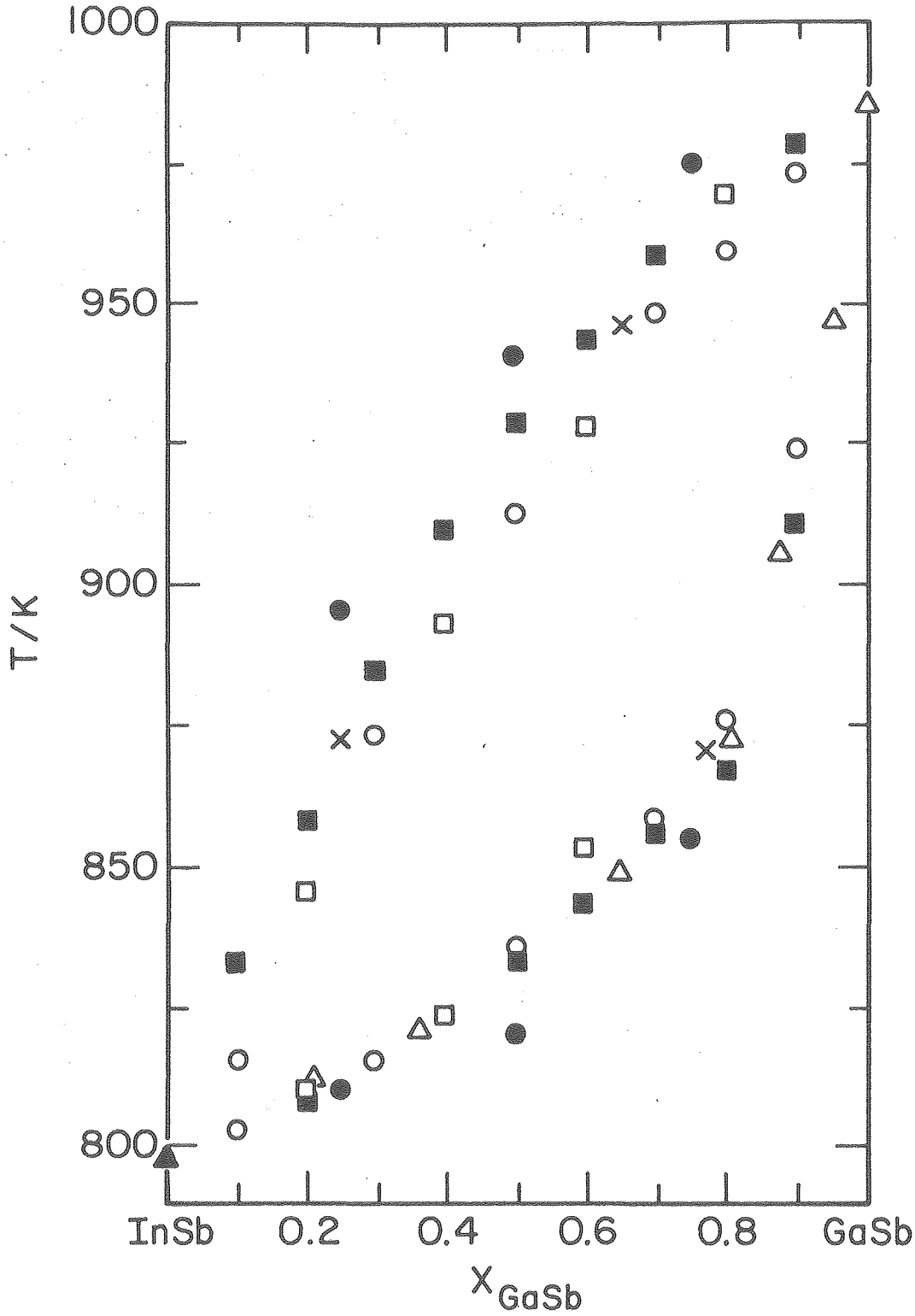

XBL 788-10382

Figure 8.

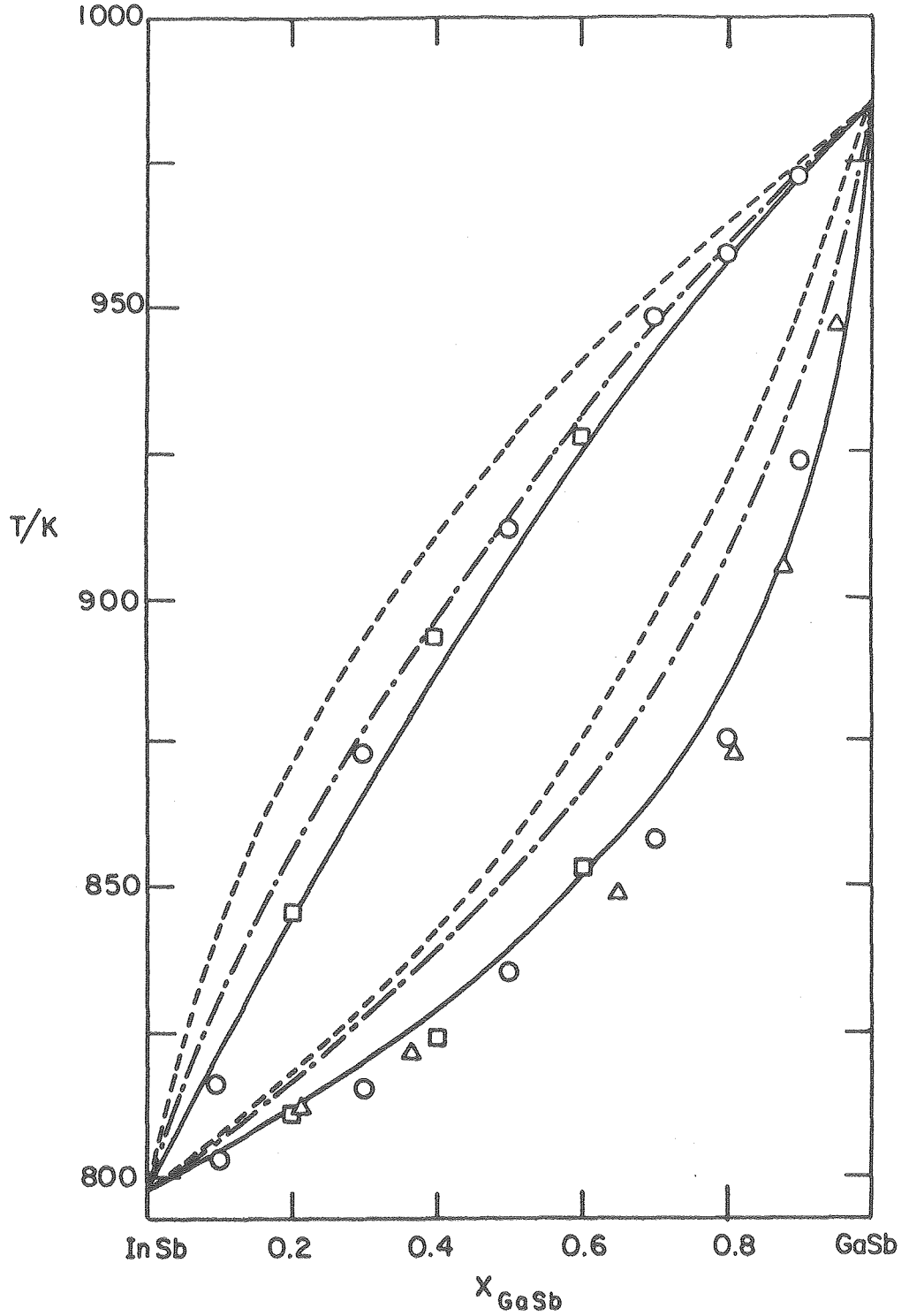

XBL 794-6063

Figure 9.

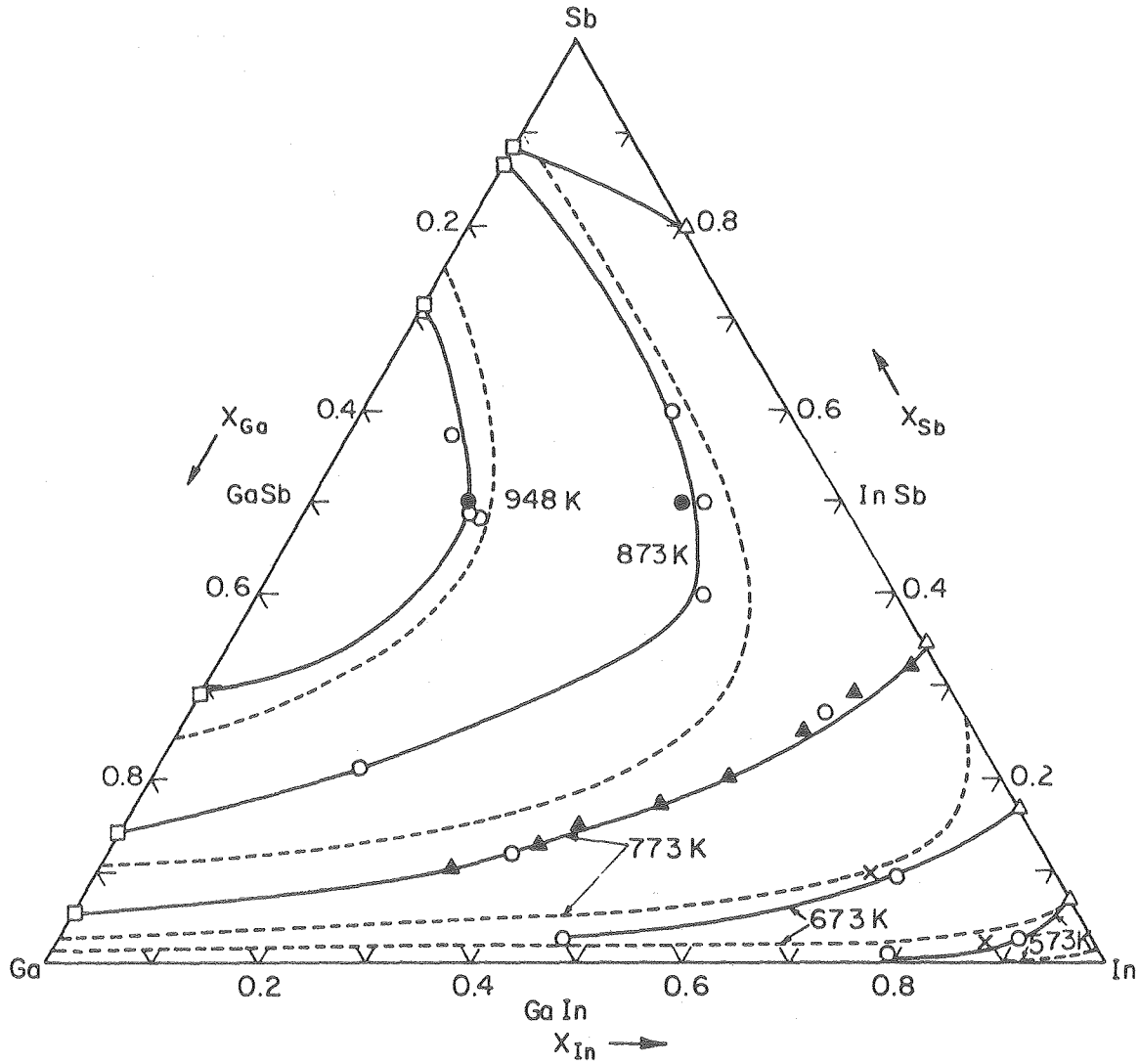

XBL794-6064

Figure 10.

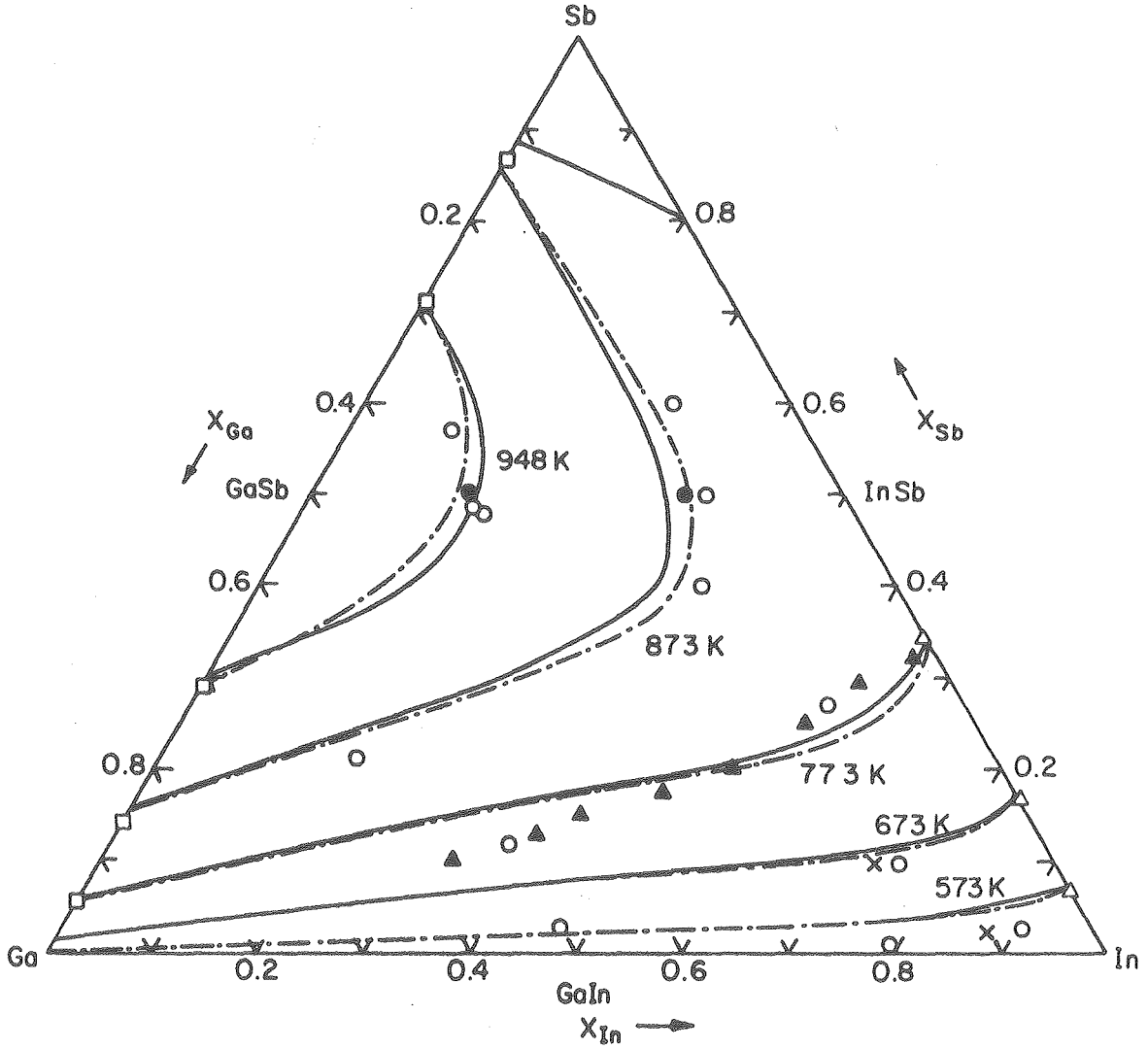

XBL794-6065

Figure 11.

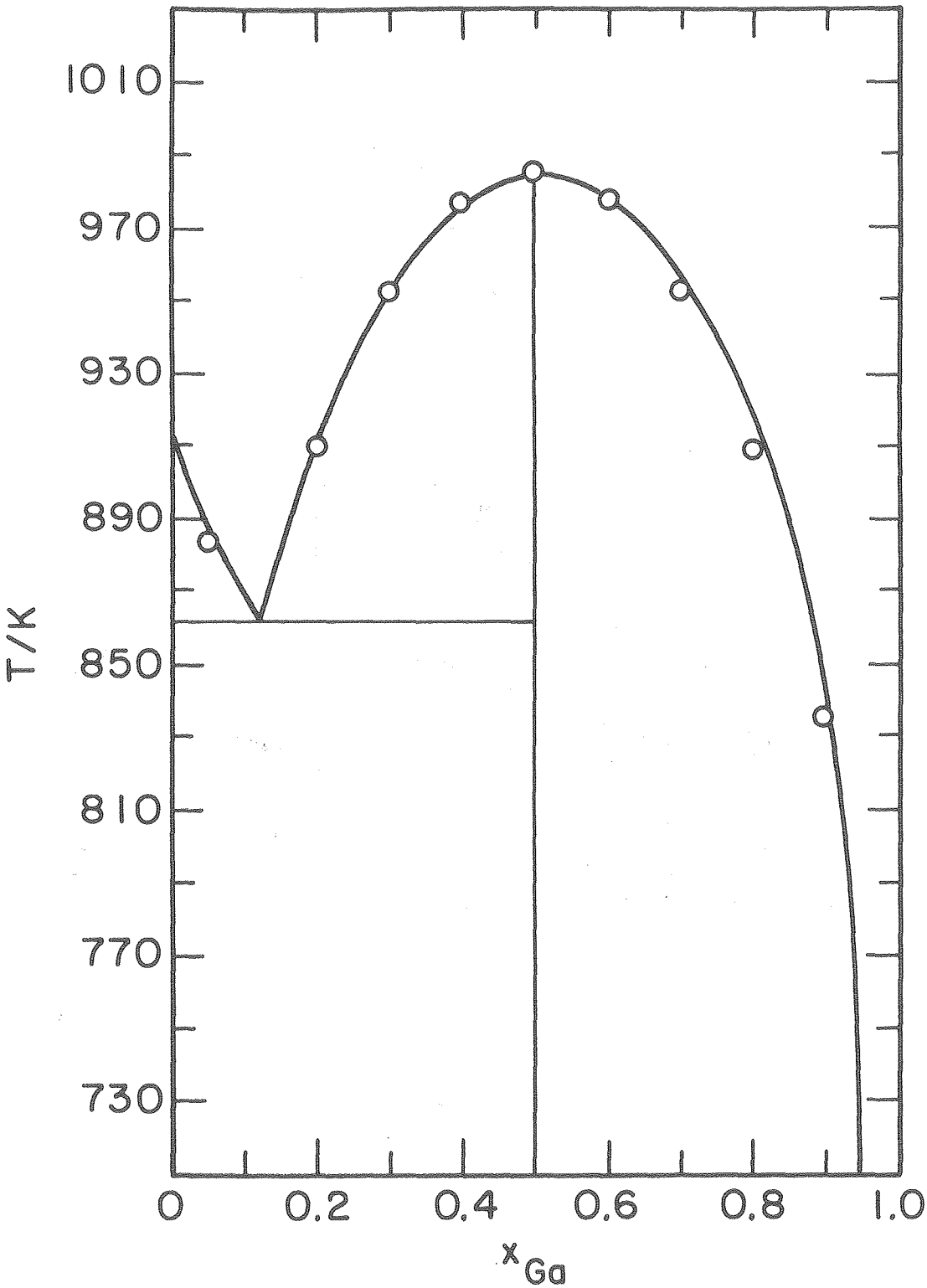

XBL 788-10380

Figure 12.

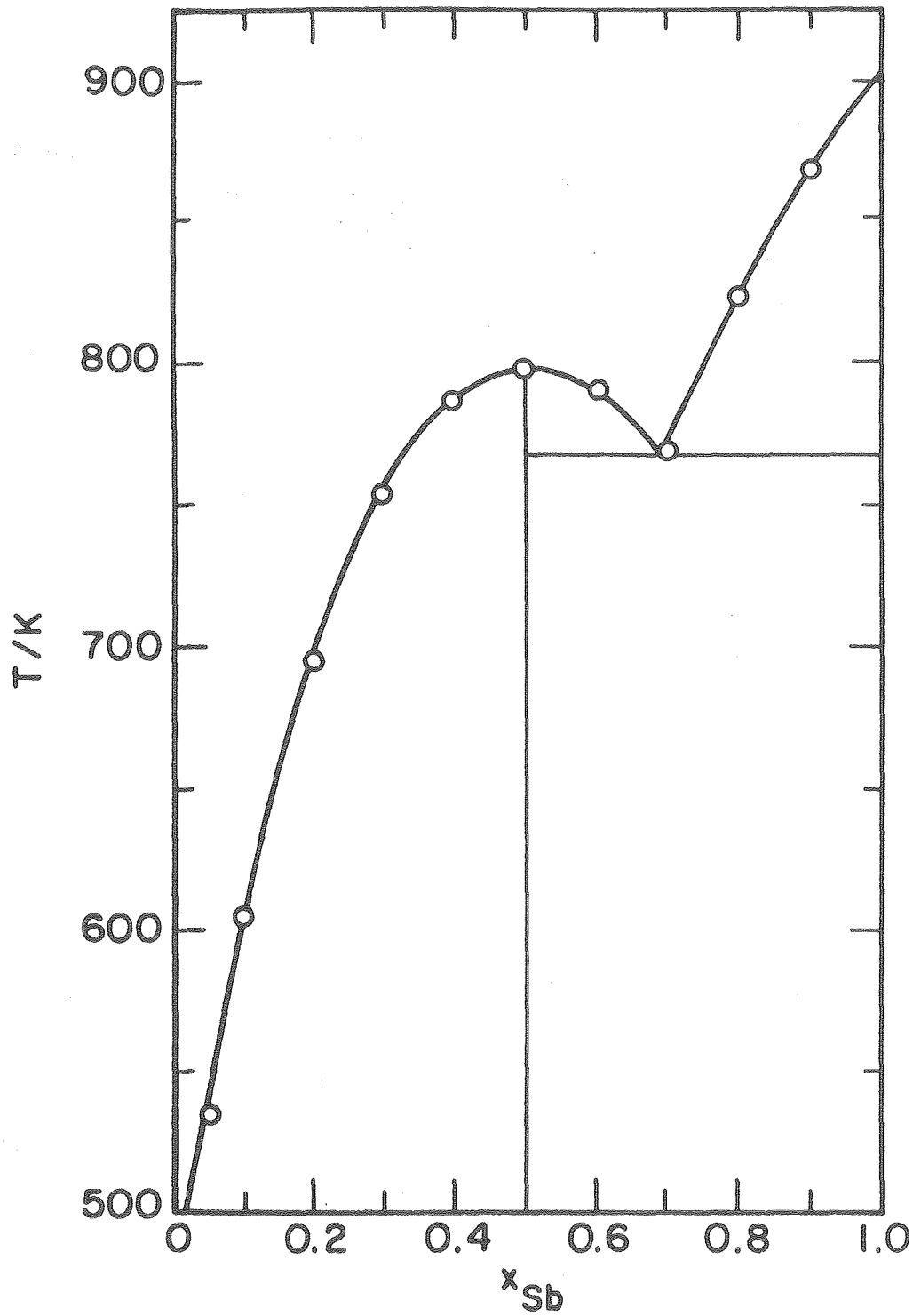

XBL 788-10381

Figure 13.

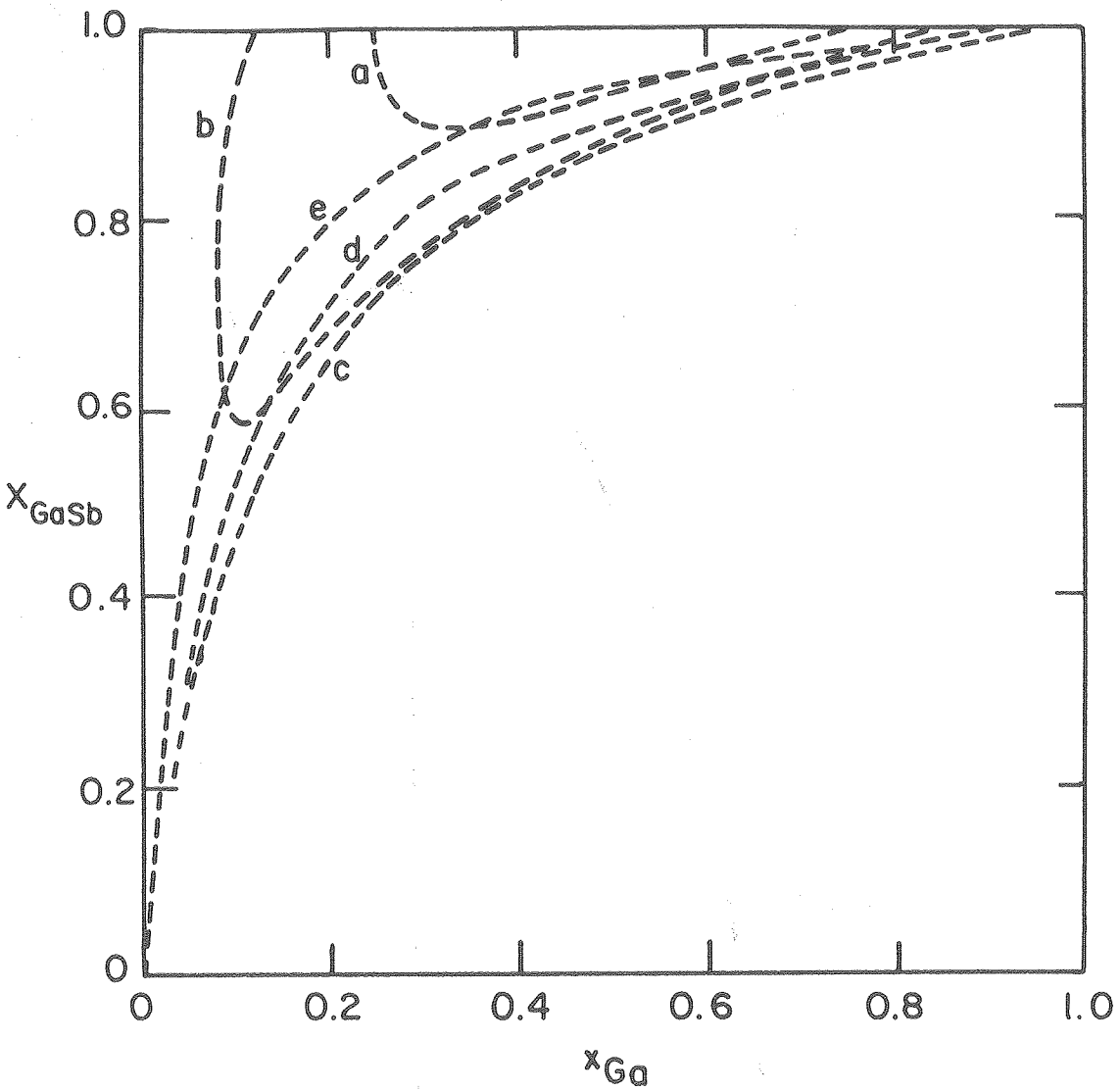

Figure 14.

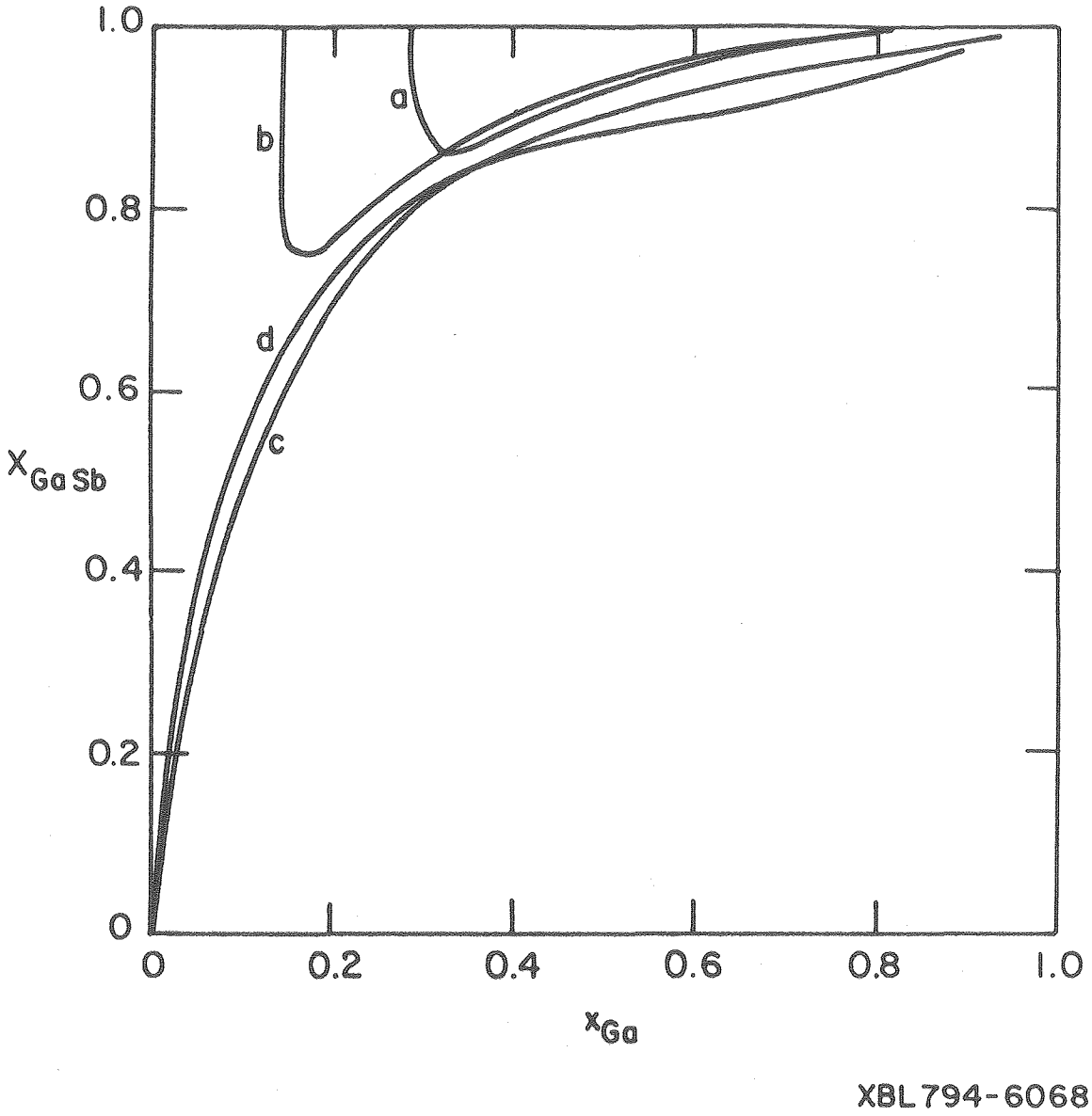

Figure 15.

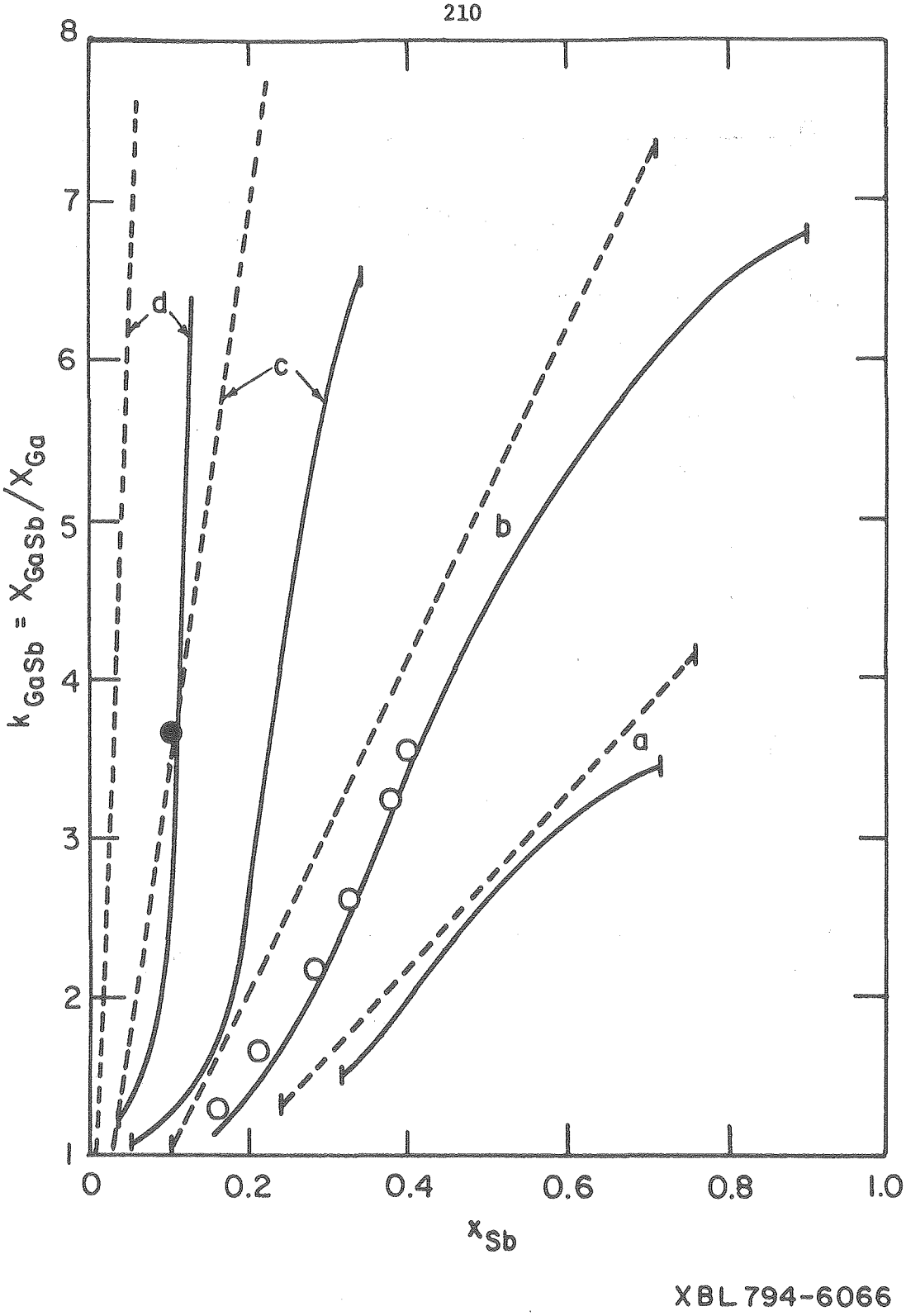

Figure 16.

0 0 0 0 5 1 0 5 1 9 8

CHAPTER VII. SUMMARY

The importance of Group III-V ternary and quaternary solid solutions as materials for improved solid-state electronic devices is currently being realized. As the growth of many of these solid solutions is accomplished by precipitation from the liquid phase, knowledge of the solid-liquid phase diagrams is essential, especially for the exploratory investigation of new systems. Unfortunately, an experimental determination of all the phase diagrams of current interest would require an enormous effort. A more expeditious method of providing the required phase equilibria information would be to develop reliable calculation techniques based upon observed thermodynamic behavior. The first stage of this effort was presented here and consisted of performing a comprehensive thermodynamic analysis of a single III-V ternary system, supplying missing information where discovered. In this way the system may serve as a basis for the development of an appropriate model for predicting phase equilibria in the remaining III-V systems. Thus, a thermodynamic analysis of the ternary Ga-In-Sb system was given here as an inaugural effort for accomplishing the long range objective of describing the solid-liquid phase fields of all III-V ternary and quaternary solutions. The goal of this initial investigation was then to develop a consistent thermodynamic property set for the Ga-In-Sb ternary system that could be used to accurately predict the corresponding solid-liquid phase diagram. This manuscript contains Gibbs energy, enthalpy and entropy values, for both the liquid and solid phases and throughout the entire composition range, that are internally consistent and that correctly yield the experimental

phase diagram. As a result of the work presented here several general conclusions and new results regarding the thermodynamics of III-V systems can be stated:

1. Experimental determinations of the Gibbs energy of formation of Ga_2O_3 and In_2O_3 and of Group III component activities in Ga-Sb, In-Sb, and $Ga_xIn_{1-x}Sb$ melts were performed. Consistent values of Gibbs energies, enthalpies and entropies were suggested for the solid materials Ga_2O_3, In_2O_3, GaSb, InSb and $Ga_xIn_{1-x}Sb$ and the contained elements and for the liquid solutions Ga-Sb, In-Sb, Ga-In, and Ga-In-Sb.

2. The mixing of a solution of Group III atoms with a solution of Group V atoms produces a <u>negative</u> enthalpy change and a <u>positive</u> excess volume and entropy change.

3. Component activities in concentrated III-V liquid mixtures exhibit negative deviations from ideal behavior.

4. Previous models (ideal solution, regular solution, and quasichemical theory) used to predict unknown multicomponent phase diagrams are unable to provide a correct description of this observed behavior. The limited success of these models is a result of forcing model parameters to match the known binary limits and therefore extrapolation to higher order systems yields dubious results.

5. Ancillary studies (transport properties, X-ray and neutron diffraction, etc.) indicate a tendency for pairing between Group III and V atoms. A model incorporating this observation predicts successfully the Ga-In-Sb ternary phase diagram.

In summary, a significant contribution has been made to understanding the solution thermodynamics of III-V systems. This work should serve as a basis for future investigations aimed at describing the necessary physical properties of these technologically important III-V materials. A list of possible future endeavors might contain:

1. Extend the use of solid-state electrochemical methods to other systems that include:

a. Investigate aluminum activities in III-V melts with a fluorine-ion conducting electrolyte.

b. Extend the Ga-In-Sb pseudobinary Gibbs energy measurements throughout the entire ternary composition range.

c. Galvanostatic/Potentiostatic determinations of oxygen diffusivities in III-V melts as a function of composition.

d. Determine binary compound activities in ternary and quaternary solid solutions.

2. Investigate models for describing the melt thermodynamics of III-V and II-VI solutions, giving particular attention to short range ordering chemical association and two-liquid theories.

3. Examine in greater detail the III-V solid phase, with emphasis placed on both the solid solution and the homogeneity range of the line compounds. In particular, considerable success has recently been exhibited with quantum mechanical calculations in predicting energy band diagrams.

APPENDIX I

SOLID-STATE ELECTROCHEMICAL STUDY OF THE GIBBS ENERGY OF FORMATION OF β-GALLIUM SESQUIOXIDE

A. INTRODUCTION

Gallium has become important in the semiconductor microelectronics industries as a component of compounds for electroluminescent and microwave devices. Gallium is also an important solvent for liquid-phase epitaxial crystal growth of compound semiconductors where oxygen is an electrically active impurity. Gallium sesquioxide added to Ga-GaP solutions has been used to achieve high electroluminescence efficiency in Zn-doped GaP light-emitting diodes.[1-4] Effective design of semiconductor device processes involving gallium should be aided by accurate thermodynamic data for gallium oxide. Additionally, knowledge of the Gibbs energy of formation of $\beta - Ga_2O_3$ is required to compute the gallium activity in liquid solution measured with a solid state electrochemical cell employing a non-gallium based reference electrode.

The Gibbs energy of formation of β-Ga_2O_3 by the reaction

$$2Ga(\ell) + \frac{3}{2} O_2(g) = Ga_2O_3(c) \qquad (1)$$

has been estimated by Coughlin[5] and measured using solid-state electrochemical methods by Klinedinst and Stevenson[6] and Smith and Chatterji.[7] Pankratz and Kelley[8] determined the high temperature heat content of $\beta - Ga_2O_3$ by calorimetric methods. More recently Mills[9] measured the heat capacity of $\beta - Ga_2O_3$ by drop calorimetry. Unfortunately, the Gibbs energies of formation as determined in the previous studies show

marked discrepancies, especially in the temperature dependence, i.e., the standard entropy of formation, and therefore, further experimentation and critical review of the data is appropriate. In this study the Gibbs energy of formation of $\beta - Ga_2O_3$ was measured in a high-temperature solid-state electrochemical cell with a $CO + CO_2$ gaseous mixture as the reference electrode. A microcomputer system was utilized for automated experimental control and for data acquisition, thereby providing continuous detection of any non-equilibrium conditions and of inconsistencies in experimental data.[10]

B. THEORY

The solid-electrolyte galvanic cell employed in measuring the Gibbs energy of formation of $\beta - Ga_2O_3$ can be represented schematically as

$$Pt|C|Ga(\ell),Ga_2O_3(c)||Ca_{0.15}Zr_{0.85}O_{1.85}||CO,CO_2|Pt \quad . \qquad (2)$$

The equilibrium partial pressures of oxygen in the two electrodes are related to the cell potential E, by the Nernst equation:

$$E/mV = \{R/4F\}(T/K)[\ell n\ \{p(O_2;CO+CO_2)/atm\} - \ell n\ \{p(O_2;Ga+Ga_2O_3)/atm\}]. \quad (3)$$

In this equation $p(O_2;CO+CO_2)$ indicates the oxygen fugacity of the $CO - CO_2$ gas mixture, $p(O_2;Ga,Ga_2O_3)$ represents that of the $Ga + Ga_2O_3$ mixture, R is the gas constant, T is the thermodynamic temperature and F is the Faraday constant.

The Gibbs energy of formation of $\beta - Ga_2O_3$ is related to the oxygen partial pressure over the $Ga + Ga_2O_3$ mixture by the equilibrium constant for the formation reaction:

$$K_f(Ga_2O_3) = a(Ga_2O_3)\ a(Ga)^{-2} p(O_2;Ga_2O_3,Ga)^{-3/2} \tag{4}$$

or

$$K_f(Ga_2O_3) = \exp\left\{-\Delta G_f^o(Ga_2O_3,c,T)/RT\right\} . \tag{5}$$

Equations 3 through 5 allow one to calculate $\Delta G_f^o(Ga_2O_3,c,T)$ from the measured experimental temperature and cell voltage:

$$\Delta G_f^o(Ga_2O_3,c,T) = 1.5\ RT\ \ell n\ p(O_2,CO + CO_2) - 6FE . \tag{6}$$

Here unit activities for $Ga(\ell)$ and $Ga_2O_3(c)$ in the mixture are assumed.

The reference oxygen partial pressure is established by the equilibrium reaction,

$$CO + \frac{1}{2} O_2 = CO_2 \tag{7}$$

and is related to the Gibbs energy change for this reaction, $\Delta G(7)$, by:

$$p(O_2;CO + CO_2) = \left(\frac{p(CO_2)}{p(CO)}\right)^2 \exp\{2\Delta G(7)/RT\} \tag{8}$$

where $\Delta G(7)/cal_{th}mol^{-1} = -68,270 - 0.18T\ \ell n\ T - 0.34 \times 10^{-3}T^2 + 0.87\ 10^5/T + 23.28T$, can be deduced from the equations given by Wicks and Block[11] for the Gibbs energies of formation of CO and CO_2.

C. EXPERIMENTAL

1. The Experimental Cell

The basic, solid-state galvanic cell design is depicted in figure 1. The cell consisted of a 5.08 cm diameter, closed-end alumina tube 45.7 cm in length secured by a Viton O-ring to a water-cooled, brass cell-head. Three 0.318 cm Cajon through-bore fittings were located on the cell head symmetrically around a 0.635 cm Cajon through-bore fitting. The thermocoupole lead wires contained in

ceramic sheaths were passed through the 0.318 cm fittings. The larger, centered fitting was used to seal to a 0.634 cm diameter calcia-stabilized zirconia (CSZ) electrolyte tube, closed at the bottom.

Included in the brass head were bores for gas entrance and exit. The exit placement was such that the gas had to flow downward to the experimental cell, then through an alumina pushrod. Three spring-loaded tungsten wires provided support for a graphite chamber containing liquid gallium and $\beta - Ga_2O_3$ in contact with the CSZ tube.

The electrode materials were contained in a 5.08 cm diameter closed graphite crucible fitted with a screw cap containing a closely fitting hole through which the CSZ tube was inserted into the gallium electrode. Powdered graphite was added to seal the CSZ tube to the graphite lid. Details of electrode compartments are shown in cross-section in figure 2.

The cell was heated with a Marshall resistance-heated furnace 51 cm in length with a 6.35 cm bore. Excellent temperature control was furnished by an integrating, temperature-regulated, power supply designed and built at the Lawrence Berkeley Laboratory. Temperature uniformity and stability was held to within ± 0.5 K in the vicinity of the electrodes. Stray cell voltages induced by the temperature regulation circuit were eliminated by a metal ground shield placed around the 5.08 cm alumina tube. Type-S thermocouples (0.051 cm diameter, Pt - Pt 10%Rh) were calibrated in the cell under vacuum against a thermocouple calibrated at the National Bureau of Standards.

The calibration was performed with the standard thermocouple occupying the position normally that of the electrode, while the unknown thermocouple was placed in the normal operating positions. Each thermocouple emf was amplified using a X100 thermocouple amplifier calibrated with a Leeds and Northrup Type K-3 potentiometer facility.

The cell emf was measured with a Keithley 640 electrometer. High-isolation, triaxial cable was used to connect the experimental cell to the input head of the electrometer. The inner conductor of the triaxial cable was connected to the positive lead wire of the cell. The outer conductor was driven by the unity-gain feedback from the electrometer, thus acting as a driven guard. Leakage sources at the input head were negligible since the cable was guarded up to the sapphire insulated electrometer contact.

2. Materials

Gallium metal used in the study was semiconductor grade, 99.9999% pure, obtained from Cominco American. Gallium oxide was obtained from Alfa Products, and had a purity of 99.99%. The oxide was confirmed to be $\beta - Ga_2O_3$ and to show no detectable second phases by X-ray diffraction analysis.

The calcia-stabilized zirconia tubes containing 7.5 weight per cent calcia were obtained from the Zircoa Corporation of America. The tubes were confirmed to be leak tight both before and after the experiments. Spectroscopic-grade graphite was employed in the electrode compartment containing the liquid metal and a small amount of the oxide. Platinum lead wires were attached to the graphite

compartment and to a platinum electrode made from Englehard unfluxed platinum paste (No. 6926) inside the CSZ tube end.

The $CO + CO_2$ reference electrode gas mixture was obtained from Matheson Gas Products. Chemical analysis showed the mixture to contain (25.29 ± 0.02) percent CO_2 and (2.45 ± 0.02) percent CO in high-purity argon. The ratio of the partial pressure of CO_2 to the partial pressure of CO in the primary standard gas was 10.322 ± .092.

Pure argon for use in purging the experimental cell was prepared by passing high-purity argon over Linde 4A molecular sieve at 195 K, then through a special, alumina-lined titanium-sponge purifer heated to 800 K. This gas was used as an inert purge gas for the metal-oxide electrode compartment, with the purge flow rate adjusted to $1\ cm^3 s^{-1}$.

Reagent dibutyl phthalate was used in gas exhaust traps to prevent back-diffusion of oxygen into the experimental cell.

3. Microcomputer Control System

Operation of the electrochemical experiments and data acquisition were automated with a microcomputer system based on an Intel 8008 microprocessor. The facility is schematically shown in figure 3. The system had the capability of setting the cell operation temperature to a predetermined, cyclical sequence of values and monitoring the cell emf and thermocouple output voltages on a specified time base until equilibrium had been established, thus allowing continuous cell operation without operator assistance. A 4 1/2 digit panel meter

alternately displayed the cell voltage and temperature, while a permanent record was obtained on a teletype. The microcomputer was constructed from components stocked at the Lawrence Livermore Laboratory.

4. Procedure

In each of several experiments the cell compartments were leak-checked using a high vacuum system, then purged with high purity argon. The cell temperature was programmed to rise at 0.02 Ks^{-1} to the lowest measurement temperature, after which the reference gas flow was initiated. The cell temperature was then sequentially incremented and decremented throughout the experimental range, with the cell voltage measured and periodically recorded at each temperature until equilibrium was reached and confirmed. Reference gas and argon flow rates did not affect the cell voltage in the ranges selected. At the conclusion of each experiment the cell compartments were again checked for leaks and the metal electrode examined for evidence of oxidation. The electrode material was then analyzed by X-ray diffraction to confirm the absence of side-reaction products.

D. RESULTS

Table 1 shows the measured cell potentials, the partial pressures of oxygen in the reference gas mixture, the calculated equilibrium partial pressures of oxygen in the $Ga + Ga_2O_3$ mixture, and the calculated values of the Gibbs energy of formation of $\beta - Ga_2O_3$ over the experimental temperature.

Table 1 Summary of Experimental and Derived Data*

T/K	$E_{measured}$/mV	$\log_{10} \frac{p(O_2;CO+CO_2)}{atm}$	$\log_{10} \frac{p(O_2;Ga+Ga_2O_3)}{atm}$	$\frac{\Delta G_f^o \ (Ga_2O_3,c,T)}{kcal_{th}mol^{-1}}$
776.9	421.1(±0.1)	-26.782(±.008)	-37.710(±.002)	-201.08(±.01)
815.1	418.4	-24.998	-35.347	-197.74
855.4	416.5	-23.288	-33.105	-194.36
902.3	415.4	-21.491	-30.773	-190.58
933.4	414.0	-20.400	-29.342	-187.98
967.9	412.4	-19.271	-27.861	-185.09
1004.4	410.9	-18.162	-26.410	-182.06
1039.9	409.1	-17.158	-25.090	-179.08
1044.7	408.5	-17.028	-24.911	-178.62
1048.8	408.5	-16.917	-24.770	-178.31
1051.1	407.9	-16.856	-24.680	-178.04
1059.5	408.0	-16.633	-24.397	-177.41
1091.2	406.9	-15.824	-23.342	-174.82

*atm = 101 325 Pa
cal_{th} = 4.184 J

A linear least-squares analysis of the experimental data obtained in the present study resulted in the following expression:

$$\Delta G_f^o(Ga_2O_3,c,T)/kcal_{th}mol^{-1} = (-265.83\pm0.16) + (0.08345\pm0.00016)(T/K). \quad (9)$$

The uncertainties given in this expression are those computed from the standard errors of the mean values. The constant term appearing in Equation 9 corresponds to the standard enthalpy change while the temperature coefficient represents the standard entropy change.

E. DISCUSSION

A comparison of the data obtained in this study with data reported in previous studies is shown in figure 4. This figure shows the experimental values of $\Delta G_f^o(Ga_2O_3,c,T)$ plotted against temperature, with the least-squares straight line drawn through the data points for each study. Also shown are the estimated Gibbs energies of formation versus temperature of Coughlin,[5] the calorimetric results of Pankratz and Kelley[8] and the emf measurements of Smith and Chatterji[7] and of Klinedinst and Stevenson.[6]

The $\Delta G_f^o(Ga_2O_3,c,T)$ values calculated from the experimental data of the present study showed excellent internal consistency with a standard error at 1000 K of only ±0.31 $kcal_{th}mol^{-1}$. In comparison to the results of other studies, the magnitude of $\Delta G_f^o(Ga_2O_3,c,T)$ found in this study was more negative, except at temperatures above 1000 K. Since electronic conduction in the solid electrolyte tends to reduce the cell voltage, and thus the magnitude of the Gibbs energy

of formation, the higher magnitudes of $\Delta G_f^o(Ga_2O_3,c,T)$ are supportive of complete ionic conduction in the solid electrolyte with possible electronic conduction at temperature above 1000 K. The possibility of electrolyte failure suggested separate data analyses in the low and high temperature ranges of measurement.

In order to evaluate the internal consistency of the experimental results, and to facilitate comparison to calorimetric data, a third-law analysis was performed. The values of the standard enthalpy of formation of $\beta - Ga_2O_3$, $\Delta H_f^o(Ga_2O_3,c,298.15)$, were calculated from the following equation:

$$\Delta H_f^o(Ga_2O_3,c,T) = \Delta G_f^o(Ga_2O_3,c,T) - \Delta_f\{H(T) - H(298.15)\}$$

$$+ T\,\Delta S_f^o(Ga_2O_3,c,T) + \Delta_f\{S(T) - S(298.15)\} \quad .$$

The values of $\Delta_f\{H(T) - H(298.15)\}$ and $\Delta_f\{S(T) - S(298.15)\}$ for $O_2(g)$ were taken from Hultgren et al.,[12] although similar values are given by Wicks and Block,[11] that for $Ga(\ell)$ from Hultgren et al.,[12] and that for $\beta - Ga_2O_3(c)$ from Mills.[9] The value $-72.87\ cal_{th}mol^{-1}K^{-1}$ for $\Delta S_f^o(Ga_2O_3,c,298.15)$ was determined from the data taken from Kelley[13] for $O_2(g)$ and from Adams, Johnston and Kerr[14] for $Ga(\ell)$ and $\beta - Ga_2O_3(c)$.

The results of the third-law analysis are presented in table 2. The overall mean value of $\Delta H_f^o(Ga_2O_3,c,298.15)$ and standard error of the mean were found to be −260.72 and 0.16 $kcal_{th}$, respectively, as indicated in analysis I. In this analysis, the cluster of data points near 1050 K were weighted so as to produce a uniform weighting of the

Table 2 Second-Law and Third-Law Analyses of the Experimental Data

	Third-Law Analysis		Second-Law Analysis		
T	$\Delta H_f^o(Ga_2O_3,c,298.15)$ / $kcal_{th}mol^{-1}$	δ_1 / $kcal_{th}mol^{-1}$	Observed log K_p	Calculated log K_p	δ_2
776.9	-261.46	-.74	-56.565	-56.543	-.022
815.1	-261.19	-.48	-53.019	-53.038	0.019
855.4	-260.98	-.26	-49.657	-49.680	0.023
902.3	-260.90	-.19	-46.160	-46.150	-.010
933.4	-260.76	-.04	-44.014	-44.005	-.009
967.9	-260.58	0.14	-41.792	-41.786	-.006
1004.4*	-260.41	0.30	-39.614	-39.605	-.009
1039.9*	-260.21	0.51	-37.631	-37.631	-.005
1044.7*	-260.13	0.59	-37.366	-37.374	0.007
1048.8*	-260.13	0.58	-37.156	-37.156	0.000
1051.1*	-260.05	0.67	-37.018	-37.035	0.017
1059.5*	-260.07	0.64	-36.595	-36.597	0.002
1091.2*	-259.96	0.76	-35.013	-35.004	-.009

Analysis I: $\Delta H_f^o(Ga_2O_3,c,298.15)/kcal_{th}mol^{-1}=-260.7$ Standard error/$kcal_{th}mol^{-1}$ = 0.2

$\Delta H_f^o(Ga_2O_3,c,298.15)/kcal_{th}mol^{-1}=-265.2$ Standard error/$kcal_{th}mol^{-1}$ = 0.1

Analysis II: $\Delta H_f^o(Ga_2O_3,c,298.15)/kcal_{th}mol^{-1}=-261.0$ Standard error/$kcal_{th}mol^{-1}$ = 0.1

$\Delta H_f^o(Ga_2O_3,c,298.15)kcal_{th}mol^{-1}=-265.5$ Standard error/$kcal_{th}mol^{-1}$ = 0.1

*Excluded from Analysis II

data over the temperature range of measurement. The calculated values of $\Delta H_f^o(Ga_2O_3,c,298.15)$ showed a small temperature dependence. This temperature dependence can be eliminated by adding 4.54 cal_{th} $mol^{-1}K^{-1}$ to $\Delta S_f^o(Ga_2O_3,c,298.15)$.

It is interesting to note the effect of utilizing alternate sources of thermodynamic data in the third-law analysis. Glassner reports a high temperature heat capacity for liquid gallium which is 5% higher than that selected by Hultgren, et al.[12] Nevertheless, if Glassner's heat capacity data is used in the third-law calculation, the results are essentially unchanged from those given in table 2. Similarly, a third-law analysis with the thermodynamic data of Wicks and Block[11] for $O_2(g)$ substituted for the selected data of Hultgren et al[12] also gave results nearly equivalent to those shown in table 2. On the other hand, the selected thermodynamic data of Coughlin,[16] when used in the third-law analysis gave a significantly different result for $\Delta H_f^o(Ga_2O_3,c,298.15)$, given by $-261.32 - 0.00196\ T\ kcal_{th}mol^{-1}$. Not only is the mean value of $-261.32 \pm 0.06\ kcal_{th}mol^{-1}$ outside the standard error of the analysis shown in table 2, but the temperature dependence differs in sign. Other third-law analyses utilizing heat capacity data for Ga_2O_3 derived from Shchukarev et al.[17] and from Pankratz and Kelley[8] support the results shown in table 2. The temperature dependence of $\Delta H_f^o(Ga_2O_3,c,298.15)$ in the third-law analysis indicates either an error in the estimated heat capacity of gallium at high temperatures, or a measured cell-voltage error which increases with increasing temperature.

The values of $\Delta H_f^o(Ga_2O_3,c,298.15)$ calculated from the third-law analysis are compared in figure 5 to the data of Mah,[18] determined by direct combustion calorimetry and to values derived from other studies. The value obtained by Shchukarev et al.[17] from isothermal evaporation studies and the value derived from the present study are in close agreement with the calorimetrically determined value of $-261.05\ kcal_{th}mol^{-1}$. Also shown in figure 5 are the results obtained from a third-law analysis of the data of Klinedinst and Steveson.[6] The resulting values for $\Delta H_f^o(Ga_2O_3,298.15)$ exhibit a large temperature dependence with the average value lying somewhat above the calorimetrically determined value. Third-law analyses of the electrochemical results of Smith and Chatterji[7] are shown by the dashed line in figure 5. Because the actual data were not available for this calculation, a data-fitted equation was used. This equation gave a nearly temperature-independent value of the standard heat of formation of $\beta - Ga_2O_3$, but shifted approximately $1.75\ kcal_{th}mol^{-1}$ above the calorimetrically-determined value. Smith and Chatterji[7] reported an error range of $0.8\ kcal_{th}mol^{-1}$ with no apparent temperature dependence from their third-law analysis.

The values of $\Delta H_f^o(Ga_2O_3,c,2981.5)$ calculated from the present experimental data show somewhat different temperature dependences in the low and high temperature ranges of measurement, as shown in figure 5. Below 970 K the calculated values of $\Delta H_f^o(Ga_2O_3,c,298.15)$ have a temperature dependence of $4.2\ cal_{th}mol^{-1}K^{-1}$, whereas above 970 K the temperature dependence is $5.4\ cal_{th}mol^{-1}K^{-1}$. On the assumption that

the experimental results are in error in the high temperature range, an additional third-law analysis was performed on the experimental data in the range below 970 K. This analysis is denoted by analysis II in table 2. The average value of $\Delta H_f^o(Ga_2O_3,c,298.15)$ obtained from analysis II was $-260.98\ kcal_{th}mol^{-1}$ with a standard error of $0.13\ kcal_{th}mol^{-1}$. This result differs from the value obtained in analysis I by an amount only slightly larger than the standard error, indicating no significant systematic error in the high temperature range alone. Thus, the small temperature dependence in $\Delta H_f^o(Ga_2O_3,c,2981.15)$ obtained in the third-law analysis most probably indicates a systematic error in the thermodynamic functions, rather than an experimental error in the high temperature range alone.

A second-law analysis of the data obtained in the present study was also performed, and the results are shown in table 2. The least-squares value of $\Delta H_f^o(Ga_2O_3,c,T_m)$ at the mid-point experimental temperature, $T_m = 934.05$ K was found to be $-265.83\ kcal_{th}mol^{-1}$. This value was corrected to 298.15 K by adding $-\Delta_f\{H(968.5) - H(298.15)\}$ to obtain $-265.15\ kcal_{th}mol^{-1}$ for the standard heat of formation of $\beta - Ga_2O_3$ from solid gallium. This value is larger in magnitude than the third-law analysis (I) by $4.43\ kcal_{th}mol^{-1}$, which is larger than the standard error of the mean values from both second-law and third-law analyses. A second analysis (II), in which the high temperature data above 970 K was excluded, yielded a value of -265.54 for $\Delta H_f^o(Ga_2O_3,c,298.15)$ within the standard error of the value obtained in analysis I. The difference between the values of $\Delta H_f^o(Ga_2O_3,c,298.15)$ derived from second-law and third law methods is not surprising,

because of the limited range in temperature of the experimental measurements. A small difference in slope of the measured $\Delta G_f^o(T)$ can produce a large change in the value of $\Delta H_f^o(298.15)$ derived from the second-law analysis.

A comparison of the standard entropy and enthalpy of formation of $\beta - Ga_2O_3$ as derived from different sources is summarized in table 3. The enthalpy and entropy values reported by each source were corrected to the reference temperature. The values of $\Delta H_f^o(Ga_2O_3,c,298.15)$ obtained in previous electrochemical studies differ significantly from that obtained in the present study, and are more consistent with the value selected by Brewer,[19] and by Rossini et al.,[20] (-258 ± 3 $kcal_{th}$), than with the more precise value obtained by Mah.[18] The results of the present study show the highest consistency with the combustion-calorimetric data.

A potential source of error in the present study was electronic conduction in the CSZ electrolyte. Shown in figure 6 are conservative and liberal lower oxygen partial pressure limits to the electrolytic domain of CSZ as derived from the data of Schmalzreid[21] and Patterson, Bogden and Rapp.[22] Also shown in figure 6 is the Gibbs energy of formation of $\beta - Ga_2O_3$ and Ga_2O.[16] The conservative limit places the $Ga_2O_3 - Ga - O_2$ equilibrium outside the ionic electrolytic domain at temperature above 880 K. The more recent and liberal limit places the most stable equilibrium of interest well within the limits of operation, however. In this study the working temperature was maintained below 1100 K in order to prevent conditions allowing electronic conduction in the solid

Table 3 Comparison of the Standard Enthalpy and Entropy of Formation of $\beta - Ga_2O_3$ from Different Sources

Method	$\Delta H_f^o(Ga_2O_3,c,298.15)/kcal_{th}mol^{-1}$			$\Delta S_f^o(Ga_2O_3,c,298.15)/cal_{th}mol^{-1}$		
	Experimental	Third Law	Second Law	Experimental	Second Law	Reference
Combustion Calorimetry	-261.05±0.3					18
Drop Calorimetry				-72.87		13,14
Isothermal Evaporation		-260.85±1.4				17
Electrochemical Cells						
coexistence electrode			-252.3		-65.1	6
coexistence electrode		-259.2	-258.8		-72.38	7
gas reference electrode			-252.1		-66.0	6
gas reference electrode		-260.7±0.2	-265.2±0.1		-77.60	This study (I)
gas reference electrode		-261.0±0.1	-265.5±0.1		-77.45	This study (II)

electrolyte. The results showed that while the emf data did not show a change in the temperature dependence at high temperature, the values of $\Delta H_f^o(Ga_2O_3,c,298.15\ K)$ derived from the third-law analysis showed a small increase in the temperature dependence above 970 K. This result indicates possible electronic conduction in the solid electrolyte above 970 K. For this reason, the third-law analysis (II) is considered to be a more accurate test of the emf data.

The most probable cause of the variation of $\Delta H_f^o(Ga_2O_3,c,298.15)$ with temperature is that the thermodynamic data for gallium is incorrect. The specific heat data for O_2 should be very accurate, and the more recent calorimetric data of Mills[9] for $\beta - Ga_2O_3$ agreed to within 1% with the data of Pankratz and Kelley.[8] The most likely source of error is in the specific heat of gallium, for which a constant heat capacity was assumed above 700 K. Indeed, it appears that no measurements of the specific heat of gallium have been made above 720 K, and the assumption of a constant specific heat in this temperature range is probably in error. Nevertheless, the direct measurement of $\Delta G_f^o(\beta - Ga_2O_3)$ performed in this study showed much better consistency with the calorimetric data than did the data from earlier emf studies, as shown by the second-law and third-law analyses.

F. CONCLUSION

The Gibbs energy of formation of $\beta - Ga_2O_3$ was measured with high accuracy in an electrochemical cell utilizing a CO + CO gaseous reference electrode. The use of a microcomputer system for automatic

control of the experiments proved exceptionally valuable for testing the reproducibility of the experimental data. The values of $\Delta H_f^o(Ga_2O_3,c,298.15)$ determined from a third-law analysis were in close agreement with the calorimetrically determined value. A small temperature dependence of the derived values of $\Delta H_f^o(Ga_2O_3,c,298.15)$ were attributed to errors in the predicted high temperature specific heat of gallium.

REFERENCES

1. H.G. Crimmeiss, H. Scholz, Phys. Letters, 8, 233 (1964).
2. M.R. Lorenz, M.J. Pilkuhn, J. Appl. Phys., 37, 4094 (1966).
3. R.A. Logan, H.G. White, F.A. Trumbore, Appl. Phys. Letters, 10, 206 (1967).
4. L.M. Foster, J. Scardefield, J. Electrochem. Soc., 116, 494 (1969).
5. J.P. Coughlin, U.S. Bur. Mines Bull. 542, (1954).
6. K.A. Klinedinst, D.A. Stevenson, J. Chem. Thermodynamics, 4, 565 (1972).
7. J.V. Smith, D. Chatterji, J. Am. Ceram. Soc., 56, 288 (1973).
8. L.B. Pankratz, K.K. Kelley, U.S. Bur. Mines Rep. Invest., 6198 (1963).
9. K.C. Mills, High Temp.-High Press, 4, 371 (1972).
10. L. Donaghey, Proc. IEEE, 64, 975 (1967).
11. C.E. Wicks, F.E. Block, U.S. Bur. Mines Bull., 605 (1963).
12. R. Hultgren, P.D. Desai, D.T. Hawkins, M. Gleiser, K.K. Kelley, D.D. Wagman, Selected Values of the Thermodynamic Properties of the Element, Amer. Soc. for Metals (1973).
13. K.K. Kelley, U.S. Bur. Mines Bull., 477 (1950).
14. G.B. Adams, H.L. Johnston, E.C. Kerr, J. Am. Chem. Soc., 74, 4784 (1952).
15. A. Glassner, Tech. Rept. ANL-5750; Argonne National Laboratory: Argonne, Illinois (1957).
16. J.P. Coughlin, U.S. Bur. of Mines Bull., 542 (1954).
17. S.A. Shchukarev, G.A. Semerov, I.A. Rat'kovskii, Russ. J. Inorg.

0 0 0 0 5 1 0 5 2 0 9

Chem., 14, 1 (1969).

18. A.D. Mah, U.S. Bur. Mines Rep. Invest. 5965 (1962).

19. L. Brewer, Chem. Rev., 52, 1, (1953).

20. F.D. Rossini, D.D. Wagman, W.H. Evans, S. Levine, I. Jaffe, Nat. Bureau of Standards Circ. 500, 1268 (1952).

21. H.Z. Schmalzreis, Elektrochem., 66, 572 (1962).

22. J.W. Patterson, C.C. Bogden, R.A. Rapp, J. Electrochem. Soc., 114, 752 (1967).

List of Figures

Fig. 1 Schematic diagram of the experimental cell.

Fig. 2 Cross-section diagram of the electrode compartment.

Fig. 3 Schematic of the microcomputer system utilized for experimental control and data acquisition.

Fig. 4 Comparison of the Gibbs energy of formation of $\beta - Ga_2O_3$ as a function of temperature. (———) Experimental data from this study. (———) Coughlin, (•••••) Pankratz and Kelley, (• ——•——) Smith and Chatterji, (-----) Klinedinst and Stevenson (coulometrically titrated oxygen), and (—— -- ——) Klinedinst and Stevenson (Ga,$\beta - Ga_2O_3$ electrode).

Fig. 5 Third-law calculation of $\Delta H_f^o(Ga_2O_3,c,298.15)$ and comparison to the calorimetric data of (———) Mah, and to values derived from the data of (—— - ——) Shchukarev et al., (-----) Smith and Chatterji, and (x coulometric titration; Δ coexistence electrode Klinedinst and Stevenson.

Fig. 6 Gibbs energy of formation of the oxides of gallium on a molar O_2 basis, compared to the lower O_2 partial pressure limits of the ionic conduction range of calcia-stabilized zirconia electrolyte after (—— • ——) Schmalzreid and (-----) Patterson et al. The limit of the ionic conduction range of yttria-doped thoria after (—— •• ——) Tretyakov and Muan is shown for comparison.

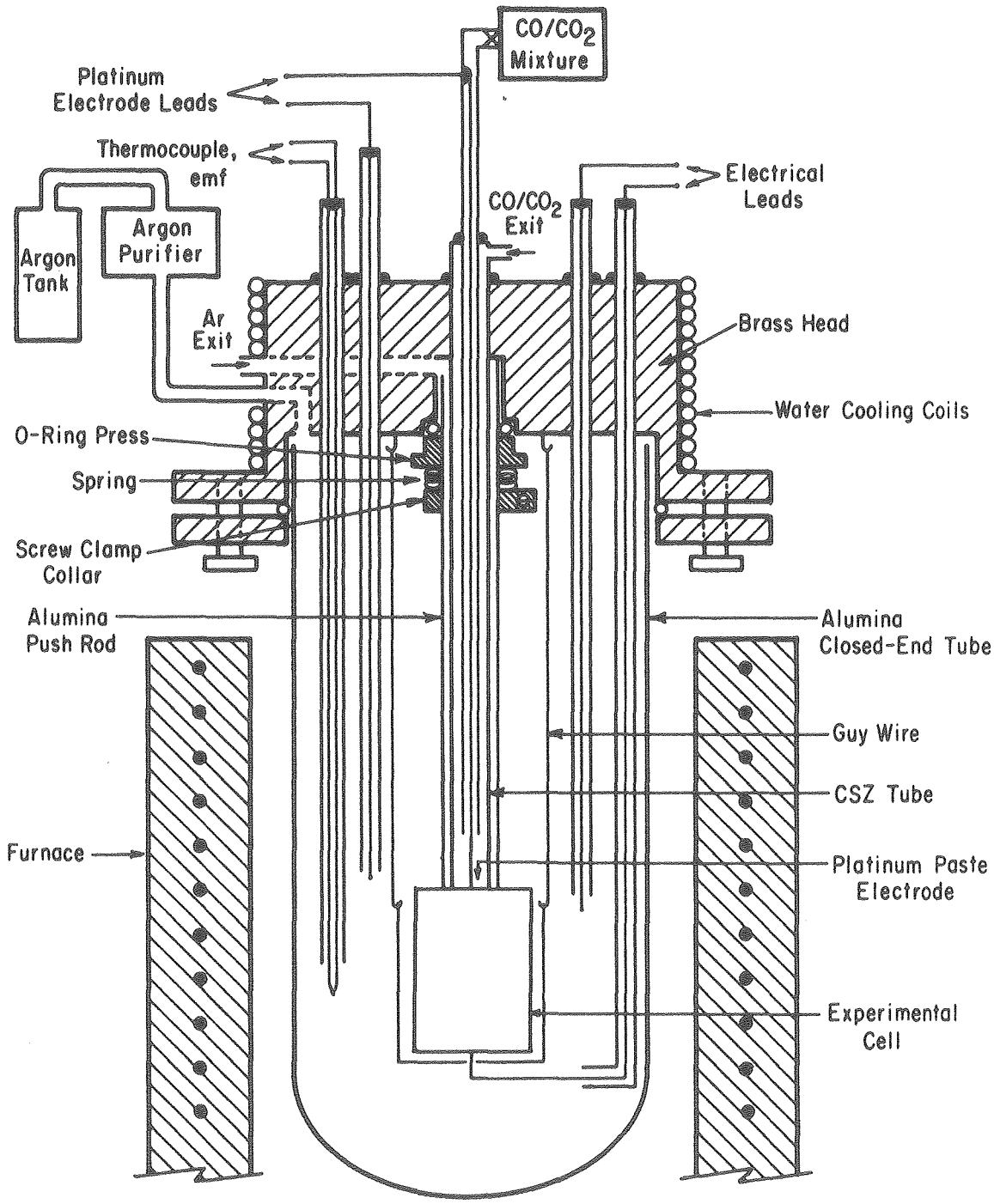

XBL 751-5566

Figure 1.

Cross Section of Electrode Compartment

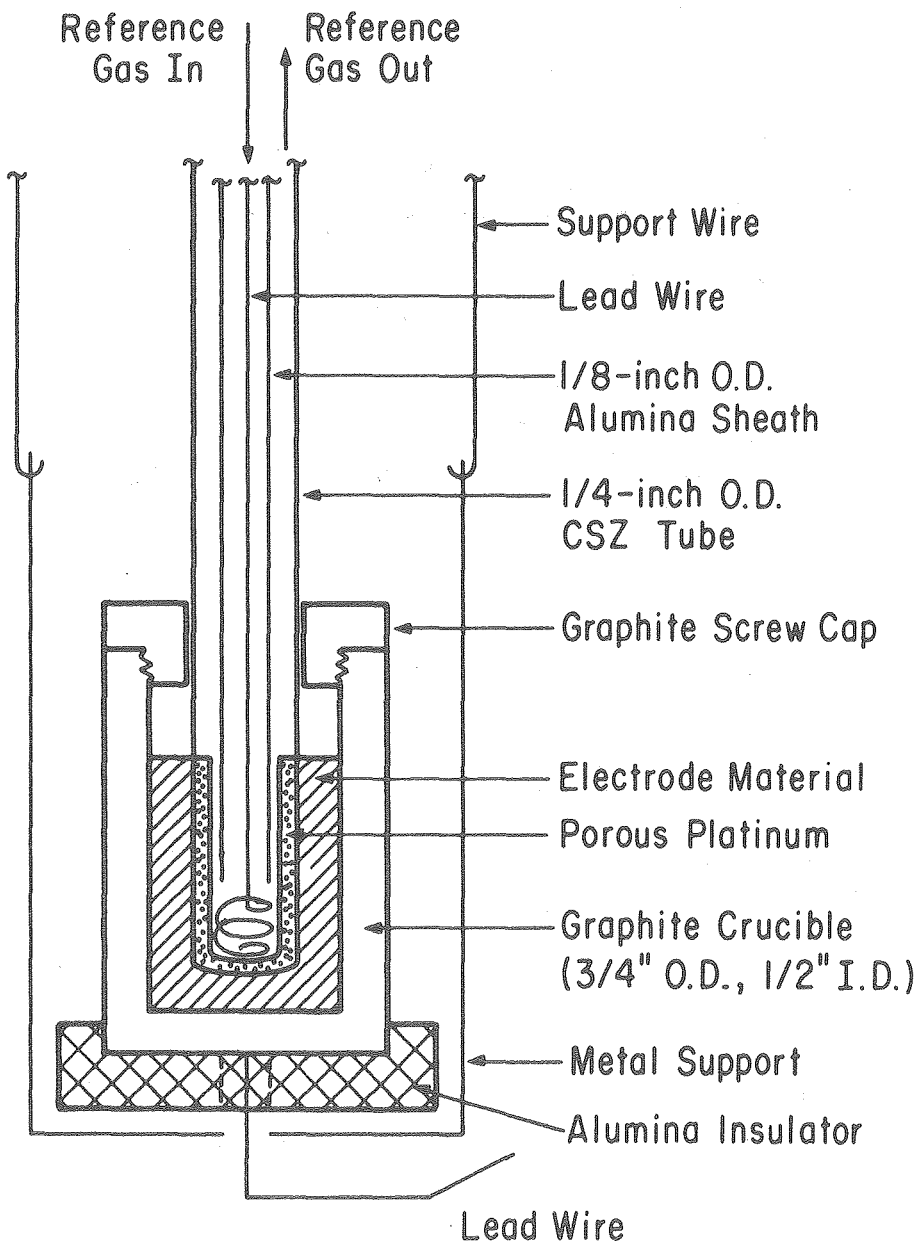

XBL 757-6782

Figure 2.

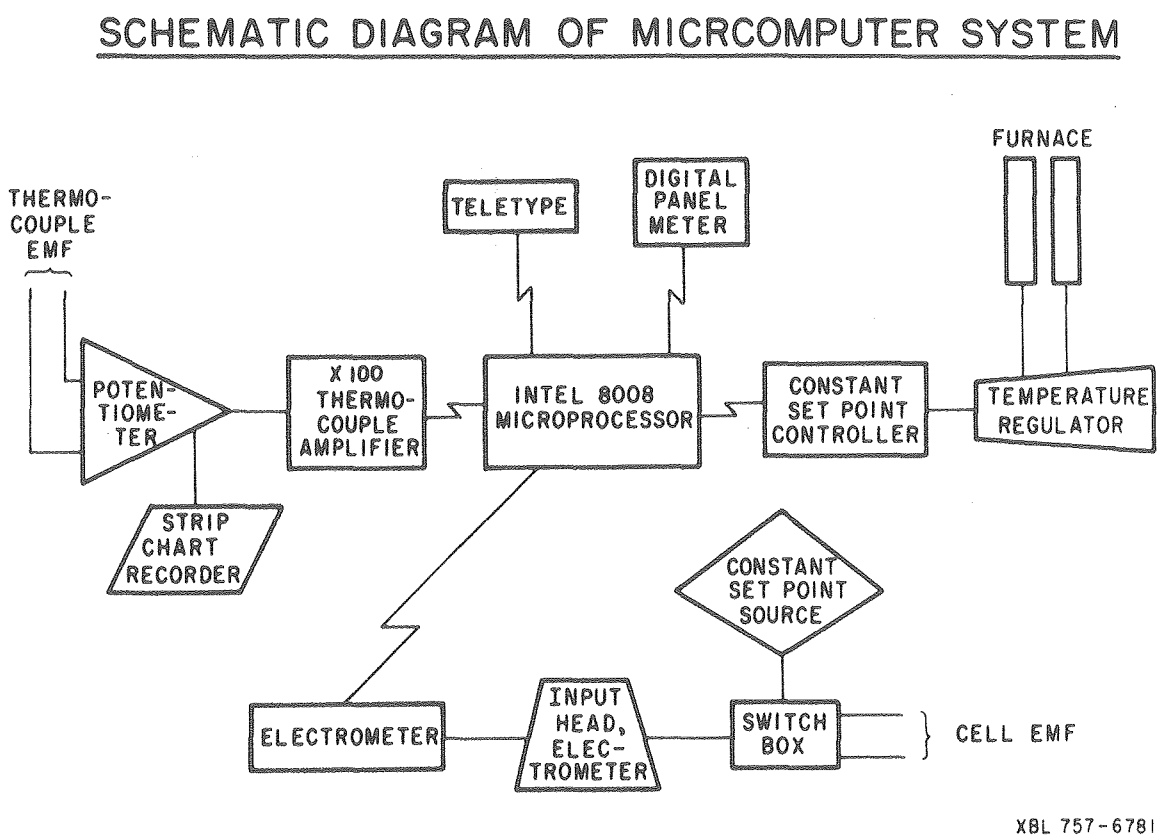
SCHEMATIC DIAGRAM OF MICRCOMPUTER SYSTEM
THERMO-
COUPLE
EMF
TELETYPE
DIGITAL
PANEL
METER
FURNACE
POTEN-
TIOME-
TER
X 100
THERMO-
COUPLE
AMPLIFIER
INTEL 8008
MICROPROCESSOR
CONSTANT
SET POINT
CONTROLLER
TEMPERATURE
REGULATOR
STRIP
CHART
RECORDER
CONSTANT
SET POINT
SOURCE
ELECTROMETER
INPUT
HEAD,
ELEC-
TROMETER
SWITCH
BOX
CELL EMF
XBL 757-6781

Figure 3.

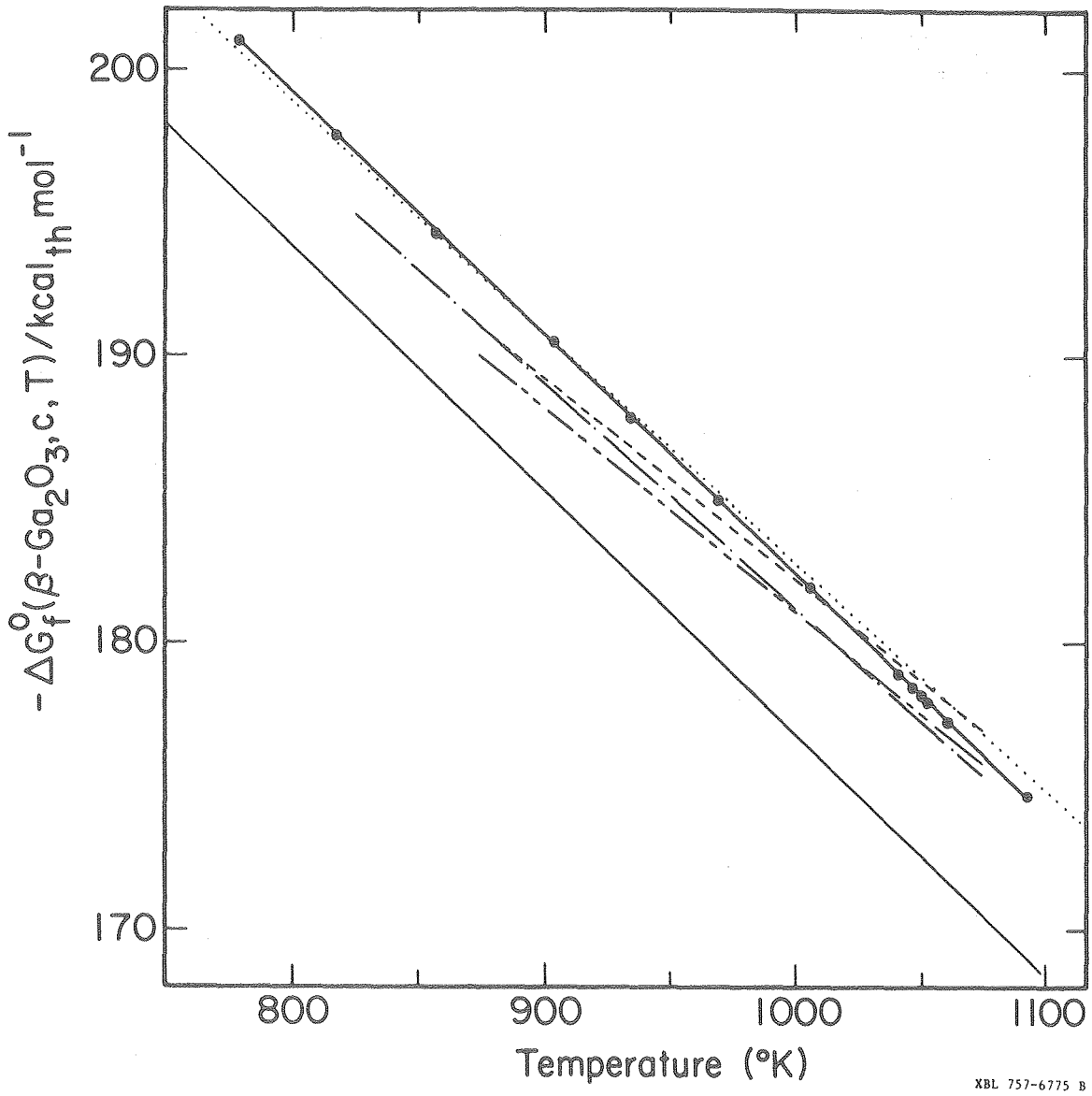
200
190
180
170
800
900
1000
1100
Temperature (°K)
$-\Delta G_f^o(\beta\text{-}Ga_2O_3, c, T)/kcal_{th}\,mol^{-1}$
XBL 757-6775 B

Figure 4.

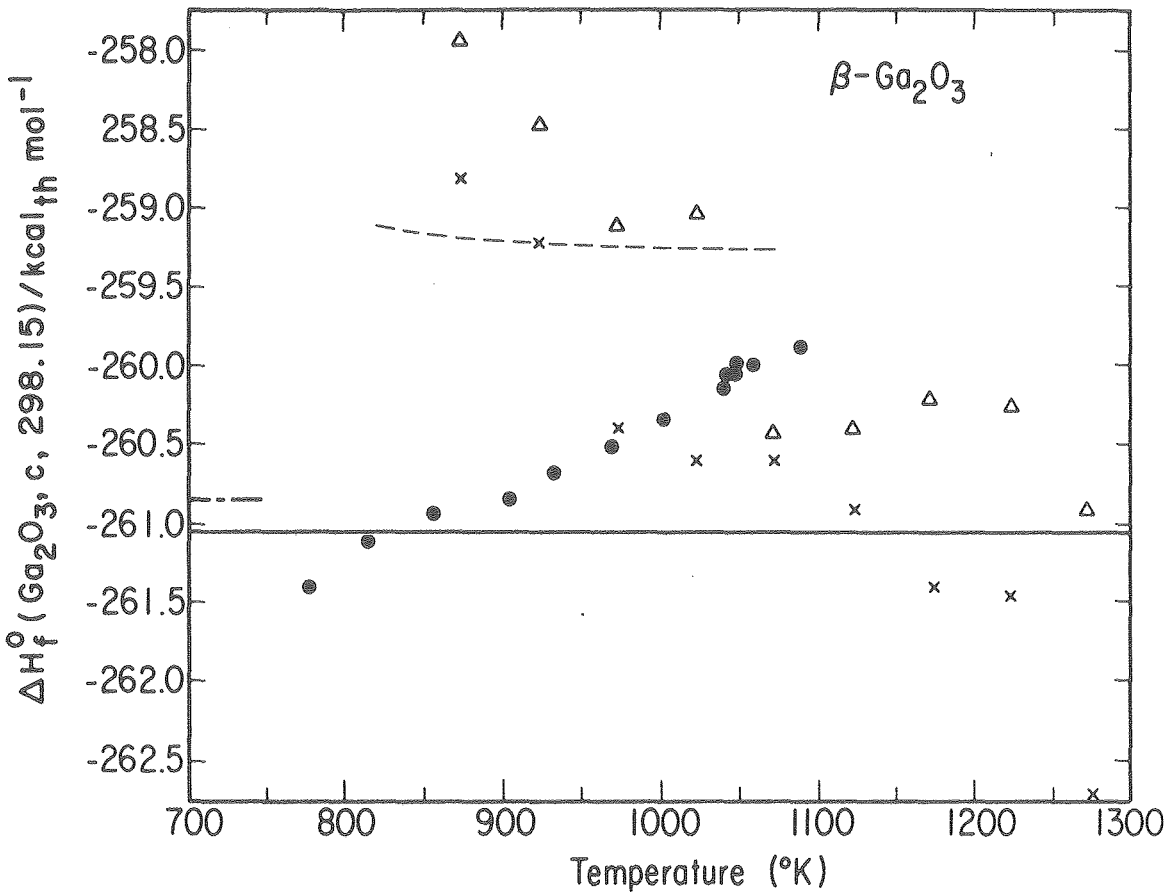

XBL 757-6774 A

Figure 5.

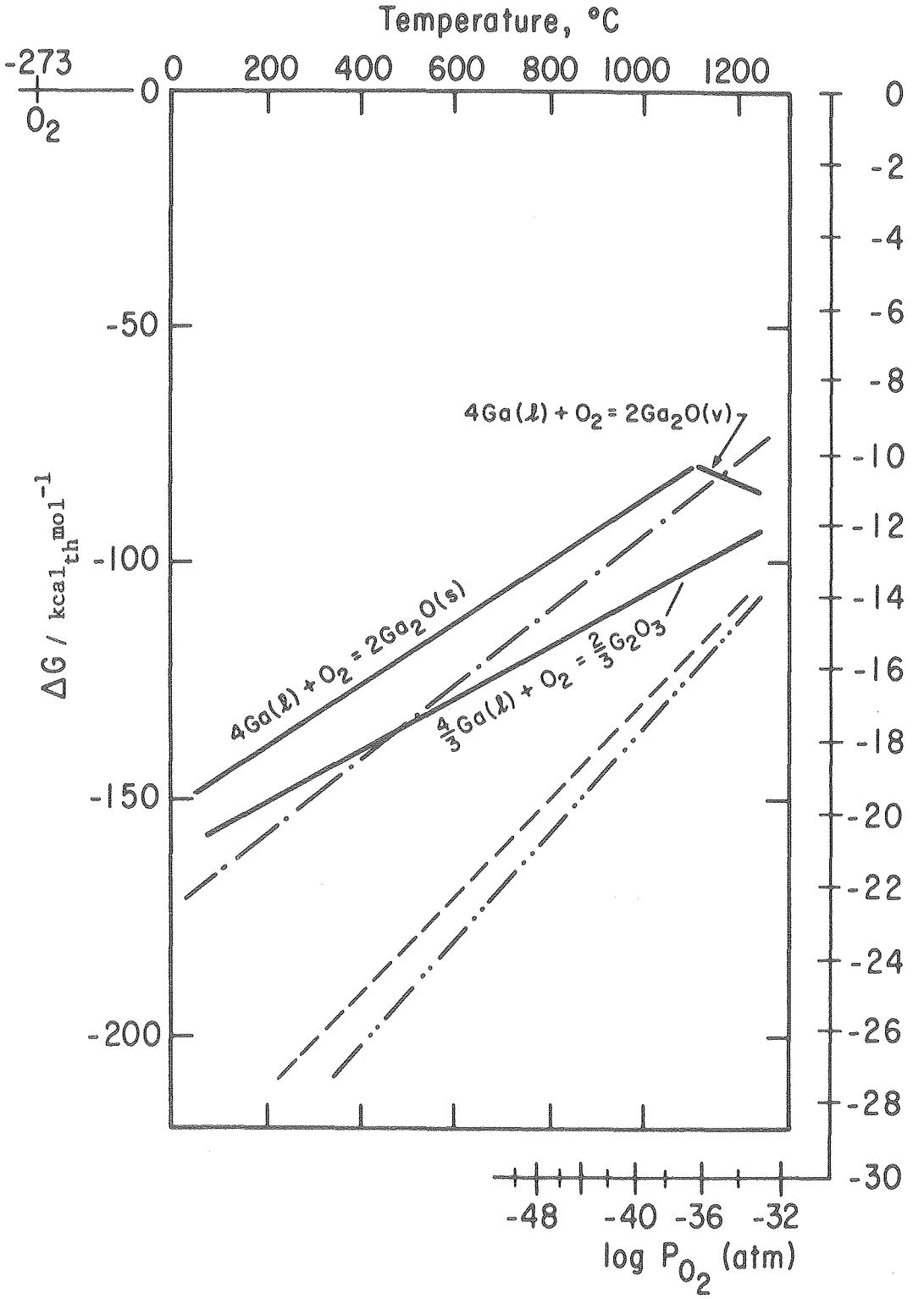

XBL 752-5923 D

Figure 6.

APPENDIX II

SOLID-STATE ELECTROCHEMICAL STUDY OF THE GIBBS ENERGY OF FORMATION OF INDIUM SESQUIOXIDE

A. INTRODUCTION

Indium sesquioxide is an n-type semiconductor with a substantial electrical conductivity of 20 $ohm^{-1}cm^{-1}$ and an electron mobility of ~160 $cm^2V^{-1}s^{-1}$ at room temperature. These properties have made In_2O_3 useful as a material for processing thick film resistors. A review of its properties has been given by de Wit.[1] For the successful processing of In_2O_3 by chemical reactions involving oxidation, accurate information on the thermodynamic properties of In_2O_3 is important. This study was undertaken to provide accurate measurements of the Gibbs energy of formation of In_2O_3 using solid-state electrochemical methods under microcomputer control. A systematic method is applied to attain a level of accuracy not previously reported.

The Gibbs energy of formation of In_2O_3 by the reaction

$$2In(\ell) + \frac{3}{2} O_2(g) = In_2O_3(c)$$

has been measured using electrochemical methods by a number of authors.[2-6] The Gibbs energy of formation has also been calculated from the equilibrium partial pressures of water and hydrogen over a mixture of In and In_2O_3.[7,8] Other studies on In_2O_3 from which thermodynamic data can be derived include vaporization studies,[9,10] thermogravametric analysis[11] and calorimetric combustion experiments.[12-14] The values of the enthalpy of formation reported by these studies show

a definite temperature dependence, and inconsistencies in the reported values of both the entropy and enthalpy of formation. These discrepancies led us to re-examine the enthalpy and entropy functions chosen for data fitting, to explore a third-law analysis of the experimental data, and to examine in detail the consequences of side reactions.

In this study a solid-state electrochemical technique was used to measure the Gibbs energy of the reaction of In_2O_3 in the temperature range from 950 to 1128 K. A solid-state galvanic cell was employed, utilizing calcia-stabilized zirconia (CSZ) as the solid electrolyte, with experiments automated under microcomputer control. The results of these experiments are compared with other available data from the literature in a third-law calculation of the standard enthalppy of formation of In_2O_3, and an analysis is presented for assessing the effect of equilibrium partial pressures of In_2O_3 over a mixture of $In(\ell) + In_2O_3(c)$, based on the results of this study and on other available data. Finally, using the results of this study we propose an alternative explanation of the recent thermogravometric data of de Wit.[11]

B. EXPERIMENTAL

An $In + In_2O_3$ coexistence electrode and a $CO + CO_2 + Ar$ gas electrode were used in the experimental cell whose structure was identical to that described in Appendix I. The coexistence electrode was prepared from 99.999% pure indium powder (Orion Chemical Co.) and 99.999% pure indium sesquioxide powder (Alfa Products). X-ray diffraction analysis

showed the oxide powder to be pure In_2O_3. Measured amounts of metal and oxide powders in the weight ratio of 10:1 were thoroughly mixed and placed in a 2.54 cm O.D. tube of graphite (spectrographic grade) closed at one end. The graphite tube was fitted with a screw cap with a central hole through which a 0.635 cm O.D., closed-end calcia-stabilized zirconia (CSZ) tube containing the gas reference electrode and a platinum lead wire were inserted into the coexistence electrode. The CSZ tube (Zirconia Corporation of America) had a nominal composition of $Ca_{0.15}Zr_{0.85}O_{1.85}$. The closed end of the tube was coated inside with unfluxed platinum paste (Englehard No. 6926) to which a spiral platinum lead wire was attached.

The $CO + CO_2 + Ar$ reference gax mixture (Matheson Gas Products) was prepared from high purity gases. Chemical analysis showed the gas mixture to contain (25.29 ± 0.02) per cent CO_2 and (2.45 ± 0.02) per cent CO, with the balance consisting of high purity argon. The pressure in the experimental cell was maintained at 1 atm.

The electrode assembly was contained within a 5.08 cm O.D. closed-end alumina tube sealed with a vitron O-ring to a water-cooled brass cell head containing Cajon seals to alumina tubes supporting electrode leads and Pt, Pt + 10% Rh thermocouples calibrated to an NBS reference thermocouple. The coexistence electrode compartment was purged with argon purified by passing it over titanium sponge heated to 1123 K.

The cell was placed in a Marshall resistance-heated furnace and shielded from rf interference from the triac-controlled temperature

regulator by a grounded platinum shield placed between the 5.08 cm O.D. alumina tube and the furnace winding. Temperatures could be maintained to within ± 0.5 K.

Cell emf was measured with a Keithley 640 electrometer which was connected to the cell leads with a triaxial cable containing a driven guard to reduce leakage currents. The electrometer output and amplified thermocouple output were monitored periodically by a microcomputer control system based on the Intel 8008 microprocessor. The control program was able to raise the cell temperature at $2\times10^{-2}Ks^{-1}$ to the operating temperature, monitor the cell temperature and emf and print the data on a teletype, test for equilibrium, and repeat the measurements at a series of fixed temperatures within the desired temperature range. The sequence of temperatures at which measurements were taken was chosen to test the reproducability of the experiments and to eliminate systematic errors arising from thermal transients.

C. RESULTS

The Gibbs energy of formation of indium sesquioxide was determined with the cell

$$Pt\ |C|\ In\ ,\ In_2O_3\ ||Ca_{0.15}Zr_{0.85}O_{1.85}||\ CO\ ,\ CO_2\ |\ Pt\ . \qquad (2)$$

The activity of oxygen in the coexistence electrode relative to that in the reference gas mixture was measured from the cell voltage E, and the Nernst equation,

Listed in table 1 are the temperatures of measurement, recorded cell emf, the partial pressures of oxygen in the reference and measured electrodes and the Gibbs energy of formation of In_2O_3 , as calculated from Equation 4.

A linear least squares regression analysis of the $\Delta G_f^o(In_2O_3,c,T)$ data shown in table 2 gave the following equation:

$$\Delta G_f^o(In_2O_3,c,T)/kcal_{th}mol^{-1} = -(223.67\pm.14) + (8.044\pm0.014)\times10^{-2}(T/K) \quad (6)$$

The error values given in this expression were obtained from the combined errors in the reference gas composition, the cell temperature and the deviation of the data from the least-squares line. The total error was found to be 0.25 kcal at 1000 K, which corresponds roughly to a 3 K error in temperature measurement or to a 1.8 mV error in cell emf measurement.

D. DISCUSSION

The calculated values of $\Delta G_f^o(In_2O_3,c,T)$ obtained in this study are shown plotted in figure 1 as function of temperature and compared to data from the emf studies of Klinedinst and Stevenson[5] (using an oxygen reference electrode), of Schaefer[2] (using a Cu - Cu_2O reference electrode), of Newns and Pelmore[4] (using a Ni - NiO reference electrode), of Chatterji and Vest[3] (also using a Ni - NiO reference electrode), and of Bird et al.,[6] (also using a Ni - NiO reference electrode). Also plotted in figure 1 are the values measured by Hochgeshwender and Ingraham employing a flowing gas equilibration technique.[7]

$$E = \frac{RT}{4F} \ln \{p(O_2;CO + CO_2)/p(O_2;In + In_2O_3)\} \qquad (3)$$

where R is the gas constant, T the absolute temperature, F is the Faraday constant, $p(O_2;CO + CO_2)$ the oxygen partial pressure over the $CO + CO_2$ mixture and $p(O_2;In + In_2O_3)$ that over the coexistence electrode.

The Gibbs energy of formation of In_2O_3 is related to the cell emf through the equilibrium constant of the reaction given in Equation 1. Assuming unity activities for $In(\ell)$ and $In_2O_3(c)$, $\Delta G_f^o(In_2O_3,c,T)$ is given by:

$$\Delta G_f^o(In_2O_3,c,T) = 1.5\ RT\left(P_{CO_2}/P_{CO}\right)^2 + 3\Delta G_{ref}^o - 6\ FE\ . \qquad (4)$$

The ratio of partial pressures of the reference gas components, $\left(P_{CO_2}/P_{CO}\right)$, was determined by chemical analysis to be (10.322 ± 0.092). The term ΔG_{ref}^o in Equation 4 is the Gibbs energy of reaction for the reference gas equilibrium,

$$CO + \frac{1}{2}\ O_2 = CO_2 \qquad (5)$$

and was calculated from the data of Wicks and Block[15] to have the form,

$$\Delta G_{ref}^o/kcal_{th}mol^{-1} = -68.27 - 1.8\times10^{-4}T\ln T$$
$$- 3.4\times10^{-7}T^2 + 87./T + 0.02328(T/K)\ .$$

Table 1 Summary of Experimental and Derived Data *

T/K	$E_{measured}$/mV	$\log_{10} \frac{p(O_2, CO+CO_2)}{atm}$	$\log_{10} \frac{p(O_2, In+In_2O_3)}{atm}$	$\frac{\Delta G_f^o(In_2O_3, c, T)}{kcal_{th} mol^{-1}}$
950.8	128.9(±0.1)	-19.820(±.008)	-22.553(±.002)	-147.18(±.01)
953.6	129.0	-19.729	-22.487	-146.98
986.1	128.4	-18.708	-21.716	-144.38
988.2	128.2	-18.644	-21.288	-144.19
1021.6	127.5	-17.667	-20.565	-141.52
1026.0	127.1	-17.543	-20.041	-141.12
1041.8	126.8	-17.107	-19.737	-139.86
1059.0	126.6	-16.646	-19.243	-138.51
1067.8	126.0	-16.417	-18.899	-137.75
1094.9	125.8	-15.732	-18.330	-135.64
1128.3	124.7	-14.935	-17.515	-132.91

* cal_{th} = 4.184 J
atm = 101325 Pa

In order to better ascertain the reliability of the experimental data, a third-law calculation was performed. The values of $\Delta H_f^o(In_2O_3,c,298.15)$ were calculated from the equation,

$$\Delta H_f^o(In_2O_3,c,298.15) = \Delta G_f^o(In_2O_3,c,T) - \Delta_f^o\{H(T) - H(298.15)\}$$

$$+ T[\Delta S_f^o(In_2O_3,c,298.15) + \Delta_f^o\{S(T) - S(298.15)\}] \ . \qquad (7)$$

The values of the entropy and enthalpy functions were taken from Coughlin.[16] The value of $\Delta S_f^o(298.15)$ was taken to be -0.0735 $kcal_{th}$ $mol^{-1}k^{-1}$, as suggested by Hart.[17] Component values were combined according to the stoichiometry of the formation reaction, Equation 1, to determine the magnitudes of the terms in Equation 7.

The results of the third-law analysis are summarized in table 2. A statistical study of the third-law results showed that

$$\Delta H_f^o(In_2O_3,c,298.15)/kcal_{th}mol^{-1} = -222.09 \pm 0.01 \qquad (8)$$

with a surprisingly small standard error from the mean value. The derived values of the enthalpy of formation show a negligible temperature dependence of 0.00045 $kcal_{th}mol^{-1}k^{-1}$.

A comparison of the derived enthalpy of formation with calorimetrically determined values is presented in table 3. The value derived in the present study is within the error limits of the calorimetric results of Becker and Roth,[13] but differs by twice the standard error from the more recent, and more accurate, results of Holley et al.[14] Therefore, it is probable that the thermodynamic functions of Coughlin[16] are in error by about 0.2%.

Table 2 Second-Law and Third-Law Analyses of the Experimental Data

	Third-Law Analysis		Second-Law Analysis		
T/K	$\Delta H_f^o(In_2O_3,c,298.15)$ / $kcal_{th}mol^{-1}$	δ_1 / $kcal_{th}mol^{-1}$	Observed log K_p	Calculated log K_p	δ_2
950.8	-222.11	-.02	-33.830	-33.832	0.002
953.6	-222.14	-.05	-33.685	-33.681	-.004
986.1	-222.13	-.04	-31.998	-31.991	-.007
988.2	-222.12	-.03	-31.888	-31.886	-.002
1021.6	-222.11	-.02	-30.275	-30.269	-.006
1026.0	-222.07	0.02	-30.060	-30.064	0.004
1041.8	-222.07	0.02	-29.339	-29.341	0.002
1059.0	-222.10	-.01	-28.584	-28.579	-.005
1067.8	-222.04	0.05	-28.193	-28.199	0.006
1094.9	-222.10	-.01	-27.074	-27.065	-.009
1128.3	-222.04	0.05	-25.744	-25.744	0.000

Mean/$kcal_{th}mol^{-1}$ -222.09

Standard error/$kcal_{th}mol^{-1}$ = ±0.01

$\Delta H_f^o(In_2O_3,c,298.15)/kcal_{th}mol^{-1}$
= -222.53

Table 3. Comparison of Calorimetric Data with the Derived Enthalpy of Formation of In_2O_3

$\Delta H_f^o(In_2O_3,c,298.15)$ / $kcal_{th}mol^{-1}$	Source
-220.*	Ditte[12]
-222.5±0.7	Becker and Roth[13]
-221.27±0.40	Holley et al.[14]
-222.09±0.01	This work (third-law)

*As corrected by Becker and Roth[13]

On the assumption that the third-law analytical results could be affected by an error in the estimated entropy of formation of In_2O_3, entropy data were re-examined. The values of S(In,ℓ,298.15) and S(O_2,g,298.15) have been very well determined by Kelley[18] and are not expected to be in significant error. Becker and Roth[13] estimated the entropy of cubic In_2O_3 at 298.15°K to be 0.0270 ± 0.0025 $kcal_{th}mol^{-1}K^{-1}$ while Stubbs et al.,[8] calculated a value of 0.0301 $kcal_{th}mol^{-1}K^{-1}$ from their phase equilibria studies. Another alternative calculation of $\Delta S_f^o(In_2O_3,c,298.15)$ is based on the assumption that $C_p(In_2O_3,c,T)$ is equal to $C_p(\beta\text{-}Ga_2O_3,c,T)$, where the coefficients for a linear temperature-dependent expression for $C_p(In_2O_3,c,T)$ are given by Glassner.[19] Using these values as extrema leads us to estimate a range from -0.07431 to -0.07121 $kcal_{th}mol^{-1}K^{-1}$ for $\Delta S_f^o(In_2O_3,c,298.15)$. The variation of $\Delta S_f^o(In_2O_3,c,298.15)$ within this range in the third-law calculation does not, however, change the resulting temperature dependence of the derived values of $\Delta H_f^o(In_2O_3,c,298.15)$, but does shift the magnitude of the enthalpy of formation by ±1.6 $kcal_{th}mol^{-1}$. An entropy of formation of -0.726 $kcal_{th}mol^{-1}$ is needed to give a temperature-independent value of $\Delta H_f^o(In_2O_3,c,298.15)$ which is in exact agreement with the calorimetric results of Holley et al.[14]

The results of the third-law analysis applied to the present experimental data and to that from other electrochemical studies are compared in figure 2. The results obtained in this study exhibit the most temperature-independent values of $\Delta H_f^o(In_2O_3,c,298.15)$ of all

the electrochemical studies conducted to date, with all calculated values falling between the calorimetric determinations of Becker and Roth[13] and Holley et al.[14] The values of $\Delta H_f^o(In_2O_3,c,298.15)$ obtained from the other four emf studies (where actual data points were available) showed a definite temperature dependence of about $-0.0075\ kcal_{th}mol^{-1}K^{-1}$. It is interesting to note that all of the previous electrochemical studies utilized metal-metal oxide, reference electrodes, whereas a gaseous reference electrode was used in the present study. Polarization of the coexistence electrode would have the effect of raising the value of the derived enthalpy of formation. Thus the negative temperature dependence of the third-law results could be explained if experimental measurements were made in the direction of decreasing temperatures while electrode polarization increased. In the present study, measurements were repeated several times as the cell temperature was cycled between chosen limits, so as to test for long-term, cell degradation effects.

The third-law analysis was repeated with other thermodynamic functions in order to test their effect on the derived values of $\Delta H_f^o(In_2O_3,c,298.15)$. Values of $\{S(T) - S(298.15)\}$ and $\{H(T) - H(298.15)\}$ for gaseous oxygen were taken from the study of Wicks and Block[15] from Hultgren et al,[20] and from Kelley.[18] Values for liquid indium were obtained from the selected values of Hultgren et al,[20] and from Kelley.[18] For indium sesquioxide values were calculated by integrating the heat capacity data of Shchukarev et al.[9] In the latter calculation the heat capacity data was reduced to the form,

$$C_p(In_2O_3,c,T)/cal_{th}mol^{-1}K^{-1} = 29.36 + 7.0\times10^{-3}T \quad -7.66\times10^{5}(T/K)^{-2}$$

by a least squares calculation. These analyses gave lower values of $\Delta H_f^o(In_2O_3,c,298.15)$ with mean values in the range from -217.3 to -217.5 $kcal_{th}mol^{-1}$ with a temperature dependences of about 0.4 $kcal_{th}mol^{-1}K^{-1}$. These third-law analytical results are primarily influenced by the heat capacity data of Shchukarev et al.,[9] and the lack of agreement of the derived enthalpy of formation with calorimetric data suggests possible error in their data.

A second-law test of the experimental data was also performed. These results are presented in table 2, and compared to values derived from other studies in table 4. The second-law test results are in fair agreement with the results of the third-law analysis, and differ by only 0.06%, well within the error in tabulated thermochemical data. The second-law test results of the data of Newns and Pelmore[4] are in best agreement with the calorimetric results of Holley et al.,[14] whereas other electrochemical studies gave higher second-law values of $\Delta H_f^o(In_2O_3,c,298.15)$.

An important side reaction to consider at high temperatures is the decomposition of $In_2O_3(c)$ to form $In_2O(g)$. The existence of $In_2O(c)$ above 1085 K has been suggested by Klinedinst and Stevenson[5] to explain a discontinuity in the temperature dependence of the measured oxygen activity of a coexistence electrode containing In(ℓ) and indium oxides formed by electrochemical titration. No such discontinuity was found in the present study for a coexistence electrode containing In(ℓ) and $In_2O_3(c)$. It is possible, therefore,

Table 4. Comparison of Enthalpy and Entropy of Formation of In_2O_3 from Second-Law Analyses

$\Delta H_f^o(In_2O_3,c,298.15)$	$\Delta S_f^o(In_2O_3,c,298.15)$	
$kcal_{th}mol^{-1}$	$cal_{th}mol^{-1}$	Source
-222.53	-78.01	This work
-217.63	-72.91	Schaefer[2]
-214.39	-70.2	Chatterji and Vest[3]
-221.6	-75.7	Newns and Pelmore[4]
-217.5	-73.2	Klinedinst and Stevenson[5]
-219.5	-74.3	Bird et al.[6]
-216.8	-68.4	Stubbs et al.[8]
-221.27±0.4	-	Holley et al.[14] (calorimetric)
-	-73.5±2.5	Hart[17] (selected)

that $In_2O(c)$ is produced by the titration of oxygen ions into $In(\ell)$ above 1085 K.

It is of interest to calculate the partial pressure of $In_2O(g)$ that would exist in the $In(\ell) + In_2O(c)$ electrode if equilibrium conditions prevailed. For the reaction,

$$4/3\ In(\ell) + \frac{1}{3}\ In_2O_3(c) \rightleftarrows In_2O(c) \qquad (9)$$

the Gibbs energy change is found by subtracting $\frac{1}{3}\ \Delta G_f^o(In_2O_3,c,T)$, obtained in this study, from that for $In_2O(c)$ suggested by Klinedinst and Stevenson.[5] The result is

$$\Delta G(9)/kcal_{th}mol^{-1} = 20.56 - 0.01891\ (T/K)\ . \qquad (10)$$

The Gibbs energy change for this reaction is zero at 1087 K. Therefore above this temperature solid In_2O could form. The Gibbs energy of vaporization of In_2O by the reaction,

$$In_2O(c) = In_2O(g) \qquad (11)$$

can now be found by combining the Gibbs energies of formation of the two species.[5] The result is

$$\Delta G(11)/kcal_{th}mol^{-1} = 32.0 - 1.8\times10^{-2}\ (T/K)\ . \qquad (12)$$

Assuming ideal equilibrium conditions, the pressure of $In_2O(g)$ over solid In_2O is then given by

$$\log_{10}\{p(In_2O)/atm\} = 3.9 - 6774\ (T/K)^{-1}\ . \qquad (13)$$

This equation gives a value of 2.6 Torr at 1100 K.

If, on the other hand, $In_2O_3(c)$ is present, the oxygen partial pressure is found from the equilibrium reaction,

$$In_2O_3(c) = 2In(\ell) + 3/2\ O_2(g)\ . \tag{14}$$

Then, the reaction

$$2In(\ell) + \frac{1}{2}\ O_2 = In_2O(g) \tag{15}$$

is an additional source of In_2O in the gas phase. Combining the last two reactions, one obtains

$$\log_{10}\{p(O_2)/atm\} = 11.7 - 3.26 \times 10^4\ (T/K)^{-1}\ . \tag{16}$$

$$\log_{10}\{p(In_2O)/atm\} = 8.0 - 1.15 \times 10^4\ (T/K)^{-1}\ . \tag{17}$$

These expressions also give a value of 3.0 Torr for the partial pressure of $In_2O(g)$ at 1100 K. Shchukarev et al.[9] found the pressure of $In_2O(g)$ over a stoichiometric mixture of $In(\ell) + In_2O_3(c)$ to be 0.641 Torr at 1101 K. Shown in figure 3 are the partial pressures of $In_2O(g)$ established by a direct formation reaction in the presence of $In_2O_3(c)$ or by vaporization of $In_2O(c)$. The mass spectrometer data is not sufficient for one to discern which mechanism is controlling, although the formation of $In_2O(c)$ after vacuum sublimation of the $In_2O_3(c) + In(\ell)$ mixture has been reported.[9]

Also of importance to the present study is the equilibrium pressure of $In_2O(g)$ over $In_2)_3(c)$ produced by reaction (11), and

$$In_2O_3(c) = In_2O(c) + O_2(g)\ . \tag{18}$$

Reaction (18) has a Gibbs energy change given by

$$\Delta G(18)/\mathrm{kcal}_{th}\mathrm{mol}^{-1} = 169.67 - 0.07254\ (T/K)\ . \qquad (19)$$

Combining this reaction with the Gibbs energy of vaporization for solid In_2O one can obtain an expression for the partial pressure of $In_2O(g)$, which is

$$\log_{10}\{p(In_2O)/atm\} = 19.8-4.41 \times 10^4(T/K)^{-1} - \log_{10}\{P(O_2)/atm\}\ . \qquad (20)$$

This expression is somewhat different from that given by Van Dillen[21] which has the form

$$\log_{10}\{p(In_2O)/atm\} = 17.7-42{,}189(T/K)^{-1} - \log_{10}\{p(O_2)/atm\}\ . \qquad (21)$$

The formation of $In_2O(c)$ as a reaction product during $In_2O_3(c)$ decomposition is suggested by the thermogravimetry studies of de Wit[11] who found a small (0.017 μgs^{-1}) linear weight loss of $In_2O_3(c)$ over the temperature range from 1173 to 1473 K. De Wit attributed this result to a defect reaction involving either the formation of oxygen vacancies or indium interstitials in $In_2O_3(c)$, however, rather than to the formation of an $In_2O(c)$ surface reaction product. In our study of the $In(\ell) + In_2O_3(c)$ existence electrode, no discontinuities in cell emf with temperature were observed, in spite of some vaporization of $In(\ell)$. Therefore, we conclude that $In_2O(c)$ could be produced by a rapid dissociative decomposition reaction from $In_2O_3(c)$ above 1173 K, but that $In_2O(c)$ is not present in the $In(\ell) + In_2O_3(c)$ coexistence electrode. This conclusion also is supported by X-ray diffraction analysis on our coexistence electrodes following high-temperature studies.

Finally, it is important to determine whether electronic conduction in the solid electrolyte could have introduced an error in the cell emf. Shown in figure 4 are the ionic-conduction domain limits for CSZ, as determined by Schmalzreid[22] and by Patterson et al.,[23] along with the Gibbs energy of formation of the various oxides of indium plotted as a function of temperature. The Gibbs energy of formation of $In_2O_3(c)$ is well within the conservative limit for the ionic-conduction domain, over the entire temperature range used in the present study. The experimental data was tested for evidence of electronic conduction by statistically examinng the second derivative was found to be essentially zero, indicating that the magnitude of the cell emf was not reduced by partial electrolyte failure at the higher experimental temperatures.

E. CONCLUSION

The Gibbs energy of formation of In_2O_3 was readily measurable utilizing a solid-state electrochemical cell with a $CO + CO_2$ reference electrode. The microcomputer automation of the study proved exceptionally beneficial for automatic testing of thermodynamic equilibrium and of the reproducibility of the data. The results of the study gave the most temperature-independent values of $\Delta H_f^o(In_2O_3,c,298.15)$ of all the emf studies of the $In_2O_3(c)$ formation reaction, and in close agreement with calorimetric data. No evidence was found for the formation of $In_2O(c)$ over an $In(\ell) + In_2O_3(c)$ coexistence electrodes.

REFERENCES

1. J.H.W. De Wit, J. Solid State Chem., 8, 142 (1973).

2. S. Schaefer, U.S. Bur. Mines Rep. Invest. No. 7549. U.S. Govt. Printing Office: Washington (1971).

3. D. Chatterji, R.W. Vest, J. Amer. Ceram. Soc., 55, 575 (1972).

4. G.R. Newns, J.M. Pelmore, J. Chem. Soc. (A), 360 (1968).

5. K.A. Klinedinst, D.A. Stevenson, J. Chem. Thermo., 5, 21 (1973).

6. J.M. Bird, A.W. Bryant, J.N. Pratt, J. Chem. Thermo., 7, 577 (1975).

7. K. Hochgeschwender, T.R. Ingrahm, Can. Met. Quart. 6, 293 (1967).

8. M.F. Stubbs, J.A. Schufler, A.J. Thompson, J. Amer. Chem. Soc., 74, 6201 (1952).

9. S.A. Shchukarev, G.A. Semenov, I.A. Ratkovskii, Russ. J. Inorg. Chem., 14, 1 (1969).

10. R.P. Burns, G. DeMaria, J. Drowart, M.G. Inghram, J. Chem. Phys., 38, 1035 (1963).

11. J.H.W. De Wit, J. Solid State Chem., 13, 192 (1975).

12. A. Ditte, Compt. rend. 72, 858 (1871).

13. G. Becker, W.A. Roth, Z. Phys. Chem. A, 161, 69 (1932).

14. C.E. Holley, E.J. Huber, Jr., E.H. Neierkord, J. Amer. Chem. Soc., 74, 1084 (1952).

15. C.E. Wicks, F.F. Block, U.S. Bur. Mines Bull. 605. U.S. Govt. Printing Office: Washington, p. 29 (1963).

16. J.P. Coughlin, U.S. Bur. Mines Bull. 542. U.S. Govt. Printing Office: Washington, p. 21 (1954).

17. D. Hart, J. Phys. Chem., 56, 202 (1952).

18. K.K. Kelley, U.S. Bur. Mines Bull. 477. U.S. Govt. Printing Office: Washington (1950).

19. A. Glassner, Tech. Rept. ANL-5750. Argonne National Laboratory: Argonne, Illinois (1957).

20. R. Hultgren, P.D. Desai, D.T. Hawkins, M. Gleizer, K.K. Kelley, Selected Values of the Thermodynamic Properties of the Elements. American Soc. Metals: Ohio (1973).

21. A.J. Van Dillen, Thesis. University of Utrecht: The Netherlands. To be published.

22. H.Z. Schmalzreid, Electrochem., 66, 572 (1962).

23. J.W. Patterson, C.C. Bogden, R.A. Rapp, J. Electrochem. Soc., 114, 752 (1967).

0 0 0 0 3 1 0 5 2 2 3

List of Figures

Fig. 1 Gibbs energy of formation of $In_2O_3(c)$ as a function of temperature: (——) This study; (—— -- ——) Schaefer; (•••••) Klinedinst and Stevenson; (———) Chatterji and Vest; (—— - ——) Newns and Pelmore; (—— • ——) Bird et al.; (—— •• ——) Stubbs et al.

Fig. 2 Standard enthalpy of formation of $In_2O_3(c)$ obtained by a third-law analysis of the experimental data: (•) This work; (x) Schaefer; (Δ) Klinedinst and Stevenson; (---) Chatterji and Vest; (—— - ——) Newns and Pelmore; (—— • ——) Bird et al.; (———) Holley, Huber and Neierkord; (—— -- ——) Becker and Roth.

Fig. 3 Partial pressure of $In_2O(g)$ as a function of temperature for two possible formation reactions.

Fig. 4 Gibbs energies of formation of the oxides of indium on a molar O_2 basis compared to the ionic-conduction domain limits of calcia-stabilized zirconia after Schmalzreid, (—— • ——) and Patterson et al., (---).

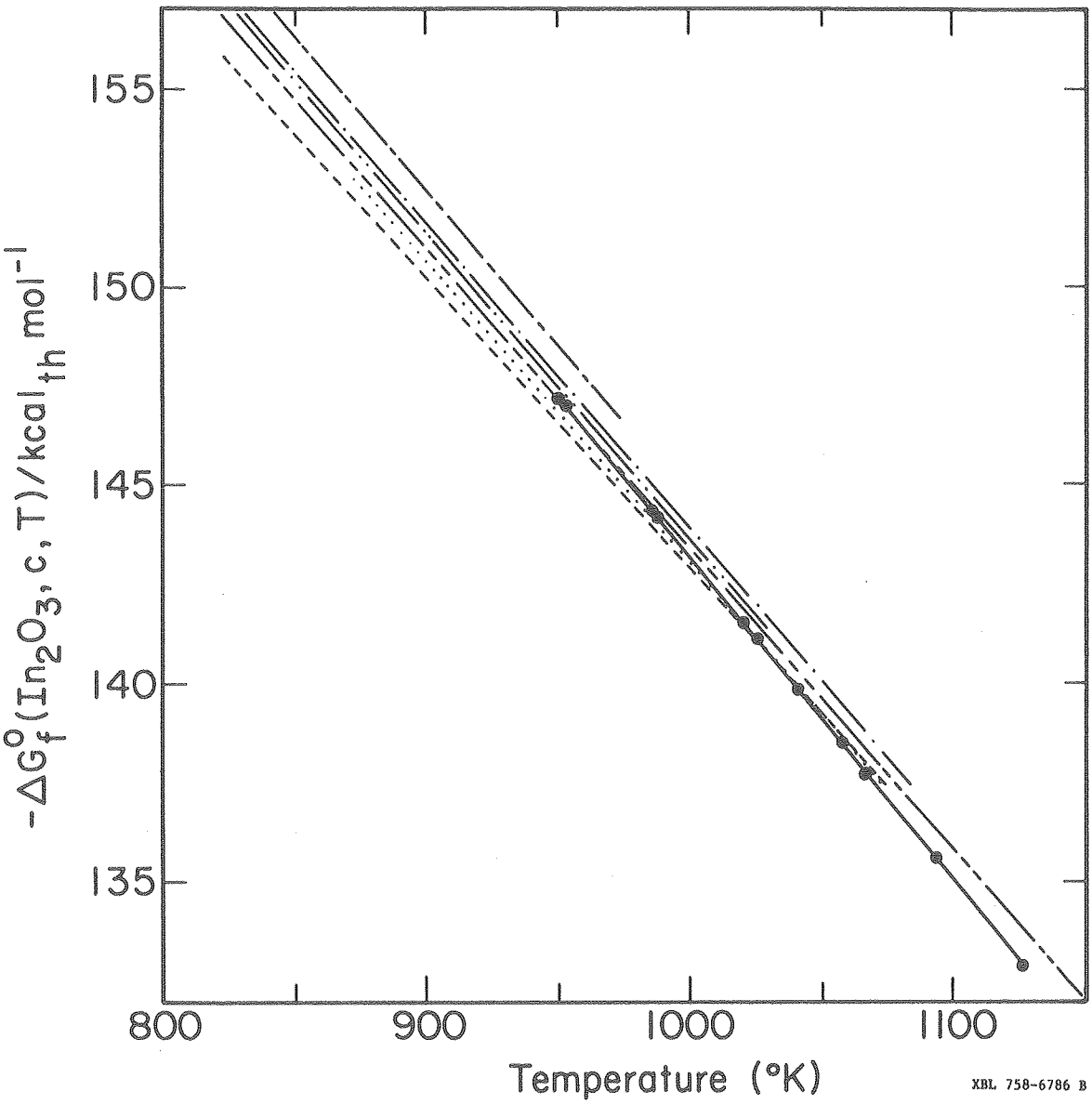
155
150
145
140
135
800
900
1000
1100
Temperature (°K)
$-\Delta G_f^o(In_2O_3, c, T)/kcal_{th}\,mol^{-1}$
XBL 758-6786 B

Figure 1.

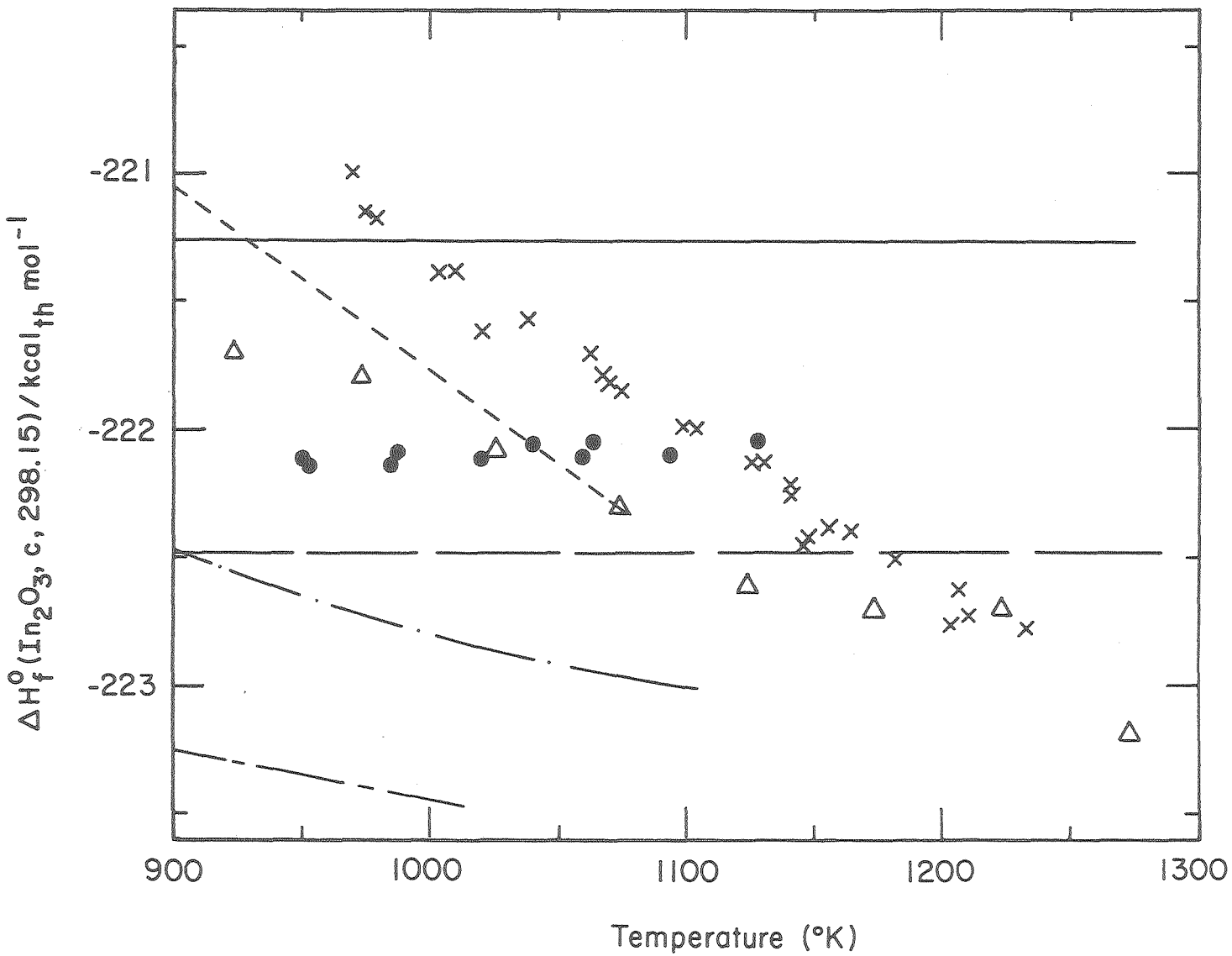

XBL 758-6785 A

Figure 2.

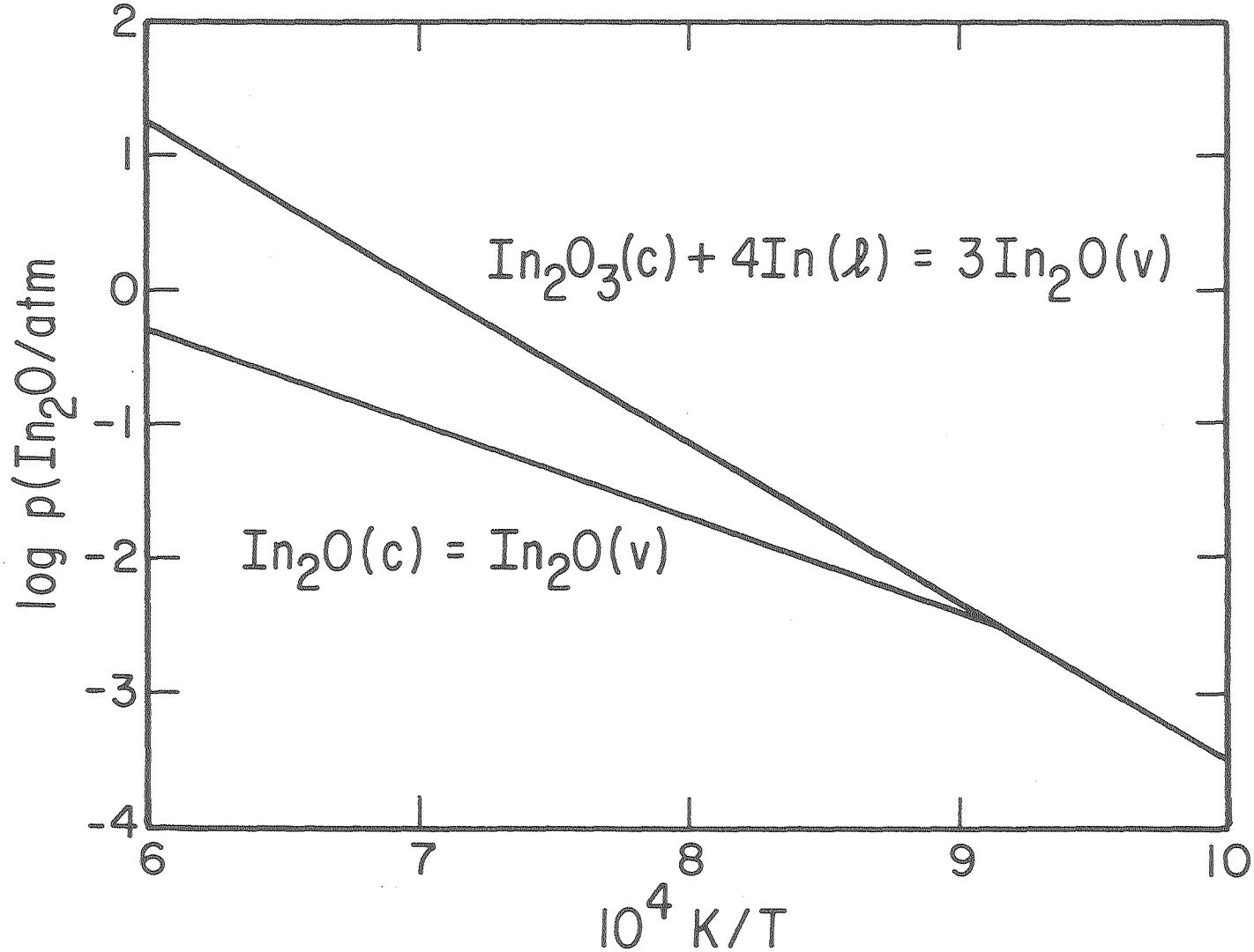

XBL 757-6791

Figure 3.

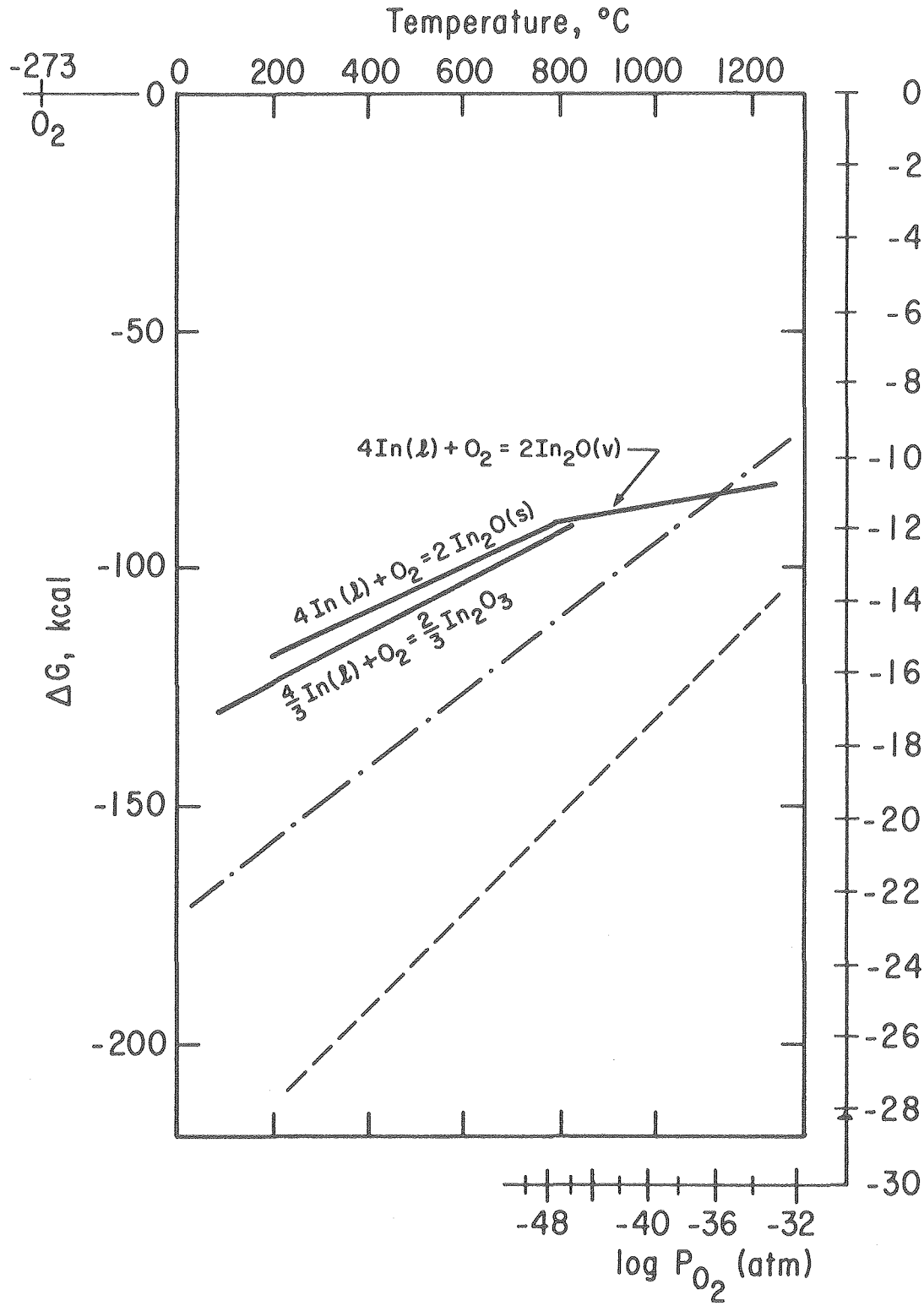

XBL 752-5923 E

Figure 4.

APPENDIX III

CALCULATION OF LIQUIDUS TEMPERATURES IN A BINARY SYSTEM FORMING A SOLID SOLUTION OF NARROW HOMOGENEITY RANGE

A. INTRODUCTION

The calculation of binary phase diagrams from available thermodynamic data has been presented in the literature. Unfortunately, the available developments are not in a convenient form with respect to the binary systems and the thermodynamic data analyzed here - liquid solution Gibbs energies and enthalpies. Thus equations for calculating liquidus temperatures in Group III-V binary systems are derived here.

B. DEVELOPMENT OF THE FORMATION EQUATION

Consider the formation of a solid compound, A_mB_n (c) from pure liquid elements.

$$mA(\ell) + nB(\ell) = A_mB_n\ (c) \qquad (1)$$

The Gibbs energy of formation of A_mB_n (c), $\Delta G_f^o(A_mB_n)$, is then given by

$$\Delta G_f^o(A_mB_n) = m\mu_A^c + n\mu_B^c - m\mu_A^{\ell,o} - n\mu_B^{\ell,o} \qquad (2)$$

where μ_A^c and μ_B^c are the chemical potentials of A and B in the solid compound A_mB_n and $\mu_A^{\ell,o}$ and $\mu_B^{\ell,o}$ are the chemical potentials of the pure liquid elements A and B, respectively. Actually the designation of A_mB_n (c) as a compound is somewhat arbitrary in that what exists for the compounds of interest here is a solid solution of very small homogeneity range (on the order of 10^{-6} mole fraction) close to the composition $x = m/n+m \cong \frac{1}{2}$. The liquidus line represents

a condition of equilibrium between the solid and liquid solution. Therefore the chemical potentials of A or B in both phases can be equated.

$$\mu_A^{\ell} = \mu_A^{c} \tag{3}$$

$$\mu_B^{\ell} = \mu_B^{c} \tag{4}$$

Multiplying Equation (3) by m and Equation (4) by n and adding yields

$$m\mu_A^{\ell} + n\mu_B^{\ell} = m\mu_A^{c} + n\mu_B^{c} \tag{5}$$

It is advantageous to express the liquid phase chemical potentials in terms of activities according to

$$\mu_i = \mu_i^{\ell,o} + RT\ \ell n\ a_i^{\ell} \tag{6}$$

Inserting this expression into Equation (5) produces

$$m\ RT\ \ell n\ a_A^{\ell} + n\ RT\ \ell n\ a_B^{\ell} = m(\mu_A^{c} - \mu_A^{\ell,o}) + n(\mu_B^{c} - \mu_B^{\ell,o}) \tag{7}$$

As can be seen, the right hand side of Equation (7) is equivalant to Equation (2) and is just $\Delta G_f^o(A_mB_n)$. Thus

$$m\ RT\ \ell n\ a_A^{\ell} + n\ RT\ \ell n\ a_B^{\ell} = \Delta G_f^o(AmBn) \tag{8}$$

Since the variable desired to isolate is temperature while both the activity and standard Gibbs energy of formation are temperature dependent, these quantities must be expressed in terms of temperature-insensitive and measurable quantities. Over small temperature ranges the standard enthalpy and entropy of formation are nearly constant (and

exactly constant if the Neumann-Kopp rule is valid). Similarly the activity can be expressed in terms of temperature-insensitive partial molar enthalpy and entropy. Equation (8) then reduces to

$$m\Delta\overline{H}_A - mT\Delta\overline{S}_A + n\Delta\overline{H}_B - nT\Delta\overline{S}_B = \Delta\overline{H}_f^o(A_mB_n) - T\Delta\overline{S}_f^o(A_mB_n) \qquad (9)$$

where $\Delta\overline{H}_i$ and $\Delta\overline{S}_i$ are the relative partial molar enthalpy and entropy of component i and $\Delta H_f^o(A_mB_n)$ and $\Delta S_f^o(A_mB_n)$ and the standard enthalpy and entropy changes, respectively, for the formation of A_mB_n (c). Thus Equation (9) can be solved for the liquidus temperature.

$$T_\ell = \frac{\Delta H_f^o(A_mB_n) - m\Delta\overline{H}_A(x) - n\Delta\overline{H}_B(x)}{\Delta S_f^o(A_mB_n) - m\Delta\overline{S}_A(x) - n\Delta\overline{S}_B(x)} \qquad (10)$$

Taking m=n, Equation (10) reduces to the applicable "formation" equation for the liquidus temperature.

$$T_\ell = \frac{2\Delta H_f^o(AB) - \Delta\overline{H}_A(x) - \Delta\overline{H}_B(x)}{2\Delta S_f^o(AB) - \Delta\overline{S}_A(x) - \Delta\overline{S}_B(x)} \qquad (11)$$

Here all quantities are expressed on a g°atom basis. The derivation of the liquidus temperature utilized the following assumptions:

i) ΔC_p^o for the formation Reaction (1) can be neglected.

ii) The relative partial molar enthalpy and entropy are independent over the temperature range of the calculated liquidus temperature.

iii) The homogeneity range is very small, thus producing neglible variation in $\Delta G_f^o(A_mB_n)$ with composition.

iv) The values of m and n are each taken as equal.

For Group III-V compounds the above assumptions are all excellent assumptions. Thus the liquidus temperature can be calculated from experimental Gibbs energy of formation data (usually emf results), relative partial molar enthalpies (calorimetric enthalpies of mixing) and relative partial molar entropies (derived from activity measurements of this study).

C. DEVELOPMENT OF THE FUSION EQUATION

A second expression for the liquidus temperature can be derived by considering an alternative expression for $\Delta G_f^o(A_mB_n)$. The binary system of interest here all melt congruently, thus at the maximum liquidus temperature (the reported melting point, Tm, of the compound)

$$\Delta G_f^o(A_mB_n) = \Delta G_f^o(s.l.) \qquad (12)$$

where $\Delta G_f^o(s.l.)$ refers to the Gibbs energy of formation of the stoichiometric liquid of composition $X_A = m/m+n$. At a temperature different from that of Tm $\Delta G_f^o(A_mB_n)$ can be approximated by

$$\Delta G_f^o(A_mB_n) = \Delta G_f^o(s.l.) + \Delta H_f^c(A_mB_n)\ (T/Tm - 1) \qquad (13)$$

where $\Delta H_f^c(A_mB_n)$ is the enthalpy of fusion of the compound A_mB_n. Here it is assumed that the heat capacity change for Reaction (1) is negligible. An expression for $\Delta G_f^o(s.l.)$ can be formulated by combining Equations (8) and (12) as

$$\Delta G_f^o(s.l.) = mRT \ln a_A^{s.l.} + nRT \ln a_B^{s.l.} \quad (14)$$

Here $a_A^{s.l.}$ and $a_B^{s.l.}$ are liquid phase activities of A and B, respectively, in a solution of composition $x_A = m/m+n$. It is noted that for $T < Tm$ the stoichoimetric liquid is supercooled. Combining Equations (8), (9), (13) and (14) gives

$$m\Delta\overline{H}_A(x) + n\Delta\overline{H}_B(x) - T(m\Delta\overline{S}_A(x) + n\Delta\overline{S}_B(x)) = \Delta H_f^c(A_mB_n)(\frac{T}{Tm} - 1)$$

$$+ m\Delta\overline{H}_A^{s.l.} + n\Delta\overline{H}_B^{s.l.} - T(m\Delta\overline{S}_A^{s.l} + n\Delta\overline{S}_B^{s.l.}) \quad (15)$$

Solving for T in the above equation yields the second expression for the liquidus temperature

$$T_\ell = \frac{\Delta H_f^c(A_mB_n) + m\Delta\overline{H}_A(x) + n\Delta\overline{H}_B(x) - m\Delta\overline{H}_A^{s.l.} - n\Delta\overline{H}_B^{s.l.}}{\Delta S_f^c(A_mB_n) + m\Delta\overline{S}_A(x) + n\Delta\overline{S}_B(x) - m\Delta\overline{S}_A^{s.l.} - n\Delta\overline{S}_B^{s.l.}} \quad (16)$$

where $\Delta S_f^c(A_mB_n)$ is the entropy of fusion for A_mB_n and is equal to $\Delta H_f^c(A_mB_n)/Tm$. Taking A_mB_n as perfectly stoichiometric ($m=n$ or $x_A = m/(m + n) = \frac{1}{2}$ for the application here) gives the "fusion" equation used.

$$T_\ell = \frac{2\Delta H_f^c(AB) + \Delta\overline{H}_A(x) + \Delta\overline{H}_B(x) - \Delta\overline{H}_A(0.5) - \Delta\overline{H}_B(0.5)}{2\Delta S_f^c(AB) + \Delta\overline{S}_A(x) + \Delta\overline{S}_B(x) - \Delta\overline{S}_A(0.5) - \Delta\overline{S}_B(0.5)} \quad (17)$$

All quantities are on a g°atom basis. The assumptions listed in the previous derivation were again used here. It should be emphasized that these assumptions produce negligible errors compared to the errors introduced by the experimentally determined quantities found

in the two liquidus equations. The alternative experimental quantity needed in this equation is the enthalpy of fusion and the melting temperature which are readily available.

D. DEVELOPMENT OF THE COMPONENT-RICH EUTECTIC LIQUIDUS EQUATIONS

The phase diagrams of binary Group III-V compounds also exhibits eutectic compositions. Since the pure solid metals show negligible solubility of the other metal, the liquid solution rich in either metal shows a composition range where equilibrium is with the pure metal.

An equation for calculating liquidus temperatures in component-rich solutions can be derived by considering the following reaction sequence for forming the pure metal solid phase

$$B \text{ (in liquid alloy)} = B(\ell) \tag{18}$$

and

$$B(\ell) = B(c) \tag{19}$$

The corresponding Gibbs energy changes are

$$\Delta G\ (18) = \mu_B - \mu_B^o = RT_\ell \ln a_B^{T_\ell} \tag{20}$$

and

$$\Delta G\ (19) = 0 = \Delta H_f^c(B) - T_\ell \Delta S_f^c(B) \tag{21}$$

The overall reaction is the formation of pure solid metal B from a saturated liquid solution. The Gibbs energy change for this equilibrium process is zero and results in a liquidus temperature given by

$$T_\ell = \Delta H_f^c(B)/(\Delta S_f^c(B) - R\ell n a_B^{T_\ell}) \tag{22}$$

Here the activity of B is that at the liquidus temperature. Equation (22) can be put into a more convenient form by relating $a_B^{T_\ell}$ at the liquidus temperature to the quantities measured and tabulated - the relative partial molar enthalpy and entropy at same reference temperature. The activity of B at the liquidus temperature, $a_B^{T_\ell}$, is related to the activity at a new temperature, a_B^T, by

$$\ell n\ a_B^{T_\ell} = \ell n\ a_B^T + \Delta\overline{H}_B(x)/R(\frac{1}{T_\ell} - \frac{1}{T}) \tag{23}$$

Substituting Equation (23) into Equation (22) and solving for T_ℓ yields

$$T_\ell = \frac{\Delta H_f^c(B) + \Delta\overline{H}_B(x)}{\Delta S_f^c(B) - R\ell n a_B^T + \Delta\overline{H}_B(x)/T} \tag{24}$$

Realizing that

$$R\ell n\ a_B^T = \Delta\overline{H}_B(x)/T - \Delta\overline{S}_B(x) \tag{25}$$

Equation (24) reduces to the equation desired

$$T_\ell = \frac{\Delta H_f^c(B) + \Delta\overline{H}_B(x)}{\Delta S_f^c(B) + \Delta\overline{S}_B(x)} \tag{26}$$

0 0 1 0 3 1 0 0 4 2 9

REFERENCES

1. A.S. Jordan and M.E. Weiner, J. Phys. Chem. Solids, 36, 1335 (1975).
2. L.J. Vieland, Acta Met., 11, 137 (1963).
3. H. Gaye and C.H.P. Lupis, Met. Trans., 6A, 1049 (1975).
4. L.S. Darken, Trans. Met. Soc. AIME, 239, 80 (1967).
5. C. Wagner, Acta Met., 6, 309 (1958).
6. R.F. Brebrick, Met. Trans., 2, 3377 (1971).
7. H. Hoshino, Y. Nakamura, M. Shimoji and K. Niwa, Ber. Bensenges, 69, 114 (1965).

APPENDIX IV

A LATTICE THEORY FOR LIQUID METAL SOLUTIONS

A. INTRODUCTION

Liquid solutions containing elements from the Group III and V columns have been found to have unusual properties near the temperature of compound formation. As the temperature is varied near the melting temperature anomalous heat capacities,[1] a maximum in the velocity of sound,[2,3] changing temperature coefficients of viscosity,[4-6] and abrupt structure changes[7,8] have all been observed. These results lead to the conclusion that the liquid phase is similar in behavior to a solid solution. A cell theory describing the liquid solution thermodynamic behavior is developed here similar to that of Averbach[9] and others.[10,11]

It is assumed that the entire potential energy is described completely by nearest neighbor mean potentials. For a binary system the energy of a mixture is

$$E = P_{11}E_{11} + P_{22}E_{22} + P_{(12)}E_{(12)} \tag{1}$$

where P_{ij} is the number of ij pairs - the parenthesis indicating the ij pairs are not distinguishable from ji pairs and E_{ij} is the effective mean potential energy of a ij pair. The number of unlike pairs, $P_{(ij)}$, is related to the probability, P_i, of finding an atom i as a nearest neighbor of an atom j. A short range order parameter is defined as

$$\alpha = 1 - P_i/x_i \ . \tag{2}$$

Thus α is zero if $P_i = x_i$, which is the condition for a random solution, while positive values of α indicate a preference for like pairs and negative values a preference for unlike pairs. Defining the average number of nearest neighbors to an atom as Z, one can show that the number of atoms i neighboring atoms j is the probability of this occurrence times the number of atoms i available, or

$$P_{(ij)} = Z\ N_o\ x_i x_j (1 - \alpha)\ . \tag{3}$$

The number of like pairs is related to the number of unlike pairs by

$$P_{ii} = \frac{ZN_o x_i - P_{(ij)}}{2} \tag{4}$$

Substituting Equations (3) and (4) into Equation (1) one obtains

$$E = \frac{ZN_o}{2}\ (x_1 E_{11} + x_2 E_{22}) + ZN_o\ x_2 x_1 (1-\alpha)(E_{12} - \frac{(E_1+E_2)}{2} \tag{5}$$

The difference between the mean potential energy of an unlike pair and the average mean potential of the two like pairs is termed the interaction energy, w. Neglecting the PV term, the relative integral Gibbs energy of mixing is given by

$$\Delta G^M = ZN_o x_1 x_2 (1-\alpha) w - T\Delta S_c^M \tag{6}$$

where ΔS_c^M is the configurational entropy of mixing.

The configurational entropy of mixing can be calculated by considering the number of ways of arranging the four types of pairs in the liquid lattice. The four types are 11, 22, 12 and 21; it being necessary to account for the difference between 12 and 21 since the order of the pair will affect the identity of an atom at a given

lattice site. The configurational entropy is then

$$\Delta S_c^M = R \ln \frac{P!}{P_{11}!P_{22}!P_{12}!P_{21}!} = -\frac{RZ}{2} \sum_{i=j=1}^{2} x_{ij} \ln x_{ij} \qquad (7)$$

where x_{ij} is the fraction of ij pairs.

The above formulation is not exactly correct in that it contains many unallowable configurations. A correction term is applied such that Equation (7) reduces the configurational entropy of a completely random solution when the bond fractions are $x_{11} = x_1^2$, $x_{22} = x_2^2$ and $x_{12} = x_{21} = x_1 x_2$. With this correction the entropy of mixing is now given by

$$\Delta S_c^M = -\frac{RZ}{2} \sum_{i=j=1}^{2} x_{ij} \ln x_{ij} + kN_o(Z-1) \sum_{i=1}^{2} x_i \ln x_i \qquad (8)$$

Upon substituting Equations (3) and (4) for the x_{ij} terms one arrives at the result

$$\Delta S_c^M = -\frac{RZ}{2} \{[x_1 - x_1 x_2(1-\alpha)] \ln[x_1 - x_1 x_2(1-\alpha)] + 2x_1 x_2(1-\alpha)$$

$$\ln[x_1 x_2(1-\alpha)] + [x_2 - x_1 x_2(1-\alpha)] \ln[x_2 - x_1 x_2(1-\alpha)]\} + R(Z-1) \sum_{i=1}^{2} x_i \ln x_i \qquad (9)$$

Equations (6) and (9) can be expressed in terms of the bond fraction of (12) pairs, x_{12} as

$$\Delta G^M = ZN_o x_{12} w - T\Delta S_c^M \qquad (10)$$

and

$$\Delta S_C^M = -\frac{RZ}{2}\{[x_1 - x_{12}] \ln[x_1 - x_{12}] + 2x_{12} \ln[x_{12}] + [x_2 - x_{12}] \ln[x_2 - x$$

$$R(Z-1) \sum_{i=1}^{2} x_i \ln x_i \qquad (11)$$

The entropy of mixing is then given by

$$\frac{\partial \Delta G^M}{\partial T} = \Delta S^M = \Delta S^M_c - ZN_o \frac{\partial}{\partial T}(x_{12}w) + T\frac{\partial}{\partial T} S^M_c \qquad (12)$$

The interaction energy, w, is allowed to be a function of both composition and temperature. It is now assumed that these dependencies can be separated or

$$w = \mu + j(x) + g(T) \qquad (13)$$

The interaction energy can be related to bond fraction, x_{12}, by computing the bond fraction that minimizes the Gibbs energy of mixing as required by equilibrium considerations. Thus the equation

$$\left(\frac{\partial \Delta G^M}{\partial x_{12}}\right)_{T,P,x_1} = 0 = ZN_o w - T\frac{\partial \Delta S^M_c}{\partial x_{12}} \qquad (14)$$

provides a means for relating the short range order parameter to the interaction energy. Upon performing the above operation and defining a reduced interaction energy, ν, as 2Now/RT one finds the following quadratic expression

$$x_{12}^2(e^{\nu} - 1) + x_{12} - x_1x_2 = 0 \qquad (15)$$

Solving the above quadratic equation for x_{12} (which is equal to $x_1x_2(1-\alpha)$ for the real root and then expanding this result produces the following equation:

$$x_{12} = x_1x_2[1 - x_1x_2\nu - \tfrac{1}{2}x_1x_2(x_1-x_2)^2\nu^2 + \ldots] \qquad (16)$$

The short range parameter is then related to the bond fraction by

$$\alpha = x_1 x_2 \nu - \tfrac{1}{2} x_1 x_2 (x_1 - x_2)^2 \nu^2 + \ldots \tag{17}$$

The entropy of mixing can now be calculated from Equation (10). Making use of Equation (15), ΔS^M is then simply given by

$$\Delta S^M = \Delta S^M_c - ZN_o x_{12} \frac{dg(T)}{dT} \tag{18}$$

and the enthalpy of mixing by

$$\Delta H^M = ZN_o x_{12} (\mu + j(x) + g(T) - T \frac{dg(T)}{dT}) \tag{19}$$

Equations (17), (18) and (19) can be solved simultaneously from experimental enthalpy and entropy of mixing data to give values for the terms $\mu + j(x)$, $g(T)$ and α.

B. APPROXIMATIONS

1. General Approximations

The simultaneous solution of Equations (17) to (19) is not explicit but fortunately these equations can be put into an approximate form as follows. First, the short range order parameter is approximated by truncating all terms except the first in Equation (17), leaving

$$\alpha = x_1 x_2 \nu \tag{20}$$

Next, it can be shown that the entropy of mixing can be approximately given by

$$\Delta S^M = -R(1 - x_1 x_2 |\nu|) \sum_{i=1}^{2} x_i \ln x_i - ZN_o x_1 x_2 (1 - x_1 x_2 \nu) \frac{dg(T)}{dT} \tag{21}$$

These simplifications will greatly aid in the determination of the interaction energy. With these ideas several special cases exist

concerning the assumed temperature and composition dependence of the interaction energy.

2. Special Cases

a) Constant Interaction Energy

For the case of the interaction energy independent of both temperature and composition the pertinent equations reduce to

$$w = \mu \tag{22}$$

$$\alpha = 2N_o \mu x_1 x_2 / RT = x_1 x_2 \nu \tag{23}$$

$$\Delta H^M = ZN_o x_1 x_2 (1 - x_1 x_2 \nu)\mu \tag{24}$$

$$\Delta \overline{H}_1 = \Delta \overline{H}_1(\mu) = ZNo\mu[1 - 2(\nu+1)x_1 + (7\nu+1)x_1^2 - 8\nu x_1^3 + 3\nu x_1^4] \tag{25}$$

$$\Delta \overline{H}_2 = \Delta \overline{H}_2(\mu) = ZN_o\mu[(\nu+1)x_1^2 - 4\nu x_1^3 + 3\nu x_1^4] \tag{26}$$

$$\Delta S^M = -R(1 - x_1 x_2 |\nu|) \sum_{i=1}^{2} x_i \ \ell n \ x_i \tag{27}$$

$$\Delta S^E = -x_1 x_2 |\nu| \ \Delta S^{ID} \tag{28}$$

$$\Delta \overline{S}_1 = \Delta \overline{S}_1^{ID}(1 - x_2^2 |\nu|) + Rx_2^2 |\nu| (x_1 - x_2) \ell n \ x_1/x_2$$

$$\Delta \overline{S}_2 = \Delta \overline{S}_2^{ID}(1 - x_1^2 |\nu|) + Rx_1^2 |\nu| (x_1 - x_2) \ell n \ x_1/x_2$$

It can be seen that the excess entropy in this case is always negative and when μ is identically zero these formulations reduce to the ideal solution case.

b) Temperature Dependent Interaction Energy

If the composition dependence of the interaction energy is

neglected it takes the form

$$w = \mu + g(T) \tag{31}$$

The acoustic factor, g(T) may be considered as follows. This factor gives information on the solution lattice behavior as a function of temperature. As an approximation this may be assumed to correspond to the temperature coefficient of the elastic constants of the solid. The variation of the thermoelastic coefficients with temperature is linear over surprisingly large temperature ranges, and thus it will be assumed that

$$g(T) = gT \tag{32}$$

With this assumption the thermodynamic quantities are now given by

$$w = \mu + gT \tag{33}$$

$$\alpha = 2N_o(\mu + gT)x_1x_2/RT = x_1x_2\nu \tag{34}$$

$$\Delta S^M = -R(1-x_1x_2|\nu|) \sum_{i=1}^{2} x_i \ln x_i - ZNox_1x_2(1-x_1x_2\nu)g \tag{35}$$

$$\Delta S^E = x_1x_2|\nu|\Delta S^{ID} - ZNox_1x_2(1-x_1x_2\nu)g \tag{36}$$

$$\Delta\bar{S}_1 = \Delta\bar{S}_1^{ID}(1-x_2^2|\nu|) + R_2^2|\nu|(x_1-x_2)\ln\frac{x_1}{x_2} - \Delta H_1(g) \tag{37}$$

$$\Delta\bar{S}_2 = \Delta\bar{S}_2^{ID}(1-x_1^2|\nu|) + Rx_1^2|\nu|(x_1x_2)\ln\frac{x_1}{x_2} - \Delta H_2(g)$$

The enthalpy terms are as in the case of a constant interaction energy. The important characteristic of this set of equations is that a positive or negative excess entropy of mixing is now allowable.

c) Composition Dependent Interaction Energy

It is now assumed that the interaction energy is given by

$$w = \mu + jx_1 \tag{39}$$

Thus the assumption of a linear composition dependence for w is invoked. The thermodynamic quantities of interest reduce to those given below.

$$\alpha = 2N_o(\mu+jx_1)x_1x_2/RT = x_1x_2\nu \tag{40}$$

$$\Delta H^M = ZN_o x_1x_2(1-x_1x_2\nu)(\mu+jx_1) \tag{41}$$

The partial molar enthalpy of both components is now a polynomial order of six:

$$\Delta S^M = \Delta S^{ID}(1-x_1x_2|\nu|) \tag{42}$$

$$\Delta S^E = -\Delta S^{ID}x_1x_2|\nu| \tag{43}$$

$$\Delta\bar{S}_1 = \Delta\bar{S}_1^{ID}(1-x_2^2|\nu|) + Rx_2^2(x_1-x_2)|\nu|\ln\frac{x_1}{x_2} - \frac{2N_o j}{RT}x_1x_2^2\,\Delta S^{ID} \tag{44}$$

$$\Delta\bar{S}_2 = \Delta\bar{S}_2^{ID}(1-x_1^2|\nu|) + Rx_1^2(x_1-x_2)|\nu|\ln\frac{x_1}{x_2} - \frac{2N_o j}{RT}x_1^2x_2\,\Delta_S{}^{ID} \tag{45}$$

The excess entropy of mixing in the case again shows only negative values.

A final case is that allowing for both a composition and temperature dependence on the interaction energy and this case is simply a superposition of the previous two cases.

C. SUMMARY

A simple statistical model was developed to account for the tendency of unlike pairing found in most Group III-V semiconductor liquid solutions. With the approximations indicated above the terms $\mu + j(x)$, $g(T)$ and α can be solved from experimental enthalpies and entropies of mixing. The functionality of these terms can then be ascertained by the results of the calculations and the appropriate special case discussed can be applied. In this way the degree of short range order is quantified and the model used to predict thermodynamic properties of interest.

REFERENCES

1. H. Lichter and P. Sommelet, Trans. Met. Soc. AIME, 245, 99 (1969).
2. V.M. Glazov, A.A. Aivazov and V.I. Timoshenko, Sov. Phys. Solid State, 18, 1236 (1976).
3. M.B. Gitis and I.G. Mikhailov, Sov. Phys. - Acoustics, 11, 372 (1966).
4. V.M. Glazov and D.A. Petrov, Izv. AN SSSR, OTN, No. 4, 125 (1958).
5. V.M. Glazov and S.N. Chizhevskaya, Fiz. tverd. tela., 4, 1841 (1962).
6. V.M. Glazov, S.N. Chizhevskaya and N.N. Glazoleva, Liquid Semiconductors, Plenum Press, N.Y. (1969).
7. Yu. G. Poltavtsev, Russ. J. Phys. Chem., 45, 1665 (1971).
8. H. Krebs, H. Weyand and M. Haucke, Angew. Chem., 70, 468 (1958).
9. B.L. Averbach, Energetics in Metallurgical Phenomena, Vol. II, W.M. Mueller, ed., Gordon and Breach, New York, 1965.
10. C. Wagner, Thermodynamics of Alloys, Addison Wesley Publishing Co., Inc., Reading, Mass. (1952).
11. E.A. Guggenheim, Mixtures, Clarendon Press, Oxford, England (1952).

APPENDIX V

THE IMPORTANT RELATIONSHIPS FOR DESCRIBING PHASE EQUILIBRIUM IN TERNARY III-V SYSTEMS

A. INTRODUCTION

The ternary systems constituted from two elements of the Group III or V column of the periodic table and one element from either the Group V or III column, respectively, form substitutional solid solutions over the entire composition range. The pseudobinary solid solution can be represented by $A_xB_{1-x}C$, where A and B are Group III or Group V atoms and C is a Group V or III atom, respectively.

The phase field is dominated by the equimolar binary compounds AC and BC due to their unusually high melting points relative to the other solid phases (primarily the solid elements showing little solubility for the other elements). The compounds AC and BC are completely miscible and for a pseudobinary system that is depicted by a vertical slice at constant C composition, $x_C = 1/2$. This pseudobinary phase diagram is isomorphous and again its shape is dominated by the melting points of the binary compounds. The liquidus surface is of primary interest in that the important mixed crystals are generally precipitated from the liquid phase. The binary compounds are generally simple eutectics in nature though they may be isomorphous for atoms of the same Group. The eutectic type binary phase diagrams produce eutectic valleys in the ternary phase field. Except for binary phase diagrams constituted from atoms of the same Group, the pure elements show no solid solubility for the other elements. As indicated above,

the industrially important phase equilibria consists of solid solution in equilibrium with a miscible ternary liquid. Thus derived below are the important relationships that can be used to describe the phase equilibrium.

B. GENERAL RESULTS

1. Basic Equilibrium Conditions

The criteria for equilibrium are equality of all chemical potentials, for each component temperature and pressure in each phase. For two phase equilibria in a three component system the condition of equilibrium gives

$$\mu_A^c = \mu_A^\ell \tag{1}$$

$$\mu_B^c = \mu_B^\ell \tag{2}$$

$$\mu_C^c = \mu_C^\ell \tag{3}$$

$$T^c = T^\ell \tag{4}$$

$$P^c = P^\ell \tag{5}$$

The chemical potential of liquid component i is given by the relationship

$$\mu_i^\ell = \mu_i^{o,\ell} + RT \ln \gamma_i x_i \tag{6}$$

where $\mu_i^{o,\ell}$ is chemical potential of i in its standard state and is taken as the pure liquid element at T^ℓ and P^ℓ, γ_i is the activity coefficient of i in the ternary solution, and x_i is the mole fraction of i in the liquid phase. The treatment of the solid solution is

somewhat simplified by considering the system as binary system of constituents AC and BC. Thus the chemical potential of AC is given by

$$\mu^{c}_{AC} = \mu^{o,c}_{AC} + RT \ln \gamma_{AC} X_{AC} \qquad (7)$$

where the standard state chemical potential of AC, $\mu^{o,c}_{AC}$, is pure solid AC at the temperature and pressure of interest and X_{AC} is the mole fraction of AC in the mixed crystal and equivalent to X in the formulation $A_X B_{1-X} C$, at equilibrium the chemical potentials of the components AC and BC in the solid solution must be equal to the sum of the chemical potentials of their respective constituents in the liquid phase. Thus the basic equations of equilibrium are

$$\mu^{o,c}_{AC} + RT\ln \gamma_{AC} X_{AC} = \mu^{o,\ell}_{A} + \mu^{o,\ell}_{C} + RT\ln\gamma_A x_A + RT\ln \gamma_C x_C \qquad (8)$$

$$\mu^{o,c}_{BC} + RT\ln\gamma_{BC} X_{BC} = \mu^{o,\ell}_{B} + \mu^{o,\ell}_{C} + RT\ln\gamma_B x_B + RT\ln \gamma_C x_C \qquad (8)$$

$$x_A + x_B + x_c = 1 \qquad (10)$$

and

$$X_{AC} + X_{BC} = 1 \qquad (11)$$

all at constant temperature and pressure.

2. Relationship Between the Standard State Chemical Potentials

In order to produce Equations (8) and (9) into a workable form the relationship between the solid and liquid phase chemical potentials must be elucidated. Using the compound AC as an example, first consider heating the compound AC from T to the melting temperature of AC, T_m.

The chemical potential change of this process is related to the molar entropy of AC and in the integrated form is

$$\mu^c_{AC}(T_m) - \mu^c_{AC}(T) = - \int_T^{T_m} S^c_{AC}(T)dT \qquad (12)$$

The molar entropy is related to the molar heat capacity of AC, C^c_p, by

$$S^c_{AC}(T) = S^c_{AC}(T_m) + \int_{T_m}^{T} \frac{C^c_p}{T} \, dT \qquad (13)$$

Combining Equations (12) and (13) we obtain

$$\mu^c_{AC}(T_m) = \mu^c_{AC}(T) - (T_m - T) S^c_{AC}(Tm) + \int_T^{T_m} \int_T^{T_m} \frac{C^c_p}{T} \, dT^2 \qquad (14)$$

Next, the compound is melted to form a stoichiometric liquid and the chemical potential change for this equilibrium process is

$$\mu^c_{AC}(T_m) = \mu^{s\ell}_A(T_m) + \mu^{s\ell}_C(T_m) \qquad (15)$$

where $s\ell$ indicates the liquid phase chemical potential is evaluated at an equimolar composition. Finally, the stoichiometric liquid is supercooled from T_m to the original temperature, T. Using reasoning similar to that in arriving at Equation (14) the chemical potential for this process is given by

$$\mu^{s\ell}_A(T) + \mu^{s\ell}_C(T) = \mu^{s\ell}_A(T_m) + \mu^{s\ell}_B(T_m) - (T-T_m) \, S^{s\ell}_{A,C}(T_m) - \int_{T_m}^{T} \int_{T_m}^{T} \frac{C^{s\ell}_p}{T} \, dT^2 \qquad (16)$$

Combining Equations (14), (15) and (16) one obtains the relation between the compound chemical potential and the chemical potential of the liquid

components is discovered and given by

$$\mu^{c}_{AC}(T) = \mu^{s\ell}_{A}(T) + \mu^{s\ell}_{C}(T) - (T_m-T)(S^{s\ell}_{A,C}(T_m) - S^{c}_{AC}(T_m)) + \int_T^{T_m}\int_T^{T_m} \frac{C^{s\ell}_p - C^{c}_p}{T}\, dT^2 \qquad (17)$$

Defining ΔC_p as the difference between the molar heat capacity of the stoichiometric liquid and the compound and recognizing that $S^{s\ell}_{AC}(T_m) - S^{c}_{AC}(T_m)$ is equal to the entropy of fusion of the compound, $\Delta S^{c}_{f}(AC)$, Equation (17) reduces to

$$\mu^{c}_{AC}(T) = \mu^{s\ell}_{A}(T) + \mu^{s\ell}_{C}(T) = -(T_m-T)\Delta S^{f}_{c}(AC) + \int_T^{T_m}\int_T^{T_m} \frac{\Delta C_p}{T}\, dT^2 \qquad (18)$$

Finally, if ΔC_p is taken as independent of temperature Equation (18) can be integrated to give

$$\mu^{c}_{AC}(T) = \mu^{s\ell}_{A}(T) + \mu^{s\ell}_{C}(T) - (T_m-T)\Delta S^{f}_{c}(AC) + \Delta C_p[T_m - T - T\ell n \frac{T_m}{T}] \qquad (19)$$

3. Development of Working Equations for the Ternary Phase Equilibria

The general equations for phase equilibria in the ternary III-V systems are Equations (8) and (9). These equations can be put into a more useful form by writing Equation (18) for the standard state chemical potential of either compound AC or BC and making use of Equation (6). The final results are

$$RT\ell n\gamma_{AC}X_{AC} = RT\ell n \left\{\frac{4\gamma_A\gamma_C x_A x_C}{\gamma^{s\ell}_A \gamma^{s\ell}_C}\right\} + (T_m-T)\Delta S^{f}_{c}(AC) - \int_T^{T_m}\int_T^{T_m} \frac{\Delta C^{AC}_p}{T}\, dT^2 \qquad (20)$$

and

$$RT\ln\gamma_{BC}X_{BC} = RT\ln\left\{\frac{4\gamma_B\gamma_C x_B x_C}{\gamma_B^{s\ell}\gamma_C^{s\ell}}\right\} + (T_m-T)\Delta S_c^f(BC) - \int_T^{T_m}\int_T^{T_m}\frac{\Delta C_p^{BC}}{T}dT^2 \quad (21)$$

Thus, in order to calculate the liquidus surface, information on both the liquid and solid phase activity coefficients, the entropy of fusion of the compounds, and the ΔC_p terms are required.

C. PSEUDOBINARY CASE

Equations (20) and (21) reduce to a simpler form for the special case of the pseudo-binary slice of the ternary phase diagram. Using the following simplifying notation

$$\Gamma_{AC} = [(T_m-T)\Delta S_f^c(AC) - \int_T^{T_m}\int_T^{T_m}\frac{\Delta C_p^{AC}}{T}dT^2]/RT \quad (22)$$

$$\Gamma_{BC} = [(T_m-T)\Delta S_f^c(BC) - \int_T^{T_m}\int_T^{T_m}\frac{\Delta C_p^{BC}}{T}dT^2]/RT \quad (23)$$

and noting that the component mole functions are now given by

$$x_B = 1/2 - x_A \quad (24)$$

and

$$x_C = 1/2 \quad (25)$$

the governing equations for the pseudo-binary reduce to

$$\ln\gamma_{AC}X_{AC} = \ln\left\{\frac{2\gamma_A\gamma_C x_A}{\gamma_A^{s\ell}\gamma_C^{s\ell}}\right\} + \Gamma_{AC} \quad (26)$$

$$\ln\gamma_{BC}X_{BC} = \ln\frac{2\gamma_B\gamma_c(1-x_A)}{\gamma_B^{s\ell}\gamma_C^{s\ell}} + \Gamma_{BC} \quad (27)$$

D. IDEAL LIQUID AND SOLID SOLUTIONS

For purposes of comparison it is instructive to calculate the phase diagram for the special case of ideal solution behavior. In this limit all activity coefficients are taken as unity and Equation (20) and (21) reduce to

$$\ln X_{AC} = \ln\{4x_A x_C\} + \Gamma_{AC} \tag{28}$$

and

$$\ln(1-X_{AC}) = \ln\{4x_B x_C\} + \Gamma_{BC} \tag{29}$$

These equations contain 4 unknowns, x_A, x_C, X_{AC} and T, and can be solved for any two given the values of the other two variables. Solving the above equations for X_{AC} and the liquid mole fraction x_A yields the following equations for the liquidus surface

$$x_A = \frac{\frac{1}{4x_c} - (1 - x_c)e^{\Gamma_{BC}}}{e^{\Gamma_{AC}} - e^{\Gamma_{BC}}} \tag{30}$$

and

$$X_{AC} = \frac{4x_c(1-x_c) - e^{-\Gamma_{BC}}}{e^{-\Gamma_{AC}} - e^{-\Gamma_{BC}}} \tag{31}$$

Thus the liquidus surface for the case of ideal solution behavior can be easily evaluated.

0 0 0 5 1 3 0 2 5 8

Thus the liquidus surface for the case of ideal solution behavior can be easily evaluated.

ACKNOWLEDGMENTS

I would like to dedicate this manuscript to the person responsible for its initiation and inspired continuation, to the person giving endlessly of herself, to my wife - Sandy.

I am pleased to express my gratitude to Dr. Lee F. Donaghey for his support and guidance and for his friendship, under whose direction the project progressed and provided me with an invaluable educational experience. I am especially beholden to Dr. Leo Brewer for his interest and helpful advice and to the members of his research group for their suggestions and interactions. Dr. John Prausnitz deserves special recognition for his review of this work and synergistic criticism. Thanks to the faculty of the Department of Chemical Engineering for producing a creative atmosphere. The inhabitants and visitors of 210 Lewis also merit considerable credit for maintaining a healthy perspective of this research in my mind.

I would also like to thank all those people whose efforts made the success of this project possible - the employees of Lawrence Berkeley Laboratory (especially Paul, George, Brian, and Phil) and the staff of the College of Chemistry (Carl, Slim, Andy, Mike, Carl, Gigi, and Linda, to mention a few). Finally, I give appreciation to Nancy for the excellent drafting and Lorine, Shirley, Michelle, and Jean for exhibiting the virtue of patience in the preparation of this manuscript in spite of the continued harassment by the author.

This work was supported by the Department of Energy.

U.S.GPO:1980-698-169/F-111

0 0 0 0 5 1 0 0 2 3 9

This report was done with support from the Department of Energy. Any conclusions or opinions expressed in this report represent solely those of the author(s) and not necessarily those of The Regents of the University of California, the Lawrence Berkeley Laboratory or the Department of Energy.

Reference to a company or product name does not imply approval or recommendation of the product by the University of California or the U.S. Department of Energy to the exclusion of others that may be suitable.

TECHNICAL INFORMATION DEPARTMENT
LAWRENCE BERKELEY LABORATORY
UNIVERSITY OF CALIFORNIA
BERKELEY, CALIFORNIA 94720